Mechanistic Photochemistry of Inorganic and Organometallic Complexes in Solution and Inert Matrices at 85K

A Dissertation

Presented in Partial Fulfillment of the Requirements for the

Degree of Doctorate of Philosophy

with a

Major in Chemistry

in the

College of Graduate Studies

University of Idaho

by

Wyatt Aaron Thornley

Major Professor: Thomas E. Bitterwolf, Ph.D.

Committee Members: Eric B. Brauns, Ph.D.; John C. Linehan, Ph.D.;

Peter B. Allen, Ph.D.

Department Chair: Ray von Wandruszka, Ph.D.

September 2016

Authorization to Submit Dissertation

This *dissertation* of *Wyatt Aaron Thornley,* submitted for the degree of *Doctorate in Philosophy* with a Major in *Chemistry* and titled "Mechanistic Photochemistry of Inorganic and Organometallic Complexes in Solution and Inert Matrices at 85K," has been reviewed in final form. Permission, as indicated by the signatures and dates below, is now granted to submit final copies to the College of Graduate Studies for approval.

Major Professor: ______________________ Date: ____________
Thomas E. Bitterwolf, Ph.D.

Committee Members: ______________________ Date: ____________
John C. Linehan, Ph.D.

______________________ Date: ____________
Eric B. Brauns, Ph.D.

______________________ Date: ____________
Peter B. Allen, Ph.D.

Department Chair: ______________________ Date: ____________
Ray von Wandruszka, Ph.D.

Abstract

Matrix-isolation FTIR at cryogenic temperatures and traditional solution experiments have been used to study the mechanisms of new and previously reported photochemical reactions of inorganic and organometallic complexes. Spurred by lack of consensus for the mechanism of the photodecomposition of permanganate, one of the earliest reported inorganic photoreactions, a broad survey upon the photochemistry of inorganic and organometallic oxides and nitrides was conducted. These studies yielded the only known example of reversible six-electron reductive elimination and oxidative addition, coming in the form of a nitrosyl ligand from the nitridoosmate anion, the identity of the key intermediate and mechanism of the photodecomposition of permanganate, and a new competitive photopathway in the photochemistry of the O_2 adduct of Vaska's complex, an archetypal organometallic photoreaction.

As a means to study the structure and bonding of the [FeFe]-hydrogenase enzyme active, a potential model for a future hydrogen energy economy, the photochemistry of structural models of this active site has been studied. At cryogenic temperatures, photoejection of CO is observed resulting in a product that may then undergo secondary photolysis to form either a bridging carbonyl ligand as found in the natural enzyme, or result in C-H bond activation of the alkyl dithiolate bridge which may serve as a new model for proton or hydride transfer in the catalytic cycle of the [FeFe]-hydrogenase enzyme. Photodecarbonylation of dithiolene

derivatives of [FeFe]-hydrogenase model complexes results in the formation of uncommon aromatic metallacycles.

Photolysis of a series of allyl complexes in the $TpM(CO)_2(\eta^3\text{-}C_3H_4R)$, where Tp=tris(pyrazolyl)borate, M=Mo or W, and R=2-H or 2-Me, family of compounds was found to result in in *exo/gauche* rotameric isomerism of the allyl ligand, exhibiting behaviour distinct from the closely related $CpM(CO)_2(\eta^3\text{-}C_3H_4R)$ (Cp = η^5-cyclopentadienyl) complexes that undergo *endo/exo* rotameric isomerism.

Finally, a series of organometallic diazonium complexes were studied at cryogenic temperatures. Diazonium ligands are isoelectronic with the well-studied nitrosyl ligand, and these initial studies reveal, that like their nitrosyl counterparts, diazonium ligands undergo η^1 to η^2 linkage isomerism following photoexcitation. An additional photoreaction, whereby homolysis of the diazonium ligand occurs to yield two radical species is also reported.

Table of Contents

List of Tables

List of Figures

List of Schemes

Chapter 1: Photochemical Intramolecular Six-Electron Reductive Elimination and Oxidative Addition of Nitric Oxide by the Nitridoosmate(VIII) Anion

Published: W. A. Thornley, T. E. Bitterwolf, Angew. Chem. Int. Ed. Engl. **2015**, *54*, 2068–2072.

Abstract*: UV photolysis of the nitridoosmate(VIII) anion, OsO_3N^-, in low-temperature frozen matrices results in nitrogen-oxygen bond formation to give the Os(II) nitrosyl complex $OsO_2(NO)^-$. Photolysis of the Os(II) nitrosyl product with visible wavelengths results in reversion to the parent Os(VIII) complex. Formally a 6-electron reductive elimination and oxidative addition, respectively, this represents the first reported example of such an intramolecular transformation. DFT modelling of this reaction reveals a step-wise mechanism taking place through a side-on nitroxyl Os(VI) intermediate, $OsO_2(\eta^2\text{-}NO)^-$.*

Oxidative addition and reductive elimination reactions are fundamental processes observed in transition metal chemistry. These are generally two-electron processes that are associated with addition or elimination of substrates such as H_2, alkanes, arenes, silanes, and others, and have been widely exploited in a variety of catalytic cycles. Far less common are the four- or six-electron analogues of these reactions.

Four- and six-electron oxidative addition of bonds in N_2O have been observed in a number of chemical systems.[1] In frozen gas matrices, metal atoms[2-4] and vacant metal sites generated through photochemical decarbonylation,[5,6] reactions have been observed with O_2, NO, and N_2 to form OMO, NMO, and NMN species, respectively; in some cases these products may be preceded by an η^2-XY species with conversion to the insertion product being either thermally or photochemically initiated. In an examination of the photochemistry of $CpW(CO)_2NO$ (Cp = η^5-C_5H_5) in frozen gas matrices, Rest and co-workers found evidence for intramolecular formation of an isocyanate ligand to give CpW(CO)(NCO), presumably through the reaction of CO with a photochemically generated nitrene intermediate; the ultimate fate of O-atom of the nitrosyl ligand remains elusive.[7] In a solution photolysis study of the closely related $CpMo(CO)_2NO$ in the presence of an excess of PPh_3, McPhail and co-workers found that in addition to the simple PPh_3 substitution product, generation of PPh_3O, $CpMo(CO)_2(NCO)PPh_3$, and $CpMo(CO)(NCO)(PPh_3)_2$ were also observed, providing evidence for intramolecular activation of the nitrosyl ligand to give an unobserved nitrene intermediate.[8] Finally, Legzdins and co-workers have observed isomerization of some 16-electron aryl and alkyl nitrosyl complexes of tungsten to the corresponding imido oxo analogues when in the presence of O_2 or H_2O; in the latter case an η^2-NO intermediate was suggested.[9-21]

Even less common are the four- and six-electron reductive elimination counterparts to these multi-electron oxidative additions. We are only aware of two such examples that fit this category; the long-known photochemical ejection of O_2

from the permanganate ion[22] and S_2 from MS_4^{n-}, where M, n = Mo, 2; W, 2; V, 3; and Re, 1 when in the presence of O_2.[23,24]

As part of our ongoing examination of metal nitrosyl photochemistry, our attention was directed toward the possibility that the photochemical nitrosyl bond cleavage reported by Rest and McPhail may occur through oxidative addition of a photogenerated η^2-NO intermediate. Oxidative addition of an η^2-NO may give rise to several valence isomers depending upon the extent of reduction of the nitrosyl ligand, each possessing the same ligating atoms but differing in the nature of the bonds between the ligands and metal as well as the oxidation state of the metal. Formal four-electron oxidative addition of the nitrosyl ligand in $CpM(CO)_2(\eta^2\text{-NO})$ would result in formation of what could be described as an anionic η^2-NO nitroxyl group and six-electron oxidative addition would result in cleavage of the NO bond to ultimately yield a mixed nitride oxide complex (Scheme 1.1).

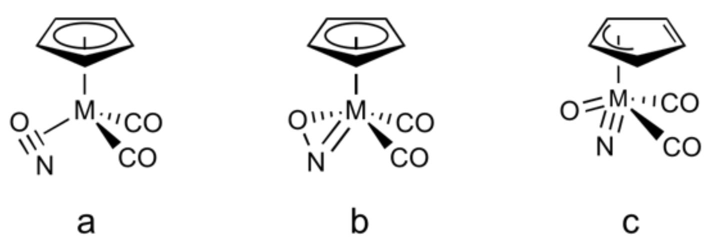

Scheme 1.1: Valence isomers of $CpM(CO)_2(\eta^2\text{-NO})$

Synthesis of four-electron valence isomers of a molybdenum nitroso-complex has been previously reported. Wentworth and Maatta synthesized the η^2-nitrosobenzene complex $Mo(\eta^2\text{-ONPh})(S_2CNEt_2)_2$, as well as its four-electron valence isomer $MoO(NPh)(S_2CNEt_2)_2$, a mixed phenylnitrene, oxo complex.[24] Though no isomerization between $Mo(\eta^2\text{-}ONPh)(S_2CNEt_2)_2$ and $MoO(NPh)(S_2CNEt_2)_2$ was found to occur thermally nor following visible photolysis, in a subsequent publication we will demonstrate that this process does, indeed, occur at higher energies of incident light.[25,26] This remarkable example does demonstrate the ability of a transition metal to support such valence isomers as those proposed for the oxidative-addition of an η^2-NO ligand.

As no direct evidence for η^2-NO valence isomerism has been reported in metal nitrosyl photochemistry literature, we directed our focus on the photochemistry of model compounds that resemble the oxidative addition valence isomers of η^2-NO, that is, complexes with oxide and nitride ligands oriented in adjacent coordination sites. Microscopic reversibility indicates that if an η^2-NO ligand is capable of undergoing oxidative addition, that this family of compounds should then be able to reductively eliminate nitric oxide (Scheme 1.2). Matching this criteria is the MO_3N^{n-} family of compounds where M, n = Mo, 3; Re, 2; and Os, 1.[8] Due to poor solubility of the polyanions, only $[(n\text{-}C_4H_9)_4N)][OsO_3N]$ was found to be compatible with the matrix materials we currently use for low-temperature photolysis experiments.

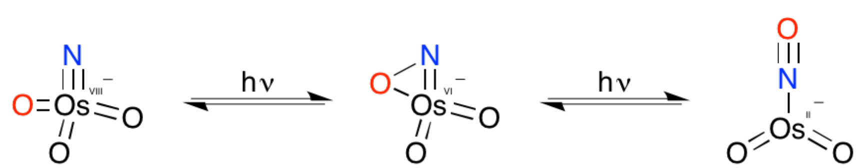

1a 1c 1e

Scheme 1.2: Proposed reductive elimination of nitric oxide by OsO_3N^-.

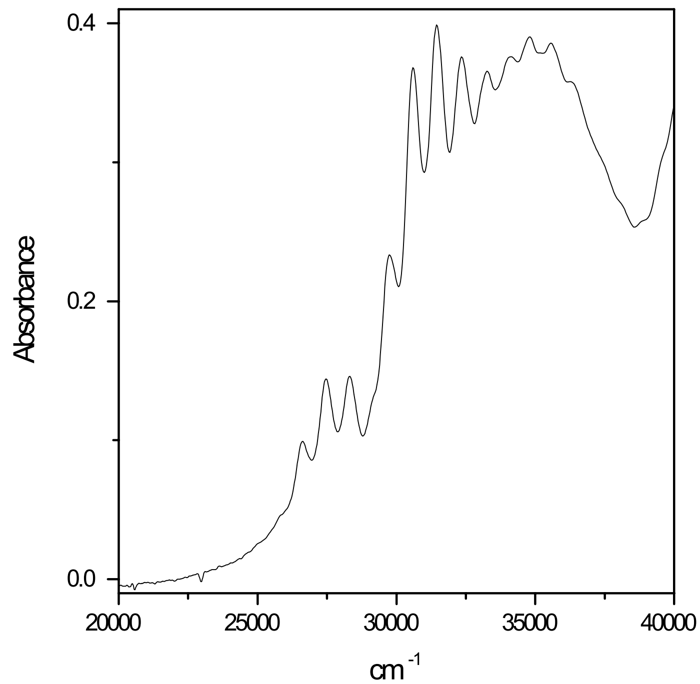

Figure 1.1: Electronic spectrum of $[(n\text{-}C_4H_9)_4N)][OsO_3N]$ as a thin film at 85 K.

The electronic spectrum of $[(n\text{-}C_4H_9)_4N)][OsO_3N]$ as a thin film at 85 K in the region of 250-500 nm (20,000-40,000 cm^{-1}) consists of three overlapping absorptions centered at 402, 357, and 315 nm with well resolved vibronic fine structure (Figure 1.1). Miskowski and coworkers have previously performed a detailed analysis of the vibronic fine structure of the electronic spectrum of nitridoosmate(VIII) at 5 K, and found an average Δν of 825 cm^{-1}, 900 cm^{-1}, and 872 cm^{-1} for the three absorptions bands, respectively.[30] This coupling corresponds to an 11-19% reduction of the Os-N stretching frequency in the excited state, consistent with LMCT from the nitride ligand. TD-DFT calculations reveal that these three absorptions consist of vertical excitations from non-bonding nitride and oxide p-orbitals to molecular orbitals that are predominantly metal d-orbital in character. It is worth noting that the non-bonding nitrogen and oxygen p-orbitals of the LUMO are oriented in such a way that occupation of this orbital, accompanied by a molecular vibration along the C_s symmetry plane, may lead to a bonding N-O interaction.

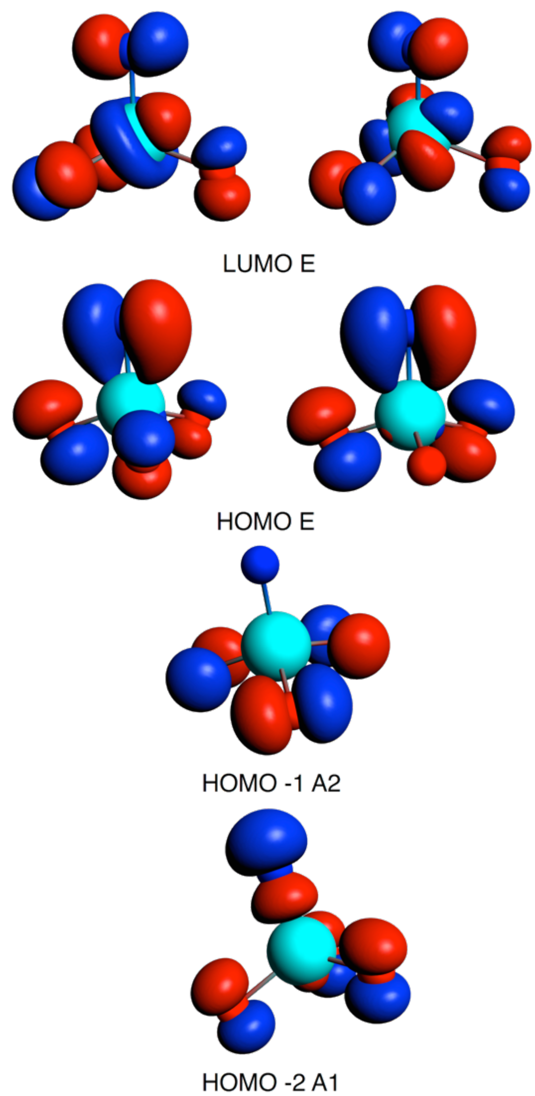

Figure 2.2: Selected Kohn-Sham orbitals of OsO_3N^- from non-relativistic QZ4P/B88P86 calculation.

In a triethyloctylammonium tetrafluoroborate matrix at 85 K, [(*n*-$C_4H_9)_4N$)][OsO_3N] exhibits three well resolved vibrational modes, an antisymmetric Os-O stretching mode at 872 cm^{-1}, a fully symmetric Os-O stretching mode at 889 cm^{-1}, and the Os-N stretch at 1014 cm^{-1} (982 cm^{-1} for the ^{15}N isotopomer) (Figure 1.3). Photolysis of the sample with 330 ± 50 nm irradiation results in bleaching of the parent vibrational bands and growth of two new strong Os-O vibrational modes at 880 cm^{-1} and 918 cm^{-1}, and an intense absorption at 1,620 cm^{-1} that shifts to 1584 cm^{-1} upon ^{15}N substitution (Figure 1.3a). Back photolysis of the 330 ± 50 nm irradiated sample with 400 ± 35 nm light results in reversion of the initial photoproduct to the parent compound (Figure 1.3b).

The most notable feature of the 330 ± 50 nm irradiation photoproducts is the ^{15}N sensitive absorption at 1620 cm^{-1}. This new band lies within the metal-nitrosyl stretching region and well beyond the typical metal-oxo or metal-nitrido stretching region, demonstrating the generation of new N-O bonds in the molecule following UV photolysis. The weaker absorption at 918 cm^{-1} shifts to 914 cm^{-1} upon ^{15}N substitution, indicating that the molecular vibration is weakly coupled to the N atom. The ratio of the intensity of these two bands is highly dependent upon the duration of photolysis, sample concentration, and the thickness of the matrix, suggesting that these vibrations belong to two different photoproducts. Back photolysis of these two products with 400 ± 35 nm light results in reversion to the parent complex at differing rates, demonstrating that the two photoproducts have overlapping electronic absorptions in this region.

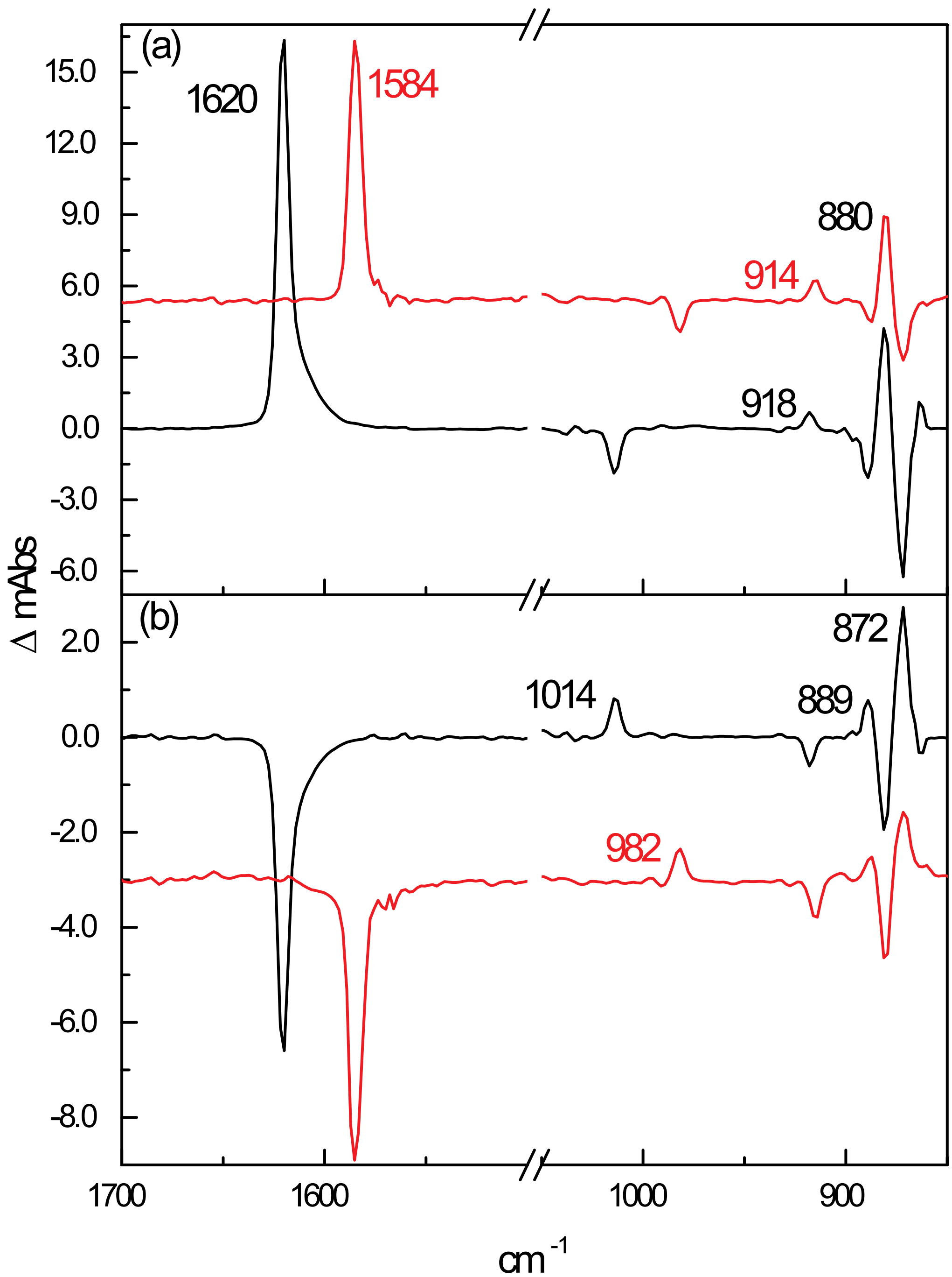

Figure 1.3: Photolysis of $[(n\text{-}C_4H_9)_4N)][OsO_3N]$ in $[Oct_3EtN][BF_4]$ matrix at 85 K. Top (a) Difference following 330 ± 50 nm irradiation from unphotolyzed sample. Bottom (b) Difference following 400 ± 35 nm backphotolysis of 330 ± 50 nm irradiated sample. Results of photolysis of $[(n\text{-}C_4H_9)_4N)][OsO_3{}^{15}N]$ presented as red trace.

While the new absorption at 1620 cm^{-1} is strongly indicative of the presence of a linear metal-nitrosyl photoproduct, the identity of the secondary photoproduct primarily characterized by an absorption at 918 cm^{-1} is less clear. One possibility is the formation of a bond between two oxide ligands which would give rise to a peroxo O-O vibrational mode that would absorb in this region, however, the lack of any new absorptions assignable to the Os-N stretching mode of such a molecule makes this assignment unlikely. A more probable candidate is a species intermediate to the parent complex and the putative nitrosyl complex, that is, a species with a partially reduced metal center and a weak N-O bond such as that of structure 1c (Scheme 1.3). To clarify the nature of the photoproducts observed in our matrix photolysis experiments, a DFT investigation was performed to identify any possible species possessing N-O and O-O bonds.

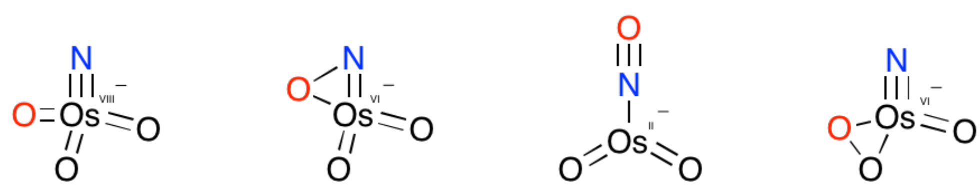

1a 1c 1e 1g

Scheme 1.3: Lowest energy DFT stationary point geometries considered.

DFT studies revealed a single stationary point with a NO group in an η^2 coordination mode, a species possessing C_s symmetry analogous to 1.1c calculated to lie 39.5 kcal mol^{-1} higher in energy than the parent complex. The elongated N-O bond length of 1.424 Å calculated for this species is consistent with a N-O single bond. Previous DFT and photocrystallography experiments have demonstrated that nitrosyl N-O bond lengths remain nearly constant upon undergoing linkage isomerism,[31] suggesting that this elongation is not due to the mode of NO coordination, but rather the NO remaining highly anionic and better being described as an η^2-nitroxyl group. This would correspond to the metal having undergone a formal two-electron reduction. Calculated vibrational modes for this species, Table 1.1, show the expected intensity of the N-O bond stretch to be much less than that of the Os-O stretching modes, offering an explanation as to why no ^{15}N sensitive N-O absorption is observed for this photoproduct. Compellingly, the fully symmetric Os-O stretching mode is weakly coupled to the N-O bond stretching mode and upon ^{15}N substitution is calculated to decrease in energy from 923 cm^{-1} to 919 cm^{-1}, consistent with the experimentally observed shift from 918 cm^{-1} to 914 cm^{-1}.

Only one stationary geometry was found that featured NO in an η^1 coordination mode, a C_{2v} symmetric complex with a linear nitrosyl group calculated to lie 27.6 kcal mol^{-1} higher in energy than the parent complex, 1.1e. This geometry gave calculated N-O and Os-O vibrational modes in excellent agreement with those observed in the matrix photolysis experiments. Formally, the Os metal center would be in the +2 oxidation state for this molecule, representing a net six-electron reduction from the parent complex. Additionally, a stationary geometry possessing a peroxo ligand, 1.1g, was found to lie 61.2 kcal mol^{-1} higher in energy than the parent complex.

Table 1.1: Calculated QZ4P SO-TPSS-D3(BJ) vibrational frequencies (cm^{-1}) and intensities ($km\ mol^{-1}$) in parentheses for selected species. Values in red are those calculated for ^{15}N substitution.

Compound	Os-N	N-O	Os-O
1a: OsO_3N^-	1039 (71.17)		892 (98.29)
	1007 (60.20)		881 (197.04)
			875 (198.78)
1c: $OsO_2(\eta^2\text{-NO})^-$	696 (11.41)	964 (40.79)	923 (231.11)
	684 (9.64)	949 (7.44)	919 (262.12)
			895 (241.60)
1e: $OsO_2(\eta^1\text{-NO})^-$	633 (38.69)	1615 (592.74)	892 (128.48)
	627 (36.07)	1577 (573.01)	873 (252.86)
		O-O	
1g: $OsON(\eta^2\text{-O}_2)^-$	1080 (82.80)	914 (58.66)	893 (212.24)
	1047 (73.11)		

To better understand the relationship between these stationary points, transition state geometries on the potential energy surface were located; the results of these calculations are presented in Scheme 1.4. In all cases, calculated vibrational modes of the transition states yielded a single large magnitude imaginary frequency and following the intrinsic reaction coordinate of these transition states yielded the expected stationary geometries. The barriers for the conversion of 1.1a to 1.1c and 1.1c to 1.1e are of very similar value at 60.4 kcal mol^{-1} and 61.5 kcal mol^{-1}, respectively. The barrier for the formation of 1.1g was calculated at 86.4 kcal mol^{-1}, significantly higher in energy than that required for the formation of the nitrosyl species.

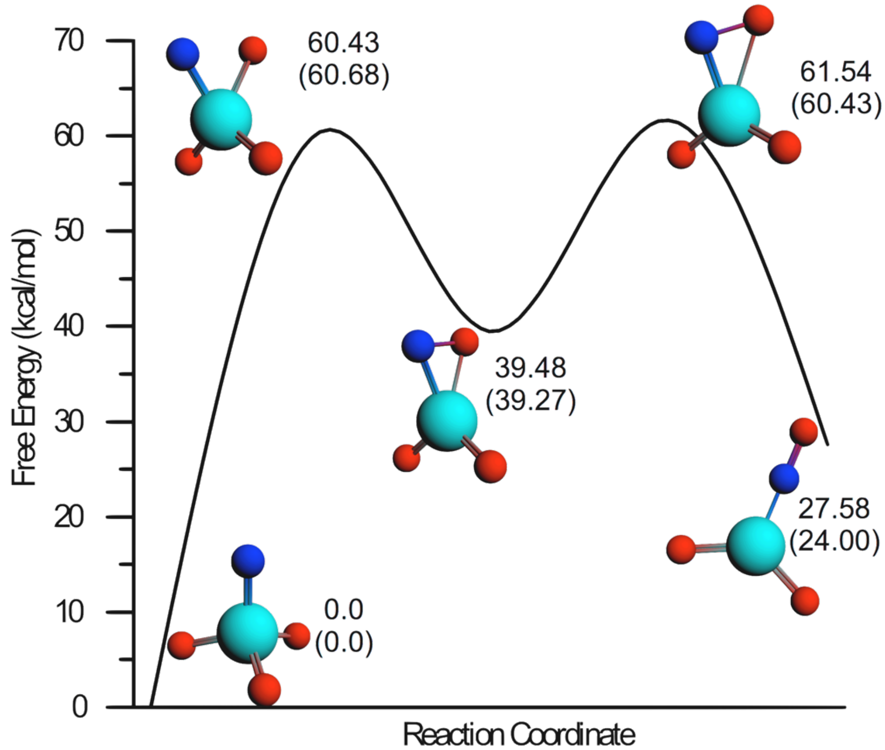

Scheme 1.4: SO-TPSS-D3(BJ) calculated reaction energy diagram for the observed photochemical transformation. Values in parentheses are from SR-B88P86 calculations.

On basis of the results of DFT calculations, we dismiss the possibility of UV-photolysis driven O-O bond formation to give an identifiable peroxo species in our low-temperature matrix photolysis experiments. The calculated barrier and stationary point energies for the peroxo complex are roughly 20 kcal mol^{-1} higher in energy than the corresponding N-O bond formation processes. Additionally, the absence of a new experimentally observable Os-N stretch in the photolysis products as well as the absence of any calculated ^{15}N coupled Os-O vibrational modes in the peroxo complex makes 1.1g inconsistent as one of the observed photoproducts.

We then identify the non-nitrosyl photoproduct generated during matrix photolysis as structure 1.1c. DFT calculations found this partially reduced Os(VI) species to connect the Os(VIII) parent complex, 1.1a, to the Os(II) nitrosyl complex, 1.1e, on the potential energy surface, making it a probable intermediate in the formation of the Os(II) nitrosyl complex. Furthermore, the small magnitude shift of the symmetric Os-O vibrational mode upon ^{15}N substitution for complex 1.1c is accurately reproduced by DFT. The identity of the species giving rise to the absorptions at 1620 cm^{-1} and 880 cm^{-1} is then assigned to complex 1.1e which is fully consistent with experimental spectroscopic data and DFT calculations.

The exact mechanism of this transformation remains unclear. As the matrix photolysis experiments are conducted under steady-state photolytic conditions, multi-step and multi-photon reactions are possible. In the present case, this would correspond to the absorption of a photon by the parent complex, 1.1a, to form complex 1.1c, which may then undergo secondary photolysis to form the nitrosyl complex 1.1e. This would necessitate electronic overlap of 1.1a and 1.1c in the 330 ± 50 nm region to proceed in this manner. Furthermore, back photolysis of 1.1c and 1.1e with 400 ± 35 nm light results in reversion of both species to the parent complex, 2.1a. Under these conditions, 1.1c reverts to the parent complex faster than 1.1e by comparison of the ratio of the two initially formed upon UV photolysis of the parent complex. This demonstrates electronic overlap of 1.1c and 1.1e assignable as MLCT in this region with reversion of 1.1c being the favored process. These data support a stepwise, two-photon process as opposed to a single-photon reaction that would be more likely to give only a single observable photoproduct.

In conclusion, a reversible photolytic six-electron reductive elimination and oxidative addition of nitric oxide by the nitridoosmate(VIII) anion has been demonstrated. To the best of our knowledge, this represents the first example of such a reaction. The results of this study offer a possible mechanism for the photochemical disproportionation of the nitrosyl ligand observed in previous studies. Moreover, this has broad implications for the development of catalytic small molecule activation that may be beneficial to the functionalization of abundant chemical feedstocks.

Experimental

[(*n*-$C_4H_9)_4N$)][OsO_3N] was prepared according to literature procedures.[30] [(*n*-$C_4H_9)_4N$)][$OsO_3{}^{15}N$] was prepared from 98% ^{15}N ammonium hydroxide supplied from Cambridge Isotope Laboratories. The apparatus and methods for matrix photochemistry have been reported elsewhere.[32] Briefly, 2-5 mg of [(*n*-$C_4H_9)_4N$)][OsO_3N] was thoroughly mixed with ~2 g [Oct_3EtN][BF_4] in a mortar and pestle. Approximately 50 mg of this waxy mixture was placed onto a 25 mm NaCl optical round and heated until the wax melted and uniformly spread across the window surface. The sample was allowed to slowly cool over the course of 60 minutes to obtain a clear, optically consistent film. The sample was then placed in a liquid N_2 cryostat (Graesby Specac GS21525), and placed under vacuum to obtain an ultimate pressure of 10^{-4} torr using a Kontes oil diffusion pump backed by an Edwards RV5 rotary vane pump. After achieving final vacuum, the sample was cooled with liquid N_2, obtaining an ultimate temperature of 85 K at the sample. A reference FTIR spectrum was taken (Perkin Elmer Spectrum 1000, 4 cm^{-1} resolution, 256 scans averaged), and the sample was photolyzed for 15 minutes in ~50 nm windows from 600 – 200 nm, collecting FTIR following each photolysis. The filtered output of a 350 W high-pressure Hg lamp was used (Newport Corporation) for all photolyses. This output was first filtered through a 5 cm pathlength quartz water jacket to absorb the infrared output of the lamp and avoid sample heating, then desired photolysis wavelengths were selected using combinations of optical bandpass and cutoff filters (Hoya, Corion, and Schott).

All DFT calculations were performed in the Amsterdam Density Functional (ADF2013.01) program.[33-35] Electronic configurations of atoms were described by an all-electron quadruple-ζ Slater-type orbital basis set modified by four polarization functions (QZ4P STO).[36] Geometry optimizations and vibrational frequency calculations were performed using the GGA functional of Becke[37] and Perdew[38,39] as well as the dispersion corrected meta-GGA TPSS-D3(BJ).[40-42] Computations carried out using the B88P86 functional utilized a scalar relativistic correction, whereas TPSS-D3(BJ) computations used spin-orbit relativistic corrections within the Zeroth Order Regular Approximation (ZORA).[43,44] Open-shell calculations were performed to identify any possible S=1 or S=2 geometries, in all cases these were strongly energetically disfavored. The intrinsic reaction coordinate (IRC) of all calculated transition state geometries was followed to confirm the relation with the expected stationary points. Electronic excitation energies were computed using SOC-B88P86 and the statistical average of orbital potentials (SAOP) model.[45,46]

References

(1) Tolman, W. B. *Angew. Chem. Int. Ed. Engl.* **2010**, *49* (6), 1018–1024.

(2) Cherry, J. P. F.; Johnson, A. R.; Baraldo, L. M.; Tsai, Y. C.; Cummins, C. C.; Kryatov, S. V.; Rybak Akimova, E. V.; Capps, K. B.; Hoff, C. D.; Haar, C. M.; Nolan, S. P. *J. Am. Chem. Soc.* **2001**, *123* (30), 7271–7286.

(3) Lentz, M. R.; Vilardo, J. S.; Lockwood, M. A.; Fanwick, P. E.; Rothwell, I. P. *Organometallics* **2004**, *23* (3), 329–343.

(4) Andrews, L.; Zhou, M. *J. Phys. Chem. A* **1999**, *103* (21), 4167–4173.

(5) Citra, A.; Andrews, L. *J. Am. Chem. Soc.* **1999**, *121* (49), 11567–11568.

(6) Zhou, M.; Citra, A.; Liang, B.; Andrews, L. *J. Phys. Chem. A* **2000**, *104* (16), 3457–3465.

(7) Zhou, M.; Andrews, L. *J. Phys. Chem. A* **2000**, *104* (17), 3915–3925.

(8) Wang, X.; Zhou, M.; Andrews, L. *J. Phys. Chem. A* **2000**, *104* (45), 10104–10111.

(9) Liang, B.; Andrews, L. *J. Phys. Chem. A* **2002**, *106* (4), 595–602.

(10) Poliakoff, M.; Smith, K. P.; Turner, J. J.; Wilkinson, A. J. *J. Chem. Soc., Dalton Trans.* **1982**, No. 3, 651.

(11) Crayston, J. A.; Almond, M. J.; Downs, A. J.; Poliakoff, M.; Turner, J. J. *Inorg. Chem.* **1984**, *23* (20), 3051–3056.

(12) Almond, M. J.; Crayston, J. A.; Downs, A. J.; Poliakoff, M.; Turner, J. J. *Inorg. Chem.* **1986**, *25* (1), 19–25.

(13) Almond, M. J.; Downs, A. J. *J. Chem. Soc., Dalton Trans.* **1988**, No. 4, 809.

(14) Hitam, R. B.; Rest, A. J.; Herberhold, M.; Kremnitz, W. *J. Chem. Soc., Chem. Commun.* **1984**, No. 7, 471.

(15) McPhail, A. T.; Knox, G. R.; Robertson, C. G.; Sim, G. A. *J. Chem. Soc., A* **1971**, 205.

(16) Legzdins, P.; Young, M. A. *Comments Inorg. Chem.* **1995**, *17* (4), 239–254.

(17) Legzdins, P.; Rettig, S. J.; Ross, K. J.; Batchelor, R. J.; Einstein, F. W. B. *Organometallics* **1995**, *14* (12), 5579–5587.

(18) Legzdins, P.; Rettig, S. J.; Ross, K. J.; Veltheer, J. E. *J. Am. Chem. Soc.* **1991**, *113* (11), 4361–4363.

(19) Pougnet, M. *J Pharm Chim* **1910**, *2*, 540.

(20) Mathews, J. H.; Dewey, L. H. *J. Phys. Chem.* **1913**, *17* (3), 211–218.

(21) Rideal, E. K.; Norrish, R. G. W. *Proc. R. Soc. A* **1923**, *103* (721), 342–366.

(22) Lee, D. G.; Moylan, C. R.; Hayashi, T.; Brauman, J. I. *J. Am. Chem. Soc.* **1987**, *109* (10), 3003–3010.

(23) Vogler, A.; Kunkely, H. *Inorg. Chem.* **1988**, *27* (3), 504–507.

(24) Maatta, E. A.; Wentworth, R. A. D. *Inorg. Chem.* **1979**, *18* (9), 2409–2413.

(25) Maatta, E. A.; Wentworth, R. A. D. *Inorg. Chem.* **1980**, *19* (9), 2597–2599.

(26) Bitterwolf, T. E.; Linehan, J. C.; Shade, J. E. *Organometallics* **2000**, *19* (23), 4915–4917.

(27) Watt, G. W.; Davies, D. D. *J. Am. Chem. Soc.* **1948**, *70* (6), 2041–2043.

(28) Clifford, A. F.; Olsen, R. R.; Kokalis, S. G.; Moeller, T. *Inorg. Syn.* **1960**, *6*, 167–169.

(29) Fritzsche, J.; Struve, H. *J. Prak. Chem.* **1847**, *41* (1), 97–113.

(30) Miskowski, V.; Gray, H. B.; Poon, C. K.; Ballhausen, C. J. *Molecular Physics* **1974**, *28* (3), 747–757.

(31) Coppens, P.; Novozhilova, I.; Kovalevsky, A. *Chem. Rev.* **2002**, *102* (4), 861–884.

(32) Bays, J. T.; Bitterwolf, T. E.; Lott, K. A.; Ollino, M. A.; Rest, A. J.; Smith, L. M. *J. Organomet. Chem.* **1998**, *554* (1), 75–85.

(33). ADF2013, SCM, Theoretical Chemistry, Vrije Universiteit, Amsterdam, The Netherlands, http://www.scm.com

(34) Guerra, C. F.; Snijders, J. G.; Velde, Te, G.; Baerends, E. J. *Theor.*

Chem. Acc. **1998**, *99*, 391–403.

(35) Velde, Te, G.; Bickelhaupt, F. M.; Baerends, E. J.; Fonseca Guerra, C.; van Gisbergen, S. J. A.; Snijders, J. G.; Ziegler, T. *J. Comp. Chem.* **2001**, *22* (9), 931–967.

(36) Lenthe, E. V.; Baerends, E. J. *J. Comp. Chem.* **2003**, *24* (9), 1142–1156.

(37) Becke, A. D. *Phys. Rev. A* **1988**, *38* (6), 3098–3100.

(38) Perdew, J. *Phys. Rev. B* **1986**, *33* (12), 8822–8824.

(39) Perdew, J. *Phys. Rev. B* **1986**, *34* (10), 7406–7406.

(40) Tao, J.; Perdew, J.; Staroverov, V.; Scuseria, G. *Phys. Rev. Lett.* **2003**, *91* (14), 146401.

(41) Grimme, S.; Antony, J.; Ehrlich, S.; Krieg, H. *J. Chem. Phys.* **2010**, *132* (15), 154104.

(42) Grimme, S.; Ehrlich, S.; Goerigk, L. *J. Comp. Chem.* **2011**, *32* (7), 1456–1465.

(43) Lenthe, E. V.; Baerends, E. J.; Snijders, J. G. *J. Chem. Phys.* **1993**, *99* (6), 4597.

(44) Lenthe, E. V.; Ehlers, A.; Baerends, E. J. *J. Chem. Phys.* **1999**, *110* (18), 8943.

(45) Gritsenko, O. V.; Schipper, P.; Baerends, E. J. *Chem Phys Lett* **1999**, *302*, 199–207.

(46) Schipper, P. R. T.; Gritsenko, O. V.; van Gisbergen, S. J. A.; Baerends, E. J. *J. Chem. Phys.* **2000**, *112* (3), 1344.

Chapter 2: Photochemistry of the Permanganate Ion in Low-Temperature Frozen Matrices.

Published: W. A. Thornley, T. E. Bitterwolf, Inorg. Chem. **2015**, *54*, 3370–3375.

ABSTRACT: *Photolysis of the permanganate anion, MnO_4^-, in tetralkylammonium tetrafluoroborate matrices at 85 K results in formation of the Mn(V) peroxo complex, $MnO_2(\eta^2\text{-}O_2)^-$. Previously postulated to be an intermediate in the photodecomposition of permanganate, results from variable temperature and intensity dependence solution photolysis experiments suggest that $MnO_2(\eta^2\text{-}O_2)^-$ does not lose O_2 thermally nor photochemically. A mechanism is proposed in which $MnO_2(\eta^2\text{-}O_2)^-$ is formed through vibrational relaxation of an excited $[MnO_4^-]^*$ species that may undergo relaxation through an alternative mechanism that results in formation of the MnO_2^- and O_2 photodecomposition products.*

The photodecomposition of permanganate was first described in 1910.[1] In this account, Pougnet reported that when in the presence of oxalic acid, photolysis of potassium permanganate solutions lead to reduction of permanganate and formation of potassium manganate. Shortly thereafter, Mathews and Dewey described the photodecomposition of potassium permanganate in the presence of sulfuric acid.[2] The first detailed studies of this photodecomposition were performed by Rideal and Norrish in 1923, who identified O_2 as a product of the reaction.[3,4]

Zimmerman later determined through ^{18}O labeling experiments that the O_2 evolved over the course of this reaction was generated intramolecularly and not through the reaction of a permanganate photoproduct and H_2O.[5] In this same work, it was also reported that there is a slight thermal dependence on the rate of photodecomposition when photolyzed with wavelengths longer than 436 nm and that the intensity of photolysis had no effect on the quantum yield of the reaction. Two overall decomposition routes were suggested, Scheme 2.1. The lack of appearance of O_2^- in subsequent EPR experiments ruled out reaction 2, leaving MnO_2^- and O_2 as the ultimate products.[6,7] Formally, this is a four-electron reductive elimination of O_2.

$$(1)\quad MnO_4^- \xrightarrow{h\nu} MnO_2^- + O_2$$

$$(2)\quad MnO_4^- \xrightarrow{h\nu} MnO_2 + O_2^-$$

Scheme 2.1: Proposed single-step photodecomposition products of permanganate.

Lee and coworkers later studied the photochemistry of permanganate in aqueous solution using oxidizable substrates as chemical traps.[8] In this elegant work, it was determined that a photochemical intermediate with a lifetime sufficiently long to undergo bimolecular reactions was generated. It was proposed that this intermediate could revert to permanganate, decompose to MnO_2^- and O_2, or react with an oxidizable substrate, Scheme 2.2. The identity of this intermediate was assigned to an unobserved Mn(V) peroxo complex, $MnO_2(\eta^2\text{-}O_2)^-$. A pair of computational studies performed by Nakai and coworkers on the formation of the putative peroxo complex demonstrated an energetically accessible pathway from permanganate to a C_{2v} symmetric $MnO_2(\eta^2\text{-}O_2)^-$ complex.[9,10] It was argued that the energy barrier associated with the change of symmetry from the T_d symmetric permanganate ion was responsible for the long lifetime of the photo-generated intermediate.

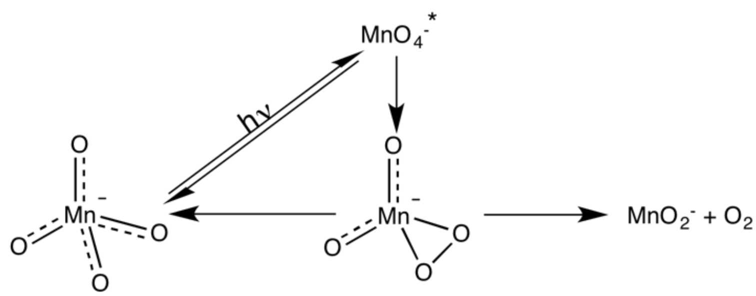

Scheme 2.2: Proposed mechanism for two-step photodecomposition of permanganate.

A subsequent computational study of this photodecomposition reaction by Gutsev and coworkers yielded two favored pathways, both occurring through a peroxo intermediate.[11] In the first proposed decomposition mechanism, photoexcitation of permanganate results in formation of the same peroxo intermediate suggested by Lee and Nakai. This intermediate then undergoes secondary excitation resulting in photoejection of an electron and formation of a neutral superoxo complex that may spontaneously lose O_2 to give MnO_2 and O_2 as products, Scheme 2.3. The second suggested mechanism begins with formation of the same peroxo intermediate followed by secondary excitation to a bis-peroxo complex, $Mn(\eta^2\text{-}O_2)_2^-$, which may undergo spontaneous O_2 loss to give MnO_2^-.

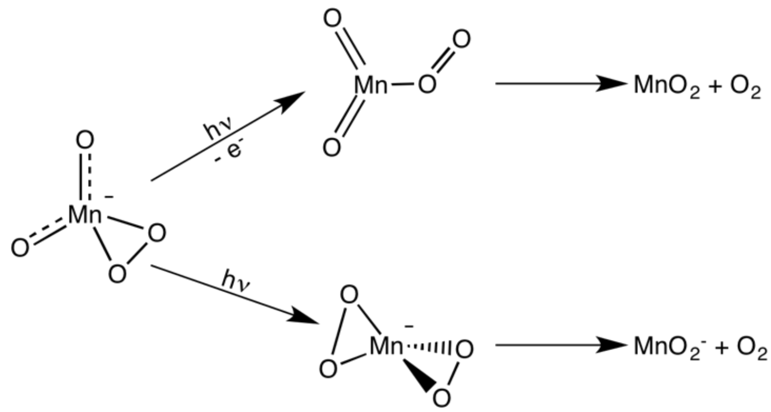

Scheme 2.3: Mechanisms of permanganate photodecomposition suggested by Gutsev *et al*.

Given the iconic stature of the permanganate ion in inorganic chemistry and ubiquitous presence in laboratories, we were surprised to find no reports of direct experimental characterization of the intermediate proposed by Lee and others. Time-resolved flash-photolysis studies of permanganate have reported no observable photoproducts,[12,13] and reported low-temperature steady-state photolyses in rigid-matrices have been characterized by EPR, allowing only paramagnetic products to be identified. As part of our group's ongoing study of photogenerated metastable species in low-temperature matrices by FTIR, we turned our attention towards the characterization of the intermediate(s) in the photochemical decomposition of permanganate.

Electronic Spectrum of the Permanganate Ion

The electronic spectrum of the permanganate ion has been the subject of numerous studies.[14-19] In aqueous solution, permanganate exhibits LMCT bands at 525, 344, 311, and 229 nm. When doped into $Ba(ClO_4)_2$ crystals at 4 K, the vibronic fine structure present in the 525 and 311 nm bands becomes well resolved and is dominated by Δv progressions of 762 and 757 cm^{-1}, respectively, corresponding to an approximately 16% reduction of the Mn-O stretching mode in the excited state. TD-DFT calculations on the electronic excitations of permanganate generally assign the 525 nm absorption as the HOMO→LUMO ($1t_1$→2e) transition, the 344 nm absorption as predominantly HOMO-1→LUMO ($6t_2$→2e), the 311 nm band as primarily HOMO→LUMO+1 ($1t_1$→$7t_2$), and the 229 absorption as HOMO-1→LUMO+1 ($6t_2$→$7t_2$), however, considerable mixing of these one-electron transitions is calculated to occur.[20-23] It is worth noting that the non-bonding oxygen p-orbitals of the 2e molecular orbital are oriented in such a way that occupation of this orbital, accompanied by a molecular vibration of e symmetry, may lead to an O-O bonding interaction that would result in the formation of a peroxo complex.

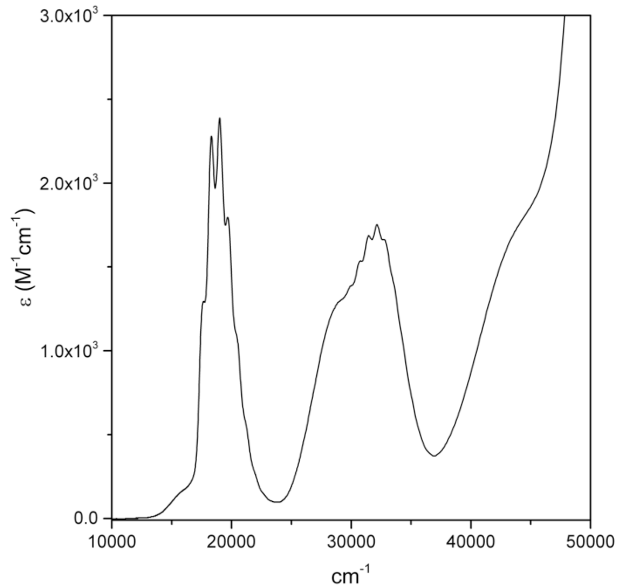

Figure 2.1: Electronic spectrum of $KMnO_4$ in H_2O.

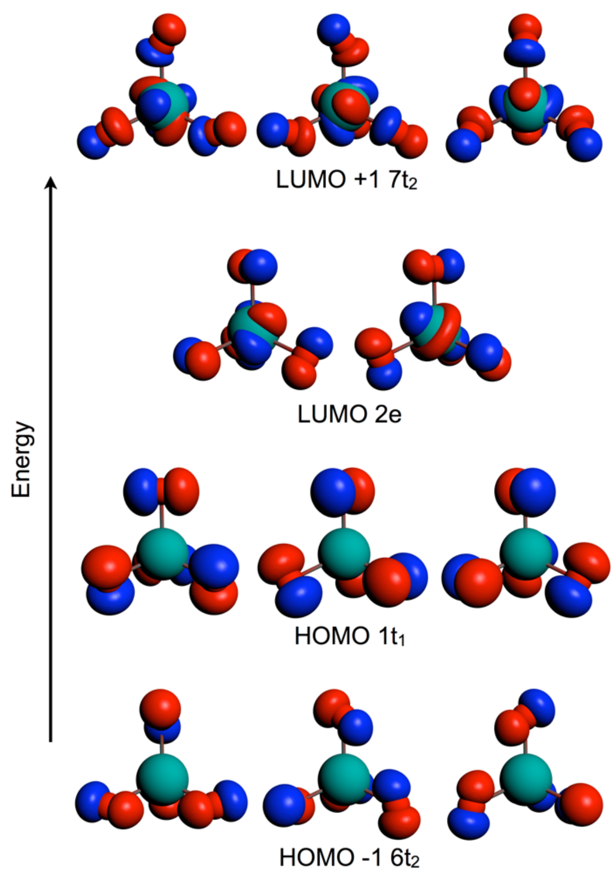

Figure 2.2: Selected molecular orbitals of MnO_4^-.

Photolysis of Permanganate in $[Et_3OctN][BF_4]$ at 85K

Photolysis of $[Et_3OctN][MnO_4]$ in a $[Et_3OctN][BF_4]$ matrix at 85 K into any of the 344, 311, or 229 nm absorptions results in bleaching of the parent vibrational band at 905 cm^{-1}, and growth of a single product with absorptions at 870, 929, and 965 cm^{-1}, Figure 2.3a. Broadband back-photolysis of the photoproduct with λ_{irr} > 400 nm results in complete reversion of the photoproduct to the parent permanganate complex, Figure 2.3b. Extended photolysis into the 525 nm transition results in formation of no observable photoproducts.

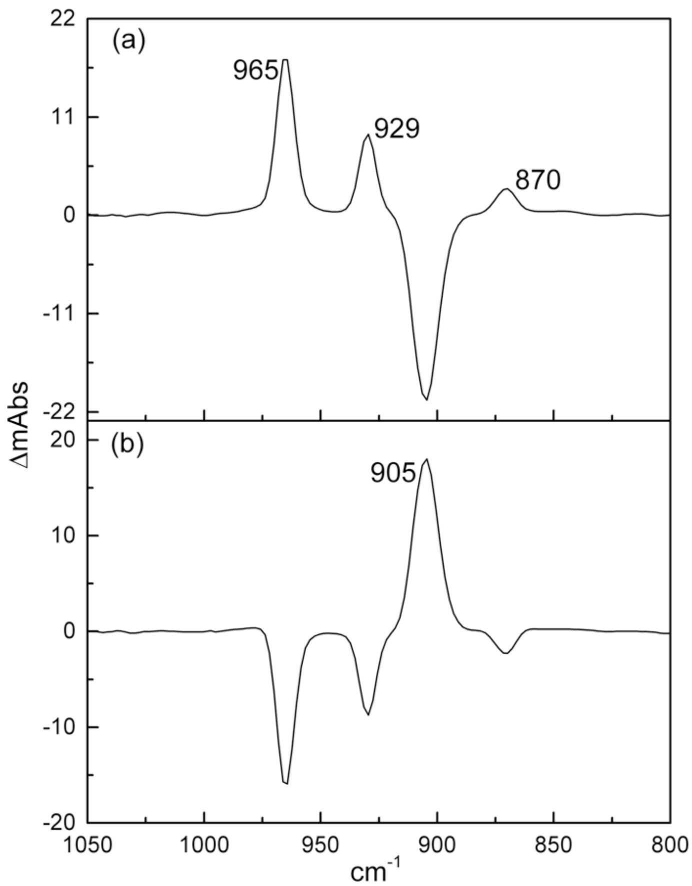

Figure 2.3: Photolysis of $[Et_3OctN][MnO_4]$ in $[Et_3OctN][BF_4]$ at 85 K. (a) 330 ± 50 nm irradiated sample minus unphotolyzed sample. (b) Difference following λ_{irr} > 400 nm back photolysis of 330 ± 50 nm irradiated sample.

The infrared spectrum of the observed photoproduct is not consistent with the formation of MnO_2^-, that would be expected to exhibit only two vibrational modes in the metal-oxo stretching region. The observed spectrum is, however, consistent with O-O bond formation to give the proposed C_{2v} peroxo complex, $MnO_2(\eta^2\text{-}O_2)^-$. This species would be expected to exhibit an antisymmetric and symmetric Mn-O vibrational absorption, assigned as the 965 and 929 cm^{-1} absorptions, respectively, as well as a peroxo vibrational mode in the 818-932 cm^{-1} region,[24] observed at 870 cm^{-1}. No new features in the superoxo vibrational region of 1100-1200 cm^{-1} are observed.

The lack of any new absorptions assignable to MnO_2^-,[25] as well as complete reversion to the parent permanganate complex upon $\lambda_{irr} > 400$ nm back photolysis, indicates that no O_2 loss is occurring under these conditions. This behavior may be suggestive of the peroxo complex formation being photochemical, with O_2 loss from this species occurring thermally. An alternative explanation may be that O_2 loss from $MnO_2(\eta^2\text{-}O_2)^-$ occurs following secondary excitation, but that the barrier for O_2 recapture by MnO_2^- is sufficiently low that this reaction occurs rapidly at 85 K. The reported independence of quantum yield with respect to photolysis intensity, however, makes such a multi-photon mechanism unlikely.

Variable Temperature Solution Photolyses

In order to differentiate between possible photochemical and thermal decomposition pathways, we sought to reproduce the temperature and intensity dependence experiments performed by Zimmerman. Solution studies were conducted under similar conditions as those used by Lee and coworkers, using an excess of sodium pyrophosphate in solution to coordinate the generated MnO_2^- and prevent deposition of a manganese oxide film on the walls of the photolysis vessel. Variable temperature photolysis experiments conducted with λ_{irr} > 590, 550 ± 50, 532, 525 ± 50, 450 ± 50, > 410, 400 ± 50, and 330 ± 75 nm from 5-75°C exhibited no appreciable thermal dependence on the rate of photodecomposition. The initial variable temperature experiments performed by Zimmerman utilized trypaflavine phosphorescence quenching to monitor O_2 evolution from permanganate. This technique would be expected to provide a lower limit of detection than simple monitoring of UV-Vis as used in our experiments, however, even a modest thermal dependence would be anticipated to be measureable over a 70°C temperature window. Also conflicting with the work of Zimmerman, we saw no evidence of rate enhancement for the decomposition reaction when using photolysis wavelengths longer than 410 nm. These data suggest that there is no thermally dependent step in the photochemical decomposition reaction.

Table 2.1: Computed QZ4P TPSS-D3(BJ) energies and vibrational modes of selected species.

	MnO_4^-	$MnO_2(\eta^2$-$O_2)^-$	$MnO_2(\eta^2$-$O_2)^-$ S=1	$MnO_2(\eta^1$-$O_2)^-$	$MnO_2(\eta^1$-$O_2)^-$S=1	MnO_2^-	MnO_2^- S=1
ΔG	0	41.9	48.8	71.1	70.9	138.5	95.7
ΔH	0	45.6	51.8	73.4	75.3	151.7	128.2
Mn-O	949 (207)	987 (311) 957 (183)	944 (176) 912 (334)	993 (287) 935 (173)	920 (296) 889 (284)	1148 (1635) 980 (272)	973 (343) 891 (66)
Mn-O_2		927 (44)	893 (7)	1152 (165)	1076 (231)		

All energies are given in kcal mol^{-1}. Vibrational frequencies are given in cm^{-1}, values in parentheses are absorption intensities (km mol^{-1}). Energy values for MnO_2^- include corrections for loss of $^3\Sigma_g^-$ O_2.

Intensity Dependence Studies

The quantum yield of the photodecomposition reaction was measured as 5.5 x 10^{-3} ± 2 x 10^{-4} with λ_{irr} = 325 ± 10 nm. This value compares favorably to the value determined by Zimmerman of 4.8 x 10^{-3} ± 2 x 10^{-4} with λ_{irr} = 313 nm. Varying the intensity of the λ_{irr} = 325 ± 10 nm photolysis of samples held at a constant 25°C gave no appreciable deviation in measured quantum yield. Plotting the rate of permanganate decomposition vs. photolysis intensity, Figure 2.5, exhibits a linear relationship with a slope of 1.04 ± 0.06, indicating that the photodecomposition is a single photon reaction.

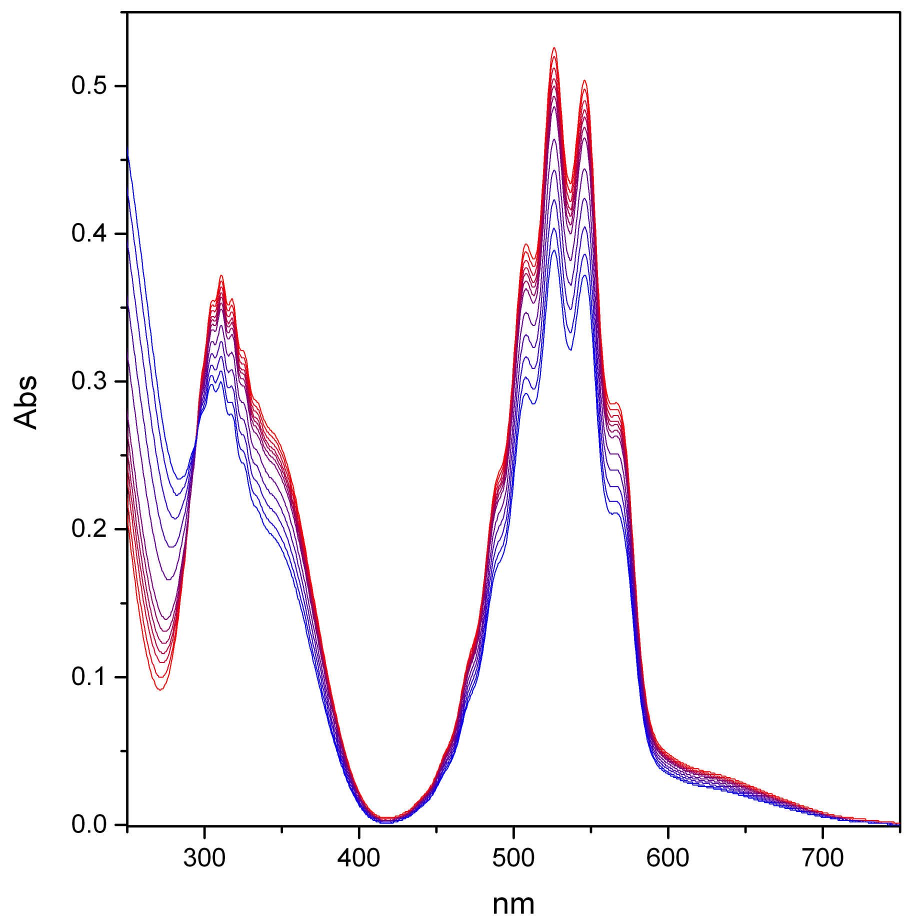

Figure 2.4: Typical spectral changes observed during variable-temperature solution photolyses.[$KMnO_4$] = 2.25 x 10^{-4} M, [$HClO_4$] = 0.115 M, [$Na_4P_2O_7$] = 4.78 x 10^{-3} M.

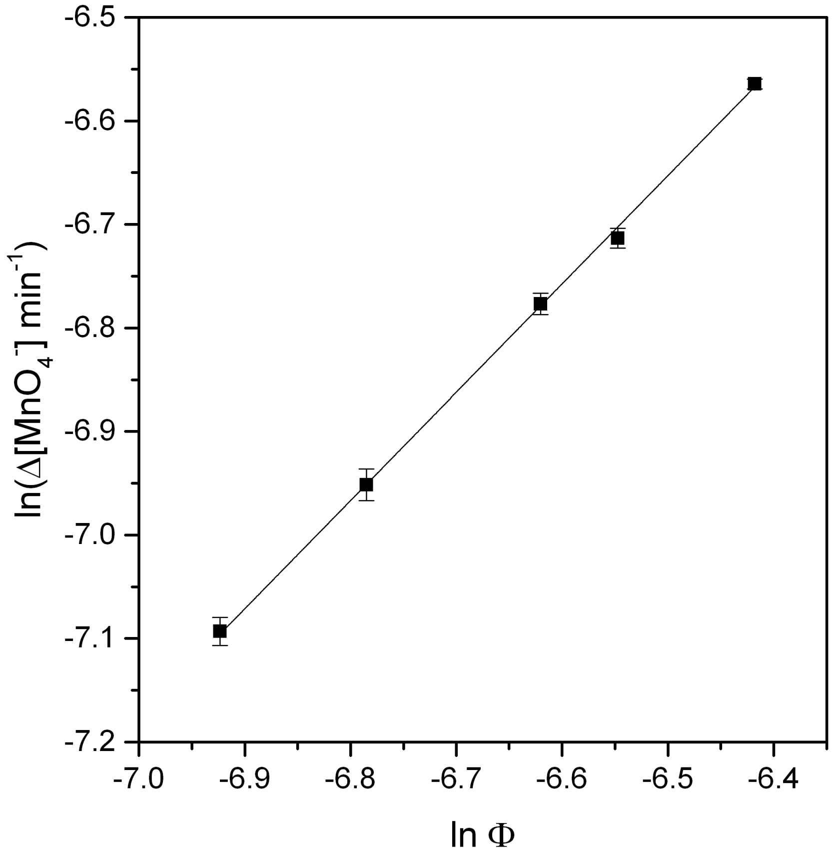

Figure 2.5: Rate of O_2 loss from permanganate solution vs. 325 ± 10 nm photolysis intensity (einsteins min^{-1}). Slope of best-fit line = 1.04 ± 0.06. [$KMnO_4$] = 2.25 x 10^{-4} M, [$HClO_4$] = 0.115 M, [$Na_4P_2O_7$] = 4.78 x 10^{-3} M.

The absence of any thermal or photolysis intensity dependence on the photodecomposition reaction implies that O_2 loss occurs via single photon reaction. These observations are perplexing when compared to the results of the low-temperature matrix photolysis where no evidence for O_2 loss is found. These seemingly contradictory observations may be rationalized if the $MnO_2(\eta^2\text{-}O_2)^-$ product observed in the matrix is not an intermediate in the photodecomposition reaction, but rather the product of relaxation of an excited-state, vibrationally-hot,

$[MnO_2(\eta^2\text{-}O_2)^-]^*$ species that may also undergo an O_2 loss relaxation pathway, Scheme 2.4.

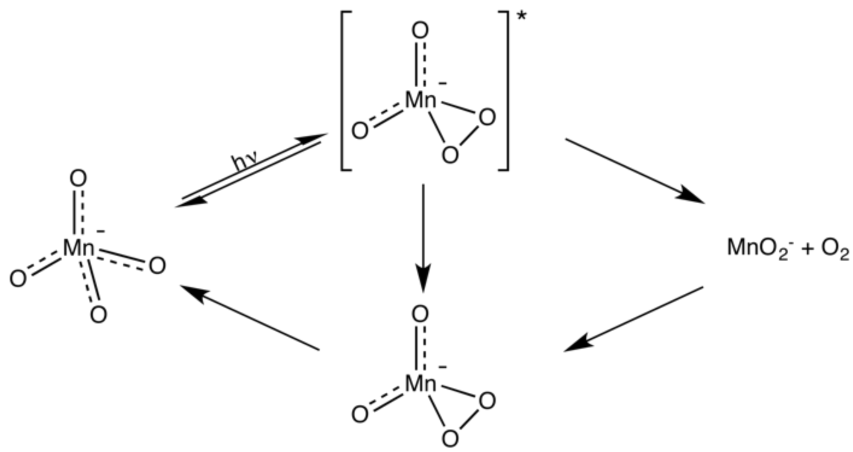

Scheme 2.4: Proposed permanganate decomposition mechanism

In the excited state, loss of O_2 from $[MnO_2(\eta^2\text{-}O_2)^-]^*$ may be effectively barrierless, being enthalpically disfavored but entropically favored. This may explain the lack of any thermal dependence on the reaction. Under rigid-matrix conditions at 85 K where any generated O_2 and MnO_2^- would be held in close proximity, rapid recapture of O_2 would be expected, explaining why no decomposition product is observed. Photolysis at $He_{(l)}$ temperatures may allow for the decomposition products to be characterized under matrix conditions. In solution, the $[MnO_2(\eta^2\text{-}O_2)^-]^*$ species may revert to the parent permanganate complex, relax to a vibrationally cool $MnO_2(\eta^2\text{-}O_2)^-$ species, or lose O_2 to give MnO_2^-. Solvent cage effects may also facilitate rapid recombination of MnO_2^- and O_2 to give a vibrationally cool $MnO_2(\eta^2\text{-}O_2)^-$ that may then revert to the parent permanganate complex or oxidize a substrate in solution. Zimmerman noted that the quantum yield of the photodecomposition reaction increases dramatically with higher energy photolysis, suggesting that high energy photons may impart more vibrational energy to the $[MnO_2(\eta^2\text{-}O_2)^-]^*$ species and favor the O_2 loss relaxation pathway.

Photoluminescence Studies

The exact nature of the O_2 evolved during the photodecomposition is unknown. Lee noted that there was no evidence for the involvement of singlet oxygen in their kinetics experiments,[8] however, generation of singlet oxygen by transition metal peroxo compounds is well known.[26,27] To clarify the nature of the generated O_2, a sample of $[Et_3OctN][MnO_4]$ in CH_3CN solution was monitored for singlet oxygen phosphorescence when subjected to 310 nm excitation.[28] No emission could be detected under these conditions, suggesting that the O_2 generated is being released in the $^3\Sigma_g^-$ ground state.

DFT Studies

To probe the mechanism and thermodynamics associated with the observed photochemical reaction in greater detail, a DFT investigation of the formation of $MnO_2(\eta^2\text{-}O_2)^-$ was performed. Following the O-Mn-O bending mode of permanganate, Figure 2.6, results in a peroxo complex stationary point possessing C_{2v} symmetry consistent with previous computational studies.[9-11] This species is calculated to lie 41.9 kcal mol^{-1} higher in energy than the parent permanganate complex. The transition state for the formation of this complex is placed 60.6 kcal mol^{-1} above the parent complex. Jahn-Teller distortion along the O-Mn-O bending mode results in Mn-O bond elongation, such that the O-O bond formation occurs in the C_s symmetry plane rather than through retention of C_{2v} symmetry. The results of these calculations are summarized in Table 2.1. The calculated vibrational frequencies of $MnO_2(\eta^2\text{-}O_2)^-$ reproduce the trends observed in the frozen-matrix photolysis studies lending support to the proposed structure of the photoproduct.

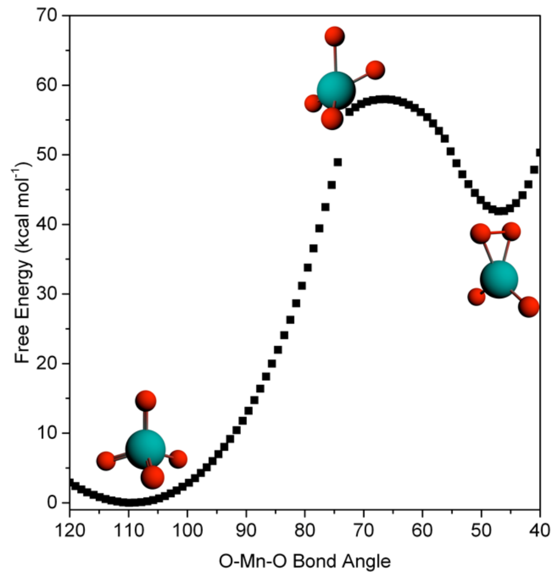

Figure 2.6: Calculated PES along the O-Mn-O bending mode.

The HOMO of $MnO_2(\eta^2\text{-}O_2)^-$ is predominantly O-O bonding and non-bonding metal dz^2 in nature, Figure 2.7. The enhanced oxidative reactivity of this complex may be rationalized by the sterically unimpeded access to the dz^2 orbital in this geometry. The observed reversion of the peroxo complex to MnO_4^- upon $\lambda_{irr} > 400$ nm back photolysis implies that MLCT must take place in this region of the spectrum.

SAOP excitation energies for $MnO_2(\eta^2\text{-}O_2)^-$ show a number of transitions lower in energy relative to those of the parent permanganate complex, Table 2.2 and Figure 2.8. The lowest energy excitation of $MnO_2(\eta^2\text{-}O_2)^-$ is calculated to be an intense 2a2→3a2 transition that can be described as charge transfer from the peroxo ligand to the manganese center. If the loss of O_2 observed in solution did occur photochemically, this transition would provide a plausible trigger for O_2 loss and concurrent two-electron reduction of Mn(V) $MnO_2(\eta^2\text{-}O_2)^-$ to Mn(III) MnO_2^-. The second and third lowest energy transitions, by contrast, are from the 14a1 orbital to the 7b1 and 15a1 molecular orbitals and are MLCT in character. MLCT to the peroxo ligand would be responsible for the reduction of the peroxo ligand to yield the parent permanganate complex.

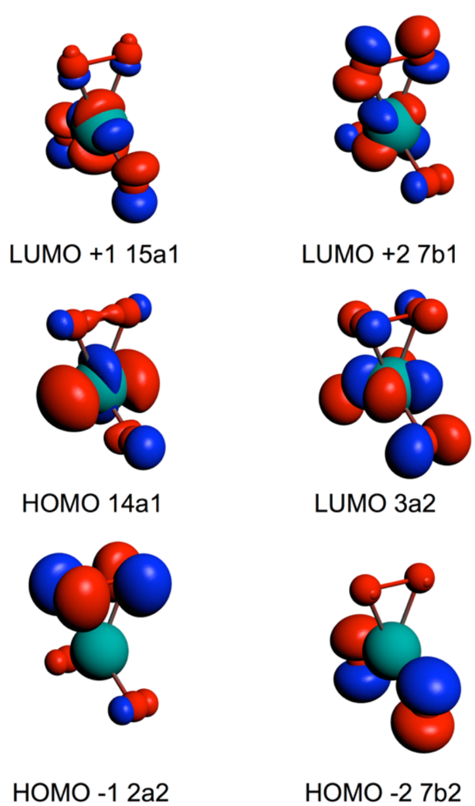

Figure 2.7: Selected molecular orbitals of $MnO_2(\eta^2\text{-}O_2)^-$.

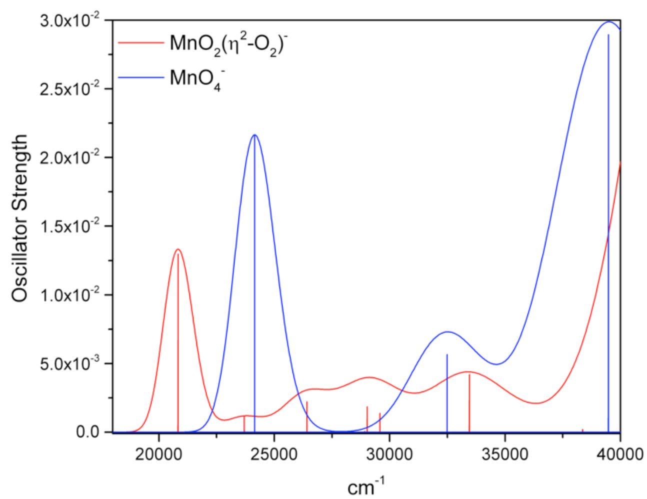

Figure 2.8: SAOP calculated absorption spectra of MnO_4^- (blue) and $MnO_2(\eta^2\text{-}O_2)^-$ (red).

Table 2.2: SAOP calculated excitation energies.

MnO_4^-		$MnO_2(\eta^2\text{-}O_2)^-$	
Transition	Energy	Transition	Energy
1t1→2e	414 nm	2a2→3a2	480 nm
6t2→2e (68%) 1t1→2e (30%)	308 nm	14a1→7b1	422 nm
1t1→7t2 (57%) 6t2→7t2 (18%) 6t2→7t2 (17%)	253 nm	14a1→15a1	379 nm
6t2→7t2 (49%) 6a1→7t2 (45%)	209 nm	2a2→8b2 (67%) 7b2→3a2 (32%)	346 nm

Conclusions

The metastable Mn(V) peroxo complex, $MnO_2(\eta^2\text{-}O_2)^-$, has been observed as a product in the photolysis of the permanganate anion. Formally the product of photochemical reductive elimination of a peroxo ligand, this is the first experimental characterization of the long-lived photoproduct speculated in previous experimental[8] and computational[9-11] studies. The absence of any species assignable as MnO_2^- in our 85 K photolysis experiments, the determination of a single photon requirement for decomposition, lack of any measureable temperature dependence, and increasing quantum yield with higher energy photolysis is highly suggestive of O_2 loss occurring through a vibrationally hot, excited state $[MnO_2(\eta^2\text{-}O_2)^-]^*$ species as opposed to O_2 loss from the observed $MnO_2(\eta^2\text{-}O_2)^-$ photoproduct.

Experimental

$[Et_3OctN][MnO_4]$ was prepared by adding an excess of $[Et_3OctN][BF_4]$ to an aqueous potassium permanganate solution. After twenty minutes of vigorous mixing at room temperature, the solution was extracted with a minimal volume cold methylene chloride. The extracts were dried over $MgSO_4$ and solvent removed on a rotary evaporator. $KMn^{18}O_4$ was prepared by the literature procedure.[29-31] 98% enriched $H_2{}^{18}O$ was supplied by Medical Isotopes, Inc. The apparatus and methods for matrix photochemistry have been reported elsewhere.[32] Variable temperature photolysis experiments were performed in a water-jacketed pyrex flask with temperatures being held to within ±0.2 K by a circulating bath. Aliquots of the photolyzed solution were periodically removed and equilibrated to 25°C prior to measuring the UV-Vis spectrum, referencing against a dark sample kept at the same temperature to account for thermal decomposition. Photon fluxes were determined by ferrioxalate actinometry. Photoluminescence spectra were measured with a Horiba Jobin-Yvon Nanolog equipped with an LN_2 cooled InGaAs detector.

All DFT calculations were performed in the Amsterdam Density Functional (ADF2013.01) program.[33-35] Electronic configurations of atoms were described by an all-electron quadruple-ζ Slater-type orbital basis set modified by four polarization functions (QZ4P STO).[36] Geometry optimizations and vibrational frequency calculations were performed using the dispersion corrected meta-GGA TPSS-D3(BJ).[37-39] Vertical electronic excitation energies were computed the statistical average of orbital potentials (SAOP) model.[40,41]

REFERENCES

(1) Pougnet, M. *J. Pharm. Chim.* **1910**, *2*, 540.

(2) Mathews, J. H.; Dewey, L. H. *J. Phys. Chem.* **1913**, *17*, 211.

(3) Rideal, E. K.; Norrish, R. G. W. *Proc. R. Soc. A* **1923**, *103*, 342.

(4) Rideal, E. K.; Norrish, R. G. W. *Proc. R. Soc. A* **1923**, *103*, 366.

(5) Zimmerman, G. *J. Chem. Phys.* **1955**, *23*, 825.

(6) Kläning, U.; Symons, M. C. R. *J. Chem. Soc.* **1959**, 3269.

(7) Yu, J.-T. *J. Phys. Chem.* **1992**, *96*, 5746.

(8) Lee, D. G.; Moylan, C. R.; Hayashi, T.; Brauman, J. I. *J. Am. Chem. Soc.* **1987**, *109*, 3003.

(9) Nakai, H.; Nakatsuji, H. *J. Mol. Struct. THEOCHEM* **1994**, *311*, 141.

(10) Nakai, H.; Ohmori, Y.; Nakatsuji, H. *J. Phys. Chem.* **1995**, *99*, 8550.

(11) Gutsev, G. L.; Rao, B. K.; Jena, P. *J. Phys. Chem. A* **1999**, *103*, 10819.

(12) Coremans, C.; Van der Waals, J. H.; Konijnenberg, J.; Huizer, A. H.; Varma, C. A. G. O. *Chem. Phys. Lett.* **1986**, *125*, 514.

(13) Kirk, A. D.; Hoggard, P. E.; Porter, G. B.; Rockley, M. G. *Chem. Phys. Lett.* **1976**, *37*, 199.

(14) Miskowski, V.; Gray, H. B.; Poon, C. K.; Ballhausen, C. J. *Mol. Phys.* **1974**, *28*, 747.

(15) Viste, A.; Gray, H. B. *Inorg. Chem.* **1964**, *3*, 1113.

(16) Johnson, L. W.; McGlynn, S. P. *Chem. Phys. Lett.* **1971**, *10*, 595.

(17) Collingwood, J. C.; Day, P.; Denning, R. G.; Robbins, D. J. *Chem. Phys. Lett.* **1972**, *13*, 567.

(18) Jaeger, Z.; Englman, R. *Chem. Phys. Lett.* **1973**, *19*, 242.

(19) Cox, P. A.; Robbins, D. J.; Day, P. *Mol. Phys.* **1975**, *30*, 405.

(20) van Gisbergen, S. J. A.; Groeneveld, J. A.; Rosa, A.; Snijders, J. G.; Baerends, E. J. *J. Phys. Chem. A* **1999**, *103*, 6835.

(21) Boulet, P.; Chermette, H.; Daul, C.; Gilardoni, F.; Rogemond, F.; Weber, J.; Zuber, G. *J. Phys. Chem. A* **2001**, *105*, 885.

(22) Neugebauer, J.; Baerends, E. J.; Nooijen, M. *J. Phys. Chem. A* **2005**, *109*, 1168.

(23) Jose, L.; Seth, M.; Ziegler, T. *J. Phys. Chem. A* **2012**, *116*, 1864.

(24) Vaska, L. *Acc. Chem. Res.* **1976**, *9*, 175.

(25) Dong, J.; Wang, Y.; Zhou, M. *Chem. Phys. Lett.* **2002**, *364*, 511.

(26) Vogler, A.; Kunkely, H. *Coord. Chem. Rev.* **2006**, *250*, 1622.

(27) Vogler, A.; Kunkely, H. *J. Am. Chem. Soc.* **1981**, *103*, 6222.

(28) Bromberg, A.; Foote, C. S. *J. Phys. Chem.* **1989**, *93*, 3968.

(29) Hall, N. F.; Alexander, O. R. *J. Am. Chem. Soc.* **1940**, *62*, 3455.

(30) Mills, G. A. *J. Am. Chem. Soc.* **1940**, *62*, 2833.

(31) Heckner, K. H.; Landsberg, R. *J. Inorg. Nucl. Chem.* **1967**, *29*, 413.

(32) Bays, J. T.; Bitterwolf, T. E.; Lott, K. A.; Ollino, M. A.; Rest, A. J.; Smith, L. M. *J. Organomet. Chem.* **1998**, *554*, 75.

(33) ADF2013, SCM, Theoretical Chemistry, Vrije Universiteit, Amsterdam, The Netherlands, http://www.scm.com.

(34) Guerra, C. F.; Snijders, J. G.; Velde, Te, G.; Baerends, E. J. *Theor. Chem. Acc.* **1998**, *99*, 391.

(35) Velde, Te, G.; Bickelhaupt, F. M.; Baerends, E. J.; Fonseca Guerra, C.; van Gisbergen, S. J. A.; Snijders, J. G.; Ziegler, T. *J. Comp. Chem.* **2001**, *22*, 931.

(36) Lenthe, E. V.; Baerends, E. J. *J. Comp. Chem.* **2003**, *24*, 1142.

(37) Tao, J.; Perdew, J.; Staroverov, V.; Scuseria, G. *Phys. Rev. Lett.* **2003**, *91*, 146401.

(38) Grimme, S.; Antony, J.; Ehrlich, S.; Krieg, H. *J. Chem. Phys.* **2010**, *132*, 154104.

(39) Grimme, S.; Ehrlich, S.; Goerigk, L. *J. Comp. Chem.* **2011**, *32*, 1456.

(40) Gritsenko, O. V.; Schipper, P.; Baerends, E. J. *Chem. Phys. Lett.* **1999**, *302*, 199.

(41) Schipper, P. R. T.; Gritsenko, O. V.; van Gisbergen, S. J. A.; Baerends, E. J. *J. Chem. Phys.* **2000**, *112*, 1344.

Chapter 3: Revisiting the Photochemistry of Vaska's O_2 Complex: Competitive Reductive and Non-Reductive Elimination Reactions.

Submitted for review and publication: W.A. Thornley, T.E. Bitterwolf *Angew. Chem. Int. Ed. Engl.* ***2016.***

***Abstract**: Low-temperature frozen matrix and solution photochemistry experiments on the dioxygen adduct of Vaska's complex, $Ir^{III}Cl(CO)O_2[P(C_6H_5)_3]_2$, reveal that a competitive non-reductive elimination of CO_2 to yield $Ir^{III}Cl(O)[P(C_6H_5)_3]_2$ competes with the long-known photochemical reductive elimination of O_2 yielding $Ir^{I}Cl(CO)[P(C_6H_5)_3]_2$. Photochemical experiments conducted in solution at room temperature also yield $OPPh_3$, arising from a secondary reaction of the CO_2 loss iridium species. DFT computations suggest that elimination of CO_2 from Vaska's O_2 complex is a thermodynamically favored photothermal side reaction, while O_2 ejection is favored through a purely photochemical reaction pathway.*

Vaska's complex is an iconic molecule in organometallic chemistry, having shaped the understanding of oxidative addition and reductive elimination reactions fundamental to homogeneous catalysis through its ability to reversibly add substrates to form stable 18-electron Ir^{III} complexes, Scheme 3.1.[1-9] One of these reactions, the addition of oxygen to Vaska's complex to yield $IrCl(CO)O_2[P(C_6H_5)_3]_2$, is particularly noteworthy as this dioxygen adduct served as an early model for molecular oxygen transport.[10-19] The reverse of this reaction, elimination of oxygen to yield 16-electron $IrCl(CO)[P(C_6H_5)_3]_2$ and O_2, is known to occur both thermally and photochemically, with the photochemical elimination reportedly being robust and able to be cycled without decomposition.[20] Following 308 nm photolysis of Vaska's O_2 adduct, the eliminated oxygen is produced in both the $^1\Delta_g$ and $^3\Sigma_g^-$ electronic states with quantum yields of 0.03 and 0.40, respectively, indicating that reductive elimination occurs directly through an electronically excited singlet state, as well as the result of an intersystem crossing (ISC).[21]

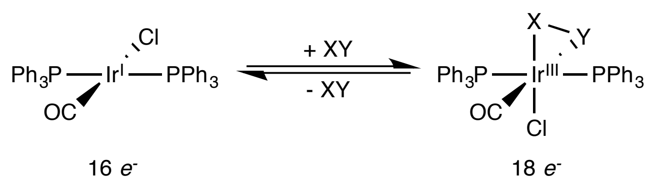

Scheme 3.1: Generalized oxidative addition and reductive elimination reactions of Vaska's complex. XY = H_2, SO_2, HCl, O_2, BF_3, halogens, etc…

Recent work in our laboratory has centered upon the photochemistry of transition metal oxides and nitrides in low-temperature frozen matrices where we've reported instances of reversible four and six-electron reductive elimination and oxidative addition reactions.[22,23] We decided to direct our attention towards this archetypal photochemical oxygen elimination from Vaska's complex in hopes that an intermediate prior to O_2 ejection (i.e. metal superoxide or η^1-O_2) or a metastable geometrical isomer of $IrCl(CO)[P(C_6H_5)_3]_2$ following O_2 ejection would be directly observed at cryogenic temperatures, further developing upon the mechanistic model for this class of reactions. The results of these experiments did not yield any evidence for non-concerted O_2 reductive elimination from this molecule, but did result in the surprising observation of photochemical elimination of CO_2.

In poly(vinyl chloride) (PVC) matrices at 85 K, photolysis at wavelengths beginning with 500 ± 50 nm result in bleaching of the parent $IrCl(CO)O_2[P(C_6H_5)_3]_2$ carbonyl (2014 cm^{-1}), triphenylphosphine (1484, 1436, and 1104 cm^{-1}), and peroxo (855 cm^{-1}) vibrational modes with concomitant growth of photoproduct absorptions at 1958, 1478, 1431, and 1096 cm^{-1}, corresponding to the O_2 elimination product, $Ir^{I}Cl(CO)[P(C_6H_5)_3]_2$, and a strong absorption at 2335 cm^{-1} belonging to matrix-trapped CO_2. Isotopic substitution with ^{13}CO results in expected infrared shifts of the product $Ir^{I}Cl(^{13}CO)[P(C_6H_5)_3]_2$ carbonyl and eliminated $^{13}CO_2$ absorption bands to 1911 cm^{-1} and 2269 cm^{-1}, respectively, while positions of features arising from changes to the peroxo and triphenylphosphine ligands remain identical to the natural abundance CO experiment. Photolysis at shorter wavelengths (450 ± 50 nm, 400 ± 50 nm, and 330 ± 70 nm) increases the extent of this reaction, but does not result in any changes to the observed photoproducts. Increasing the duration of photolysis was found to increase the intensity of the CO_2 product absorption band relative to the $IrCl(CO)[P(C_6H_5)_3]_2$ product absorption.

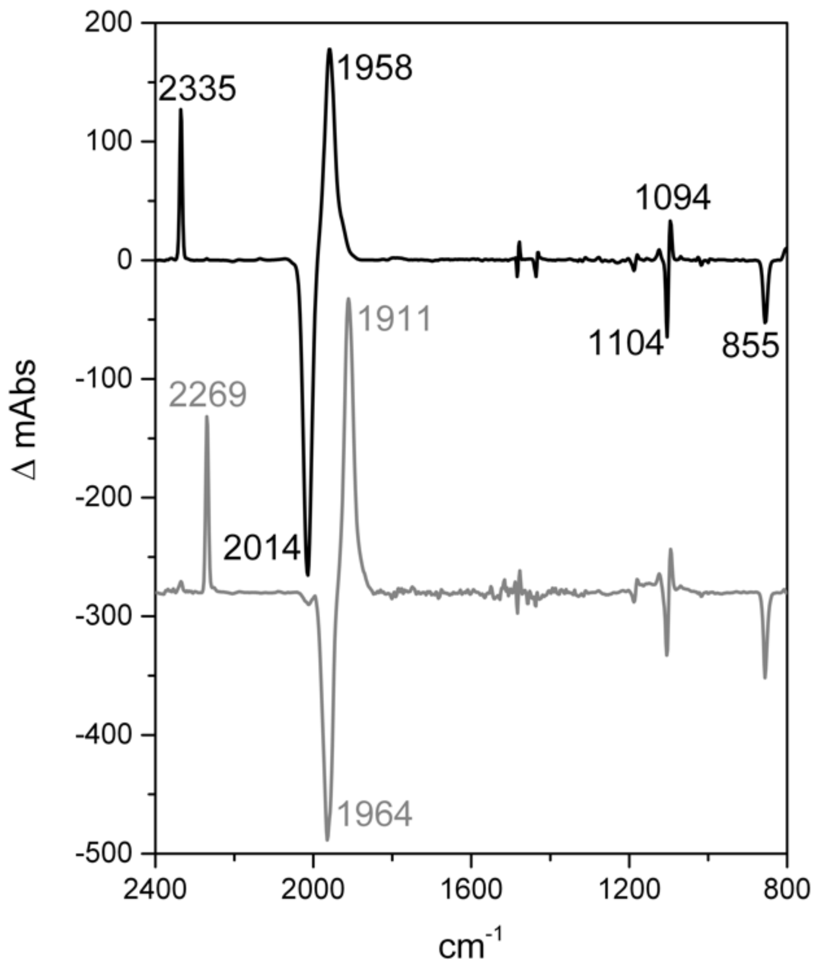

Figure 3.1: Photolysis of $IrCl(CO)O_2[P(C_6H_5)_3]_2$ in PVC matrix at 85 K. Difference following 10 minutes 400 ± 50 nm irradiation subtracted from unphotolyzed sample (black trace). Results of photolysis of the ^{13}CO isotopomer presented as grey trace (ΔAbs scaled ~3.5x to match natural abundance photolysis).

No absorption bands directly assignable to an organometallic reaction product resulting from CO_2 elimination, putatively $Ir^{III}ClO[P(C_6H_5)_3]_2$, are observed. This absence isn't necessarily surprising as the Ir=O vibration of a *trans*-$Ir^{III}ClO[P(C_6H_5)_3]_2$ species would be anticipated to be very weak due to the minor net change in dipole associated with such a vibration. Interestingly, while triphenylphosphine oxide, $OPPh_3$, may be expected to competitively eliminate with CO_2 following photochemical O-O bond activation, no vibrational mode assignable to the P=O stretch of $OPPh_3$, nor a corresponding Ir carbonyl photoproduct, are observed, indicating preferential elimination of CO_2 under these conditions.

Performing short duration (5 minutes) photolyses of $IrCl(CO)O_2[P(C_6H_5)_3]_2$ in air-free CH_2Cl_2 solution in a gas-tight FTIR sample cell at room temperature yields the same products observed in low-temperature matrix experiments, however, the ratio of the CO_2 antisymmetric vibrational mode to the $IrCl(CO)[P(C_6H_5)_3]_2$ carbonyl vibrational mode absorption areas changes from 1:5.5 in PVC at 85 K to 1:10.4 in CH_2Cl_2 at 298 K. This result, in addition to the observation that extending photolysis duration in frozen-matrix experiments favors the CO_2 elimination reaction, suggests that photoejected O_2 and $IrCl(CO)[P(C_6H_5)_3]_2$ may undergo recombination and subsequent photolysis, resulting in increasing the extent of an irreversible CO_2 elimination process relative to that of the reversible O_2 elimination photoreaction. While this recombination would be expected to occur thermally at room temperature, the fact that this appears to happen at cryogenic temperature is somewhat unexpected. We propose that at 85 K, this recombination is facilitated by a mechanism taking place through a photogenerated long-lived triplet state of $IrCl(CO)[P(C_6H_5)_3]_2$ which may undergo spin-allowed addition of O_2 at cryogenic temperatures. Consistent with this argument, a time-resolved IR study conducted on Vaska's complex following 308 nm excitation exhibited evidence for a long-lived electronically excited-state of $IrCl(CO)[P(C_6H_5)_3]_2$, which may be this proposed triplet state species.[24] Further promoting this O_2 addition reaction is the fact that photoliberated O_2 and $IrCl(CO)[P(C_6H_5)_3]_2$ are held in close proximity, poised for recapture, due to the frozen matrix conditions these experiments are performed in.

Previous solution experiments reported that photolysis of $IrCl(CO)[P(C_6H_5)_3]_2$ in benzene under O_2 purge results in generation of a dark green solution with $OPPh_3$ being identified as a by-product by FTIR.[20] In order to expand upon the nature of this photoreaction, we replicated this study on the solution photochemistry of $IrCl(CO)O_2[P(C_6H_5)_3]_2$ in toluene and CD_2Cl_2 solutions under pressures of O_2. In CD_2Cl_2 solutions under ~7 PSI O_2, 350 ± 70 nm irradiation of $IrCl(^{13}CO)O_2[P(C_6H_5)_3]_2$ yields intensely emerald green solutions (λ_{max} = 604 nm) that demonstrate remarkably clean conversion of the parent molecule to $OPPh_3$ and $^{13}CO_2$ by ^{31}P, ^{13}C, and ^{1}H NMR. No paramagnetic species were apparent by EPR in CH_2Cl_2 solutions at room temperature, and we've been unable to grow crystals satisfactory for diffraction study of the green product of this reaction, leaving the ultimate fate of the iridium unclear. As low-temperature photolysis experiments exhibited preferential elimination of CO_2 over $OPPh_3$, the formation of the $OPPh_3$ observed in solution experiments is attributed as the result of secondary reaction of the initially formed CO_2 elimination photoproduct, $Ir^{III}ClO[P(C_6H_5)_3]_2$.

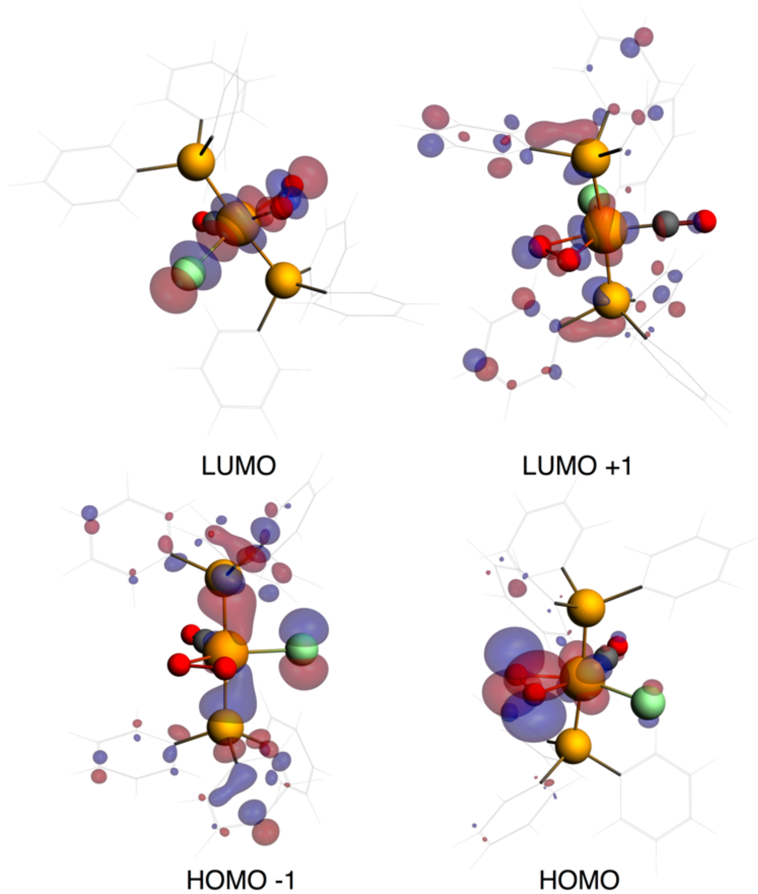

Figure 3.2: SAOP calculated frontier orbitals of $IrCl(CO)O_2[P(C_6H_5)_3]_2$.

The question as to how O-O bond activation occurs to yield CO_2 is seemingly paradoxical. One of the more surprising observations from these low-temperature frozen matrix photolyses is that the O_2 and CO_2 elimination reactions are in apparent competition at all photochemically active wavelengths. The elimination of O_2 from the parent Ir^{III} complex to yield O_2 and *trans*-$Ir^{I}Cl(CO)[P(C_6H_5)_3]_2$ would be anticipated to be the result of an excitation $Ir \leftarrow O_2$ LMCT in character, however, cleavage of the O-O bond required to yield CO_2 is suggestive of a photointermediate or transition state resembling $Ir^{V}Cl(CO)(O)_2[P(C_6H_5)_3]_2$, implying the product of $O_2 \leftarrow Ir$ MLCT excitation. In order to clarify how this transformation occurs, we performed a DFT examination on this reaction.

The frontier orbitals of $IrCl(CO)O_2[P(C_6H_5)_3]_2$ are presented in Figure 3.2. The HOMO is dominated by an O_2 π^* molecular orbital, while the LUMO is composed predominantly of Ir d_{x2-y2}, d_{z2}, and Cl p_y atomic orbitals. TD-DFT computations suggest that the electronic transitions in the region of the observed photochemistry are dominated by LUMO←HOMO excitations which may be characterized as being Ir←O_2 LMCT, fully consistent with photochemical O_2 ejection. Optimizing the geometries for the first few of these excited states yields structural changes that would be anticipated for Ir←O_2 LMCT, chiefly increasing Ir-O_2 bond lengths and a decrease in the O-O bond length. These results, suggesting purely O_2 elimination photochemistry, are particularly confounding with respect to our experimental results which demonstrates competitive O_2 and CO_2 elimination photochemistry at all photochemically active wavelengths. What we then propose is a mechanism by which O-O bond activation occurs photothermally as the result of vibrational cooling of an electronically excited $IrCl(CO)O_2[P(C_6H_5)_3]_2^*$, as opposed to occurring directly in an excited state. This explanation may rationalize how O-O bond cleavage is observed following an LMCT excitation from the O_2 ligand.

To better understand the energetics and intermediate species that may be involved in a photothermal O_2 activation mechanism, we scanned the potential energy surface (PES) of $IrCl(CO)O_2[P(C_6H_5)_3]_2$ along the O-O vibrational mode. The results of these calculations are presented in Scheme 3.2. A transition state geometry corresponding to O-O bond cleavage and O-CO bond formation was found to lie 52.4 kcal mol^{-1} higher in energy relative to the parent peroxo complex, which ultimately yields a stationary point corresponding to a CO_2 complex 25.3 kcal mol^{-1} lower in energy than the parent complex. From the CO_2 complex, a relatively small barrier of 5.6 kcal mol^{-1} is associated with the dissociation of the Ir-CO_2 bond to yield of $IrCl(O)[P(C_6H_5)_3]_2$ and CO_2, resulting in a net change of Gibbs energy to -33.5 kcal mol^{-1} relative to the parent molecule. Alternatively, if an intersystem crossing (ISC) occurs following the formation of the O-CO bond, which may be promoted by both the photochemical conditions under which this reaction is performed as well as spin-orbit coupling with Ir, the expulsion of CO_2 from the iridium complex is calculated to be effectively barrierless, and yields a triplet state *trans*-$IrClO[P(C_6H_5)_3]_2$ 13.7 kcal mol^{-1} lower in energy relative to the singlet state isomer.

Additional matrix photolysis experiments we've conducted on the H_2, D_2, and HCl adducts of Vaska's complex yielded evidence for only clean reductive elimination of the adduct and reversion to $IrCl(CO)[P(C_6H_5)_3]_2$. The absence of any secondary products in these photolyses demonstrates that a competing photothermal reductive elimination pathway may not be present for all adducts of Vaska's complex, and that the O_2 complex may be an exceptional case as the elimination of CO_2 as reaction product offers a large thermodynamic driving force. Regardless, the results of frozen-matrix and solution photochemistry experiments demonstrate an unreported, yet significant, competitive elimination pathway of CO_2 in one of the archetypal photochemical reactions in organometallic photochemistry. While detailed time-resolved studies will be necessary to elucidate the mechanism and energies involved with this transformation, results from DFT computations suggest the formation does not occur directly in an excited state of $IrCl(CO)O_2[P(C_6H_5)_3]_2$, but rather as the result of vibrational cooling of a vibrationally hot $IrCl(CO)O_2[P(C_6H_5)_3]_2^*$ species.

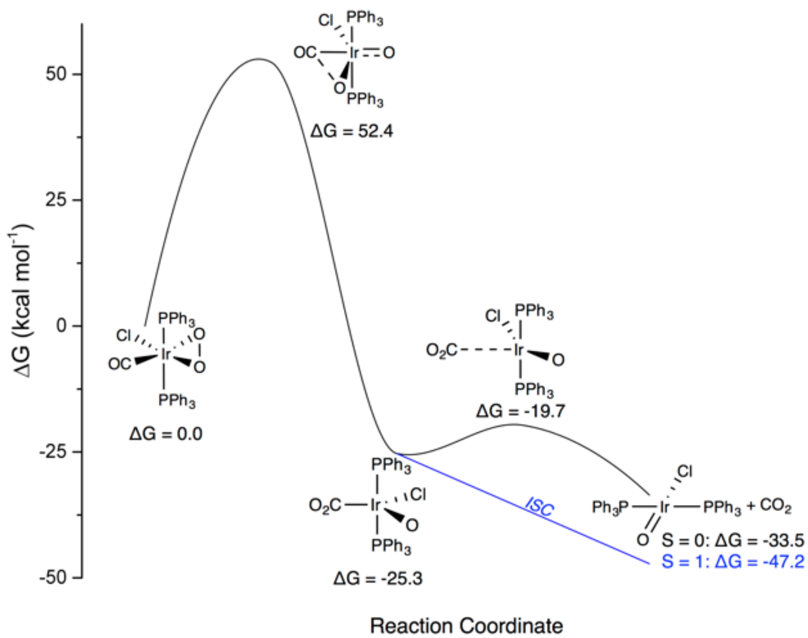

Scheme 3.2: Reaction coordinate for the elimination of CO_2 from $IrCl(CO)O_2[P(C_6H_5)_3]_2$.

Experimental

$IrCl(CO)[P(C_6H_5)_3]_2$ was prepared by literature procedure.[1] $IrCl(^{13}CO)[P(C_6H_5)_3]_2$ was synthesized by placing 120 mg of $IrCl(CO)[P(C_6H_5)_3]_2$ in methylene chloride under a 25-fold excess of ^{13}CO (Cambridge Isotope Laboratories) in an Ace pressure tube and irradiating with 350 ± 70 nm light for 12 hours. The solution was then depressurized and placed under a rapid stream of purified Ar while photolysis continued for another 6 hours to convert $IrCl(^{13}CO)_2[P(C_6H_5)_3]_2$ to $IrCl(^{13}CO)[P(C_6H_5)_3]_2$, achieving ~95% ^{13}CO enrichment by FTIR. The apparatus and methods for matrix photochemistry have been reported elsewhere.[25]

All DFT calculations were performed in the Amsterdam Density Functional (ADF2014.10) program.[26-28] Electronic configurations of atoms were described by an all-electron triple-ζ Slater-type orbital basis set modified by a polarization functions (TZP STO).[29] Geometry optimizations and vibrational frequency calculations were performed using the GGA functional of Becke[30] and Perdew[31,32] with a scalar relativistic correction within the Zeroth Order Regular Approximation (ZORA).[33,34]. Electronic excitation energies were computed using statistical average of orbital potentials (SAOP) model.[35,36]

References

(1) Vaska, L.; DiLuzio, J. W. *J. Am. Chem. Soc.* **1961**, *83* (12), 2784–2785.

(2) Vaska, L.; DiLuzio, J. W. *J. Am. Chem. Soc.* **1962**, *84* (4), 679–680.

(3) Vaska, L.; Rhodes, R. E. *J. Am. Chem. Soc.* **1965**, *87* (21), 4970–4971.

(4) Vaska, L.; Bath, S. S. *J. Am. Chem. Soc.* **1966**, *88* (6), 1333–1335.

(5) La Placa, S. J.; Ibers, J. A. *Inorg. Chem.* **1966**, *5* (3), 405–410.

(6) Vaska, L. *Acc. Chem. Res.* **1968**, *1* (11), 335–344.

(7) Collman, J. P. *Acc. Chem. Res.* **1968**, *1* (5), 136–143.

(8) Tolman, C. A. *Chem. Soc. Rev.* **1972**, *1* (3), 337–353.

(9) Brotherton, P. D.; Raston, C. L.; White, A. H.; Wild, S. B. *J. Chem. Soc., Dalton Trans.* **1976**, No. 18, 1799–4.

(10) Vaska, L. *Science* **1963**, *140* (3568), 809–810.

(11) La Placa, S. J.; Ibers, J. A. *J. Am. Chem. Soc.* **1965**, *87* (12), 2581–&.

(12) Chock, P. B.; Halpern, J. *J. Am. Chem. Soc.* **1966**, *88* (15), 3511–&.

(13) McGinnety, J. A.; Doedens, R. J.; Ibers, J. A. *Inorg. Chem.* **1967**, *6* (12), 2243.

(14) Vaska, L.; Chen, L. S. *J. Chem. Soc. D* **1971**, No. 18, 1080.

(15) Wickman, H. H.; Silverthorn, W. E. *Inorg. Chem.* **1971**, *10* (10), 2333–2335.

(16) Vaska, L. *Acc. Chem. Res.* **1976**, *9* (5), 175–183.

(17) Selke, M.; Karney, W. L.; Khan, S. I.; Foote, C. S. *Inorg. Chem.* **1995**, *34* (23), 5715–5720.

(18) Lanci, M. P.; Brinkley, D. W.; Stone, K. L.; Smirnov, V. V.; Roth, J. P. *Angew. Chem. Int. Ed. Engl.* **2005**, *44* (44), 7273–7276.

(19) Lebel, H.; Ladjel, C.; Bélanger-Gariépy, F.; Schaper, F. *J. Organomet. Chem.* **2008**, *693* (16), 2645–2648.

(20) Geoffroy, G. L.; Hammond, G. S.; Gray, H. B. *J. Am. Chem. Soc.* **1975**, *97* (14), 3933–3936.

(21) Seip, M.; Brauer, H. D. *J. Photochem. Photobiol. A: Chem.* **1994**, *79* (1-2), 19–24.

(22) Thornley, W. A.; Bitterwolf, T. E. *Angew. Chem. Int. Ed. Engl.* **2015**, *54* (7), 2068–2072.

(23) Thornley, W. A.; Bitterwolf, T. E. *Inorg. Chem.* **2015**, *54* (7), 3370–3375.

(24) Schultz, R. H. *J. Organomet. Chem.* **2003**, *688* (1-2), 1–4.

(25) Bays, J. T.; Bitterwolf, T. E.; Lott, K. A.; Ollino, M. A.; Rest, A. J.; Smith, L. M. *J. Organomet. Chem.* **1998**, *554* (1), 75–85.

(26) ADF2013, SCM, Theoretical Chemistry, Vrije Universiteit, Amsterdam, The Netherlands, http://www.scm.com

(27) Guerra, C. F.; Snijders, J. G.; Velde, Te, G.; Baerends, E. J. *Theor. Chem. Acc.* **1998**, *99*, 391–403.

(28) Velde, Te, G.; Bickelhaupt, F. M.; Baerends, E. J.; Fonseca Guerra, C.; van Gisbergen, S. J. A.; Snijders, J. G.; Ziegler, T. *J. Comp. Chem.* **2001**, *22* (9), 931–967.

(29) Lenthe, E. V.; Baerends, E. J. *J. Comp. Chem.* **2003**, *24* (9), 1142–1156.

(30) Becke, A. D. *Phys. Rev. A* **1988**, *38* (6), 3098–3100.

(31) Perdew, J. *Phys. Rev. B* **1986**, *33* (12), 8822–8824.

(32) Perdew, J. *Phys. Rev. B* **1986**, *34* (10), 7406–7406.

(33) Lenthe, E. V.; Baerends, E. J.; Snijders, J. G. *J. Chem. Phys.* **1993**, *99* (6), 4597.

(34) Lenthe, E. V.; Ehlers, A.; Baerends, E. J. *J. Chem. Phys.* **1999**, *110* (18), 8943.

(35) Gritsenko, O. V.; Schipper, P.; Baerends, E. J. *Chem Phys Lett* **1999**, *302*, 199–207.

(36) Schipper, P. R. T.; Gritsenko, O. V.; van Gisbergen, S. J. A.; Baerends, E. J. *J. Chem. Phys.* **2000**, *112* (3), 1344.

Chapter 4: Intramolecular C-H Activation and Metallacycle Aromaticity in the Photochemistry of [FeFe]-Hydrogenase Model Compounds in Low-Temperature Frozen Matrices

Published: W. A. Thornley, T. E. Bitterwolf, Chem. Eur. J. **2015**, *21*, 18218–18229.

Abstract: *The [FeFe]-hydrogenase model complexes (μ-pdt)[Fe(CO)$_3$]$_2$, (μ-edt)[Fe(CO)$_3$]$_2$, and (μ-mdt)[Fe(CO)$_3$]$_2$, where pdt = 1,3-propanedithiolate, edt = 1,2-ethanedithiolate, and mdt = methanedithiolate, undergo wavelength dependent photodecarbonylation in hydrocarbon matrices at 85 K resulting in multiple decarbonylation isomers. As previously reported in time-resolved solution photolysis experiments, the major photoproduct is attributed to a basal carbonyl loss species. Apical carbonyl loss isomers are also generated and may undergo secondary photolysis resulting in β-hydride activation of the alkyl dithiolate bridge as well as formation of bridging carbonyl isomers. For (μ-bdt)[Fe(CO)$_3$]$_2$, (bdt = 1,2-benzenedithiolate), apical photodecarbonylation results in generation of a 10 π-electron aromatic $FeS_2C_6H_4$ metallacycle that coordinates the remaining iron through an η^5 mode.*

The ability of the hydrogenase family of enzymes to reversibly catalyze the activation of hydrogen has drawn considerable interest as a model for renewable energy storage.[1-9] The organometallic active site of the [FeFe]-hydrogenase enzyme is composed of a dithiolate-bridged diiron core coordinated by CO and CN^- ligands, and a cysteinyl ligand that links the diiron active site to an electron transport network composed of $[Fe_4S_4]$ cubanes, Scheme 4.1a.[10,11] In the oxidized form, a CO ligand serves as a bridge between the diiron center and reverts to a semi-bridging or terminal coordination mode in the reduced form.[12] Crystallographic evidence indicates that the dithiolate bridgehead may be composed of a CH_2, O, or NH functionality, though the chemistry of functional model complexes seem to indicate that this bridgehead is most likely an NH functionality that serves to act as proton relay to the metal.[6,9,13-15] Extensive synthetic strategies have been developed for the preparation of [FeFe]-hydrogenase model complexes since the elucidation of the active site structure.[16-22]

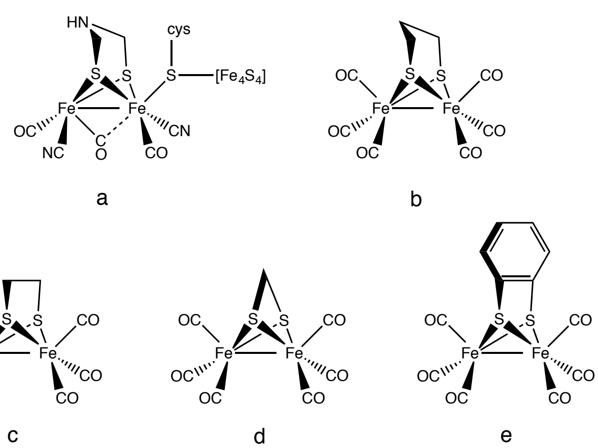

Scheme 4.1: Proposed active site of the [FeFe]-Hydrogenase enzyme (a), (μ-pdt)$[Fe(CO)_3]_2$ (b), (μ-edt)$[Fe(CO)_3]_2$ (c), (μ-mdt)$[Fe(CO)_3]_2$ (d), and (μ-bdt)$[Fe(CO)_3]_2$ (e)

As a means to study the bonding and reactivity of the hydrogenase active site and model complexes, numerous photochemical experiments have been performed in low-temperature matrices and in solution. The photochemistry of the CO-inhibited form of *Clostridium pasteurianum* has been studied at temperatures from 6 - 30 K by FTIR and EPR.[23-25] It was found that photolysis of this species at low temperature gave rise to two CO loss products, one having an identical infrared spectrum to the oxidized form of *Clostridium pasteurianum* that reverts to the CO-inhibited form at temperatures > 150 K. The second photoproduct was found to lose the characteristic bridging carbonyl functionality and revert at temperatures > 80 K.

In solution, the photochemistry of the (μ-pdt)[Fe(CO)$_3$]$_2$ (pdt = 1,3-propanedithiolate) [FeFe]-hydrogenase model complex, Scheme 4.1b, has been the subject of several investigations. Under steady-state photolysis in coordinating and non-coordinating solvents, partially reversible substitution of CO by solvent to give (μ-pdt)Fe$_2$(CO)$_5$(sol) has been reported.[26,27] On the ultrafast timescale, a CO loss species possessing solely terminal carbonyls is generated that is generally assigned to a basal CO loss species with a weakly coordinated solvent molecule occupying the vacant metal site.[28-30] This CO loss species undergoes recapture of CO following bimolecular kinetics on the microsecond timescale, though some evidence for growth of a dimeric species has been observed on longer timescales.[29] Multidimensional ultrafast IR experiments on the CO loss product support the formation of only a single pentacarbonyl species, and in contrast to other studies, suggest that CO loss and solvent coordination is occurring at an apical Fe coordination site based on anisotropic measurements and DFT simulations.[31] A generalized scheme of the observed photochemistry is presented in Scheme 4.2.

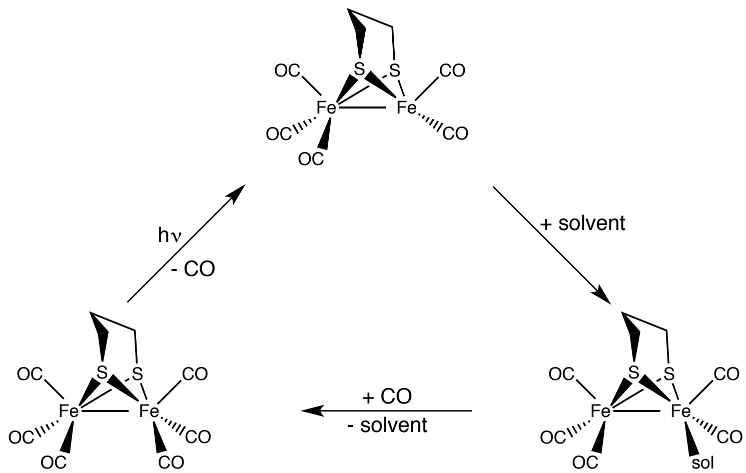

Scheme 4.2: Solution photochemistry of (μ-pdt)[Fe(CO)$_3$]$_2$

To gain a clearer understanding of the structures of the photoproducts, effect of photolysis wavelengths, and the possibility of multi-step, multi-photon reactions that may not be observed in transient pump-probe experiments, we've recently begun exploring the photochemistry of [FeFe]-hydrogenase model complexes in low-temperature frozen matrices with characterization being performed by FTIR. Herein, we report the initial findings of these experiments, investigating the steric and electronic effects of the dithiolate bridge on the decarbonylative photochemistry of these model complexes.

The electronic spectra of the [FeFe]-hydrogenase model complexes studied, Scheme 4.1b-e, are markedly similar. Their most notable features are a strong transition at ca. 335 nm and a broad, weak absorption centered at 465 nm having a tail extending to ca. 650 nm, Figure 4.1. To better understand the nature of the electronic transitions involved in the UV-Vis spectrum and how they may influence the photochemistry of these complexes, time-dependent density functional theory (TD-DFT) modelling of the electronic spectrum of (μ-pdt)$[Fe(CO)_3]_2$ using the statistical average of orbital potentials (SAOP) model was performed.[32,33] Results of these computations, summarized in Table 4.1 and Figure 4.2, give excitation energies that are slightly underestimated, but in overall excellent agreement with the experimentally measured spectrum. The computed transitions suggest that the broad, low-energy feature of this spectrum is composed of several transitions from molecular orbitals that are dominated by bonding interactions between Fe t_{2g} and sulfur p-orbitals or the Fe-Fe σ bond into an orbital that is Fe-Fe σ* in character. Consistent with this model, evidence from ultrafast 532 nm pump-probe experiments and resonance-Raman experiments suggest elongation of the Fe-Fe bond when subjected to excitation in this region.[30,34] Transitions in the region of the intense absorption at 335 nm are distinctly metal-to-ligand charge-transfer (MLCT) in character, comprised of transitions from the Fe-Fe σ bond orbital into orbitals that are largely CO π* and sulfur p-orbital in nature. Excitation into these CO π* orbitals would be expected to result in disassociation of CO as is observed in previously reported photochemical experiments. We should note that this interpretation comes in contrast to a previous study that assigned the intense 335 nm absorption to a Fe-Fe σ* ← Fe-Fe σ transition, but offers a similar interpretation of the low-energy feature.[34]

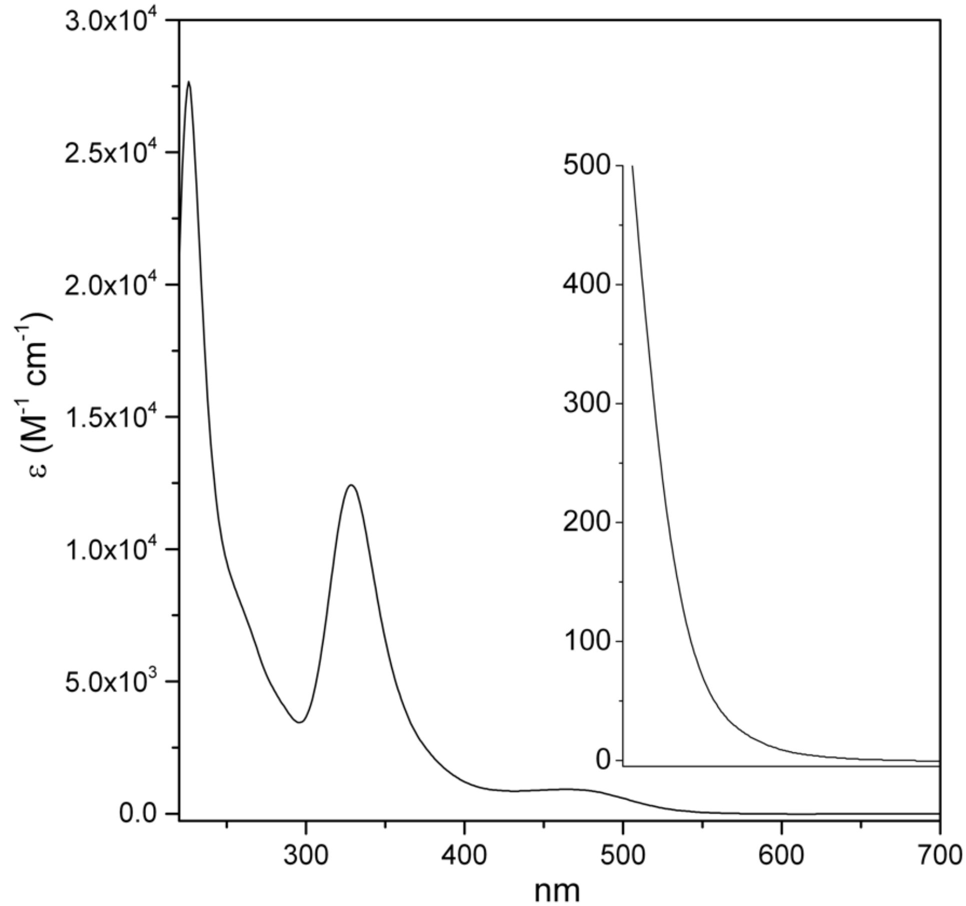

Figure 4.1: Electronic spectra of (μ-pdt)[Fe(CO)$_3$]$_2$ model complex in cyclohexane and expansion of 500-700 nm region (inset).

Table 4.1: Selected SAOP Electronic Transitions and Excitation Energies

Transition	Wavelength	Character
LUMO ← HOMO -1	557	Fe_2 σ* ← S_2Fe_2 π
LUMO ← HOMO (63%)	490	Fe_2 σ* ← Fe_2 σ
LUMO ← HOMO -2 (31%)		Fe_2 σ* ← Fe_2S_2 π
LUMO +1 ← HOMO	433	Fe_2S_2 π* ← Fe_2 σ
LUMO ← HOMO -2 (57%)	427	Fe_2 σ* ← Fe_2S_2 π
LUMO ← HOMO (20%)		Fe_2 σ* ← Fe_2 σ
LUMO +2 ← HOMO -1 (13%)		Fe_2S_2 π* ← S_2Fe_2 π
LUMO ← HOMO -3	419	Fe_2 σ* ← Fe_2S_2 π
LUMO +2 ← HOMO	414	Fe_2S_2 π* ← Fe_2 σ
LUMO +1 ← HOMO -1	370	Fe_2S_2 π* ← S_2Fe_2 π
LUMO +2 ← HOMO -1 (53%)	347	Fe_2S_2 π* ← Fe_2 σ
LUMO +3 ← HOMO (16%)		Fe-CO π* ← Fe_2 σ
LUMO +3 ← HOMO (74%)	342	Fe-CO π* ← Fe_2 σ
LUMO +2 ← HOMO -1 (13%)		Fe_2S_2 π* ← Fe_2 σ

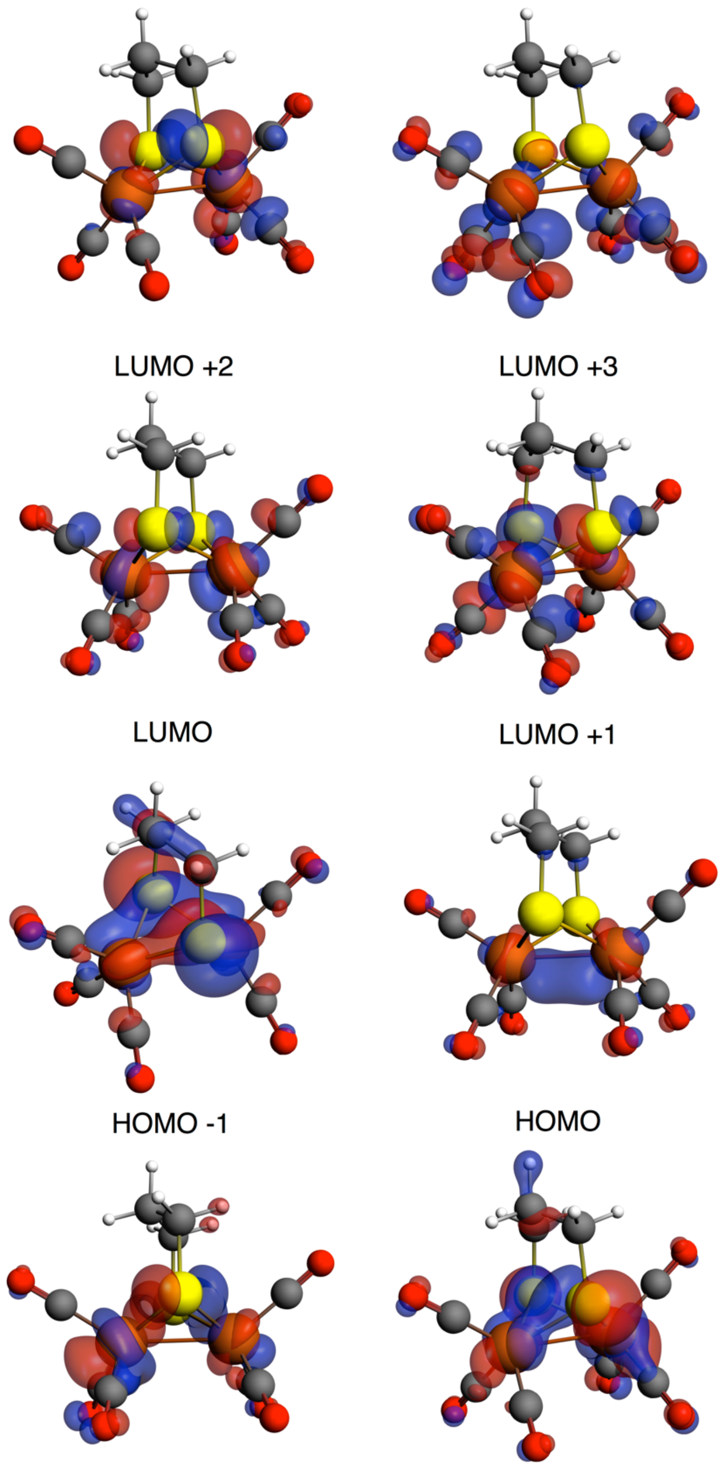

Figure 4.2. Kohn-Sham orbitals of (μ-pdt)[Fe(CO)$_3$]$_2$ model complex.

Photolysis of (μ-pdt)[Fe(CO)$_3$]$_2$ at 85 K in Hydrocarbon Matrices

Photolysis into the low energy electronic transitions of (μ-pdt)[Fe(CO)$_3$]$_2$ with λ_{irr} = 450 ± 70 nm light in Nujol glass at 85 K results in bleaching of the parent vibrational bands and growth of new absorptions at 2132, 2081, 2052, 1998, 1982, 1973, 1961, and 1942 cm^{-1}, Figure 4.3a. The feature at 2132 cm^{-1} corresponds to "free" CO, while the product bands at 2052, 1998, 1973, and 1942 cm^{-1} are in excellent agreement with those observed in heptane solution TRIR experiments.[28,29] Interestingly, the product bands at 2081, 2041, 1982, and 1961 cm^{-1} are unique to our low-temperature matrix photolysis experiments and belong to a species having no direct analogue in the reported transient solution studies. At higher energy photolysis wavelengths, λ_{irr} = 330 ± 70 nm, Figure 4.3b, an additional species exhibiting vibrational modes at 2025, 2012, and 1843 cm^{-1} appears. Annealing the photoproducts in hydrocarbon glass to 135 K and refreezing to 85 K results in clean reversion of the carbonyl loss isomers to the parent hexacarbonyl complex. Back photolysis of the λ_{irr} = 330 ± 70 nm sample at long wavelengths, λ_{irr} = 550 ± 70 nm, also results in recapture of CO and reformation of the parent complex.

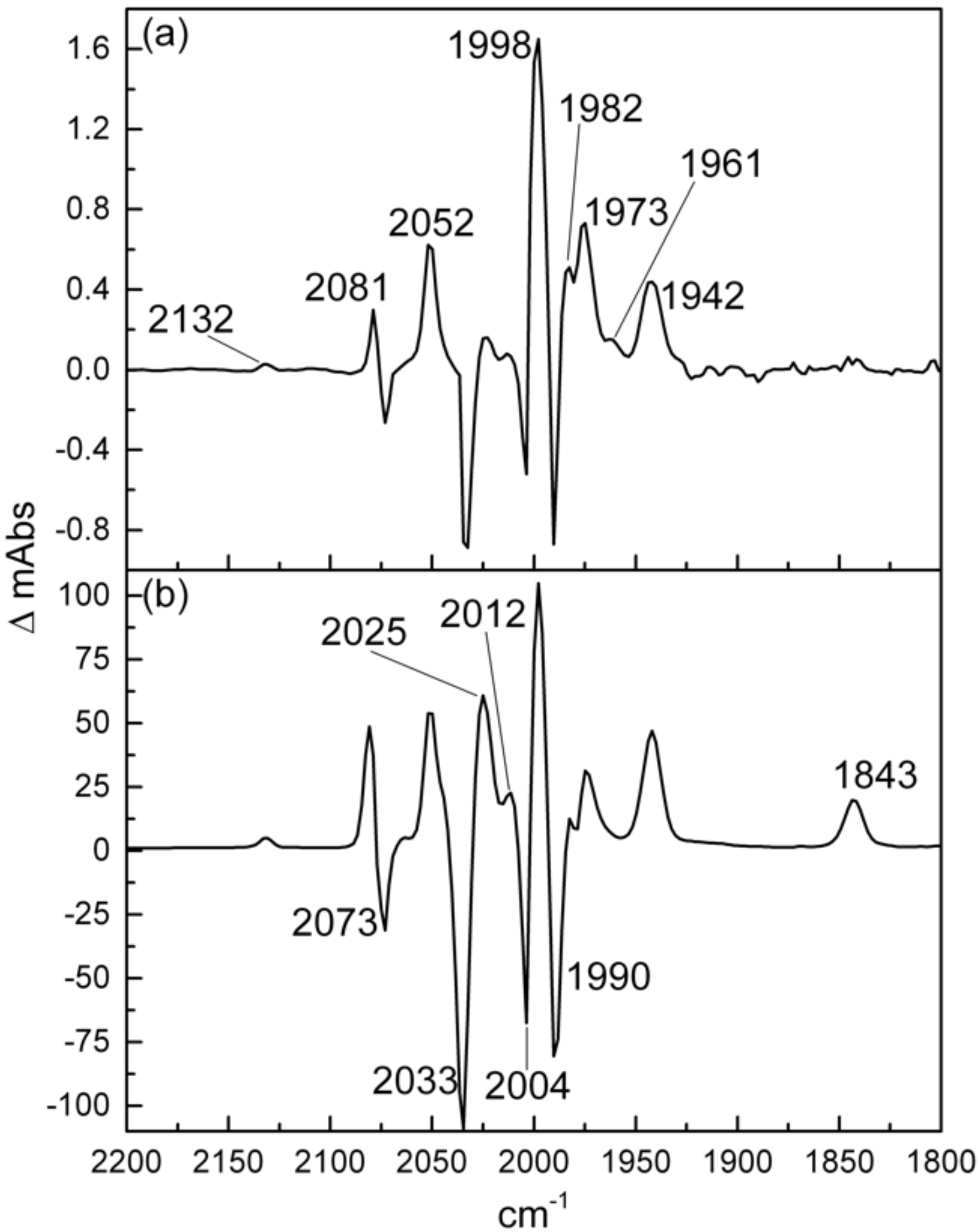

Figure 4.3. Photolysis of (μ-pdt)$[Fe(CO)_3]_2$ in glassy Nujol at 85 K. (a) 120 minute 450 ± 70 nm irradiated sample minus unphotolyzed sample. (b) Difference following 90 minutes 330 ± 70 nm irradiation

The additional product bands observed in our low-temperature matrix photolysis experiments that are absent in transient solution studies may be attributed to multi-photon reactions resulting in rearrangement of a primary photoproduct. As the matrix photolyses are performed under steady-state photolytic conditions, multi-step and multi-photon reactions like this are possible, providing a route to products not observed in transient pump-probe experiments. Varying photolysis duration between 10 and 300 minutes results in no observable change in the relative ratios of the photoproducts, suggesting that a photoequilibrium between the carbonyl loss isomers is rapidly established under steady-state photolysis conditions.

Of the unique product bands observed in the low-temperature photochemistry experiments, the two most noteworthy features are the vibrational bands at 2081 cm^{-1}, which is shifted to higher energy relative to the parent hexacarbonyl complex, implying formal oxidation of the photoproduct, and the band at 1843 cm^{-1} that lies within the bridging carbonyl stretching region. As the 2081 cm^{-1} band could conceivably be attributed to C-H bond activation of the Nujol matrix following coordination of a vacant metal site, the sample was also photolyzed in Fluorolube oil (chlorotrifluoroethylene polymer). Photolysis in Fluorolube oil leads to generation of an analogous species, suggesting that this product is the result of an intramolecular rearrangement and not engendered through reaction with the matrix material. In order to clarify the structures of and relationships between possible CO loss isomers observed in the matrix photochemistry, we carried out a DFT investigation on the isomers of (μ-pdt)$Fe_2(CO)_5$, Scheme 4.3.

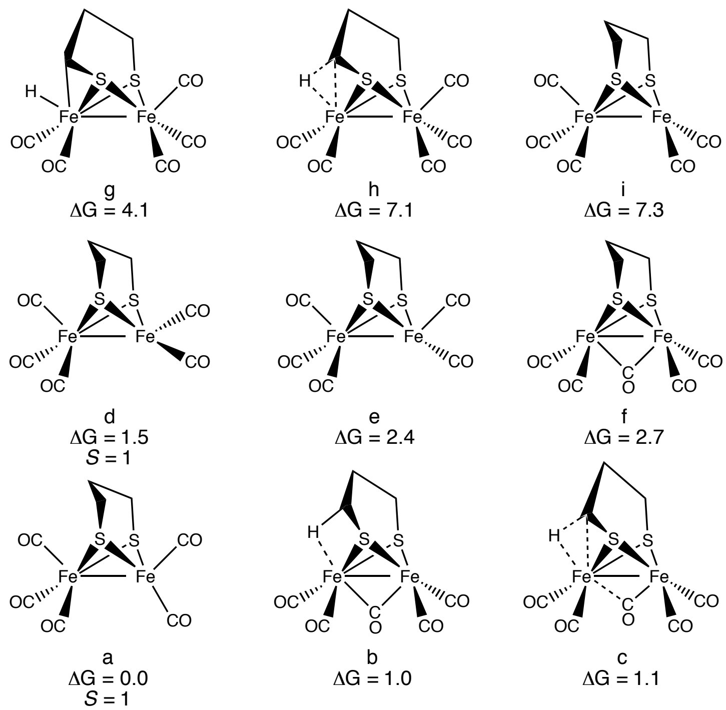

Scheme 4.3: TZP/TPSS-D3(BJ) DFT energies (kcal mol^{-1}) of the nine lowest energy isomers of (μ-pdt)[$Fe_2(CO)_5$].

Surprisingly, the lowest energy isomer of (μ-pdt)$Fe_2(CO)_5$ was found to be a triplet state species possessing C_s symmetry with the carbonyl groups of the unsaturated iron positioned within the C_s plane of the molecule, 4.3a**.** While we have no direct experimental evidence to suggest the presence of an open-shell decarbonylated species, and recognize the limitations of DFT when applied to open-shell transition metal complexes,[35] we include this result as the role of low-lying open-shell intermediates in the reaction chemistry of these models may warrant further investigation.

Of the closed-shell stationary points of (μ-pdt)$Fe_2(CO)_5$, the lowest energy isomers were found to posses a bridging carbonyl group and exhibit either agostic, 4.3b, or sigma, 4.3c, interactions between a vacant apical coordination site and a β-hydrogen of the propanedithiolate bridge. These agostic or sigma interactions stabilize the bridging carbonyl geometry by 1.7 and 1.6 kcal mol^{-1}, respectively, relative to the bridging carbonyl geometry that possesses no such interactions, 4.3f. In agreement with previous studies,[28] two all terminal carbonyl CO loss species were found possessing vacant basal, 4.3e, and apical, 4.3i, coordination sites and lay 2.4 and 7.3 kcal mol^{-1} higher in energy than the triplet state global minima respectively. The potential energy surface of 4.3i was explored in search of stationary points possessing either agostic or sigma interactions between the propanedithiolate bridge and vacant apical coordination site. These calculations led to location of a stationary point corresponding to a β-hydride activation product, 4.3g, possessing calculated Fe-H, Fe-C, and C-H bond lengths of 1.50, 2.03, and 2.40 Å respectively, and an additional species exhibiting a β-hydrogen sigma interaction, 4.3h. The β-hydride activation product is calculated to be 3.2 kcal mol^{-1} lower in energy relative to the apical carbonyl loss, 4.3i, and is the only of the nine isomers calculated to have a νCO mode higher in energy relative to the highest energy νCO band of the parent hexacarbonyl complex.

To identify the relationships between the calculated stationary points, the energies associated with their interconversion, and ultimately which isomers are formed following matrix photolysis, transition states on the potential energy surface were located. With regard to the mechanism of formation of the β-hydride activation species, the barrier for formation of the β-hydrogen sigma complex, 4.3h, was found to lay just 0.3 kcal mol^{-1} higher in energy than the apical carbonyl loss isomer, 4.3i, while the barrier associated with activation of the C-H bond to give the β-hydride complex, 4.3g, is placed 2.8 kcal mol^{-1} above the 4.3h. These low-energy transition states suggest that facile β-hydride activation may occur following apical photodecarbonylation while the molecule is still vibrationally hot, giving rise to the species possessing the high-energy νCO mode observed in our matrix photolysis experiments. Rotation of the iron tricarbonyl moiety of the β-hydride activation product results in formation of the bridging carbonyl β-hydrogen sigma complex, 4.3c, with a barrier of 5.8 kcal mol^{-1}. The results of these calculations are summarized in Scheme 4.4.

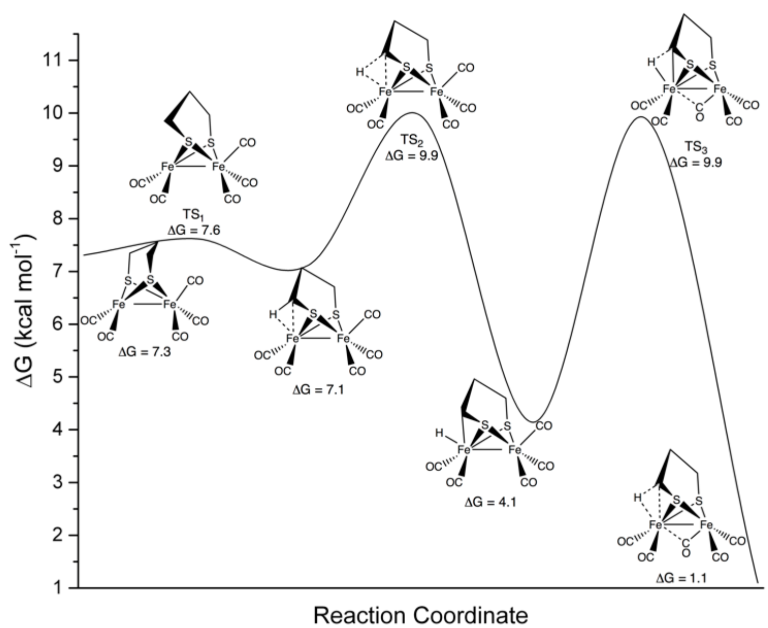

Scheme 4.4: TZP/TPSS-D3(BJ) DFT reaction energies (kcal mol^{-1}) for pathway of C-H activation of the propanedithiol bridge of (μ-pdt)$[Fe(CO)_3]_2$.

Two additional mechanisms were found that may result in formation of the various bridging carbonyl stationary points. In the first, simple rotation of the $Fe(CO)_3$ moiety of the apical carbonyl loss species 4.3i leads to the bridging carbonyl species 4.3f with a barrier of 1.4 kcal mol^{-1}. The β-hydrogen agostic species, 4.3b, may then be formed from 4.3f with a barrier of just 0.3 kcal mol^{-1}, Scheme 4.5 (solid trace). In the second mechanism, the 4.3h isomer is formed by the same mechanism in Scheme 4.4. Rotation of the $Fe(CO)_3$ moiety may then lead to 4.3b with a barrier of 1.4 kcal mol^{-1}, Scheme 4.5 (dashed trace). The barrier associated with the interconversion between β-hydrogen agostic species, 4.3b, and the β-hydrogen sigma complex, 4.3c, is placed 1.3 kcal mol^{-1} above 4.3b.

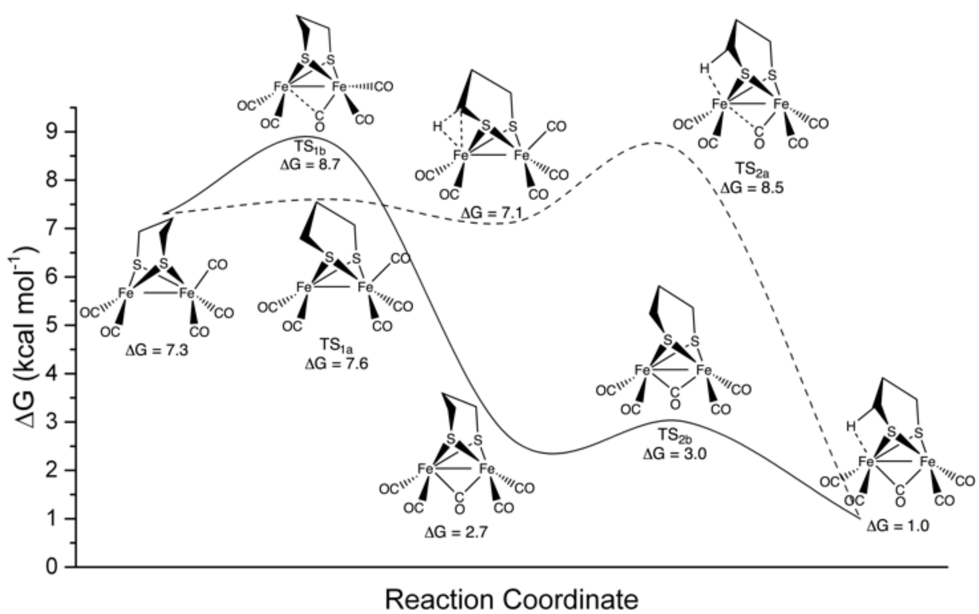

Scheme 4.5: TZP/TPSS-D3(BJ) DFT reaction pathway and energies (kcal mol^{-1}) for formation of bridging carbonyl isomers.

Based on the results of DFT computations, we assign the carbonyl loss product exhibiting νCO modes at 2052, 1998, 1973, and 1942 cm^{-1} following λ_{irr} = 450 ± 70 nm photolysis to the basal loss isomer, 4.3e, consistent with the results of ultrafast solution experiments. The additional species that grows in following photolysis at these wavelengths, possessing νCO absorptions at 2081, 1982, and 1961 cm^{-1}, is assigned to the β-hydride activation product, 4.3g. This assignment is based largely upon the 2081 cm^{-1} absorption that is shifted to higher energy relative to the parent hexacarbonyl complex, consistent with oxidative addition occurring at a vacant apical coordination site. We propose that the small barrier associated with the activation of this C-H bond is responsible for the absence of any spectral features assignable to the apical CO loss isomer, 4.3i, and that formation of the 4.3i isomer leads directly to formation of the metastable β-hydride activation product under steady-state photolysis conditions. While the formal oxidative addition reaction we propose is unique to our study, the activation of a β-hydrogen is not entirely unprecedented in this family of compounds. Previous work by Seyferth and coworkers found that reaction of alkyldithiolate bridged diiron hexacarbonyl tetrahedrane complexes with lithium diisopropyl amide (LDA) leads to abstraction of a β-hydrogen and in some cases a β-elimination product.[36] More recently, Zheng *et al*. found that oxidation of an [FeFe]-hydrogenase model complex possessing a pendant amine diphosphine ligand resulted in heterolysis of a β-CH bond and formation formation of an Fe-C bond and protonation of the pendant amine ligand.[37]

Finally, the species that is characterized by νCO absorptions at 2025, 2012, and 1843 cm^{-1} that is produced following λ_{irr} = 330 ± 70 nm photolysis is assigned to the bridging carbonyl β-hydrogen agostic structure 4.3b. This is a somewhat arbitrary assignment; the DFT calculated infrared spectra of bridging carbonyl isomers 4.3b and 4.3c are effectively identical, giving no way to distinguish between the two isomers by FTIR, and both are calculated to be nearly degenerate in energy. The relatively small calculated barrier for interconversion between the two forms of 1.3 kcal mol^{-1} implies that both forms may very well be present but simply fail to resolve in the matrix FTIR spectra. The exact mechanism for the formation of the bridging carbonyl species also remains unclear. This isomer is present as a minor product following λ_{irr} = 450 ± 70 nm irradiation, but as a major product following photolysis at wavelengths < 380 nm. These results suggest a CO loss isomer must possess appreciable vibrational energy following decarbonylation to overcome the reaction barrier associated with the formation of the bridging isomer, in the current case, this would be consistent with the mechanism presented in Scheme 4.4. The two mechanisms proposed in Scheme 4.5, while lower in energy, would be expected to result in formation of a bridging carbonyl isomer in similar population to the β-hydride activation product following λ_{irr} = 450 ± 70 nm due to the similar reaction barriers, which is not observed. Additionally, the apparent photoequilibrium that is established following λ_{irr} < 380 nm suggests interconversion between the bridging carbonyl and β-hydride activation isomers, which is also consistent with the mechanism in Scheme 4.4. The overall photochemistry is summarized in Scheme 4.6.

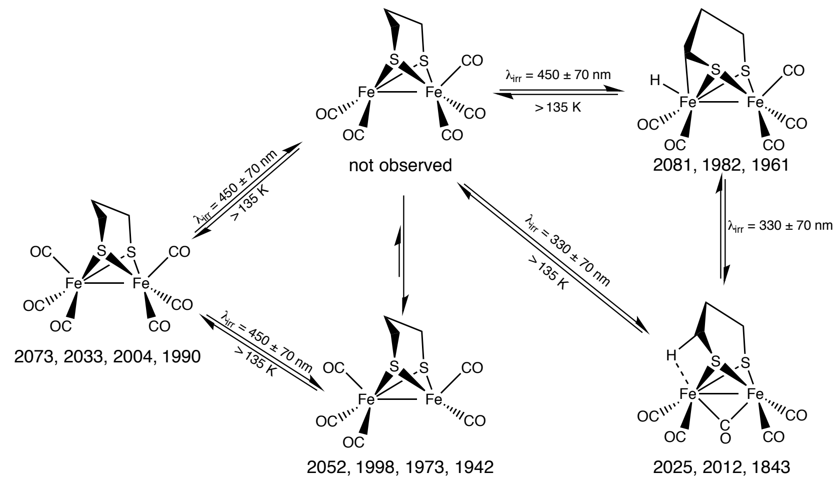

Scheme 4.6: Proposed photochemical behavior and product vibrational modes (cm^{-1}) of (μ-pdt)[$Fe(CO)_3]_2$ in hydrocarbon matrices at 85 K.

Photolysis of (μ-edt)[$Fe(CO)_3]_2$ at 85 K in Hydrocarbon Matrices

We next examined the photochemistry of the (μ-edt)[$Fe(CO)_3]_2$ (edt = 1,2-ethanedithiolate) model complex, 4.1c. While (μ-edt)[$Fe(CO)_3]_2$ has β-hydrogens capable of undergoing addition to a vacant metal coordination site as observed with the pdt model complex, the reduced flexibility of the shorter ethanedithiol bridge would be expected to increase the barrier of this reaction. We reasoned this higher-energy barrier may allow for an intermediate prior to β-hydride activation, e.g. the apical carbonyl loss species, to be observed. Photolysis of (μ-edt)[$Fe(CO)_3]_2$ in a Nujol matrix at 85 K with λ_{irr} = 330 ± 70 nm results in bleaching of the parent CO bands at 2078, 2037, 2006, and 1992 cm^{-1} with concomitant appearance of "free" CO (2132 cm^{-1}) and product bands at 2084, 2065, 2053, 2025, 2019, 1999, 1977, 1963, 1946, and 1849 cm^{-1}, Figure 4.4.

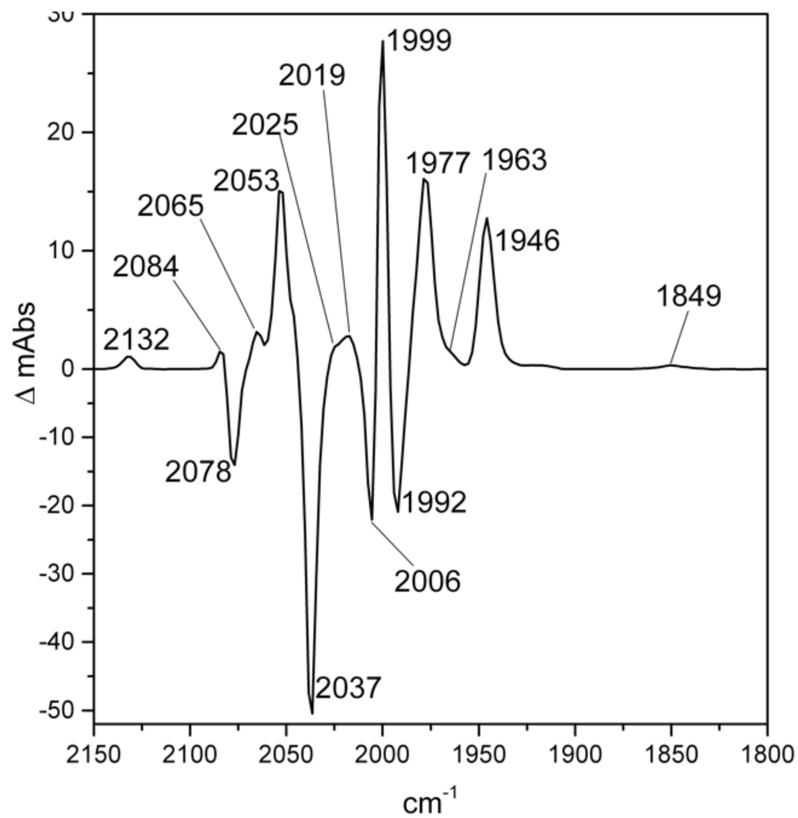

Figure 4.4. Photolysis of (μ-edt)[Fe(CO)$_3$]$_2$ in glassy Nujol at 85 K. 15 minute 330 ± 70 nm irradiated sample minus unphotolyzed sample.

By way of analogy to the (μ-pdt)[Fe(CO)$_3$]$_2$ photolysis, we assign the product bands at 2053, 1999, 1977, and 1946 cm^{-1} to a basal carbonyl loss structure, Scheme 4.7a. Similarly, the species with a vCO band shifted to higher energy relative to the parent complex at 2084 cm^{-1} is assigned to the β-hydride activation product, 4.7e. The weak product absorptions at 2025, 2019, and 1849 cm^{-1} are assigned to a minor population of the bridging carbonyl isomer, 4.7c. Finally, the remaining product vCO absorption at 2065 cm^{-1}, which has no direct analogue in the photochemistry of (μ-pdt)[Fe(CO)$_3$]$_2$, is assigned to the apical carbonyl loss isomer, 4.7b. DFT computations predict the high energy vCO transition of the apical carbonyl loss isomer to be approximately 12 cm^{-1} higher in energy relative the basal carbonyl loss isomer, in excellent agreement with the experimentally observed value. The absence of other spectral features attributable to the apical carbonyl loss product is credited to the low population of this species and significant spectral overlap with 4.7a, resulting in additional vCO vibrational modes failing to resolve.

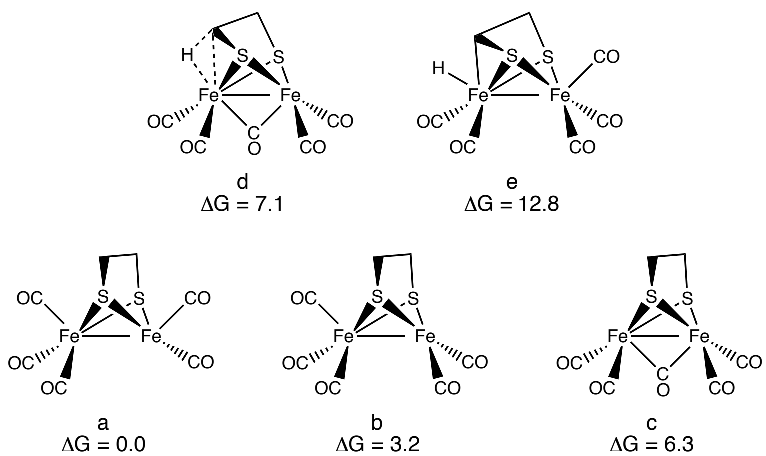

Scheme 4.7. TZP/TPSS-D3(BJ) DFT energies (kcal mol^{-1}) of the five lowest energy isomers of (μ-edt)[$Fe_2(CO)_5$].

As was found for the isomers of (μ-pdt)$Fe_2(CO)_5$, the only isomer of (μ-edt)$Fe_2(CO)_5$ that is calculated to have a vCO vibrational mode shifted to higher energy relative to any of those of the parent hexacarbonyl complex is the β-hydride activation product, 4.7e. DFT calculated energies for isomers of (μ-edt)$Fe_2(CO)_5$ show, that as expected, 4.7e is significantly higher in energy, 9.6 kcal mol^{-1}, relative to the apical carbonyl loss isomer. The barrier associated with β C-H activation and the conversion of 4.7b to 4.7e is also much higher than the analogous process for (μ-pdt)$Fe_2(CO)_5$, calculated to be 17.0 kcal mol^{-1}, Scheme 4.8. This high energetic expense for β-hydride activation in (μ-edt)$Fe_2(CO)_5$ is consistent with the minor population of 4.6e observed in these experiments compared to the matrix photochemistry (μ-pdt)$Fe_2(CO)_5$.

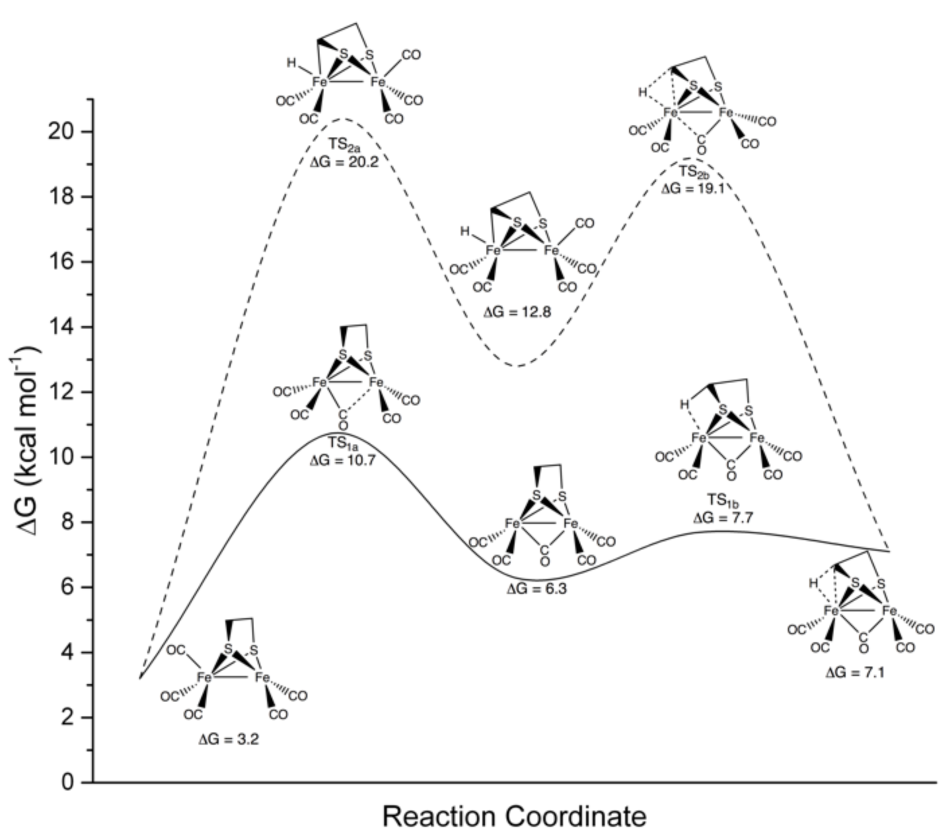

Scheme 4.8: TZP/TPSS-D3(BJ) DFT reaction pathway and energies (kcal mol^{-1}) for interconversion of isomers of (μ-edt)[$Fe_2(CO)_5$].

The major product, assigned to the basal carbonyl loss isomer, has similar band positions to those of the (μ-pdt)$Fe_2(CO)_5$ basal carbonyl loss species, and is calculated to be the lowest energy isomer of (μ-edt)$Fe_2(CO)_5$. Interestingly, the barrier for rotation of the $Fe(CO)_3$ moiety of 4.7b, a process that would yield the bridging carbonyl product 4.7c, is calculated to be 7.5 kcal mol^{-1} (Scheme 4.8, solid trace), much higher than that calculated for a similar process in (μ-pdt)$Fe_2(CO)_5$ (Scheme 4.5, solid trace). This increase in barrier energy, and decrease in barrier for the reverse process to 4.4 kcal mol^{-1}, may be responsible for the low abundance of the bridging carbonyl isomer in these matrix experiments and may also contribute to the observable population of the apical carbonyl loss isomer. Alternatively, formation of the bridging carbonyl isomer may be predicated upon the formation of the β-hydride activation product as was suggested in the photochemistry of the pdt bridged model complex. In this case, only a minor population of the β-hydride activated product is generated and available to undergo secondary rearrangement, resulting in the trace population of the bridging carbonyl isomer in the low-temperature matrix photolysis. The vibrational modes and structures of the observed photoproducts are summarized in Scheme 4.9.

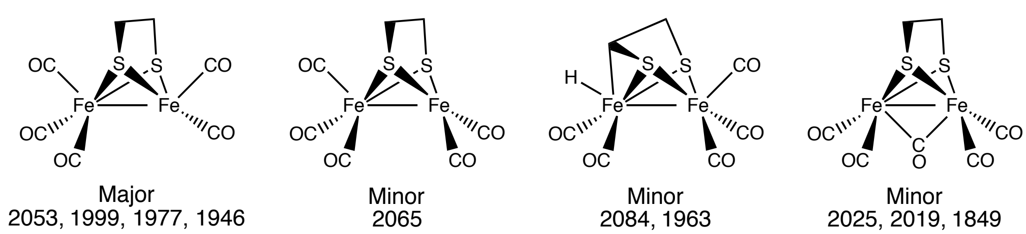

Scheme 4.9: Observed product vibrational modes (cm^{-1}) in the photochemistry of (μ-edt)$[Fe(CO)_3]_2$ in hydrocarbon matrices at 85 K.

Photolysis of (μ-mdt)[Fe(CO)$_3$]$_2$ at 85 K in Hydrocarbon Matrices

To further explore the influence of the length and flexibility of the alkyl dithiolate bridge upon the photochemistry of [FeFe]-hydrogenase model complexes, we next studied the (μ-mdt)[Fe(CO)$_3$]$_2$ (mdt = methanedithiolate) model complex, 1d. Despite the methanedithiolate bridge being more geometrically constrained than either of the pdt or edt alkyl dithiolate bridges, we anticipated facile formation of a C-H activated product due to the positioning of the CH_2 bridgehead near an iron apical coordination site. We reasoned that β-hydride activation would occur following a molecular vibration of the methaneditholate bridge within the Fe-Fe C_s plane subsequent to apical carbonyl photoejection, leading to a low-strain C-H activation product.

Photolysis of (μ-mdt)[Fe(CO)$_3$]$_2$ in a Nujol matrix at 85 K with λ_{irr} = 330 ± 70 nm results in bleaching of the parent νCO bands with concomitant appearance of "free" CO (2132 cm^{-1}) and product bands at 2083, 2068, 2055, 2027, 2013, 2001, 1978, 1947, and 1849 cm^{-1}, Figure 4.5. As anticipated, the high-energy νCO absorption characteristic of the β-hydride activation product is much more intense relative to the other photoproduct νCO bands when compared to the results of the (μ-edt)[Fe(CO)$_3$]$_2$ matrix photochemistry experiment, suggesting more facile activation of a mdt C-H bond.

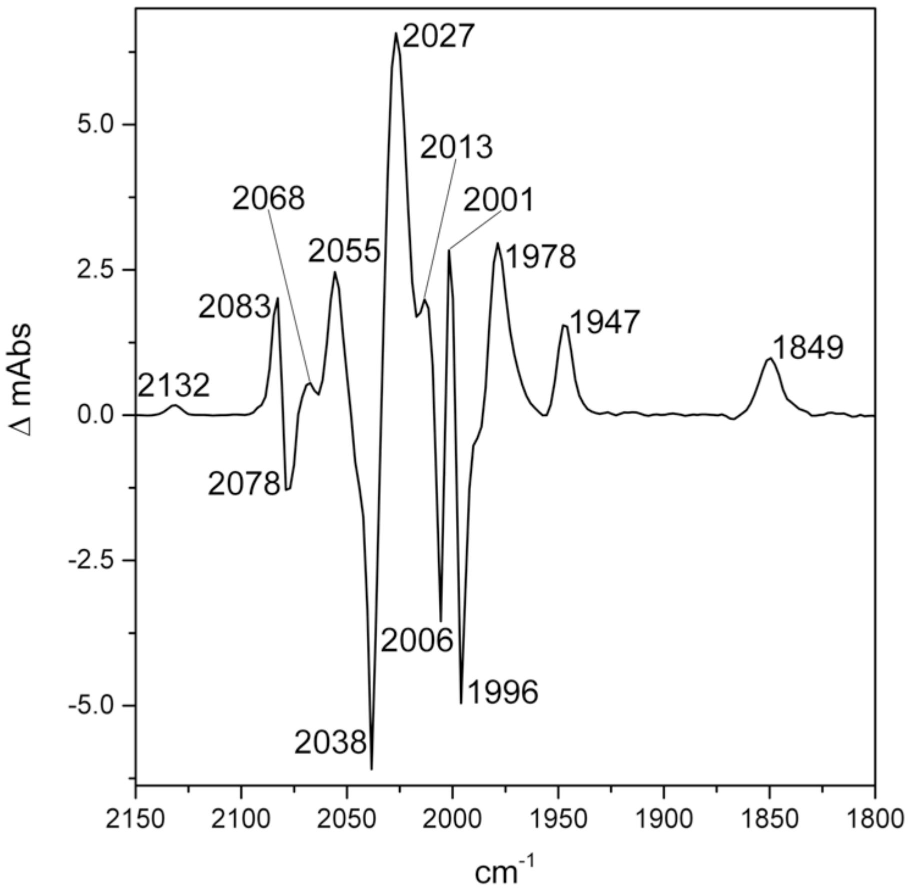

Figure 4.5: Photolysis of (μ-mdt)$[Fe(CO)_3]_2$ in glassy Nujol at 85 K. 15 minute 330 ± 70 nm irradiated sample minus unphotolyzed sample.

DFT computations on the isomers of (μ-mdt)$Fe_2(CO)_5$ reveal six stationary points, Scheme 4.10. The lowest energy geometry is again found to be the basal carbonyl loss isomer, 4.10a, with the apical carbonyl loss isomer, 4.10b, calculated to be just 1.0 kcal mol^{-1} higher in energy. Two isomers were found that possess a bridging carbonyl group, 4.10c, placed 1.8 kcal mol^{-1} above 4.10a, and 4.10e which has also undergone β-hydride activation of the mdt bridge placed 8.6 kcal mol^{-1} higher in energy than 4.10a. 4.10e is a unique geometry in the current study, among all of the alkyl dithiolate bridges studied, the mdt bridged complex is the only one found to have a stationary corresponding to a β-hydride activated bridging carbonyl complex. The remaining stationary points are the β-hydride activation product 4.10d, and the closely related β-hydride sigma complex, 4.10f. As was found in the previous experiments, the β-hydride activation isomer, 4.10d, is the only isomer calculated to have a νCO absorption shifted to higher energy relative to the parent hexacarbonyl complex.

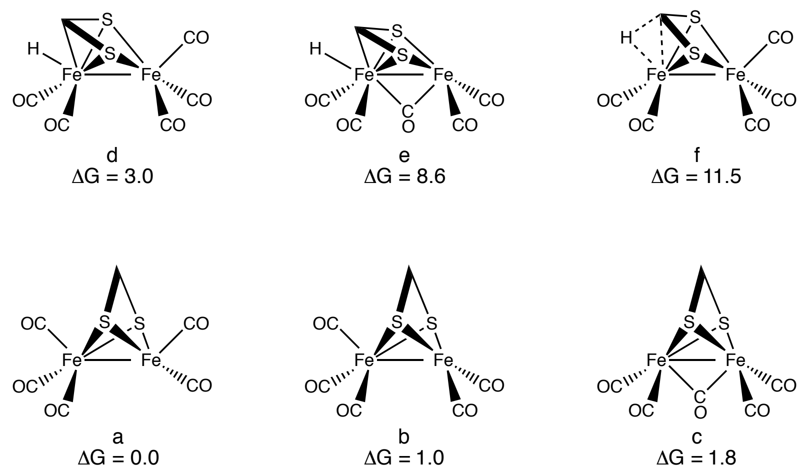

Scheme 4.10. TZP/TPSS-D3(BJ) DFT energies (kcal mol^{-1}) of the six lowest energy isomers of (μ-mdt)[$Fe_2(CO)_5$].

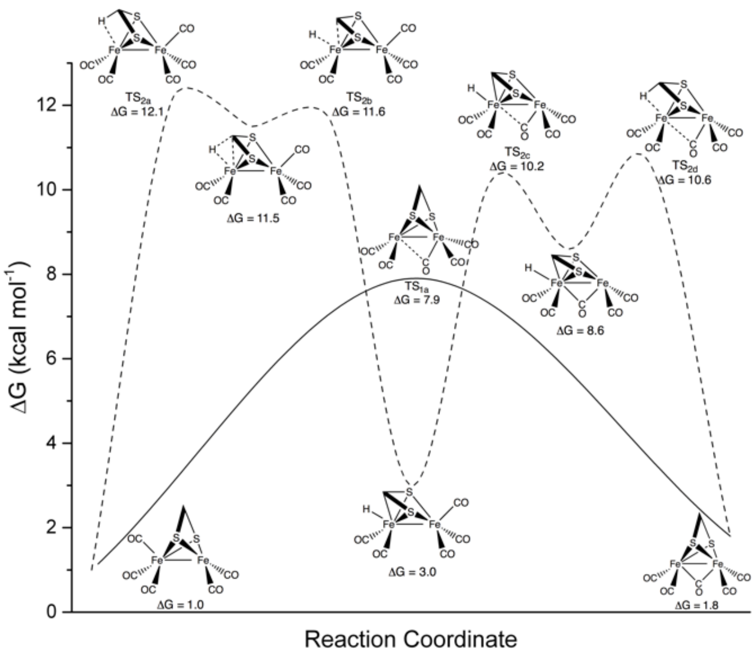

Scheme 4.11. TZP/TPSS-D3(BJ) DFT reaction pathway and energies (kcal mol^{-1}) for formation for C-H activated and bridging carbonyl isomers of (μ-mdt)[Fe(CO)$_3$]$_2$.

Exploring the potential energy surface of the apical carbonyl loss isomer of (μ-mdt)$Fe_2(CO)_5$, Scheme 4.11, reveals that the barrier for β-hydride activation of the mdt bridge to give isomer 4.10d is 4.11.1 kcal mol^{-1}, and is preceded by the formation of the β-hydride sigma complex 4.10f. This is significantly lower in energy than the analogous process for the edt bridged complex, placed at 17.0 kcal mol^{-1}, but still much higher than the 2.6 kcal mol^{-1} calculated for the pdt bridged model complex. The intermediate energy required for mdt β-hydride activation can be rationalized as being due to increased strain relative to the highly flexible pdt alkyl dithiolate bridged complex, but having lower strain relative to the edt bridged due to the position of the mdt C-H bond near the apical iron coordination site within the C_s plane of the molecule.

Two mechanisms were found that may result in the formation of the bridging carbonyl isomer 4.10c. In the first, simple rotation of the $Fe(CO)_3$ moiety of 4.10b may result in formation of the bridging carbonyl species 4.10c with a barrier of 6.9 kcal mol^{-1}. Alternatively, rotation of the $Fe(CO)_3$ moiety of the β-hydride activation product, 4.10d, may result in the formation of isomer 4.9e, which may then undergo C-H elimination of the mdt bridge to give isomer 4.10c with a barrier of 7.6 kcal mol^{-1}, Scheme 4.11 (dashed trace). It is unclear whether formation of the bridging carbonyl isomer in the low-temperature matrix photochemistry experiments proceeds exclusively through either of these mechanisms. The calculated barrier for rotation of the $Fe(CO)_3$ moiety of the apical carbonyl loss isomers of both the mdt and edt model complexes are very similar in energy, however, the bridging carbonyl isomer of (μ-edt)$Fe_2(CO)_5$ is only present as a trace photoproduct, whereas the bridging carbonyl isomer represents a major photoproduct in the photochemistry of (μ-mdt)$Fe_2(CO)_6$. This may be due to the bridging carbonyl loss isomer of (μ-mdt)$Fe_2(CO)_5$ being disfavored by just 0.8 kcal mol^{-1} relative to the apical carbonyl loss isomer versus 3.1 kcal mol^{-1} for the isomers of (μ-edt)$Fe_2(CO)_5$, leading to a greater population of the bridging isomer in the photoequilibrium of the mdt model complex. Alternatively, the results from the photochemistry of (μ-pdt)$Fe_2(CO)_5$ seem to suggest that the formation of the bridging carbonyl isomer is preceded by β-hydride activation of the alkyldithiolate bridge. In the present case, the greater population of the bridging carbonyl isomer in the photochemistry of (μ-mdt)$Fe_2(CO)_6$ relative to that of (μ-edt)$Fe_2(CO)_6$ could then be attributed to the more facile C-H bond activation of the methanedithiolate bridge relative to the 1,2-ethanedithiolate.

Using the results of DFT computations and the results of the above matrix photolysis experiments, we assign the species giving rise to the 2055, 2001, 1978, and 1947 cm^{-1} vibrational modes to the basal carbonyl loss isomer, 4.10a, and the 1968 cm^{-1} vibrational mode to a minor population of the apical carbonyl loss isomer, 4.10b. The bridging carbonyl isomer, 4.10c, is assigned to the 2027, 2013, and 1849 cm^{-1} absorptions. The remaining band at 2083 cm^{-1}, shifted to higher energy relative to the parent hexacarbonyl complex, is again assigned to the β-hydride activation product, 4.10d. The vibrational modes and structures of the observed photoproducts are summarized in Scheme 4.12.

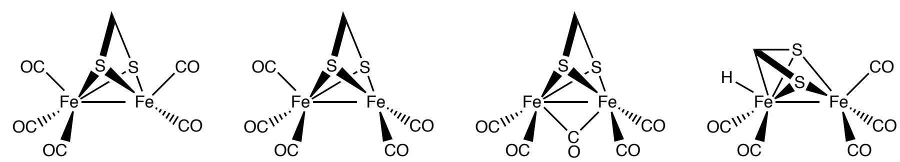

2055, 2001, 1978, 1947   2068   2027, 2013, 1849   2083

Scheme 4.12: Observed product vibrational modes (cm^{-1}) in the photochemistry of (μ-mdt)$[Fe(CO)_3]_2$ in hydrocarbon matrices at 85 K.

Photolysis of (μ-bdt)$[Fe(CO)_3]_2$ at 85 K in Hydrocarbon Matrices

Finally, we turned our attention towards the dithiolene bridged model complex (μ-bdt)$[Fe(CO)_3]_2$ (bdt = 1,2-benzenedithiolate), Scheme 4.1e. The absence of any C-H bonds on the dithiolene β-carbons eliminates the possibility of β-hydride activation, making this an attractive target for confirmation of the assignments made in the photochemistry of the alkyl dithiolate bridged complexes. The (μ-bdt)$[Fe(CO)_3]_2$

parent molecule exhibits five well-defined carbonyl stretching modes at 2079, 2044, 2004, 1969, and 1957 cm^{-1} in Nujol at 85 K.

Photolysis of (μ-bdt)$[Fe(CO)_3]_2$ with λ_{irr} = 400 ± 70 nm results in bleaching of the parent carbonyl vibrational modes and concomitant growth of a band at 2132 cm^{-1}, corresponding to matrix trapped CO, and appearance of product bands at 2065, 2056, 2009, 1995, 1987, 1980, 1953, and 1943 cm^{-1}, Figure 4.6a. Photolysis at higher energy, λ_{irr} = 330 ± 70 nm, results in the growth of bands at 2026, 2017 cm^{-1}, and a feature in the bridging carbonyl region at 1861 cm^{-1}, Figure 4.6b. Photolysis at these wavelengths also leads to reduction in the intensity of the 2065 and 1943 cm^{-1} absorptions relative to the 2056 and 1953 cm^{-1} photoproduct νCO vibrational modes. Warming of the hydrocarbon glass to 135 K results in recapture of liberated CO and reversion to the parent hexacarbonyl complex. Notably absent in these spectra are any product bands higher in energy relative to the parent hexacarbonyl complex that would be consistent with formal oxidation of a carbonyl loss photoproduct, supporting the assignment of β-hydride activation in the photochemistry of the alkyl dithiolate bridged model complexes.

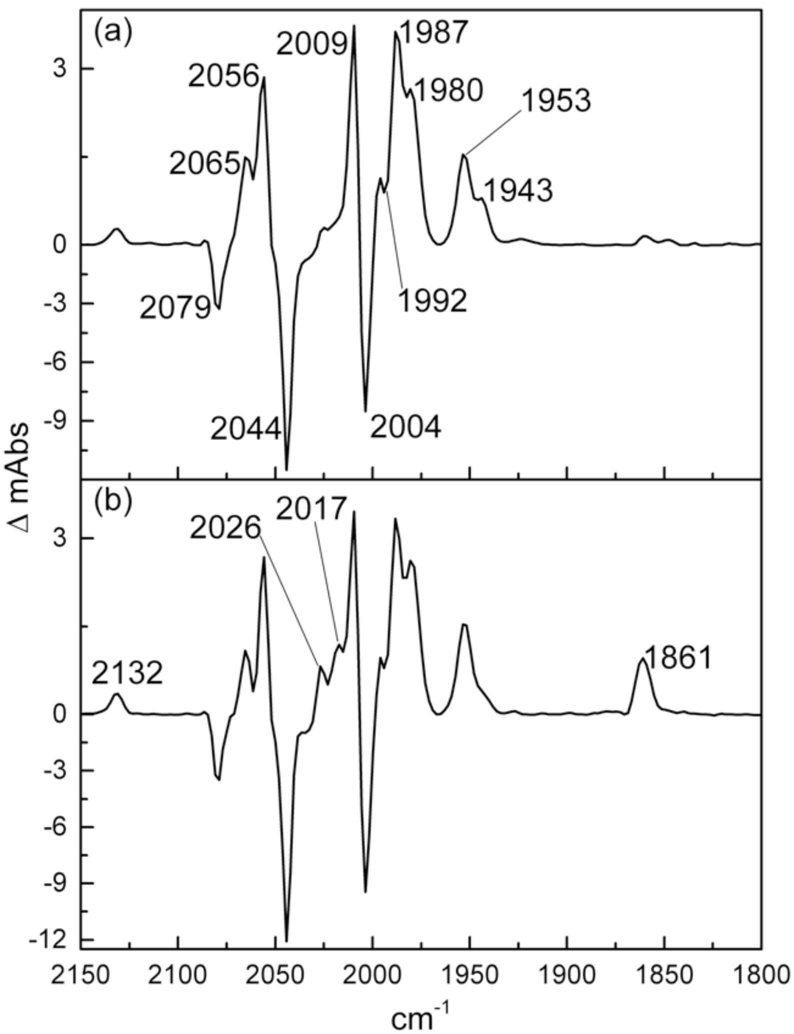

Figure 4.6. Photolysis of (μ-bdt)$[Fe(CO)_3]_2$ in glassy Nujol at 85 K. (a) 60 minute 400 ± 70 nm irradiated sample minus unphotolyzed sample. (b) 45 minute 330 ± 70 nm irradiated sample minus 400 ± 70 nm irradiated sample.

The products formed following λ_{irr} = 400 ± 70 nm photolysis are consistent with formation of two different CO loss products possessing solely terminal carbonyls, assigned to basal and apical CO loss isomers. With higher energy photolysis, λ_{irr} = 330 ± 70 nm, an isomer possessing a bridging carbonyl grows in exhibiting νCO modes at 2026, 2017, and 1861 cm^{-1} as well as a reduction in the relative population of the species responsible for the 2065 and 1943 cm^{-1}, suggesting that this species converts to the bridging carbonyl isomer at these wavelengths.

To understand the nature of the decarbonylation photoproducts of (μ-bdt)$Fe_2(CO)_6$, DFT computations were conducted on isomers of (μ-bdt)$Fe_2(CO)_5$. These computations resulted in the location of just four low-energy, singlet-state stationary points, Scheme 4.13. Interestingly, the lowest energy isomer is found to be a geometry possessing a bridging carbonyl and an FeS_2C_2 metallacycle coordinating the remaining Fe through an η^5 coordination mode, Scheme 4.13a. Isomers possessing vacant basal, 4.13b, and apical, 4.13c, coordination sites are located 5.2 and 7.1 kcal mol^{-1} higher in energy than 4.13a, respectively. The final stationary point, 13d, features an η^5-FeS_2C_2 metallacycle similar to 4.13a, but possesses solely terminal carbonyl groups, located 10.4 kcal mol^{-1} above isomer 4.13a. All but the basal CO loss isomer, 13b, were found to possess an element of C_s symmetry. No stationary points corresponding to a bridging carbonyl structure without an η^5-FeS_2C_2 were located. A C_{2v} bridging carbonyl structure in which the benzenedithiolate bridge is perpendicular to the Fe-Fe bond corresponds to a transition state for a “flopping” of η^5 coordination of the FeS_2C_2 group between the two irons with a barrier of 9.0 kcal mol^{-1}.

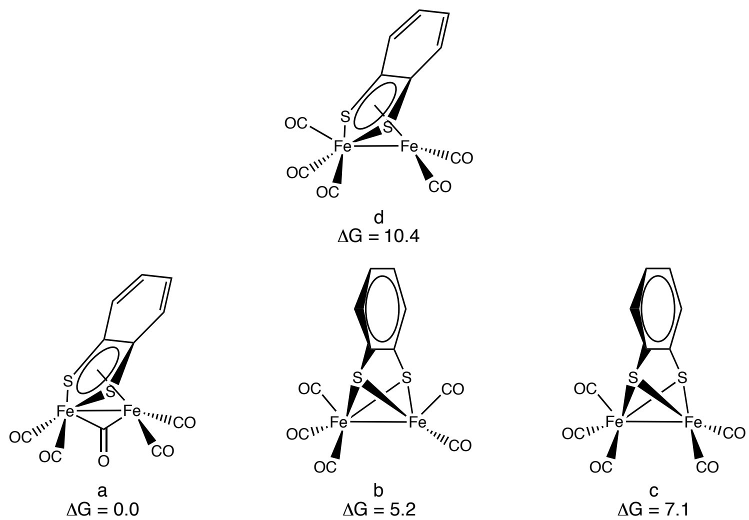

Scheme 4.13: TZP/TPSS-D3(BJ) DFT energies (kcal mol^{-1}) of the four lowest energy isomers of (μ-bdt)$Fe_2(CO)_5$.

Perhaps the most interesting result of these computations is the electronic structure of the two isomers possessing an η^5-FeS_2C_2 heterometallacycle. For structure 4.13a, the Fe-Fe, S-Fe, and C-Fe bond lengths of the η^5-FeS_2C_2 to the coordinated iron were found to be 2.53, 2.38, and 2.25 Å, respectively, while 4.13d had similar bond lengths of 2.54, 2.31, and 2.24 Å. Nucleus-independent chemical shift (NICS) calculations taken 1 Å above the plane of the ring structures results in values of -10.6 and -9.1 for the FeS_2C_2 and C_6H_4 rings, respectively for isomer 4.13a, and -13.6 and -9.6 for isomer 4.13d, consistent with these being aromatic metallacycles.[38,39] Additionally, examining the molecular orbitals of these isomers reveals a high degree of delocalization and nodal surfaces that are suggestive of the $FeS_2C_6H_4$ ring structure behaving as a 10 π-electron aromatic system, Figure 4.7. The recognition of aromatic metallacycle stationary points, while unexpected, is not necessarily surprising given the diverse chemistry of aromatic dithiolene complexes,[40-43] this is, however a rare example of an aromatic dithiolene metallacycle coordinating another metal through its π structure.

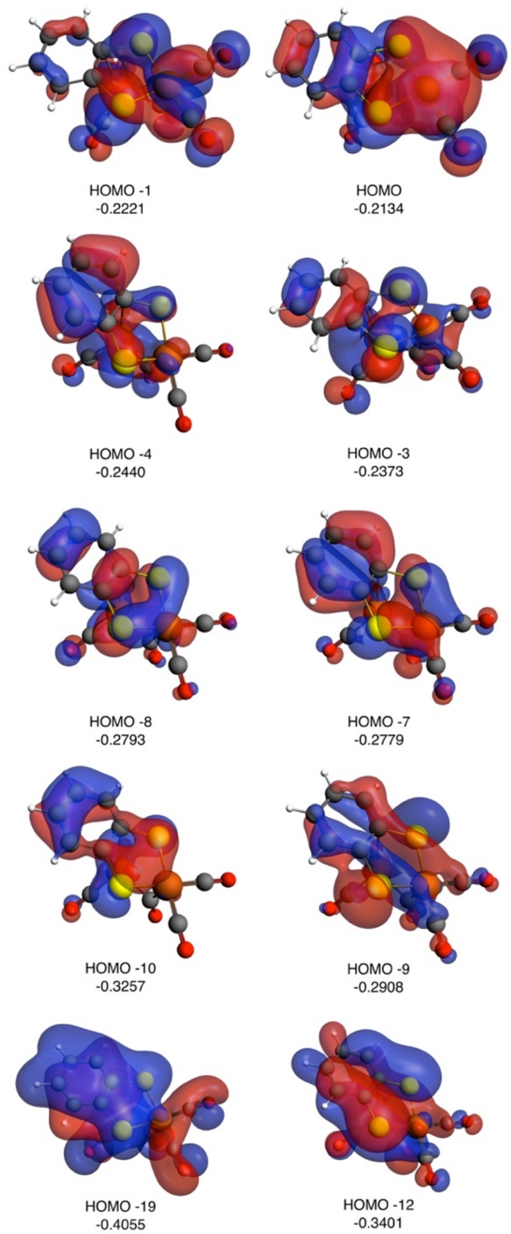

Figure 4.7: Molecular orbitals corresponding to nodal surfaces of delocalized $C_6H_4S_2Fe$ ring structure.

The potential energy surface of (μ-bdt)$Fe_2(CO)_5$ was surveyed to determine the energies associated with the formation of each of the four carbonyl loss isomers and how they may relate to one another, Scheme 4.14. A relatively small barrier of 3.9 kcal mol^{-1} associated with the collapse of the dithiolene bridge to an η^5 coordination mode to yield 4.13d from 4.13c was found. Rotation of the $Fe(CO)_3$ group of 13d is predicted to be effectively barrierless, resulting in formation of a bridging carbonyl and the (μ-bdt)$Fe_2(CO)_5$ global minima structure, 4.13a. This suggests that the 4.13d isomer is not a species present in the matrix photolysis, but is an intermediate in the formation of the bridging carbonyl species.

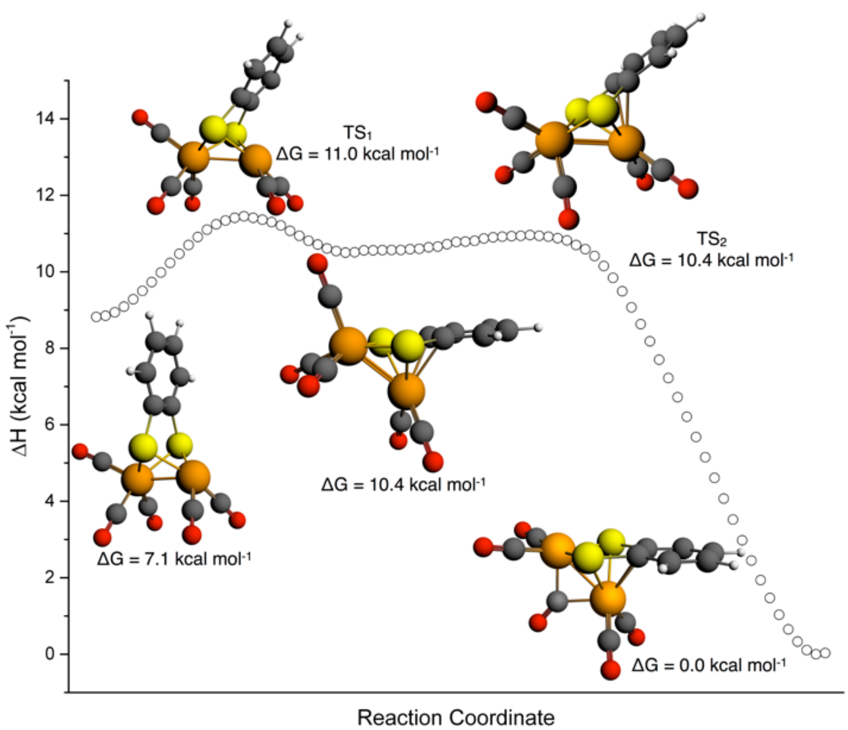

Scheme 4.14: TZP/TPSS-D3(BJ) reaction pathway for formation of bridging carbonyl species following photodecarbonylation of (μ-bdt)$[Fe(CO)_3]_2$.

Based on the results of DFT and variable wavelength matrix photochemistry experiments, we propose that irradiation of (μ-bdt)[$Fe(CO)_3]_2$ with λ_{irr} = 400 ± 70 nm results in both an apical carbonyl loss isomer (2065, 2009, 1987, 1943 cm^{-1}) and a basal carbonyl loss isomer (2056, 1980, 1953 cm^{-1}), Scheme 4.15. Photolysis at higher energies, λ_{irr} = 330 ± 70 nm, results in formation of these same isomers, however, a greater portion of the apical carbonyl loss isomer may retain the vibrational energy necessary to overcome the barrier associated with formation of the η^5-FeS_2C_2 structure, 4.13d, which then proceeds to form the bridging structure 4.13a (2026, 2017, 1861 cm^{-1}).

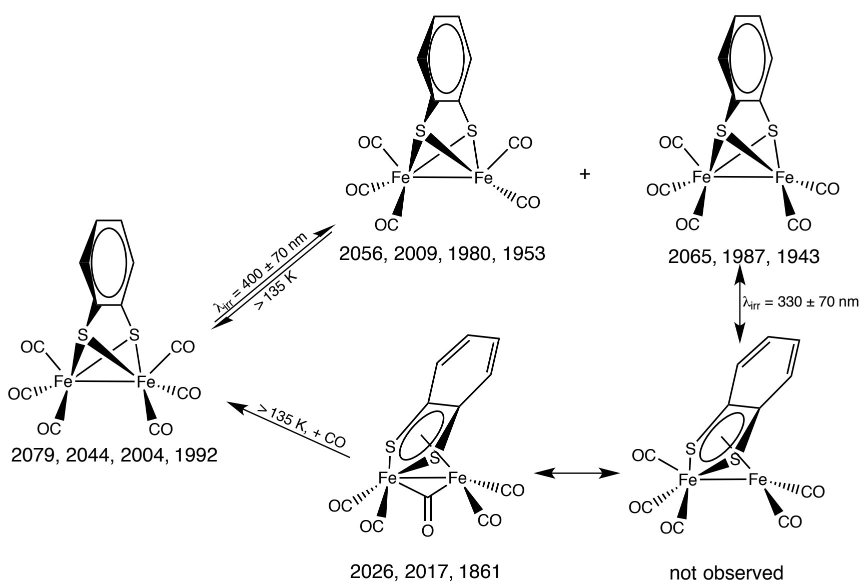

Scheme 4.15: Observed photochemical behaviour and product vibrational modes (cm^{-1}) of (μ-bdt)[$Fe(CO)_3]_2$ in hydrocarbon matrices at 85 K.

Conclusions

Photolysis of [FeFe]-hydrogenase model complexes in low-temperature matrices provides a much broader range of products than those observed in ultrafast solution studies. This is largely due to the ability of metastable photogenerated species to be maintained indefinitely at cryogenic temperatures and undergo multi-photon reactions, reaching an eventual photoequilibrium. For [FeFe]-hydrogenase model complexes possessing β-hydrogens on the dithiolate bridge, results from these low-temperature photolyses and DFT studies demonstrate that C-H bond activation of the dithiolate bridge occurs and results in reversible formation of a β-hydride activation product. Additionally, formation of photoproducts possessing bridging carbonyls, as found in the enzyme active site, are observed and appear to be preceded by β-hydride activation.

In the photolysis of (μ-bdt)$[Fe(CO)_3]_2$, which lacks any β-hydrogens that may undergo activation and has an element of unsaturation in the dithiol bridge, formation of a 10 π aromatic metallacycle is observed in addition to the initial apical and basal carbonyl loss products. This aromatic photoproduct appears to be a rare instance in which a dithiolene based aromatic metallacycle is able to coordinate another metal through the π structure resulting in an η^5 coordination mode.

Experimental

All complexes were prepared by reported procedures.[16,36,44-46] The apparatus and methods for matrix photochemistry have been reported elsewhere.[47] All DFT calculations were performed in the Amsterdam Density Functional (ADF2014.02) program.[48-50] Electronic configurations of atoms were described by an all-electron triple-ζ Slater-type orbital basis set modified by a polarization function (TZP STO).[51] Geometry optimizations and vibrational frequency calculations were performed using the GGA functional of Becke[52] and Perdew[53,54] as well as the dispersion corrected meta-GGA TPSS-D3(BJ).[55-57] The intrinsic reaction coordinate (IRC) of all calculated transition state geometries was followed to confirm the relation to the expected stationary points. Electronic excitation energies were computed using the statistical average of orbital potentials (SAOP) model,[32,33] with cyclohexane solvent interactions modelled using the COSMO model.[58-60]

References

(1) Evans, D. J.; Pickett, C. J. *Chem. Soc. Rev.* **2003**, *32* (5), 268–275.

(2) Frey, M. *Chembiochem* **2002**, *3* (2-3), 153–160.

(3) Vincent, K. A.; Parkin, A.; Armstrong, F. A. *Chem. Rev.* **2007**, *107* (10), 4366–4413.

(4) Bullock, R. M.; Appel, A. M.; Helm, M. L. *Chem. Commun.* **2014**, *50* (24), 3125–3143.

(5) Cracknell, J. A.; Vincent, K. A.; Armstrong, F. A. *Chem. Rev.* **2008**, *108* (7), 2439–2461.

(6) Yang, J. Y.; Smith, S. E.; Liu, T.; Dougherty, W. G.; Hoffert, W. A.; Kassel, W. S.; DuBois, M. R.; DuBois, D. L.; Bullock, R. M. *J. Am. Chem. Soc.* **2013**, *135* (26), 9700–9712.

(7) Darensbourg, M. Y.; Lyon, E. J.; Smee, J. J. *Coord. Chem. Rev.* **2000**, *206*, 533–561.

(8) DuBois, D. L. *Inorg. Chem.* **2014**, *53* (8), 3935–3960.

(9) Helm, M. L.; Stewart, M. P.; Bullock, R. M.; DuBois, M. R.; DuBois, D. L. *Science* **2011**, *333* (6044), 863–866.

(10) Nicolet, Y.; Piras, C.; Legrand, P.; Hatchikian, C. E.; Fontecilla-Camps, J. C. *Structure* **1999**, *7* (1), 13–23.

(11) Fontecilla-Camps, J. C.; Volbeda, A.; Cavazza, C.; Nicolet, Y. *Chem. Rev.* **2007**, *107* (10), 4273–4303.

(12) Nicolet, Y.; de Lacey, A. L.; Vernède, X.; Fernandez, V. M.; Hatchikian, E. C.; Fontecilla-Camps, J. C. *J. Am. Chem. Soc.* **2001**, *123* (8), 1596–1601.

(13) Schilter, D.; Rauchfuss, T. B. *Angew. Chem. Int. Ed. Engl.* **2013**, *52* (51), 13518–13520.

(14) Wiese, S.; Kilgore, U. J.; Ho, M.-H.; Raugei, S.; DuBois, D. L.; Bullock, R. M.; Helm, M. L. *ACS Catal.* **2013**, *3* (11), 2527–2535.

(15) Hulley, E. B.; Welch, K. D.; Appel, A. M.; DuBois, D. L.; Bullock, R. M. *J. Am. Chem. Soc.* **2013**, *135* (32), 11736–11739.

(16) Li, H.; Rauchfuss, T. B. *J. Am. Chem. Soc.* **2002**, *124* (5), 726–727.

(17) Gloaguen, F.; Rauchfuss, T. B. *Chem. Soc. Rev.* **2008**, *38* (1), 100–108.

(18) Tard, C.; Pickett, C. J. *Chem. Rev.* **2009**, *109* (6), 2245–2274.

(19) Darensbourg, M. Y.; Lyon, E. J.; Zhao, X.; Georgakaki, I. P. *Proc. Natl. Acad. Sci. U.S.A.* **2003**, *100* (7), 3683–3688.

(20) Singleton, M. L.; Bhuvanesh, N.; Reibenspies, J. H.; Darensbourg, M. Y. *Angew. Chem. Int. Ed. Engl.* **2008**, *47* (49), 9492–9495.

(21) Lawrence, J. D.; Li, H.; Rauchfuss, T. B. *Chem. Commun.* **2001**, No. 16, 1482–1483.

(22) Liu, T.; Darensbourg, M. Y. *J. Am. Chem. Soc.* **2007**, *129* (22), 7008–7009.

(23) Lemon, B. J.; Peters, J. W. *J. Am. Chem. Soc.* **2000**, *122* (15), 3793–3794.

(24) Chen, Z.; Lemon, B. J.; Huang, S.; Swartz, D. J.; Peters, J. W.; Bagley, K. A. *Biochemistry* **2002**, *41* (6), 2036–2043.

(25) Kowal, A. T.; Adams, M. W.; Johnson, M. K. *Journal of Biological Chemistry* **1989**, *264* (8), 4342–4348.

(26) Brown-McDonald, J.; Berg, S.; Peralto, M.; Works, C. *Inorganica Chimica Acta* **2009**, *362* (2), 318–324.

(27) Marhenke, J.; Pierri, A. E.; Lomotan, M.; Damon, P. L.; Ford, P. C.; Works, C. *Inorg. Chem.* **2011**, *50* (23), 11850–11852.

(28) Ridley, A. R.; Stewart, A. I.; Adamczyk, K.; Ghosh, H. N.; Kerkeni, B.; Guo, Z. X.; Nibbering, E. T. J.; Pickett, C. J.; Hunt, N. T. *Inorg. Chem.* **2008**, *47* (17), 7453–7455.

(29) Kaziannis, S.; Santabarbara, S.; Wright, J. A.; Greetham, G. M.; Towrie, M.; Parker, A. W.; Pickett, C. J.; Hunt, N. T. *J. Phys. Chem. B* **2010**, *114* (46), 15370–15379.

(30) Bingaman, J. L.; Kohnhorst, C. L.; Van Meter, G. A.; McElroy, B. A.; Rakowski, E. A.; Caplins, B. W.; Gutowski, T. A.; Stromberg, C. J.; Webster, C. E.; Heilweil, E. J. *J. Phys. Chem. A* **2012**, *116* (27), 7261–7271.

(31) Stewart, A. I.; Wright, J. A.; Greetham, G. M.; Kaziannis, S.; Santabarbara, S.; Towrie, M.; Parker, A. W.; Pickett, C. J.; Hunt, N. T. *Inorg. Chem.* **2010**, *49* (20), 9563–9573.

(32) Gritsenko, O. V.; Schipper, P.; Baerends, E. J. *Chem Phys Lett* **1999**, *302*, 199–207.

(33) Schipper, P. R. T.; Gritsenko, O. V.; van Gisbergen, S. J. A.; Baerends, E. J. *J. Chem. Phys.* **2000**, *112* (3), 1344.

(34) Fiedler, A. T.; Brunold, T. C. *Inorg. Chem.* **2005**, *44* (6), 1794–1809.

(35) Jacob, C. R.; Reiher, M. *Int. J. Quant. Chem.* **2012**, *112* (23), 3661–3684.

(36) Seyferth, D.; Womack, G. B.; Gallagher, M. K.; Cowie, M. *Organometallics* **1987**, *6* (2), 283–294.

(37) Zheng, D.; Wang, N.; Wang, M.; Ding, S.; Ma, C.; Darensbourg, M. Y.; Hall, M. B.; Sun, L. *J. Am. Chem. Soc.* **2014**, *136* (48), 16817–16823.

(38) Schleyer, P. R.; Maerker, C.; Dransfeld, A. *J. Am. Chem. Soc.* **1996**, *118*, 6317–6318.

(39) Mauksch, M.; Tsogoeva, S. B. *Chem. Eur. J.* **2010**, *16* (26), 7843–7851.

(40) Schrauzer, G. N.; Mayweg, V. P.; Finck, H. W. *J. Am. Chem. Soc.* **1966**, *88* (20), 4604–4609.

(41) Cui, Y.-H.; Tian, W. Q.; Feng, J.-K.; Li, W.-Q.; Liu, Z.-Z. *Journal of Molecular Structure: THEOCHEM* **2009**, *897* (1-3), 61–65.

(42) Damas, A.; Chamoreau, L.-M.; Cooksy, A. L.; Jutand, A.; Amouri, H. *Inorg. Chem.* **2013**, *52* (3), 1409–1417.

(43) Schrauzer, G. N. *Acc. Chem. Res.* **1969**, *2* (3), 72–&.

(44) Li, P.; Wang, M.; He, C.; Li, G.; Liu, X.; Chen, C.; Åkermark, B.; Sun, L. *Eur. J. Inorg. Chem.* **2005**, *2005* (12), 2506–2513.

(45) Wright, J. A.; Webster, L.; Jablonskytė, A.; Woi, P. M.; Ibrahim, S. K.; Pickett, C. J. *Faraday Discuss.* **2010**, *148*, 359.

(46) Cabeza, J. A.; Martinez-Garcia, M. A.; Riera, V.; Ardura, D.; Garcia-Granda, S. *Organometallics* **1998**, *17* (8), 1471–1477.

(47) Bays, J. T.; Bitterwolf, T. E.; Lott, K. A.; Ollino, M. A.; Rest, A. J.; Smith, L. M. *J. Organomet. Chem.* **1998**, *554* (1), 75–85.

(48) ADF2013, SCM, Theoretical Chemistry, Vrije Universiteit, Amsterdam, The Netherlands, http://www.scm.com

(49) Guerra, C. F.; Snijders, J. G.; Velde, Te, G.; Baerends, E. J. *Theor. Chem. Acc.* **1998**, *99*, 391–403.

(50) Velde, Te, G.; Bickelhaupt, F. M.; Baerends, E. J.; Fonseca Guerra, C.; van Gisbergen, S. J. A.; Snijders, J. G.; Ziegler, T. *J. Comp. Chem.* **2001**, *22* (9), 931–967.

(51) Lenthe, E. V.; Baerends, E. J. *J. Comp. Chem.* **2003**, *24* (9), 1142–1156.

(52) Becke, A. D. *Phys. Rev. A* **1988**, *38* (6), 3098–3100.

(53) Perdew, J. *Phys. Rev. B* **1986**, *33* (12), 8822–8824.

(54) Perdew, J. *Phys. Rev. B* **1986**, *34* (10), 7406–7406.

(55) Tao, J.; Perdew, J.; Staroverov, V.; Scuseria, G. *Phys. Rev. Lett.* **2003**, *91* (14), 146401.

(56) Grimme, S.; Antony, J.; Ehrlich, S.; Krieg, H. *J. Chem. Phys.* **2010**, *132* (15), 154104.

(57) Grimme, S.; Ehrlich, S.; Goerigk, L. *J. Comp. Chem.* **2011**, *32* (7), 1456–1465.

(58) Klamt, A.; Schüürmann, G. *J. Chem. Soc., Perkin Trans. 2* **1993**, No. 5, 799.

(59) Klamt, A. *J. Phys. Chem.* **1995**, *99* (7), 2224–2235.

(60) Klamt, A.; Jonas, V. *J. Chem. Phys.* **1996**, *105* (22), 9972–11.

Chapter 5: Rotameric Transformations in the Photochemistry of $TpM(CO)_2(\eta^3\text{-}C_3H_4R)$, where Tp=tris(pyrazolyl)borate, M=Mo or W, and R=H or Me

Published: W. A. Thornley, T. E. Bitterwolf, Dalton Trans. **2015**, *44*, 8007–8012.

Abstract: *Low energy photolysis of $TpM(CO)_2(\eta^3\text{-}C_3H_4R)$, where Tp=tris(pyrazolyl)borate, M=Mo or W, and R=2-H or 2-Me in PVC matrices at 85 K results in exo/gauche isomerism of the allyl ligand. This transformation comes in contrast to the behaviour observed in cyclopentadienyl analogues which undergo exo/endo isomerism. DFT computations reveal an $\eta^3 \rightarrow \eta^{1*} \rightarrow \eta^3$ mechanism for the allyl rotameric interconversion where the η^{1*}-allyl intermediate is generated upon MLCT excitation.*

Introduction

Rotameric fluxionality of the allyl ligand in transition metal complexes is a long recognized process for this class of compounds.[1-4] The interconversion between *endo* and *exo* forms of the allyl rotamers is known to occur both thermally and photochemically.[5,6] Experimental evidence for two mechanisms of the thermal isomerism have been reported, one occurring through rotation along the metal-allyl axis with retention of the η^3 bonding mode,[4,7] as well as through an η^1-allyl intermediate.[5,8] A theoretical study suggests that the degree of antibonding character between the metal and ancillary ligands in the η^3 rotational transition state dictates which of the two isomerism mechanisms is favored; rotation along the metal-allyl axis being preferred when only a small degree of antibonding character is present in the transition state, and the $\eta^3 \rightarrow \eta^1 \rightarrow \eta^3$ mechanism being preferred when a high degree of metal-ligand antibonding is present in the η^3 rotational transition state.[9]

In 1967, Trofimenko reported the synthesis of $TpM(CO)_2(\eta^3\text{-}C_3H_4R)$ (Tp = trispyrazolylborate, M = Mo, W and R = H, Me), through the reaction of $TpM(CO)_3^-$ with the corresponding allyl halide.[10] In subsequent publications, the solution dynamics of these fluxional molecules were studied through variable temperature NMR and evidence for rotation of the Tp ligand about the B-M axis was found, but nothing was observed to suggest rotation of the allyl ligand.[11,12] In CH_2Cl_2 solution, these compounds exhibit only two vibrational modes in the metal carbonyl stretching region. The simplicity of this spectrum suggests the presence of a single allyl rotamer in solution. More than two carbonyl vibrational bands, or significant asymmetry arising from overlapping absorptions, would be expected if multiple isomers were present in solution.

The crystal structure of $TpMo(CO)_2(\eta^3$-2-methylallyl) has been reported previously.[13] Perhaps unexpectedly due to steric considerations, the allyl ligand is found in the *exo* rotameric form with the allyl methyl group oriented towards the trispyrazolylborate ligand. This comes in contrast to the analogous cyclopentadienyl compounds that favor the *endo* rotamer with the allyl methyl group facing away from the cyclopentadienyl ring.[4,7,14-16] For $TpMo(CO)_2(\eta^3\text{-}C_3H_4Me)$, the Mo-allyl bond lengths are 2.337(5) and 2.364(4) Å for the terminal carbons with the bond to the central allyl carbon slightly shorter at 2.258(4) Å.

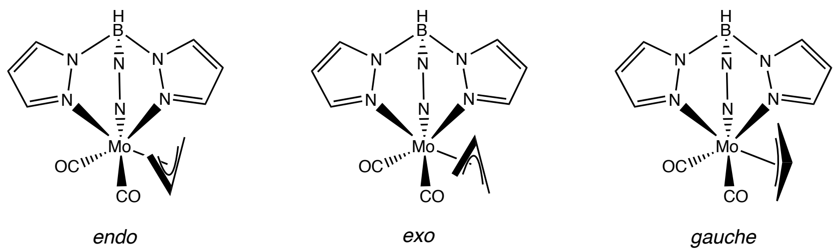

Scheme 5.1: Possible allyl rotamers of $TpMo(CO)_2(\eta^3-C_3H_5)$.

Previous work from our group has established that wavelength dependent photolysis of isoelectronic $CpM(CO)_2(\eta^3-C_3H_4R)$ (M = Mo and R = H, Me) results in selective population of either the *exo* or *endo* rotameric forms, Scheme 5.2.[6] As an extension of these studies, we sought to examine the photochemistry of the corresponding Tp compounds to study the influence of the increased steric demands of the trispyrazolylborate ligand on the allyl rotamers.

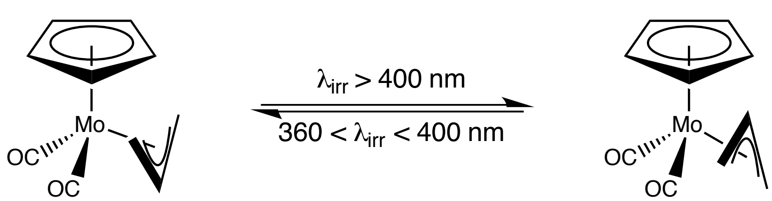

Scheme 5.2: Photochemical rotameric isomerism of the allyl ligand of $CpMo(CO)_2(\eta^3-C_3H_5)$.

Table 5.1: DFT calculated energies (kcal mol^{-1}) and CO vibrational frequencies (cm^{-1}) for rotamers of $TpM(CO)_2(\eta^3\text{-}C_3H_4R)$.

M	R	*exo*			*gauche*			*endo*		
		ΔH	ΔG	νCO (sym, antisym)	ΔH	ΔG	νCO (sym, antisym)	ΔH	ΔG	νCO (sym, antisym)
Mo	H	0.0	0.0	1926, 1859	6.6	6.5	1928, 1850	7.8	7.8	1929, 1860
Mo	Me	0.0	0.0	1925, 1857	5.7	5.2	1931, 1840	6.1	6.0	1922, 1853
W	H	0.0	0.0	1921, 1852	7.0	7.0	1919, 1847	8.6	8.7	1923, 1854
W	Me	0.0	0.0	1921, 1853	5.2	6.6	1918, 1843	6.1	7.6	1915, 1844

Results and Discussion

PVC Matrix Photochemistry at 85 K

Photolysis of $TpM(CO)_2(\eta^3\text{-}C_3H_4R)$ (M = Mo, W and R = H, Me) with λ_{irr} = 450 ± 50 nm results in bleaching of the parent vibrational bands with concomitant growth of two new product bands; no new absorbance assignable to "free" CO is present, Figure 5.1. This photoproduct displays an apparent shift of the antisymmetric CO vibrational mode to lower energy, whereas the symmetric CO stretching mode shifts to higher energy. A simple *exo/endo* rotameric isomerization would be expected to result in a shift of both vibrational bands to either higher or lower energy dependent upon the donor/acceptor ability of the two rotameric forms due to retention of approximate C_s molecular symmetry. The shift of the antisymmetric CO mode to lower energy and increase in energy of the symmetric CO mode may be attributed to a more pronounced change in molecular symmetry. In the present case, this may correspond to a photogenerated *gauche* rotamer that would possess only an element of C_1 symmetry. Back photolysis of the λ_{irr} = 450 ± 50 nm irradiated sample with λ_{irr} = 550 ± 50 nm results in reversion to the parent complex. Annealing the λ_{irr} = 450 ± 50 nm irradiated sample to ca. 155 K also results in reversion to the parent complex. Prolonged λ_{irr} = 550 ± 50 nm photolysis of a sample prepared in the dark exhibits no growth of bands assignable to the *exo* rotamer, suggesting that a single isomer is present in PVC matrices at these temperatures.

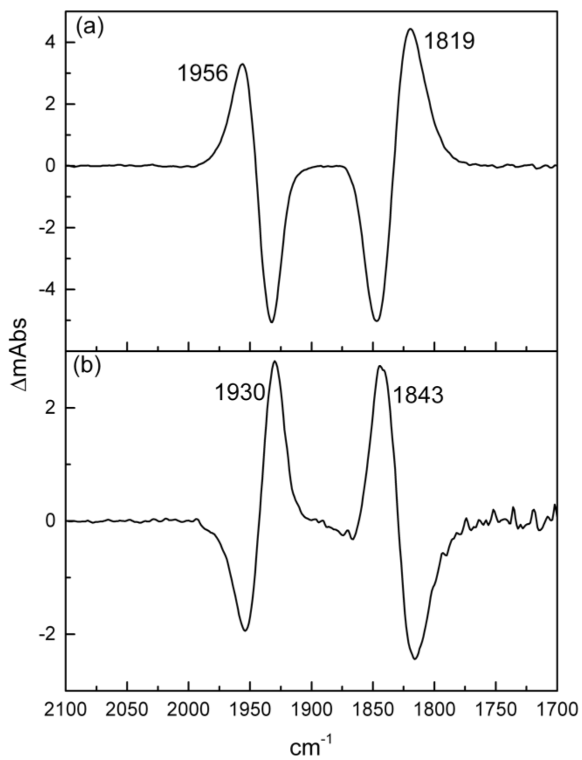

Figure 5.1: Photolysis of $TpMo(CO)_2(\eta^3\text{-}C_3H_5)$ in PVC at 85 K. (a) Difference spectrum obtained following λ_{irr} = 450 ± 50 nm photolysis of unphotolyzed sample. (b) Difference following λ_{irr} = 550 ± 50 nm back photolysis of λ_{irr} > 450 nm irradiated sample.

DFT Study

Potential Energy Surface Along the η^3-C_3H_5 Rotational Axis

To gain a clearer understanding of the observed photochemical behaviour, a DFT investigation was carried out in order to identify stationary points along the η^3-C_3H_4R rotational axis. For the four complexes studied, each was found to possess local minima featuring the allyl ligand in *exo*, *gauche*, and *endo* rotameric forms, the results of these calculations are summarized in Table 5.1. In all cases, the *exo* rotamer was found to be the lowest energy conformation followed by *gauche* and *endo*. For $TpMo(CO)_2(\eta^3$-$C_3H_5)$, the transition state between the *exo* and *gauche* rotamers was calculated to lay 9.7 kcal mol^{-1} higher in energy than the *exo* geometry. The transition state for the *gauche* to *endo* transformation was placed at 1.3 kcal mol^{-1}. Interestingly, for all four complexes, the local minima of the *endo* rotamer is calculated to be exceedingly shallow with the transition state for the *endo* to *gauche* rotameric isomerism calculated to be less than ca. 0.2 kcal mol^{-1}, Figure 5.2. The near barrierless *endo* → *gauche* isomerization suggests that if the *endo* isomer were produced photochemically in the matrix, it would likely retain sufficient energy to relax to the *gauche* rotamer even at cryogenic temperatures.

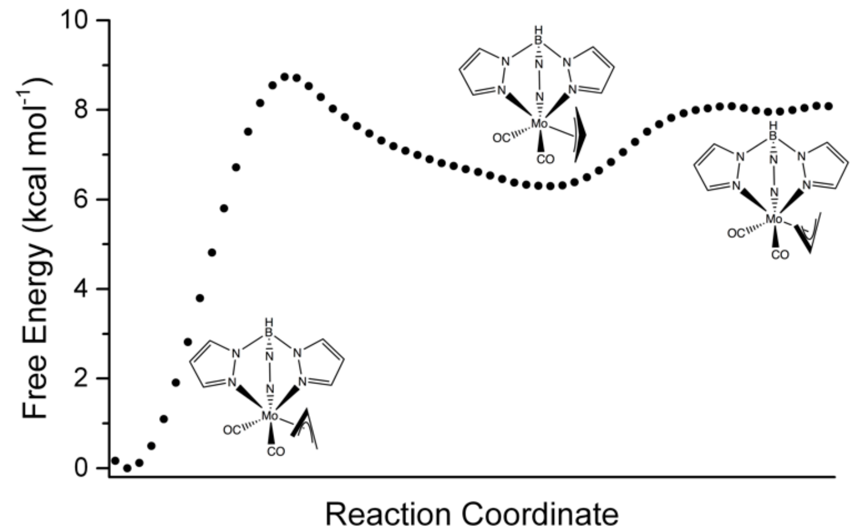

Figure 5.2: Calculated energy surface along the η^3-C_3H_5 rotational mode.

For M = Mo, DFT calculated νCO frequencies are consistent with the assignment of photochemical generation of the *gauche* rotamer at 85 K. Relative to the *exo* rotamer, the symmetric νCO mode of the *gauche* form is calculated to be higher in energy while the antisymmetric νCO mode lower in energy. For M = W, both the symmetric and antisymmetric νCO vibrational modes of the *gauche* rotamers are calculated to be lower in energy relative to those of the *exo* rotamers, though the symmetric νCO modes are effectively degenerate.

In the *gauche* orientation, the Mo-allyl bond lengths are calculated at 2.360 and 2.377 Å for the terminal carbons while the bond to the central carbon is placed at 2.313 Å. The similar Mo-C bond lengths demonstrate that the allyl ligand is coordinating roughly equally in an η^3 manner between each of the allyl carbons; the change to *gauche* orientation is not the result of the formation of a 17-electron complex with the allyl group coordinating in an η^2 fashion.

Frontier orbitals for the *exo*⟷*gauche* (TS_1) and *gauche*⟷*endo* (TS_2) transition states are presented in Figure 5.3. In both cases the HOMO corresponds to orbitals that are dominated by backbonding interactions between metal d and CO π^* orbitals. This interaction may lead to a stabilizing effect on the rotational transition states that results in the low computed energy barrier. What remains unclear is why no evidence for rotation of the allyl ligand has been observed in previous NMR experiments or in the current solution study.[11,12,17] It is possible that the rotational barrier is sufficiently low in energy that the experiments conducted in $CDCl_3$ solvent simply were unable to attain a low enough temperature to observe any broadening or coalescence of the allyl ^1H resonances. However, this argument fails to account for the presence of only a single rotamer in the current PVC matrix photolyses.

The energies for an electronic ground state $\eta^3 \rightarrow \eta^1 \rightarrow \eta^3$ isomerism mechanism were also computed. The barrier for this pathway was calculated to be substantially higher than the $\eta^3 \rightarrow \eta^3 \rightarrow \eta^3$ rotational mechanism at ca. 32 kcal mol^{-1} and was not considered further as a ground state rotational mechanism.

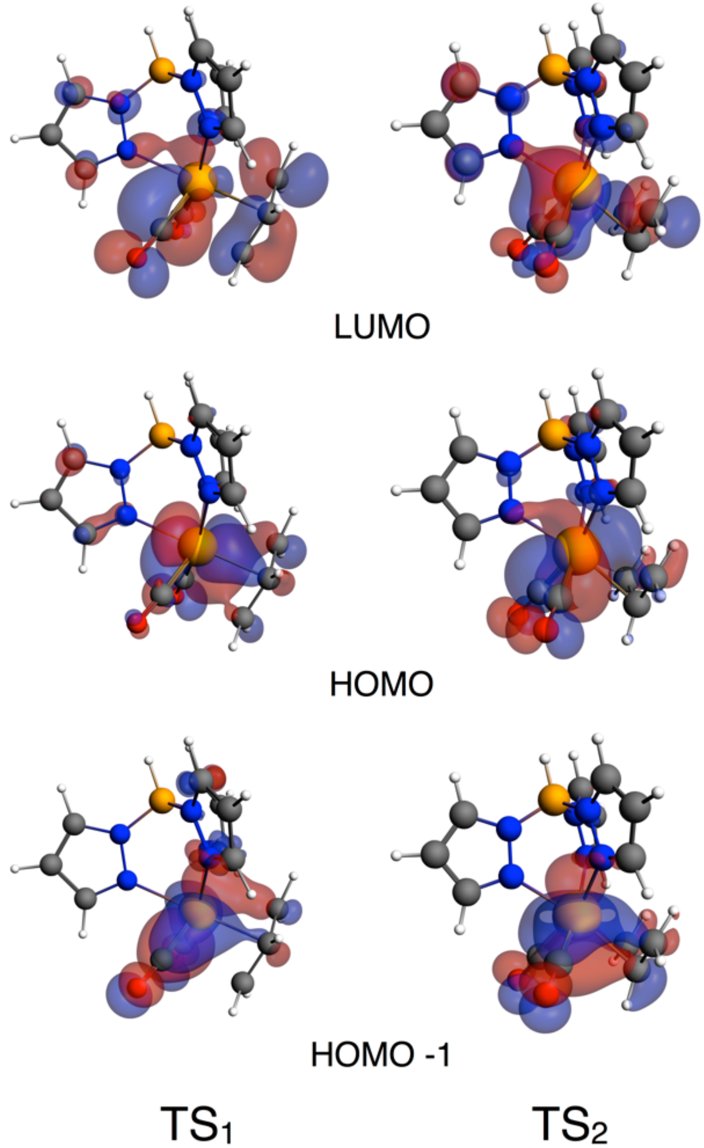

Figure 5.3: Frontier orbitals of the *exo*↔*gauche* (TS_1) and *gauche*↔*endo* (TS_2) transitions states.

Electronic Structure of TpM(CO)$_2$(η^3-C_3H_4R)

The electronic spectra of TpM(CO)$_2$(η^3-C_3H_4R) are presented in Figure 5.4. For M = Mo, the primary feature in the region of the spectrum that the observed photochemical transformation occurs is an absorbance with maxima centered at 378 nm (ε = 1.35 and 1.38 x 10^3 M^{-1} cm^{-1} for R = H, Me respectively) with a tail that extends to ca. 510 nm. For M = W, this band is slightly blue shifted, centered at 368 nm (ε = 1.68 and 1.74 x 10^3 M^{-1} cm^{-1} for R = H, Me respectively), with a tail extending to ca. 500 nm. Time-dependent density functional theory (TD-DFT) calculations of electronic excitation energies using the statistical average of model orbital potentials (SAOP) model suggest that this low energy absorption consists of two overlapping electronic transitions, a HOMO→LUMO excitation (3.260 eV) and a HOMO-1→LUMO excitation (3.355 eV), Figure 5.5. For the *exo* geometry, the HOMO-1 orbital predominantly corresponds to a bonding interaction between the allyl π* antibonding orbital with the metal d_{xz}, d_{z^2}, and d_{yz} orbitals. The HOMO is dominated by a bonding interaction between the metal $d_{x^2-y^2}$ orbital and CO π* orbitals. Finally, the LUMO is composed primarily of an antibonding interaction between the metal d_{xy} orbital with the allyl π non-bonding orbital. Excitation from either the HOMO or HOMO-1 into the LUMO would be expected to result in reduction of the bond order between the metal and allyl fragment that may facilitate the rotameric isomerization observed in the low-temperature matrix photolysis experiments.

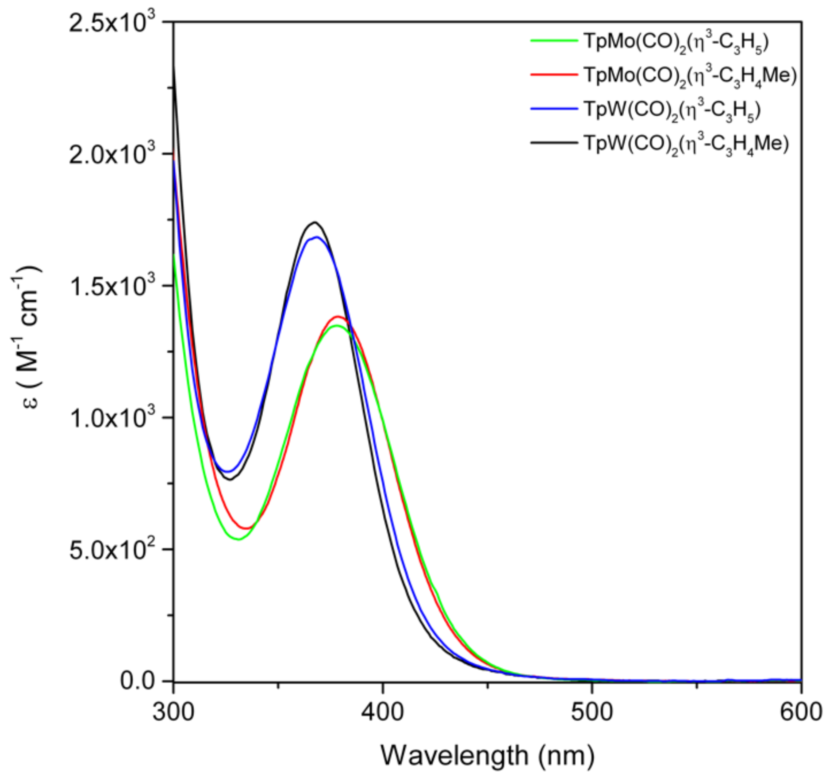

Figure 5.4: Electronic spectra of $TpM(CO)_2(\eta^3\text{-}C_3H_4R)$ compounds studied in CH_2Cl_2 solution.

As the observed photoproduct, putatively the *gauche* rotamer, reverts to *exo*-$TpM(CO)_2(\eta^3\text{-}C_3H_4R)$ upon λ_{irr} = 550 ± 50 nm photolysis, it may be assumed that this rotamer has an electronic absorption in this portion of the spectrum. Accordingly, SAOP excitation energies place two transitions lower in energy than those observed for *exo*-$TpM(CO)_2(\eta^3\text{-}C_3H_4R)$; a HOMO→LUMO excitation (3.013 eV) and a HOMO-1→LUMO excitation (3.230 eV). For the *gauche* isomer, the HOMO-1 corresponds to a bonding interaction between the CO π* antibonding orbitals and metal $d_{x^2-y^2}$, d_{yz}, d_{xz}, and d_{z^2} orbitals. The HOMO is composed of a bonding interaction between the allyl π* antibonding orbital with the metal d_{xz}, $d_{x^2-y^2}$, and d_{xy} orbitals. The LUMO is predominantly ligand based, featuring a bonding interaction between a CO π* orbital and metal. The reduction of symmetry of the allyl group in the *gauche* orientation leads to an allene-like π bonding orbital that forms a bonding interaction with the metal d orbitals. Occupation of this orbital may be expected to result in localization of the π electrons and give rise to a formal C-C double bond in the excited state.

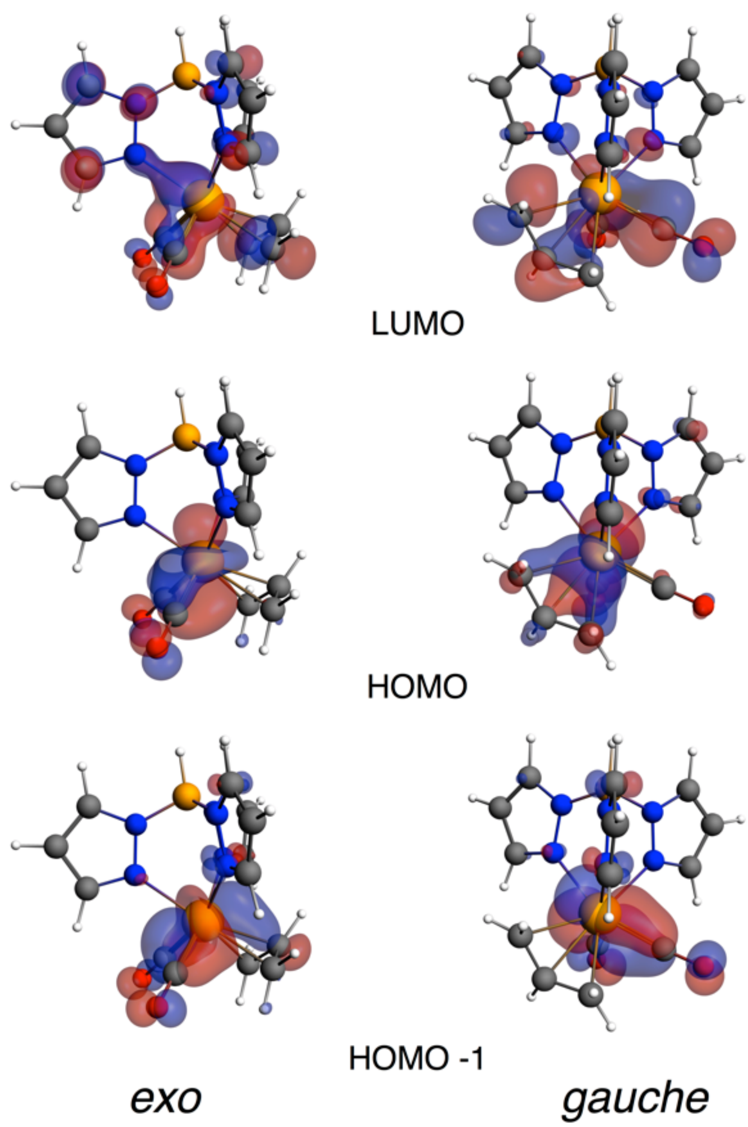

Figure 5.5: Frontier orbitals of *exo* and *gauche*, rotamers of $TpMo(CO)_2(\eta^3\text{-}C_3H_5)$

Excited State Geometries

To further explore how population of the low energy electronic excited states of the *exo* rotameric form may facilitate rotameric interconversion, excited-state geometry optimizations were performed for the two lowest energy electronic excited states.

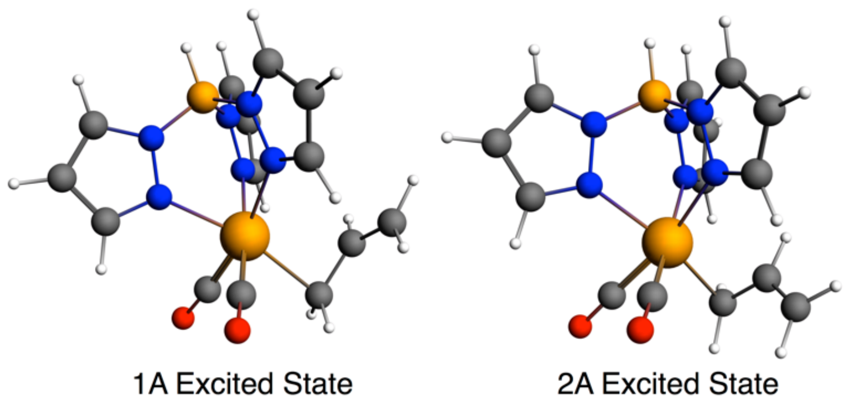

Figure 5.6: Calculated excited state geometries of $TpMo(CO)_2(\eta^3\text{-}C_3H_5)$ compounds.

Optimizing for the 1A state of *exo*-$TpM(CO)_2(\eta^3\text{-}C_3H_5)$, corresponding to the HOMO→LUMO excitation, results in localization of the allyl π electrons to give a double bond between a terminal allyl carbon and the central allyl carbon, the remaining terminal carbon is found to be approximately sp^3 hybridized with a single bond to the metal center, Figure 5.6. The bond length between the metal and sp^3 allyl carbon is placed at 2.29 Å, while the distance to the central carbon is 2.57 Å. The sp^2 terminal carbon shares little bonding character with the metal at a distance of 3.40 Å. The sp^3 terminal carbon to central carbon bond length is calculated as 1.45 Å while the bond length between the central carbon and sp^2 terminal carbon is placed at 1.39 Å, consistent with greater double bond character. Worth noting is the rotation of the allyl group, such that the B-Mo-C-C dihedral is reduced to only 12°, approaching the near 0° dihedral of the *gauch*e rotamer. Relaxation of this excited state represents a viable route to the *gauche* rotamer.

The 2A excited state, arising from the HOMO-1→LUMO excitation, which is also calculated to occur in the region of the observed photochemistry, shares much in common with the 1A excited state. Localization of the π electrons is found to occur accompanied by approximate sp^3 hybridization of a terminal carbon. The Mo-allyl bond lengths are found at 2.29 Å for the sp^3 carbon, 2.44 Å for the central carbon, and 3.24 Å for the sp^2 terminal carbon. The sp^3 carbon to central carbon bond length is placed at 1.44 Å and the central carbon to sp^2 terminal carbon at 1.40 Å. Unlike the 1A excited state, the overall rotational orientation of the allyl ligand remains largely unchanged from the ground state *exo* geometry.

Both the 1A and 2A excited states feature a substantially decreased Mo-allyl bond order, each more closely resembling a 16-electron $TpMo(CO)_2(\eta^1\text{-}C_3H_5)^*$ species. Vibrational relaxation of the $TpMo(CO)_2(\eta^1\text{-}C_3H_5)^*$ like excited state may facilitate rotation along the Mo-C axis resulting in formation of either the *exo* or *gauche* rotamers upon relaxation to a $TpMo(CO)_2(\eta^3\text{-}C_3H_5)$ ground state.

The results of these excited state DFT computations suggest that despite the presence an energetically accessible $\eta^3 \rightarrow \eta^3 \rightarrow \eta^3$ allyl rotation mechanism in the ground state, the photochemical *exo* ↔ *gauche* isomerism observed at low temperature occurs through an excited state η^{1*} species. The proposed mechanism for rotameric interconversion is summarized in Scheme 5.3.

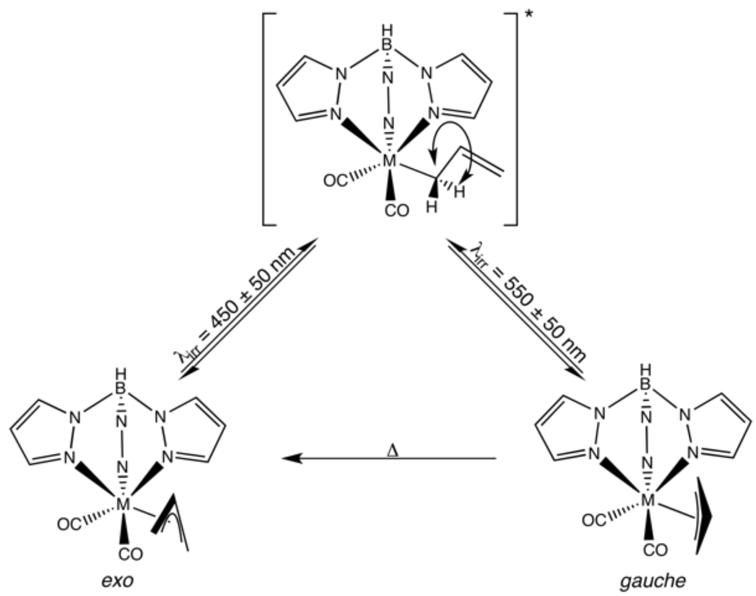

Scheme 5.3: Proposed photochemical mechanism for the allyl rotameric isomerism $TpM(CO)_2(\eta^3\text{-}C_3H_4R)$.

Conclusions

Low-temperature matrix FTIR and DFT studies demonstrate that photolysis of *exo*-$TpM(CO)_2(\eta^3\text{-}C_3H_4R)$ results in reversible rotameric isomerization to *gauche*-$TpM(CO)_2(\eta^3\text{-}C_3H_4R)$. Excited state DFT calculations suggest that when subjected to low energy photolysis, *exo*-$TpM(CO)_2(\eta^3\text{-}C_3H_5)$ forms an excited state species resembling 16-electron $TpM(CO)_2(\eta^1\text{-}C_3H_4R)^*$. The photochemically generated $TpM(CO)_2(\eta^1\text{-}C_3H_4R)^*$ excited state species may undergo vibrational relaxation to yield either of the *exo* or *gauche* forms of $TpM(CO)_2(\eta^3\text{-}C_3H_5)$.

Experimental

All complexes were synthesized by literature procedures.[18,19] The apparatus and methods for matrix photochemistry have been reported elsewhere.[20]

All DFT calculations were performed in the Amsterdam Density Functional (ADF2014.01) program.[21-23] Electronic configurations of atoms were described by an all-electron triple-ζ Slater-type orbital basis set modified by a polarization function (TZP STO).[24] Geometry optimizations and vibrational frequency calculations were performed using the GGA functional of Becke[25] and Perdew[26,27] using a scalar relativistic corrections within the Zeroth Order Regular Approximation (ZORA).[28,29] Excited state geometries were computed using the B88P86 functional in conjunction with an all-electron triple-ζ Slater-type orbital basis set modified by a polarization function and a diffuse function (ATZP STO). The intrinsic reaction coordinate (IRC) of all calculated transition state geometries was followed to confirm the relation with the expected stationary points. Electronic excitation energies were computed using the statistical average of orbital potentials (SAOP) model.[30,31]

References

1. F. A. Cotton, J. W. Faller, and A. Musco, *Inorg. Chem.*, 1967, **6**, 179–182.
2. K. C. Ramey and G. L. Statton, *J. Am. Chem. Soc*, 1966, **88**, 1327–1328.
3. J. K. Becconsall and S. O'Brien, *Chem. Commun. (London)*, 1966, 302–303.
4. J. W. Faller and M. J. Incorvia, *Inorg. Chem.*, 1968, **7**, 840–842.
5. R. W. Fish, W. P. Giering, and D. Marten, *J. Organomet. Chem.*, 1976, **105**, 101–118.
6. T. E. Bitterwolf, J. T. Bays, B. Scallorn, C. A. Weiss, M. W. George, I. G. Virrels, J. C. Linehan, and C. R. Yonker, *Eur. J. Inorg. Chem.*, 2001, **2001**, 2619–2624.
7. A. Davison and W. C. Rode, *Inorg. Chem.*, 1967, **6**, 2124–2125.
8. D. H. Gibson, W. L. Hsu, A. L. Steinmetz, and B. V. Johnson, *J. Organomet. Chem.*, 1981, **208**, 89–102.
9. A. Ariafard, S. Bi, and Z. Lin, *Organometallics*, 2005, **24**, 2241–2244.
10. S. Trofimenko, *J. Am. Chem. Soc.*, 1967, **89**, 3904–3905.
11. S. Trofimenko, *J. Am. Chem. Soc.*, 1969, **91**, 3183–3189.
12. P. Meakin, S. Trofimenko, and J. P. Jesson, *J. Am. Chem. Soc.*, 1972, **94**, 5677–5681.
13. E. M. Holt, S. L. Holt, and K. J. Watson, *J. Chem. Soc., Dalton Trans.*, 1973, 2444–2447.
14. J. W. Faller, D. F. Chodosh, and D. Katahira, *J. Organomet. Chem.*, 1980, **187**, 227–231.
15. J. W. Faller and A. Jakubowski, *J. Organomet. Chem.*, 1971, **31**, C75–C78.
16. N. W. Murrall and A. J. Welch, *Acta Cryst. C.*, 1984, **C40**, 401–403.
17. M. D. Santa María, R. M. Claramunt, I. Alkorta, and J. Elguero, *Dalton Trans.*, 2007, 3995–3999.
18. S. Trofimenko, *J. Am. Chem. Soc.*, 1969, **91**, 588–595.
19. A. J. Pearson and E. Schoffers, *Organometallics*, 1997, **16**, 5365–5367.
20. J. T. Bays, T. E. Bitterwolf, K. A. Lott, M. A. Ollino, A. J. Rest, and L. M. Smith, *J. Organomet. Chem.*, 1998, **554**, 75–85.

21. ADF 2014.01, SCM, Theoretical Chemistry, Vrije Universiteit, Amsterdam, The Netherlands, http://www.scm.com.

22. C. F. Guerra, J. G. Snijders, G. Te Velde, and E. J. Baerends, *Theor. Chem. Acc.*, 1998, **99**, 391–403.

23. G. Te Velde, F. M. Bickelhaupt, E. J. Baerends, C. Fonseca Guerra, S. J. A. van Gisbergen, J. G. Snijders, and T. Ziegler, *J. Comp. Chem.*, 2001, **22**, 931–967.

24. E. V. Lenthe and E. J. Baerends, *J. Comp. Chem.*, 2003, **24**, 1142–1156.

25. A. D. Becke, *Phys. Rev. A*, 1988, **38**, 3098–3100.

26. J. Perdew, *Phys. Rev. B*, 1986, **33**, 8822–8824.

27. J. Perdew, *Phys. Rev. B*, 1986, **34**, 7406–7406.

28. E. V. Lenthe, E. J. Baerends, and J. G. Snijders, *J. Chem. Phys.*, 1993, **99**, 4597.

29. E. V. Lenthe, A. Ehlers, and E. J. Baerends, *J. Chem. Phys.*, 1999, **110**, 8943.

30. O. V. Gritsenko, P. Schipper, and E. J. Baerends, *Chem Phys Lett*, 1999, **302**, 199–207.

31. P. R. T. Schipper, O. V. Gritsenko, S. J. A. van Gisbergen, and E. J. Baerends, *J. Chem. Phys.*, 2000, **112**, 1344.

Chapter 6: Evidence for Photochemical Linkage Isomerism of the Phenylazo Ligand in $M(CO)_2(N_2Ph)(PPh_3)_2$ Cations, where M = Fe and Ru.

Published: W. A. Thornley, T. E. Bitterwolf, Eur. J. Inorg. Chem. **2015**, 1946–1949.

Abstract: *Frozen matrix photolysis studies of $M(CO)_2(N_2Ph)(PPh_3)_2$ cations, where M = Fe and Ru, have revealed end-on/side-on photochemical linkage isomerism of the phenylazo ligand. Previously reported solvent dependent vibrational bands of the $Ru(CO)_2(N_2Ph)(PPh_3)_2$ cation have now been identified as an equilibrium between the two linkage isomers. DFT calculations have been carried out on the end-on and side-on isomers of the iron and ruthenium complexes.*

Numerous photochemical studies of metal nitrosyl compounds have established that the nitrosyl ligand undergoes linkage isomerism yielding a side-on, π-bound nitrosyl ligand or an oxygen bound isonitrosyl ligand.[1] These linkage isomers may be observed directly at low temperature, but revert to the nitrogen bound nitrosyl isomer at room temperature. Two extraordinary examples of side-on nitrosyl groups stable at room temperature have been reported in the molecular structures of copper nitrite reductase enzymes.[2,3]

Arylazo ligands are isoelectronic with the well-known nitrosyl ligand, and like their nitrosyl counterparts, may serve as either 1 or 3 electron donors to a metal center. These 1 or 3 electron-donating isomers are referred to as doubly and singly bent, respectively, Scheme 6.1a and 6.1b. The bending in the singly bent arylazo ligands arises due to back bonding into the N_2 π* orbitals, breaking the degeneracy of the two N_2 π and π* orbitals. In the doubly bent geometry it is assumed that reduction of the phenylazo group has taken place such that the ligand is best described as an N_2Ph anion. A side-on linkage isomer is also possible, Scheme 6.1c, and indeed two such derivatives, $CpTiCl_2(\eta^2-N_2Ph)$[4,5] and $[(t-Bu_2P)_2C_2H_4]Ni(\eta^2-N_2Ph)$,[6] have been isolated. The molecular structure of the titanium compound has been reported. A bimetallic compound in which a side-on arylazo ligand serves as a bridge between two cobalt atoms is also known.[7]

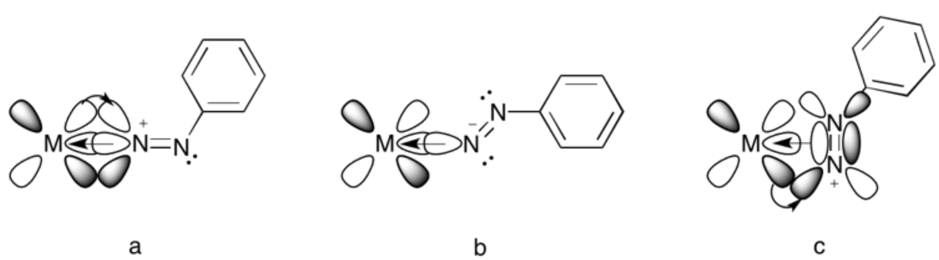

Scheme 6.1: Known binding geometries of the phenyldiazonium ligand.

The present study of the diazonium ligand is an extension of our ongoing examination of photochemical linkage isomerism of the nitrosyl ligand. Our initial exploration of the photochemistry of compounds possessing the phenylazo ligand has led us to the well known class of arylazo compounds, $[M(CO)_2(N_2Ph)(PPh_3)_2]BF_4$ (M = Fe and Ru). The results of these studies are reported below.

Frozen Matrix Photochemistry of $[Fe(CO)_2(N_2Ph)(PPh_3)_2]$ BF_4

The molecular structure of $[Fe(CO)_2(\eta^1\text{-}N_2Ph)(PPh_3)_2]BF_4$ has previously been reported by Haymore and Ibers.[8] $[Fe(CO)_2(\eta^1\text{-}N_2Ph)(PPh_3)_2]BF_4$ was found to possess a trigonal bipyramidal geometry with the carbonyl and arylazo ligands in the equatorial plane and phosphine ligands occupying the axial positions. The arylazo ligand is singly bent with a Fe-N-N bond angle of 179.2(5)°, and an N-N-Ph bond angle of 124.2(6)°. A single N-N vibrational band is observed in its infrared spectrum.

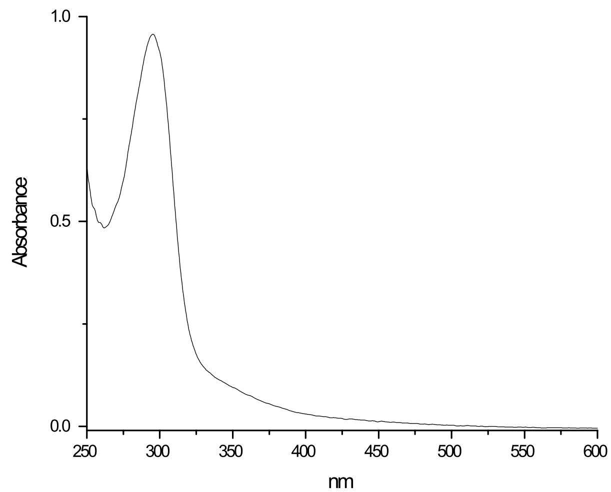

Figure 6.1: UV-Vis absorption spectrum of $Fe(CO)_2(\eta^1\text{-}N_2Ph)(PPh_3)_2$ in CH_2Cl_2.

The electronic spectrum of $[Fe(CO)_2(\eta^1\text{-}N_2Ph)(PPh_3)_2]BF_4$ in CH_2Cl_2, Figure 6.1, has a broad absorption extending from ca. 350 nm into the visible. The results of TD-DFT calculations suggest that these low energy electronic transitions are predominantly ligand based transitions into metal d and N_2 π^* antibonding orbitals. Kohn-Sham orbitals for $[Fe(CO)_2(\eta^1\text{-}N_2Ph)(PPh_3)_2]^+$ are presented in Figure 6.2. The HOMO corresponds to a back bonding interaction between the iron and the N_2 π^* orbital. The resemblance between this orbital and Scheme 6.1a suggests that this interaction is responsible for the development of a lone pair like orbital on the second nitrogen atom and the subsequent bending of the aryl group from linearity with the N_2 group.

Photolysis of this compound in a poly(vinyl chloride) (PVC) film matrix at ca. 85 K into the broad electronic absorption (350 nm < λ_{max} < 400 nm), Figure 6.3a, results in bleaching of the parent carbonyl and arylazo ligand bands and growth of new bands belonging to the photoproduct. Two new carbonyl bands are shifted to slightly higher energy in the photoproduct. ^{15}N labeling of the terminal nitrogen in the arylazo ligand, Figure 6.3b, established that the new bands at 1628 and 1570 cm^{-1} of the unlabeled sample are coupled to the N-N vibrational mode of the arylazo ligand. The absorptions at 1589 and 1579 cm^{-1} of the parent complex, as well as additional bands below 1400 cm^{-1} (not shown), are assigned to phenyl ring vibrational modes that are shifted as a result of the photochemical transformation but are not necessarily coupled to the N-N vibration. $Fe(CO)_2(\eta^1-N_2-4-C_6H_4F)(PPh_3)_2]BF_4$ and its ^{15}N isotopomer were also photolyzed and exhibited similar spectral changes. The new N-N phenylazo vibrational bands fall in the same region as those of the reported side-on arylazo derivatives, $CpTiCl_2(\eta^2-N_2Ph)$, 1550 cm^{-1}, and (dtbpe)$Ni(\eta^2-N_2Ph)$, 1602 cm^{-1}, therefore we assign the second isomer to an analogous side-on arylazo isomer.

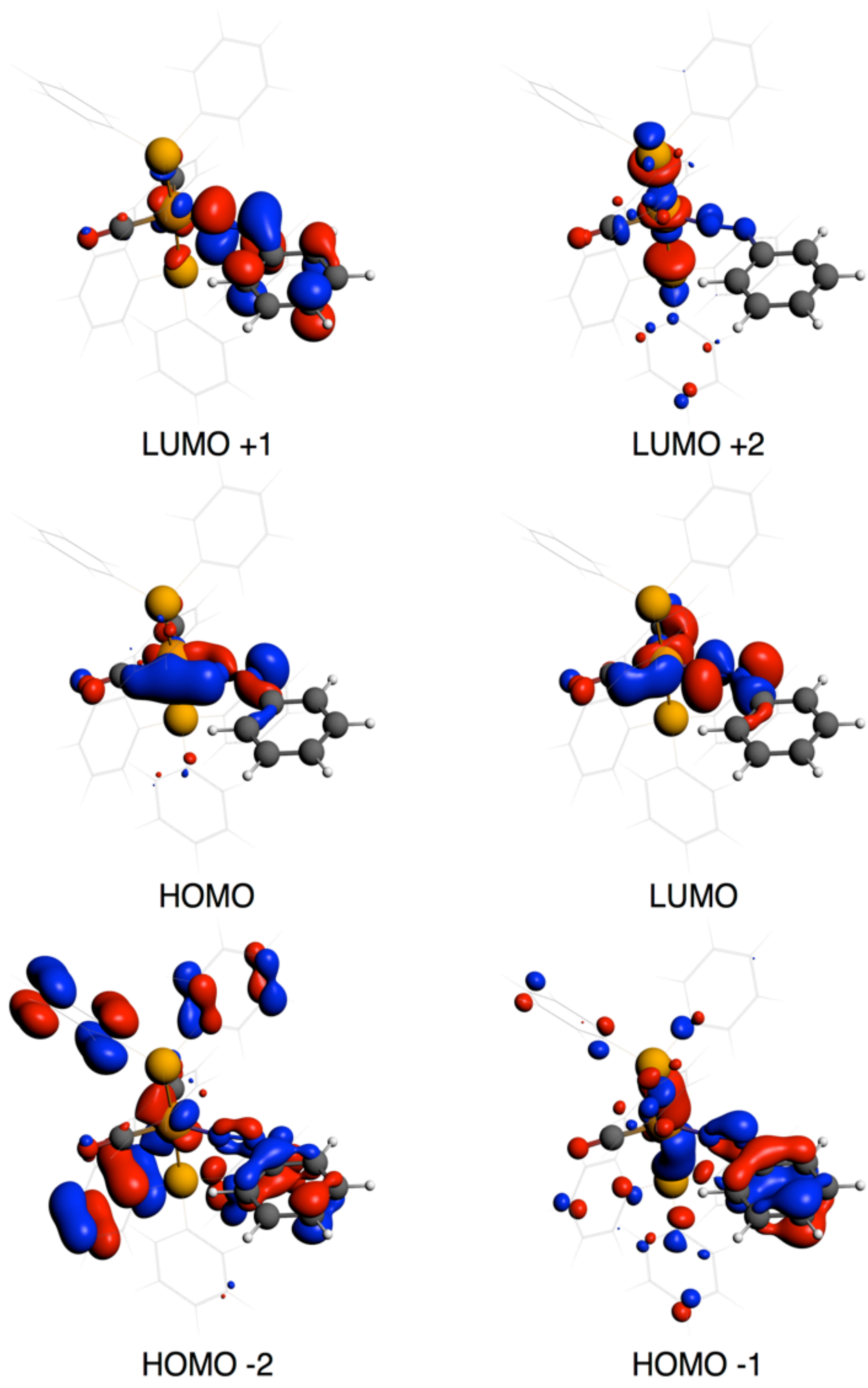

Figure 6.2: Kohn-Sham orbitals of $Fe(CO)_2(\eta^1\text{-}N_2Ph)(PPh_3)_2^+$.

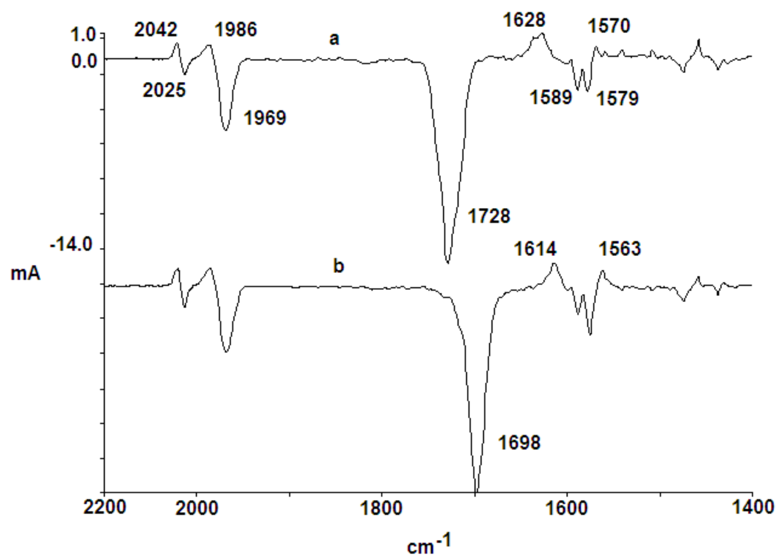

Figure 6.3: Photolysis of $Fe(CO)_2(\eta^1\text{-}N_2Ph)(PPh_3)_2$ (a) and its ^{15}N isotopomer (b) in a PVC film matrix at ca. 90 K. Spectra are the difference of a 10 min photolysis (350 nm < λ_{max} < 400 nm) minus a 10 min photolysis (λ_{max} = 500 ± 35 nm).

Table 6.1: Calculated energies (kcal mol^{-1}) and observed and calculated carbonyl and aryldiazonium vibrational frequencies (cm^{-1}) for $Fe(CO)_2(\eta^1\text{-}N_2Ph)(PPh_3)_2$ and $Fe(CO)_2(\eta^1\text{-}N_2Ph)(PPh_3)_2$, calculated intensities are given in parentheses (km mol^{-1}).

	η^1-N_2Ph		η^2-N_2Ph	
	Obs	Calc	Obs	Calc
ΔH		0.0		+11.4
ΔG		0.0		+8.3
CO (sym)	2025	1985 (400)	2042	1992
CO (antisym)	1969	1940 (565)	1986	1949
NN	1728	1744 (497)	1628	1629 (39)
NN-Ph coupled			1570	1556 (11)

The results of DFT calculations carried on the η^1 and η^2 linkage isomers of $[Fe(CO)_2(N_2Ph)(PPh_3)_2]^+$ are summarized in Table 6.1. In the side-on orientation, vibrational coupling between the N-N stretching vibration and phenyl bending motions gives rise to two weak bands that correspond to the two bands observed in the matrix spectra at 1628 cm^{-1} and 1570 cm^{-1}. The calculated phenyl azo vibrational frequencies are in good agreement with the observed frequencies. Further, these calculations reproduce the direction of the carbonyl vibrational band shifts observed in moving from the η^1 to η^2 isomer. $[Fe(CO)_2(\eta^1\text{-}N_2Ph)(PPh_3)_2]^+$ is calculated to lie 8.3 kcal mol^{-1} lower in energy than its $[Fe(CO)_2(\eta^2\text{-}N_2Ph)(PPh_3)_2]^+$ isomer.

Frozen Matrix Photochemistry of $[Ru(CO)_2(N_2Ph)(PPh_3)_2]$ BF_4

The molecular structure of the $[Ru(CO)_2(N_2Ph)(PPh_3)_2]^+$ cation has not been reported. Haywood and Ibers noted an unusually complex pattern of isotopically sensitive vibrational bands for this compound.[9] In contrast to the iron compound where a single N-N vibrational band was observed, three vibrational bands were found to be sensitive to ^{15}N substitution of the phenylazo ligand. The highest energy of these N-N vibrational modes was assigned to an end-on, η^1, arylazo group, while the two additional bands were attributed to a second isomer that was tentatively assigned to a doubly bent arylazo group. One of these bands was assumed to arise from coupling of phenyl and N_2 vibrational modes. Only one set of carbonyl bands was observed. The ratio of the two isomers was found to be dependent upon the sample medium; the end-on isomer being favored in Nujol mulls, while the second isomer was favored in CH_2Cl_2 solutions.

While $[Ru(CO)_2(N_2Ph)(PPh_3)_2]BF_4$ is stable as a microcrystalline solid, its solutions in halocarbon solvents are both air and light sensitive. Samples for photolysis had to be prepared in the dark under a flow of purified nitrogen to evaporate the 1,1,2,2-tetrachloroethane solvent used for casting the PVC films used in the low-temperature photolysis experiments. Even under stringent conditions a trace of a second species was always evident in the samples. Fortunately, this species did not undergo photolysis at visible wavelengths.

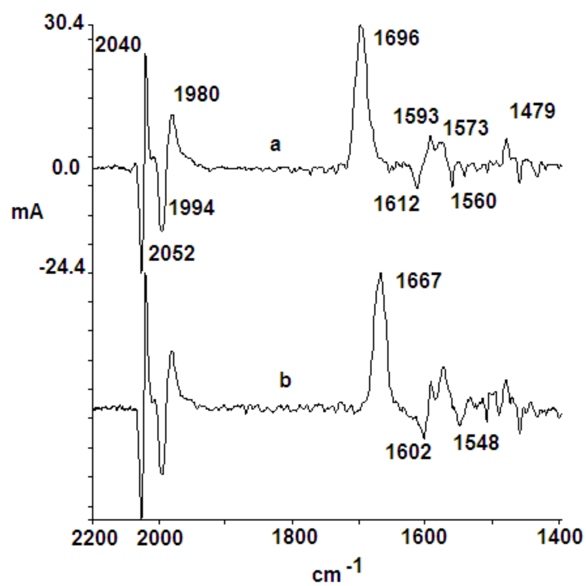

Figure 6.4. Photolysis of $Ru(CO)_2(\eta^1\text{-}N_2Ph)(PPh_3)_2$ (a) and its ^{15}N isotopomer (b) in a PVC film matrix at ca. 90 K. Spectra are the difference of a 10 min photolysis (λ_{max} = 450 ± 35 nm) minus a 10 min photolysis (λ_{max} = 500 ± 35 nm). Bands whose positions do not vary upon isotopic substitution are only marked in 6.4a.

The IR spectrum of $[Ru(CO)_2(N_2Ph)(PPh_3)_2]BF_4$ in PVC exhibits no absorptions in the 1700 – 1600 cm^{-1} region that may be assigned to an η^1-N_2Ph species. Small features could be observed in the 1625 – 1500 cm^{-1} region where vibrational modes arising from the phenyl rings as well as bands of the second isomer reported by Haymore and Ibers would be expected. Upon visible photolysis (λ_{max} = 450 ± 35 nm) of this compound, Figure 6.4a, new carbonyl absorptions, as well as an absorption at 1696 cm^{-1} were found to grow in. The carbonyl bands were slightly lower in energy than those of the initial species. In the spectral region between 1625 – 1500 cm^{-1} bands at 1612 and 1560 cm^{-1} were found to decrease in intensity while the intensity of bands at 1593 and 1573 cm^{-1} increased. Photolysis of the ^{15}N isotopomer, Figure 6.4b, established that the bands at 1612 and 1560 cm^{-1} and the new, strong absorption at 1696 cm^{-1} were associated with the N-N vibrational mode of the arylazo ligand. We reject the possibility that the new isomeric species has the doubly bent arylazo group suggested by Haymore and Ibers since the transformation from a singly bent to doubly bent ligand implies a formal oxidation of the metal. The relatively small shifts in the carbonyl stretching frequencies are not consistent with a dramatic shift of electron density away from the metal.

Comparison of Figures 6.3 and 6.4 clearly establish that the iron sample undergoes a photochemical transformation from the η^1-N_2Ph isomer to a new isomer, while the ruthenium compound displays exactly the opposite behavior. DFT calculations place $[Ru(CO)_2(\eta^2\text{-}N_2Ph)(PPh_3)_2]^+$ just 1.3 kcal mol^{-1} higher in energy than $[Ru(CO)_2(\eta^1\text{-}N_2Ph)(PPh_3)_2]^+$, consistent with the observed solvent dependent isomerization that would require a near barrierless interconversion.

Table 6.2. Calculated energies (kcal mol^{-1}) and observed and calculated carbonyl and aryldiazonium vibrational bands (cm^{-1}) for $Ru(CO)_2(\eta^1\text{-}N_2Ph)(PPh_3)_2$ and $Ru(CO)_2(\eta^1\text{-}N_2Ph)(PPh_3)_2$, calculated intensities are given in parentheses (km mol^{-1}).

	η^1-N_2Ph		η^2-N_2Ph	
	Obs	Calc	Obs	Calc
ΔH		0.0		+4.1
ΔG		0.0		+1.3
CO (sym)	2040	1994 (437)	2052	1999 (375)
CO (antisym)	1980	1943 (594)	1994	1949 (555)
NN	1696	1686 (258)	1612	1615 (24)
NN-Ph coupled			1560	1551 (12)

Conclusions

Photochemical linkage isomerism is well established for the nitrosyl ligand and appears to also be possible for at least a few examples of the isoelectronic phenylazo ligand. Interestingly, it appears that the phenylazo ligand in $Ru(CO)_2(N_2Ph)(PPh_3)_2$ may flip from one geometry to the other at room temperature under the influence of solvent. Unlike the case of the nitrosyl ligand where the lifetime of linkage isomers at room temperature is fleetingly small, the side-on phenylazo ligand may be sufficiently long lived to exhibit chemistry distinct from that of the end-on isomer.

Experimental

$[Fe(CO)_2(\eta^1\text{-}N_2Ph)(PPh_3)_2]BF_4$,[10] $[Fe(CO)_2(\eta^1\text{-}N_2Ph)[(4\text{-}F\text{-}C_6H_4)_3P]_2\}BF_4$,[10] and $[Ru(CO)_2(N_2Ph)(PPh_3)_2]BF_4$,[9] were prepared by literature procedures. The apparatus and methods for matrix photochemistry have been reported elsewhere.[11]

All DFT calculations were performed in the Amsterdam Density Functional (ADF2013.01) program.[12-14] Electronic configurations of atoms were described by an all-electron triple-ζ Slater-type orbital basis set modified by a polarization function (TZP STO).[15] Geometry optimizations and vibrational frequency calculations were performed using the GGA functional of Becke[16] and Perdew[17,18] utilizing a single-component scalar relativistic correction within the zeroth order regular approximation (ZORA).[19,20] Vertical electronic excitation energies were computed with the statistical average of orbital potentials (SAOP) model. [21,22]

References

(1) Bitterwolf, T. E. *Coord. Chem. Rev.* **2006**, *250* (9-10), 1196–1207.

(2) Antonyuk, S. V.; Strange, R. W.; Sawers, G.; Eady, R. R.; Hasnain, S. S.; Petsko, G. A. *Proc. Natl. Acad. Sci. U.S.A.* **2005**, *102* (34), 12041–12046.

(3) Tocheva, E. I.; Rosell, F. I.; Mauk, A. G.; Murphy, M. E. P. *Science* **2004**, *304* (5672), 867–870.

(4) Latham, I. A.; Leigh, G. J.; Huttner, G.; Jibril, I. *J. Chem. Soc., Dalton Trans.* **1986**, No. 2, 377.

(5) Dilworth, J. R.; Latham, I. A.; Leigh, G. J.; Huttner, G.; Jibril, I. *J. Chem. Soc., Chem. Commun.* **1983**, No. 22, 1368.

(6) Iluc, V. M.; Miller, A. J. M.; Hillhouse, G. L. *Chem. Commun.* **2005**, No. 40, 5091.

(7) DeBlois, R. E.; Rheingold, A. L.; Samkoff, D. E. *Inorg. Chem.* **1988**, *27* (20), 3506–3510.

(8) Haymore, B. L.; Ibers, J. A. *Inorg. Chem.* **1975**, *14* (6), 1369–1376.

(9) Haymore, B. L.; Ibers, J. A. *Inorg. Chem.* **1975**, *14* (11), 2784–2795.

(10) Carroll, W. E.; Lalor, F. J. *J. Chem. Soc., Dalton Trans.* **1973**, No. 17, 1754.

(11) Bays, J. T.; Bitterwolf, T. E.; Lott, K. A.; Ollino, M. A.; Rest, A. J.; Smith, L. M. *J. Organomet. Chem.* **1998**, *554* (1), 75–85.

(12) ADF 2014.01, SCM, Theoretical Chemistry, Vrije Universiteit, Amsterdam, The Netherlands, http://www.scm.com.

(13) Guerra, C. F.; Snijders, J. G.; Velde, Te, G.; Baerends, E. J. *Theor. Chem. Acc.* **1998**, *99*, 391–403.

(14) Velde, Te, G.; Bickelhaupt, F. M.; Baerends, E. J.; Fonseca Guerra, C.; van Gisbergen, S. J. A.; Snijders, J. G.; Ziegler, T. *J. Comp. Chem.* **2001**, *22* (9), 931–967.

(15) Lenthe, E. V.; Baerends, E. J. *J. Comp. Chem.* **2003**, *24* (9), 1142–1156.

(16) Becke, A. D. *Phys. Rev. A* **1988**, *38* (6), 3098–3100.

(17) Perdew, J. *Phys. Rev. B* **1986**, *33* (12), 8822–8824.

(18) Perdew, J. *Phys. Rev. B* **1986**, *34* (10), 7406–7406.

(19) Lenthe, E. V.; Baerends, E. J.; Snijders, J. G. *J. Chem. Phys.* **1993**, *99* (6), 4597.

(20) Lenthe, E. V.; Ehlers, A.; Baerends, E. J. *J. Chem. Phys.* **1999**, *110* (18), 8943.

(21) Gritsenko, O. V.; Schipper, P.; Baerends, E. J. *Chem Phys Lett* **1999**, *302*, 199–207.

(22) Schipper, P. R. T.; Gritsenko, O. V.; van Gisbergen, S. J. A.; Baerends, E. J. *J. Chem. Phys.* **2000**, *112* (3), 1344.

Chapter 7: Photolysis of Isoelectronic Ruthenium Nitrosyl and Diazonium Complexes in Frozen PVC Matrices. Retention of Dinitrogen on Ruthenium Following Photochemical Phenyl Radical Loss.

Published: W. A. Thornley, T. E. Bitterwolf, Eur. J. Inorg. Chem. **2016**, 464–468.

Abstract: *Photolysis of $RuCl_3(\eta^1\text{-}NO)(PPh_3)_2$ in polyvinyl chloride (PVC) matrices at 85 K results in reversible linkage isomerism of the nitrosyl ligand to form the isonitrosyl complex $RuCl_3(\eta^1\text{-}ON)(PPh_3)_2$. Metal-to-ligand charge-transfer (MLCT) excitation of the isoelectronic phenylazo complex, $RuCl_3(\eta^1\text{-}N_2Ph)(PPh_3)_2$, has previously been shown to result in generation of the phenyl radical, presumably through decomposition a photogenerated diazenyl radical. Examination of this photolysis in a PVC matrix at cryogenic temperatures has permitted direct observation of an isotopically sensitive product band that may be assigned to a 17-electron ruthenium dinitrogen species, suggesting that this photochemical decomposition does not proceed through formation of a diazenyl intermediate but through homolytic cleavage of the parent diazonium complex to give the phenyl radical and the 17-electron $RuCl_3(\eta^1\text{-}N_2)(PPh_3)_2$.*

The ability of the nitrosyl ligand to undergo linkage isomerism following photolysis to yield side-on, π-bound isomers and oxygen bound, isonitrosyl isomers is well known.[1] These isomers may be generated and characterized at low temperature, but rapidly revert to the nitrogen bound nitrosyl isomer at noncryogenic temperatures. Like the nitrosyl ligand, arylazo ligands may act as either 3 or 1 electron donors to a metal; these isomers are referred to as singly and doubly bent, respectively, Scheme 7.1a and 7.1b. A side-on linkage isomer is also known, Scheme 7.1c, and several such derivatives, have been isolated.[2-4] Despite the similarities between the nitrosyl and arylazo ligands, the photochemistry of arylazo complexes has largely gone unexplored since the discovery of this class of compounds by King and Bisnette in 1964. [5,6].

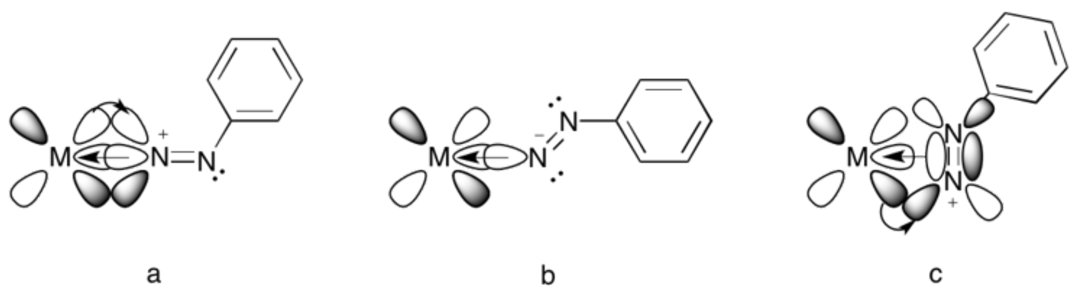

Scheme 7.1: Known coordination modes of the phenyldiazonium ligand. (a) η^1-singly-bent, (b) η^1- doubly-bent, (c) η^2.

Our attention has recently turned to the photochemistry of diazonium complexes as an extension of our ongoing study of the nitrosyl ligand. Initial findings from this work indicate that like the nitrosyl ligand, diazonium ligands may also undergo photochemical linkage isomerism.[7] Prior to this work, the only examination of the photochemistry of a phenylazo metal complex that we are aware of is the solution photochemistry of $RuCl_3(\eta^1\text{-}N_2Ph)(PPh_3)_2$ performed by Kunkely and Vogler.[8] In this work, it is reported that photolysis of $RuCl_3(\eta^1\text{-}N_2Ph)(PPh_3)_2$ in acetonitrile results in formation of $RuCl_3(NCMe)(PPh_3)_2$, N_2, and biphenyl with $\Phi = 7 \times 10^{-3}$ at λ_{irr} = 520 nm. The proposed mechanism for production of N_2 and biphenyl involves metal-to-ligand charge-transfer (MLCT) to the phenylazo ligand resulting in loss of a neutral phenyldiazenyl radical. The phenyldiazenyl radical is well known to decompose to yield N_2 and phenyl radical which may then couple to produce the biphenyl, Scheme 7.2.[9-21]

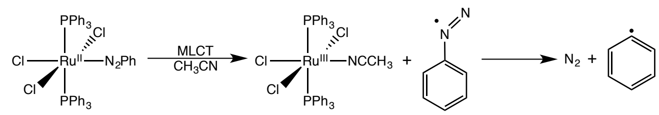

Scheme 7.2: Mechanism for phenyl radical formation proposed by Kunkely and Vogler.

In light of the report by Kunkely and Vogler, we thought it fruitful to carry out low temperature photolyses of $RuCl_3(\eta^1\text{-}N_2Ph)(PPh_3)_2$ and its nitrosyl analogue with the expectation of observing a side-on, $RuCl_3(\eta^2\text{-}N_2Ph)(PPh_3)_2$ photointermediate that we anticipated may be a precursor to diazenyl radical loss. The surprising results of these studies are reported below.

Photolysis of $RuCl_3(\eta^1\text{-}NO)(PPh_3)_2$

$RuCl_3(NO)L_2$ derivatives are readily prepared by reaction of an appropriate ligand with $[RuCl_3(NO)]_n$ in ethanol.[22] $RuCl_3(NO)(PPh_3)_2$ has a strong charge transfer band at 342 nm (ε = 15,200 M^{-1} cm^{-1}, CH_2Cl_2) with a tail that extends to ca. 510 nm. The relatively high nitrosyl stretching frequency of $RuCl_3(NO)(PPh_3)_2$ at 1873 cm^{-1} is consistent with other Ru^{II} complexes. By way of comparison, the related Ru^{II} nitrosyl species $Na_2[Ru(CN)_5NO] \cdot 2H_2O$ and $K_2[RuCl_5(NO)]$ exhibit nitrosyl stretching modes at 1932 and 1921 cm^{-1}, respectively[23,24]

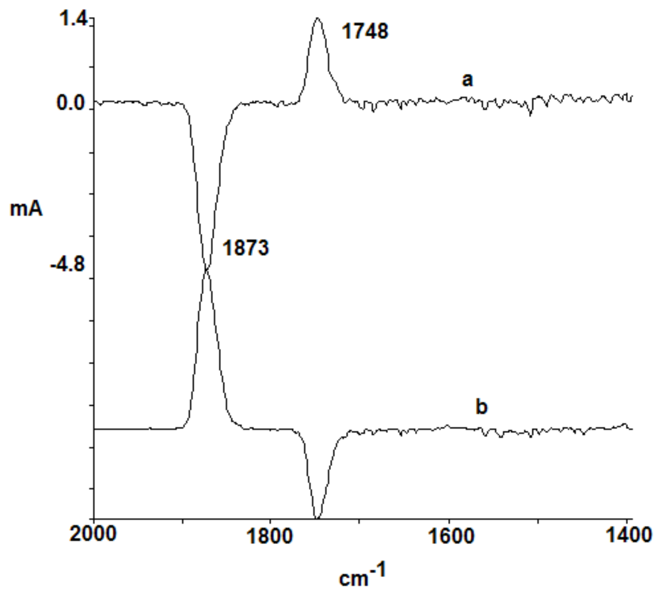

Figure 7.1. Difference spectra following photolysis of $RuCl_3(PPh_3)_2(NO)$ at 85 K in PVC: (a) sample following 10 min photolysis (λ_{Irr} = 500 ± 50 nm) minus sample before photolysis. (b) Sample after 10 min λ_{Irr} > 525 nm back photolysis minus λ_{Irr} = 500 ± 50 nm irradiated sample.

Photolysis of $RuCl_3(NO)(PPh_3)_2$ in PVC matrices at 85 K with λ_{irr} = 500 ± 50 nm results in bleaching of the parent nitrosyl band at 1873 cm^{-1} and appearance of a photoproduct absorption at 1748 cm^{-1} (Δv = 125 cm^{-1}), Figure 7.1a. Photolysis at shorter wavelengths, 330 < λ_{irr} < 400 nm, increases the extent of conversion between these two species but does not result in the appearance of any additional product bands. Long wavelength back-photolysis of 330 < λ_{irr} < 500 nm photolyzed samples with λ_{irr} > 525 nm, Figure 7.1b, cleanly reverses the transformation. The photoproduct band is shifted 125 cm^{-1} lower in energy relative to the parent nitrosyl band, consistent with formation of the isonitrosyl linkage isomer.[24]

Theoretical models[25,26] of nitrosyl linkage isomerism suggest that their interconversion are stepwise in the order: M-NO ⇄ M-(η^2-NO) ⇄ M-ON. In the current case, the failure to observe a side-on nitrosyl species argues for an overlap of the electronic absorption bands of the side-on nitrosyl species with those of the starting nitrosyl compound, thus giving rise to the isonitrosyl species with a low equilibrium population of the side-on isomer. The low-temperature matrix photochemistry of $RuCl_3(NO)(PPh_3)_2$ is summarized in Scheme 7.3.

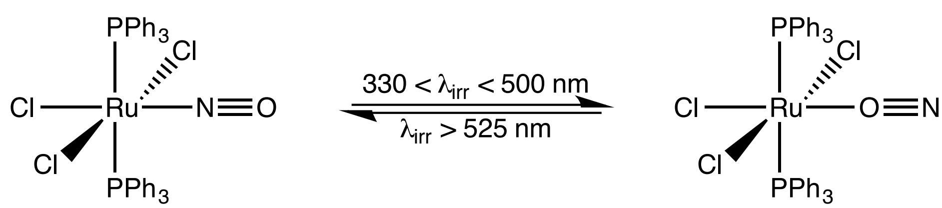

Scheme 7.3: Observed photochemical behavior of $RuCl_3(NO)(PPh_3)_2$ in PVC matrices at 85 K.

Photolysis of $RuCl_3(\eta^1\text{-}N_2Ph)(PPh_3)_2$

Acetonitrile solutions of $RuCl_3(\eta^1\text{-}N_2Ph)(PPh_3)_2$ are reported to have two absorptions in the visible (520 nm, sh, ε = 120 M^{-1} cm^{-1} and 420 nm, sh, ε = 600 M^{-1} cm^{-1}) and a strong charge transfer band in the UV (310 cm^{-1}, 12,000 M^{-1} cm^{-1}) that parallels the band observed in the nitrosyl derivative.[8] The infrared spectrum exhibits an intense N=N vibrational mode of the diazonium ligand at 1872 cm^{-1}, consistent with a singly-bent, η^1 coordination mode.

Irradiation of $RuCl_3(\eta^1\text{-}N_2Ph)(PPh_3)_2$ in PVC matrices at 85 K using wavelengths from 550 to 245 nm results in a single photochemical process; bleaching of the phenylazo band at 1872 cm^{-1} and appearance of a species possessing a low-intensity absorption at 2170 cm^{-1}, Figure 7.3a. Photolysis of the ^{15}N isotopomer, $RuCl_3(\eta^1\text{-}^{15}NNPh)(PPh_3)_2$, Figure 7.3b, bleaches the parent phenylazo N=N band at 1845 cm^{-1} and shifts the resulting product band to 2135 cm^{-1}, consistent with this photoproduct possessing an end-on N_2 oscillator. Dinitrogen complexes of ruthenium are known to have N_2 vibrational frequencies from 2100 – 2182 cm^{-1}, with the closely related $(PPh_3)_2ClRu(\mu\text{-}Cl)_3Ru(PPh_3)_2(N_2)$ having an N_2 stretching mode at 2165 cm^{-1}.[27] Low energy (λ_{Irr} > 590 nm) back-photolysis of the irradiated sample did not result in reversion of the photoproduct to the parent complex, and annealing of the matrix to 160 K resulted only in depletion of the 2170 cm^{-1} photoproduct absorption with no evidence for reversion to the parent diazonium species.

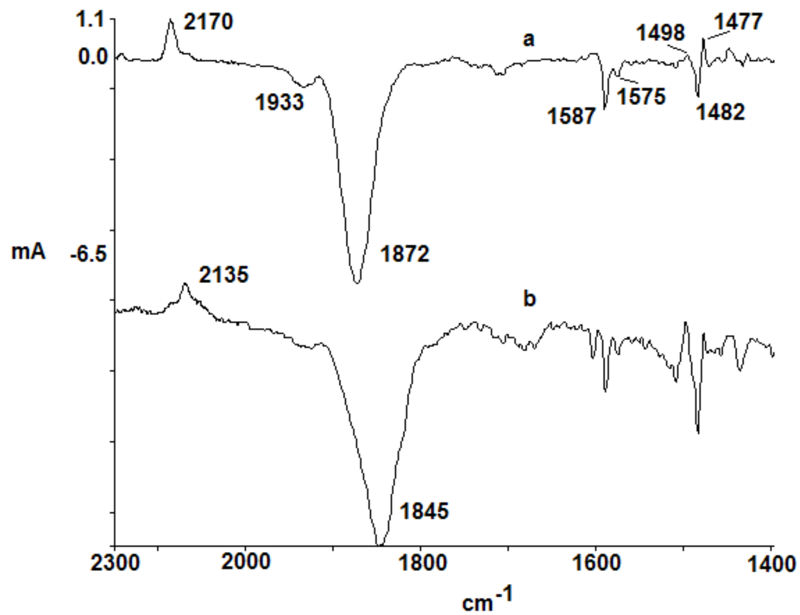

Figure 7.2. Difference spectra of the photolysis of $RuCl_3(PPh_3)_2(N_2Ph)$ (a) and its $^{15}NNPh$ isotopomer (b). Sample after 10 min photolysis (λ_{Irr} = 500 ± 50 nm) minus sample before photolysis.

In light of the work of Kunkely and Vogler that established generation of phenyl radicals in the solution photochemistry of $RuCl_3(\eta^1\text{-}N_2Ph)(PPh_3)_2$,[8] and the results of our low-temperature photolysis experiments demonstrating the formation of a Ruthenium dinitrogen complex following photolysis, we propose photochemical homolysis of the arylazo N-Ph bond to yield a 17-electron $RuCl_3(\eta^1\text{-}N_2)(PPh_3)_2$ and the phenyl radical. Though the phenyl radical has been observed in frozen inert gas matrices,[28,29] we are unable to make any spectral assignments directly attributable to this species in our 85 K PVC matrix experiments. This absence may be the product of the broad spectral bandwidths observed in PVC matrices relative to those in gas matrices, as well as a high degree of spectral overlap with PPh_3 phenyl ring vibrational modes, resulting in a failure of these product vibrational bands to resolve. Moreover, given the high reactivity of the phenyl radical, any phenyl radical that is photochemically generated may undergo secondary reaction with the PVC matrix material through halogen abstraction or addition to any residual unsaturated bonds of the polymer. Such reactions would effectively “trap” the phenyl radical, and help facilitate observation of the $RuCl_3(\eta^1\text{-}N_2)(PPh_3)_2$ radical by preventing recombination of the radical pair. Regardless, the ultimate fate of the phenylazo phenyl group remains elusive under these experimental conditions.

To better understand the observed matrix photochemistry of $RuCl_3(\eta^1\text{-}N_2Ph)(PPh_3)_2$, a DFT investigation was carried out. Geometric parameters from these calculations are summarized in Table 7.1. Calculations carried out on the products of N-Ph bond homolysis, 17-electron $RuCl_3(\eta^1\text{-}N_2)(PPh_3)_2$ and the phenyl radical, predict an N_2 vibrational frequency of 2194 cm^{-1} for the dinitrogen photoproduct, in good agreement with the species observed in the matrix photochemistry experiments. The calculated N=N vibrational mode of the parent diazonium complex was slightly underestimated relative to the experimental value at 1825 cm^{-1} and 1872 cm^{-1}, respectively. Fully consistent with a low-energy photochemical homolysis reaction, the change in free energy for N-Ph bond cleavage in $RuCl_3(\eta^1\text{-}N_2Ph)(PPh_3)_2$ to give $RuCl_3(\eta^1\text{-}N_2)(PPh_3)_2$ and the phenyl radical is calculated to be just 14.7 kcal mol^{-1}. Ph-N heterolysis pathways resulting in formation of either cationic or anionic $RuCl_3(\eta^1\text{-}N_2)(PPh_3)_2$ species were both highly energetically disfavored. Based on the large energetic expense of either heterolysis pathways, as well as the evidence for phenyl radical formation in solution studies, we dismiss both the cationic and anionic forms of $RuCl_3(\eta^1\text{-}N_2)(PPh_3)_2$ as the possible dinitrogen species observed in the matrix photochemistry experiments.

Table 7.1. Calculated bond lengths (Å) and angles (°) for $RuCl_3(\eta^1\text{-}N_2Ph)(PPh_3)_2$, $RuCl_3(\eta^1\text{-}N_2)(PPh_3)_2$, and observed values for $RuCl_3(\eta^1\text{-}N_2Tol)(PPh_3)_2$.

Bond	$RuCl_3(\eta^1\text{-}N_2Ph)(PPh_3)_2$	$RuCl_3(\eta^1\text{-}N_2)(PPh_3)_2$,	$RuCl_3(\eta^1\text{-}N_2Tol)(PPh_3)_2$ [a]
Ru-N	1.797	2.015	1.796(9)
N-N	1.190	1.117	1.144(10)
N-Ph	1.414		1.402(1)
Ru-Cl (trans)	2.384	2.340	2.385(3)
Ru-Cl (cis)	2.435, 2.458	2.388	2.386(3), 2.292(3)
Ru-P	2.486, 2.481	2.454, 2.465	2.438(4), 2.429(4)
Ru-N-N	176.8	179.7	171.2(9)
N-N-Ph	132.2		135.9(11)
N-Ru-Cl (trans)	174.0	179.4	175.5(3)
N-Ru-Cl (cis)	91.4, 87.9	82.2, 82.4	89.7(3), 88.3(3)
N-Ru-P	93.6, 94.8	92.9, 92.4	90.7(3), 90.1(3)
Cl-Ru-Cl	179.3	164.6	177.1(1)
P-Ru-P	170.0	174.7	173.5(1)

[a] From ref. [30]

To understand what electronic transitions contribute to the observed photochemical behaviour, the electronic structure of $RuCl_3(\eta^1\text{-}PhN_2)(PPh_3)_2$ was analyzed. The computed Kohn-Sham frontier orbitals of $RuCl_3(\eta^1\text{-}PhN_2)(PPh_3)_2$ are presented in Figure 7.3. The HOMO and HOMO - 1 orbitals are dominated by Cl p and Ru d_{xy} and d_{xz} orbitals. The HOMO -1 exhibits a degree of back-bonding between ruthenium and an N_2 π* orbital. The resemblance that this molecular orbital bears towards Scheme 7.1a is indicative of this interaction developing the lone pair like orbital on the second diazonium nitrogen atom and the subsequent bending of the aryl group from linearity with the N_2 group. The LUMO and LUMO + 1 are predominantly antibonding in character composed of ruthenium d orbitals and diazonium N_2 π* orbitals. MLCT, corresponding to a transition from either the HOMO - 1 or HOMO to the LUMO or LUMO + 1, would result in a formally reduced diazonium ligand, which would be expected to result in a doubly-bent diazonium coordination mode in the excited state, Scheme 7.1b.

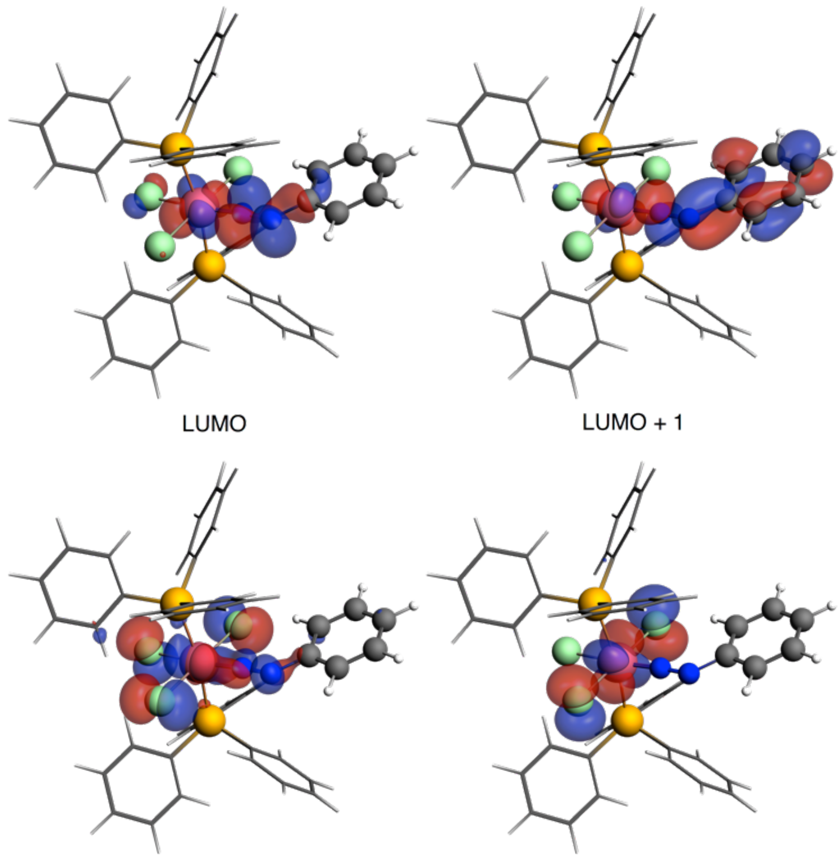

Figure 7.3: Frontier orbitals of $RuCl_3(\eta^1\text{-}N_2Ph)(PPh_3)_2$

Time-dependent DFT (TD-DFT) calculations suggest that the lowest energy electronic transitions are composed of HOMO → LUMO and HOMO - 1 → LUMO transitions at 1.687 and 1.798 eV, respectively. Optimizing for the first excited state geometry results in the expected doubly-bent diazonium coordination mode with the Ru-N-N angle decreasing from 176.8° in the ground state to 150.5° in the 1A excited state, Figure 7.4. Surprisingly, only a negligible increase of the N-Ph bond length occurs, changing from 1.414 Å in the ground state to 1.436 Å in the 1A excited state, despite photolysis into the lowest energy transitions resulting in loss of a phenyl radical. This may suggest that N-Ph homolysis is not directly occurring in the excited state, but rather as the result of vibrational relaxation of the excited state species.

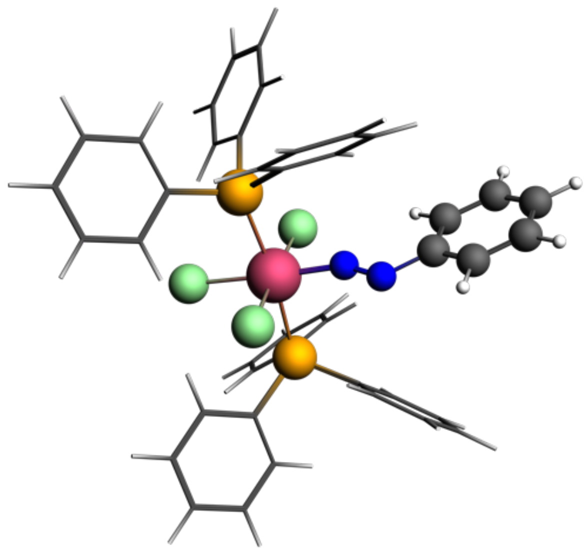

Figure 7.4. Calculated 1A excited state geometry of $RuCl_3(\eta^1\text{-}N_2Ph)(PPh_3)_2$

Conclusions

Photolysis of the nitrosyl complex $RuCl_3(\eta^1\text{-}NO)(PPh_3)_2$ in PVC matrices at 85 K results in simple linkage isomerism to yield the isonitrosyl complex, $RuCl_3(\eta^1\text{-}ON)(PPh_3)_2$. For the isoelectronic phenyldiazonium complex, $RuCl_3(\eta^1\text{-}N_2Ph)(PPh_3)_2$, the appearance of an isotopically sensitive vibrational band in the metal dinitrogen stretching region following photolysis in PVC matrices at 85 K, evidence of phenyl radical formation in solution studies, and the results of DFT computations, support a photomechanism involving homolysis of the N-Ph bond of the diazonium ligand following low-energy MLCT excitation with no evidence for linkage isomerism. Though excited-state DFT geometry optimizations show only a marginal elongation of the N-Ph bond, cleavage of this bond may occur as a result of relaxation of a vibrationally hot, excited state species. The proposed mechanism for this reaction is presented in Scheme 7.4.

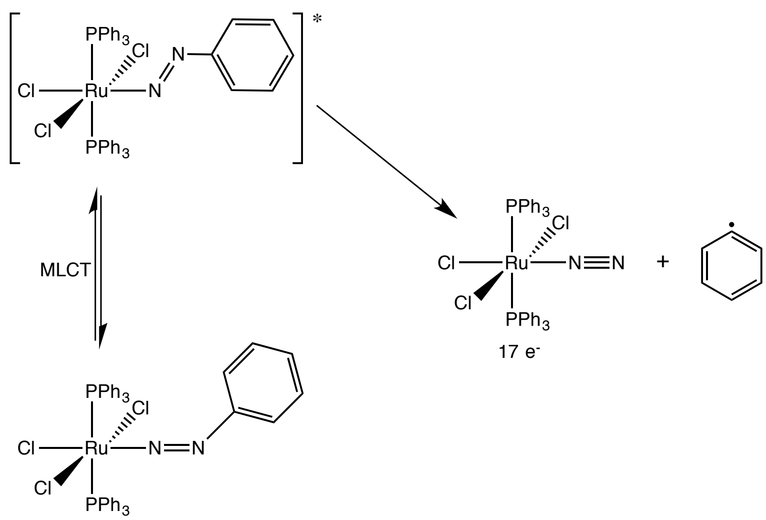

Scheme 7.4: Proposed photolytic N-Ph bond homolysis of $RuCl_3(\eta^1\text{-}N_2Ph)(PPh_3)_2$

While phenyldiazonium salts are well known to undergo reductive dediazotization by a variety of metal reducing agents to yield aryl radicals, $RuCl_3(\eta^1\text{-}N_2Ph)(PPh_3)_2$ appears to be a unique example in which an isolable metal phenylazo complex may undergo photochemical charge transfer initiated phenyl radical loss with retention (at least at cryoscopic temperatures) of the dinitrogen group.

Experimental

$RuCl_3(PPh_3)_2(NO)$ and $RuCl_3(PPh_3)_2(N_2Ph)$ were prepared by literature methods.[22,30] The apparatus and methods for matrix photochemistry have been reported elsewhere.[31] All DFT calculations were performed in the Amsterdam Density

Functional (ADF2014.02) program.[32-34] Electronic configurations of atoms were described by an all-electron triple-ζ Slater-type orbital basis set modified by a polarization function (TZP STO).[35] Geometry optimizations and vibrational frequency calculations were performed using the GGA functional of Becke[36] and Perdew[37,38] utilizing a single-component scalar relativistic correction within the zeroth order regular approximation (ZORA).[39,40] Vertical electronic excitation energies were computed with the statistical average of orbital potentials (SAOP) model.[41,42]

References

(1) Bitterwolf, T. E. *Coord. Chem. Rev.* **2006**, *250* (9-10), 1196–1207.

(2) Latham, I. A.; Leigh, G. J.; Huttner, G.; Jibril, I. *J. Chem. Soc., Dalton Trans.* **1986**, No. 2, 377.

(3) Dilworth, J. R.; Latham, I. A.; Leigh, G. J.; Huttner, G.; Jibril, I. *J. Chem. Soc., Chem. Commun.* **1983**, No. 22, 1368.

(4) Iluc, V. M.; Miller, A. J. M.; Hillhouse, G. L. *Chem. Commun.* **2005**, No. 40, 5091.

(5) Bruce King, R.; Bisnette, M. B. *J. Am. Chem. Soc.* **1964**, *86* (24), 5694–5695.

(6) Bruce King, R.; Bisnette, M. B. *Inorg. Chem.* **1966**, *5* (2), 300–306.

(7) Thornley, W. A.; Bitterwolf, T. E. *Eur. J. Inorg. Chem.* **2015**, n/a–n/a.

(8) Kunkely, H.; Vogler, A. *Inorganic Chemistry Communications* **2005**, *8* (12), 1185–1186.

(9) Galli, C. *Chem. Rev.* **1988**, *88* (5), 765–792.

(10) Beckwith, A. L. J.; Norman, R. O. C. *J. Chem. Soc., B:* **1969**, 403–410.

(11) Cepanec, I.; Litvić, M.; Udiković, J.; Pogorelić, I.; Lovrić, M. *Tetrahedron* **2007**, *63* (25), 5614–5621.

(12) Lockhart, T. P. *J. Am. Chem. Soc.* **1983**, *105* (7), 1940–1946.

(13) Andrieux, C. P.; Pinson, J. *J. Am. Chem. Soc.* **2003**, *125* (48), 14801–14806.

(14) Bard, A. J.; Gilbert, J. C.; Goodin, R. D. *J. Am. Chem. Soc.* **1974**, *96* (2), 620–621.

(15) Kochi, J. K. *J. Am. Chem. Soc.* **1955**, *77* (12), 3208–3211.

(16) Daasbjerg, K.; Sehested, K. *J. Phys. Chem. A* **2002**, *106* (46), 11098–11106.

(17) Doyle, M. P.; Guy, J. K.; Brown, K. C. *J. Am. Chem. Soc.* **1987**, *109* (5), 1536–1540.

(18) Suehiro, T. *Rev. Chem. Intermed.* **1988**, *10* (2), 101–137.

(19) Weaver, M. N.; Janicki, S. Z.; Petillo, P. A. *J. Org. Chem.* **2001**, *66* (4), 1138–1145.

(20) Glaser, R.; Horan, C. J.; Lewis, M.; Zollinger, H. *J. Org. Chem.* **1999**, *64* (3), 902–913.

(21) Doctorovich, F.; Escola, N.; Trápani, C.; Estrin, D. A.; González Lebrero, M. C.; Turjanski, A. G. *Organometallics* **2000**, *19* (19), 3810–3817.

(22) Fairy, M. B.; Irving, R. J. *J. Chem. Soc., A* **1966**, 475–475.

(23) Güida, J. A.; Piro, O. E.; Schaiquevich, P. S.; Aymonino, P. J. *Solid State Commun.* **1997**, *101* (6), 471–475.

(24) Güida, J. A.; Ramos, M. A.; Piro, O. E.; Aymonino, P. J. *J. Mol. Struct.* **2002**, *609* (1-3), 39–46.

(25) Gorelsky, S. I.; Lever, A. B. P. *Int. J. Quant. Chem.* **2000**, *80* (4-5), 636–645.

(26) Fomitchev, D. V.; Novozhilova, I.; Coppens, P. *Tetrahedron* **2000**, *56* (36), 6813–6820.

(27) Gosser, L. W.; Knoth, W. H.; Parshall, G. W. *J. Am. Chem. Soc.* **1973**, *95* (10), 3436–3437.

(28) Radziszewski, J. G.; Nimlos, M. R.; Winter, P. R.; Ellison, G. B. *J. Am. Chem. Soc.* **1996**, *118*, 7400–7401.

(29) Friderichsen, A. V.; Radziszewski, J. G.; Nimlos, M. R.; Winter, P. R.; Dayton, D. C.; David, D. E.; Ellison, G. B. *J. Am. Chem. Soc.* **2001**, *123* (9), 1977–1988.

(30) McArdle, J. V.; Schultz, A. J.; Corden, B. J. *Inorg. Chem.* **1973**, *12* (7), 1676–1681.

(31) Bays, J. T.; Bitterwolf, T. E.; Lott, K. A.; Ollino, M. A.; Rest, A. J.; Smith, L. M. *J. Organomet. Chem.* **1998**, *554* (1), 75–85.

(32) ADF 2014.01, SCM, Theoretical Chemistry, Vrije Universiteit, Amsterdam, The Netherlands, http://www.scm.com.

(33) Guerra, C. F.; Snijders, J. G.; Velde, Te, G.; Baerends, E. J. *Theor. Chem. Acc.* **1998**, *99*, 391–403.

(34) Velde, Te, G.; Bickelhaupt, F. M.; Baerends, E. J.; Fonseca Guerra, C.; van Gisbergen, S. J. A.; Snijders, J. G.; Ziegler, T. *J. Comp. Chem.* **2001**, *22* (9), 931–967.

(35) Lenthe, E. V.; Baerends, E. J. *J. Comp. Chem.* **2003**, *24* (9), 1142–1156.

(36) Becke, A. D. *Phys. Rev. A* **1988**, *38* (6), 3098–3100.

(37) Perdew, J. *Phys. Rev. B* **1986**, *33* (12), 8822–8824.

(38) Perdew, J. *Phys. Rev. B* **1986**, *34* (10), 7406–7406.

(39) Lenthe, E. V.; Baerends, E. J.; Snijders, J. G. *J. Chem. Phys.* **1993**, *99* (6), 4597.

(40) Lenthe, E. V.; Ehlers, A.; Baerends, E. J. *J. Chem. Phys.* **1999**, *110* (18), 8943.

(41) Gritsenko, O. V.; Schipper, P.; Baerends, E. J. *Chem Phys Lett* **1999**, *302*, 199–207.

(42) Schipper, P. R. T.; Gritsenko, O. V.; van Gisbergen, S. J. A.; Baerends, E. J. *J. Chem. Phys.* **2000**, *112* (3), 1344.

Appendix A: DFT Calculated Geometries and Energies for "Chapter 1: Photochemical Intramolecular Six-Electron Reductive Elimination and Oxidative Addition of Nitric Oxide by the Nitridoosmate(VIII) Anion"

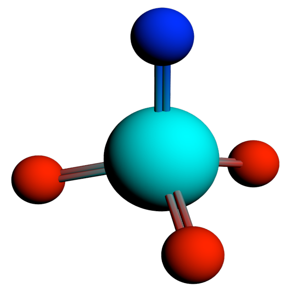

1.1a: OsO_3N^-

QZ4P/BP

Coordinates (XYZ):

Os	0.00002727	0.00000054	2.11547051
O	-0.83471115	-1.44548464	2.67659437
O	-0.83470474	1.44548173	2.67660650
O	1.66914904	0.00000315	2.67658009
N	-0.00006908	-0.00000771	0.41560768

Vibrational Frequencies (^{15}N Isotopic shifts in parentheses):

Frequency cm^{-1}	Dipole Strength 1e-40 esu2 cm2	Absorption Intensity km/mole
----------	----------	----------
302.859387	54.083886	4.105698
302.906106	54.477127	4.136188
323.442563	41.138430	3.335208
364.265097 (357.27)	27.617647	2.521635
364.265097 (357.27)	27.617647	2.521635
865.553935	894.403306	194.046405
865.568023	893.955089	193.952318
884.389522	417.156630	92.474248
1032.511509 (1001.44)	281.438277	72.837685

ΔH = 0.0 kcal mol^{-1}
ΔG = 0.0 kcal mol^{-1}

QZ4P/TPSS-D3(BJ)

Coodinates (XYZ):

Os	-0.00026400	2.11527000	0.00000000
O	-0.83164600	2.67653000	1.44280000
O	-0.83164600	2.67653000	-1.44280000
O	1.66525000	2.67597000	0.00000000
N	0.00138000	0.41920000	0.00000000

Vibrational Frequencies (^{15}N Isotopic shifts in parentheses):

Frequency cm^{-1}	Dipole Strength 1e-40 esu2 cm2	Absorption Intensity km/mole
----------	----------	----------
294.591319	70.521578	5.207389
314.668919	47.260022	3.727570
319.683050	45.552526	3.650145
360.919521 (353.81)	38.305063	3.465330
367.110246 (360.51)	24.901396	2.291386
875.397484	905.909315	198.777896
880.680777	892.602489	197.040128
892.457781	439.375256	98.288192
1038.862573 (1001.07)	273.321015	71.172004

ΔH = 0.0 kcal mol^{-1}
ΔG = 0.0 kcal mol^{-1}

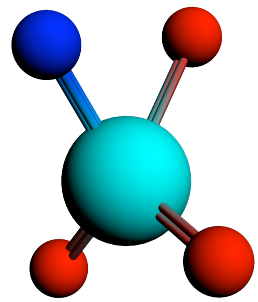

1.1b: $OsO_2(N\text{-}O)^-$ Transition State

QZ4P/BP

Coordinates (XYZ):

Os	0.01049140	-0.22071700	0.00000000
O	0.11796700	-1.13244000	-1.49156000
O	0.11796700	-1.13244000	1.49156000
O	0.85394700	1.54425000	0.00000000
N	-1.08420000	1.11031000	0.00000000

Vibrational Frequencies:

Frequency cm^{-1}	Dipole Strength 1e-40 esu2 cm2	Absorption Intensity km/mole
----------	----------	----------
-569.775249	346.204650	-49.444108
247.918097	30.255831	1.880163
248.616916	39.182078	2.441722
296.343988	72.804249	5.407928
322.612674	3.159374	0.255482
648.535265	392.154666	63.748365
881.464292	950.282128	209.959416
887.263745	675.699825	150.274265
984.631055	32.738887	8.080077

ΔH = + 60.74 kcal mol^{-1}
ΔG = + 60.68 kcal mol^{-1}

QZ4P/TPSS-D3(BJ)

Coordinates (XYZ):

Os	0.00908000	-0.22084800	0.00000000
O	0.12499800	-1.12569000	-1.49138000
O	0.12499800	-1.12569000	1.49138000
O	0.85741300	1.53232000	0.00000000
N	-1.08488000	1.11032000	0.00000000

Vibrational Frequencies:

Frequency cm^{-1}	Dipole Strength 1e-40 esu2 cm2	Absorption Intensity km/mole
----------	----------	----------
-596.131792	306.812034	-45.845081
246.897356	34.583000	2.140214
247.224785	55.145599	3.417283
288.859550	84.389531	6.110171
316.913348	5.146838	0.408845
657.607668	390.644680	64.391249
891.385661	974.920123	217.827521
894.165683	700.636832	157.032315
980.170378	24.996060	6.141171

ΔH = + 60.46 kcal mol^{-1}
ΔG = + 60.43 kcal mol^{-1}

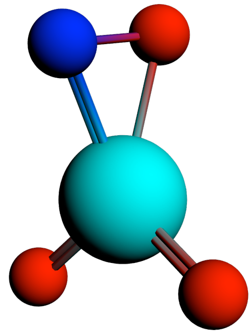

1.1c: $OsO_2(\eta^2\text{-}NO)^-$

QZ4P/BP

Coordinates (XYZ):

Os	-0.02840042	-0.00000310	2.13310915
O	-0.80310168	-1.46534772	2.66068370
O	-0.80295888	1.46532658	2.66086825
O	1.77739526	0.00001445	1.40378145
N	0.74593875	0.00013530	0.44025930

Vibrational Frequencies (^{15}N Isotopic shifts in parentheses):

Frequency cm^{-1}	Dipole Strength 1e-40 esu2 cm2	Absorption Intensity km/mole
----------	----------	----------
228.073792	26.314083	1.504325
248.386027	11.429179	0.711574
293.592462	81.145105	5.971526
385.760443 (379.48)	11.438977	1.106071
558.568401 (548.77)	24.666600	3.453534
680.443388 (667.57)	52.656074	8.980873
886.520252	1049.560839	233.224596
916.189495 (914.05)	900.008679	206.685531
974.424845 (957.91)	237.301204	57.959731

ΔH = + 39.44 kcal mol^{-1}
ΔG = + 39.27 kcal mol^{-1}

QZ4P/TPSS-D3(BJ)

Coordinates (XYZ):

Os	-0.02853400	-0.00006500	2.13218000
O	-0.79667500	-1.46609000	2.65998000
O	-0.79609400	1.46627000	2.65983000
O	1.77416000	0.00036900	1.41574000
N	0.73627500	0.00035900	0.44138700

Vibrational Frequencies (^{15}N Isotopic shifts in parentheses):

Frequency cm^{-1}	Dipole Strength 1e-40 esu2 cm2	Absorption Intensity km/mole
----------	----------	----------
220.569414	15.920063	0.880173
240.072877	31.284699	1.882579
284.125540	96.371484	6.863362
391.300939 (384.33)	10.884175	1.067541
577.416674 (571.36)	10.255376	1.484291
696.066996 (683.57)	65.395459	11.409765
894.665808	1077.370914	241.604020
922.682287 (918.67)	999.299356	231.113791
964.468529 (948.58)	168.709342	40.785450

ΔH = + 39.51 kcal mol^{-1}
ΔG = + 39.48 kcal mol^{-1}

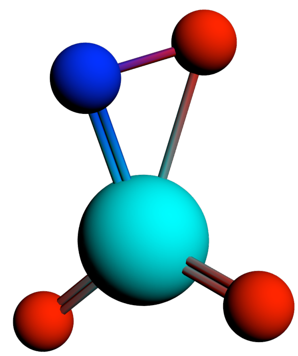

1d: $OsO_2(\eta^{2\rightarrow1}\text{-NO})^-$ Transition State

QZ4P/BP

Coordinates (XYZ):

Os	-0.06691700	-0.03727200	-0.68799500
O	-1.04954000	0.50172200	1.22873000
O	0.12922700	1.60421000	-1.21576000
O	0.44834400	-1.44608000	-1.58035000
N	0.11437500	-0.16384500	1.16825000

Vibrational Frequencies:

Frequency cm^{-1}	Dipole Strength 1e-40 esu2 cm2	Absorption Intensity km/mole
----------	----------	----------
-504.463716	156.351480	-19.770152
155.951181	55.792769	2.180945
201.414113	49.472858	2.497669
262.913741	5.416778	0.356971
321.269233	16.367999	1.318083
763.209242	78.455512	15.008772
879.521119	915.981920	201.934835
893.115202	802.767741	179.711332
1026.516076	625.941593	161.056270

ΔH = + 61.63 kcal mol^{-1}
ΔG = + 61.54 kcal mol^{-1}

QZ4P/TPSS-D3(BJ)

Coordinates (XYZ):

Os	-0.06292500	-0.03896600	-0.68193400
O	-1.07157000	0.48181500	1.17387000
O	0.08665800	1.60593000	-1.21704000
O	0.43806700	-1.43345000	-1.60366000
N	0.10294000	-0.20893800	1.15358000

Vibrational Frequencies:

Frequency cm^{-1}	Dipole Strength 1e-40 esu2 cm2	Absorption Intensity km/mole
----------	----------	----------
-502.172249	153.328739	-19.299868
145.374839	66.073335	2.407651
203.296296	72.486852	3.693744
251.867661	1.771661	0.111849
322.558837	18.640447	1.507104
757.647925	123.082285	23.374432
877.069574	951.916698	209.271969
887.304060	1037.176158	230.676346
991.920854	458.114674	113.901461

ΔH = + 60.92 kcal mol^{-1}
ΔG = + 60.43 kcal mol^{-1}

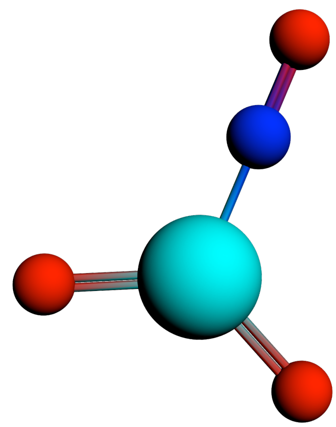

1.1e: $OsO_2(\eta^1\text{-}NO)^-$

QZ4P/BP

Coordinates (XYZ):

Os	0.00000163	-0.00000241	-0.67921067
O	0.00000069	0.00001638	2.28639652
O	0.00000186	1.58676221	-1.43136001
O	0.00000186	-1.58675286	-1.43139023
N	0.00000108	0.00000368	1.05937180

Vibrational Frequencies (^{15}N Isotopic shifts in parentheses):

Frequency cm^{-1}	Dipole Strength 1e-40 esu2 cm2	Absorption Intensity km/mole
----------	----------	----------
69.829627	220.279529	3.855600
107.207829	30.499396	0.819588
161.647311	7.028193	0.284767
265.898366	0.721187	0.048066
471.625693 (459.49)	15.704859	1.856562
633.772456 (628.68)	234.115235	37.191278
864.801696	1144.392403	248.067328
886.131544	555.558174	123.397343
1624.213553 (1586.40)	1378.547	561.232718

ΔH = + 25.67 kcal mol^{-1}
ΔG = + 24.00 kcal mol^{-1}

QZ4P/TPSS-D3(BJ)

Coordinates (XYZ):

Os	0.00000000	0.00000000	0.63998800
O	0.00000000	0.00000000	-2.32597000
O	0.00000000	-1.58412000	1.39232000
O	0.00000000	1.58412000	1.39232000
N	0.00000000	0.00000000	-1.09780000

Vibrational Frequencies (^{15}N Isotopic shifts in parentheses):

Frequency cm^{-1}	Dipole Strength 1e-40 esu2 cm2	Absorption Intensity km/mole
----------	----------	----------
38.209629	426.165403	4.081587
103.777720	58.901232	1.532169
168.086484	1.839365	0.077496
264.070040	0.046515	0.003079
472.177358 (460.10)	14.358213	1.699353
632.567922 (627.47)	243.982107	38.685054
873.044057	1155.484828	252.859036
891.997871	574.635100	128.479559
1614.586943 (1577.03)	1464.610	592.736592

ΔH = + 27.89 kcal mol^{-1}
ΔG = + 27.58 kcal mol^{-1}

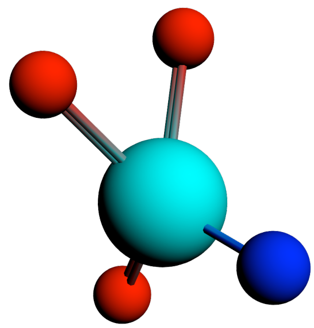

1f: OsNO(O-O)⁻ Transition State

QZ4P/BP

Coordinates (XYZ):

Os -0.0127817 -0.22899 -0.010731
O 0.229949 -1.21837 -1.44011
N 0.224958 -1.07551 1.43352
O 0.898844 1.586 0.0571551
O -1.05544 1.20394 0.0709925

Vibrational Frequencies:

Frequency cm^{-1}	Dipole Strength 1e-40 esu2 cm2	Absorption Intensity km/mole
----------	----------	----------
-425.261012	14.790533	-1.576585
124.226740	882.303566	27.473323
166.661905	47.165120	1.970314
287.825820	72.789421	5.251412
370.347982	25.675423	2.383448
759.624657	533.990100	101.674098
821.726817	784.154842	161.512954
1078.914717	236.221653	63.882939
1264.074495	190.966462	60.507309

ΔH = + 83.90 kcal mol^{-1}
ΔG = + 83.37 kcal mol^{-1}

QZ4P/TPSS-D3(BJ)

Coordinates (XYZ):

Os 0.238701 0.00548767 0.0
O 1.36201 -1.33996 0.0
N 0.987474 1.51587 0.0
O -1.38294 -0.0681627 -0.972738
O -1.38294 -0.0681627 0.972738

Vibrational Frequencies:

Frequency cm^{-1}	Dipole Strength 1e-40 esu2 cm2	Absorption Intensity km/mole
----------	----------	----------
-425.261012	14.790533	-1.576585
124.226740	882.303566	27.473323
166.661905	47.165120	1.970314
287.825820	72.789421	5.251412
370.347982	25.675423	2.383448
759.624657	533.990100	101.674098
821.726817	784.154842	161.512954
1078.914717	236.221653	63.882939
1264.074495	190.966462	60.507309

ΔH = + 86.38 kcal mol^{-1}
ΔG = + 86.32 kcal mol^{-1}

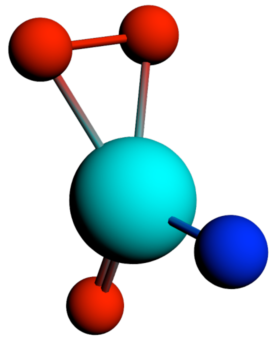

1g: $OsNO(\eta^2\text{-}O_2)^-$

QZ4P/BP

Coordinates (XYZ):

Os -0.0471143 -0.0178931 2.12026
O -0.82472 -1.41916 2.82413
N -0.651867 1.44363 2.68378
O 1.80205 0.0899507 1.45135
O 0.833185 0.0976274 0.364289

Vibrational Frequencies:

Frequency cm^{-1}	Dipole Strength 1e-40 esu2 cm2	Absorption Intensity km/mole
----------	----------	----------
217.114469	1.256979	0.068406
218.288553	17.393894	0.951713
266.240118	0.256093	0.017090
340.437016	1.498657	0.127884
500.556954	21.437152	2.689668
555.780002	323.273911	45.035153
886.164048	915.098681	203.263840
925.359533	271.125396	62.886695
1073.842093	297.362209	80.039482

ΔH = + 62.66 kcal mol^{-1}
ΔG = + 62.19 kcal mol^{-1}

QZ4P/TPSS-D3(BJ)

Coordinates (XYZ):

Os -0.0463695 -0.0173749 2.12019
O -0.821154 -1.42079 2.81848
N -0.650498 1.44344 2.67987
O 1.79892 0.0876068 1.4603
O 0.822614 0.0955416 0.365243

Vibrational Frequencies:

Frequency cm^{-1}	Dipole Strength 1e-40 esu2 cm2	Absorption Intensity km/mole
----------	----------	----------
199.899118	26.081454	1.306835
236.331000	6.134160	0.363374
272.722788	1.112144	0.076026
335.599870	4.549939	0.382741
515.435435	23.645824	3.054969
566.105594	326.030847	46.263044
893.266299	947.922995	212.242366
914.175265	255.988129	58.658015
1079.716456	305.926445	82.795134

ΔH = + 61.20 kcal mol^{-1}
ΔG = + 61.16 kcal mol^{-1}

1a SOC-TDDFT Excitations

Label	Hartree	cm^{-1}	nm	Oscillator Strength a.u.
A2 1	0.107	23483.785	425.82572	0
E 1	0.1077	23637.417	423.05805	3E-05
A1 1	0.1118	24537.263	407.54340	3.25E-06
A2 2	0.1119	24559.211	407.17920	0
E 2	0.1147	25173.740	397.23934	7.72E-05
E 3	0.1179	25876.058	386.45761	1.3E-05
A1 2	0.1194	26205.270	381.60261	0.0016042
E 4	0.1201	26358.903	379.37845	1.13E-05
A2 3	0.1264	27741.593	360.46956	0
E 5	0.1302	28575.596	349.94894	0.0111945
E 6	0.1378	30243.604	330.64842	2.93E-05
A1 3	0.1396	30638.658	326.38504	0.0328417
E 7	0.1399	30704.500	325.68515	0.0004529
A2 4	0.1423	31231.239	320.19221	0
A1 4	0.143	31384.872	318.62484	0.0088725
E 8	0.1469	32240.823	310.16577	0.0014566
E 9	0.1476	32394.455	308.69480	6.49E-05
A2 5	0.1506	33052.879	302.54550	0
A1 5	0.1518	33316.248	300.15383	0.0058011
E 10	0.1594	34984.256	285.84286	0.0004407
E 11	0.163	35774.364	279.52977	0.0296032
A1 6	0.1631	35796.312	279.35838	6.37E-05
A2 6	0.1633	35840.207	279.01624	0
A2 7	0.164	35993.839	277.82532	0
E 12	0.1659	36410.841	274.64347	0.0014262
A1 7	0.1668	36608.368	273.16158	0.0002753
E 13	0.1709	37508.214	266.60826	0.0049746
E 14	0.1726	37881.321	263.98234	6.85E-05
A2 8	0.1784	39154.273	255.39995	0
E 15	0.1789	39264.011	254.68615	7.11E-05
E 16	0.1796	39417.643	253.69350	0.0011574
E 17	0.1837	40317.489	248.03131	1.13E-05
E 18	0.184	40383.331	247.62691	0.0001362
A2 9	0.1845	40493.069	246.95584	0
A1 8	0.1845	40493.069	246.95584	0.0001146
A2 10	0.1864	40910.071	244.43858	0
A1 9	0.1883	41327.072	241.97213	0.0020082
A1 10	0.191	41919.654	238.55158	1.6E-05
E 19	0.1917	42073.286	237.68050	0.0012735
A2 11	0.1928	42314.708	236.32444	0
E 20	0.1937	42512.235	235.22639	0.0578364
E 21	0.2001	43916.873	227.70291	0.0363222
E 22	0.202	44333.875	225.56115	0.0139508
E 23	0.2023	44399.717	225.22665	0.0002035
A2 12	0.2034	44641.139	224.00861	0
A1 11	0.2036	44685.034	223.78856	1.95E-05
E 24	0.2104	46177.462	216.55585	0.0017583
E 25	0.212	46528.621	214.92147	0.0023737
A1 12	0.2129	46726.148	214.01293	6.2E-05
E 26	0.2149	47165.097	212.02118	0.0415724

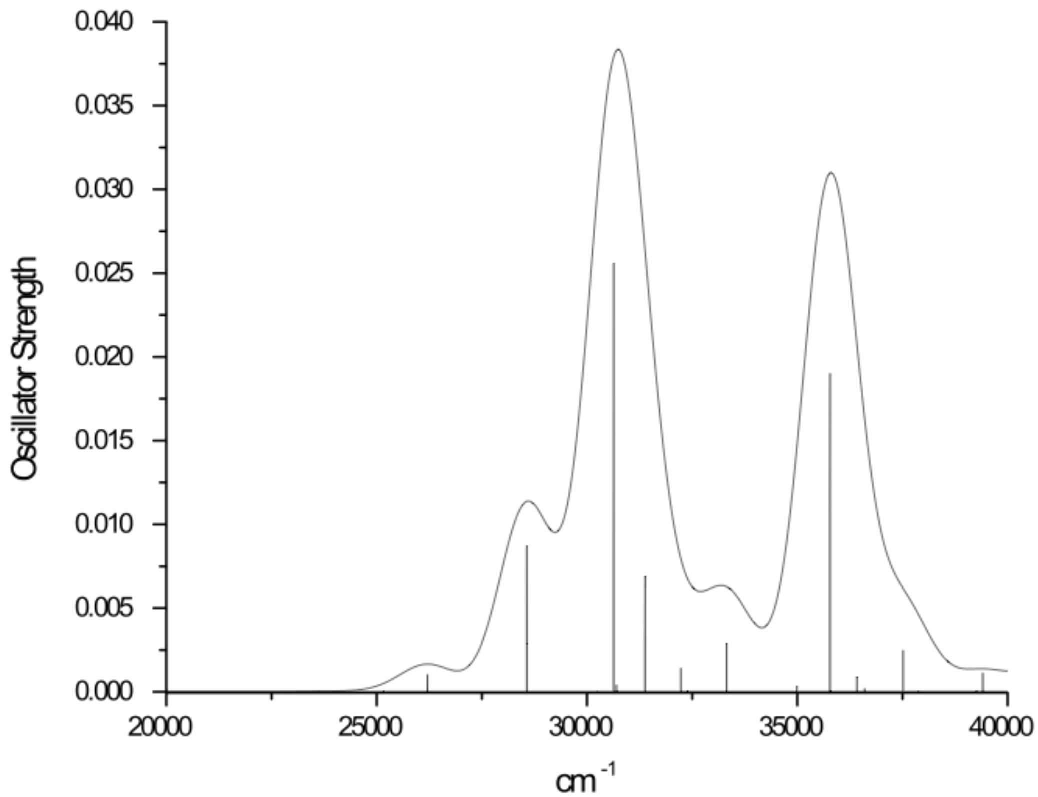

Figure A1: Calculated SOC-B88P86 TDDFT Electronic Spectrum of 1.1a

1c SOC-TDDFT Excitations

Label	Hartree	cm^{-1}	nm	Oscillator Strength a.u.
A"_1	0.0543	11917.472	839.1	3.33E-06
A'_1	0.0543	11917.472	839.1	6.71E-06
A"_2	0.0544	11939.419	837.56	1.82E-05
A'_2	0.0737	16175.280	618.23	0.0003124
A"_3	0.074	16241.122	615.72	7.43E-05
A'_3	0.0742	16285.017	614.06	0.0005189
A"_4	0.0894	19621.031	509.66	7.08E-05
A'_4	0.0945	20740.352	482.15	0.0255923
A"_5	0.0987	21662.145	461.63	1.97E-05
A'_5	0.0988	21684.093	461.17	8.13E-06
A'_6	0.1038	22781.466	438.95	0.0289456
A"_6	0.1046	22957.046	435.6	9.56E-07
A"_7	0.1079	23681.312	422.27	8.72E-05
A'_7	0.1089	23900.787	418.4	0.0075846
A"_8	0.1099	24120.261	414.59	0.0001349
A'_8	0.1198	26293.060	380.33	0.0044046
A"_9	0.1274	27961.067	357.64	1.65E-05
A'_9	0.1278	28048.857	356.52	0.0024696
A'_10	0.1284	28180.542	354.85	0.0005181
A"_10	0.1293	28378.069	352.38	0.0003125
A'_11	0.13	28531.701	350.49	0.0006192
A"_11	0.1303	28597.544	349.68	9.92E-05
A'_12	0.1383	30353.341	329.45	0.0011140
A"_12	0.1384	30375.288	329.21	2.58E-05
A'_13	0.1395	30616.710	326.62	0.0015602
A"_13	0.1407	30880.080	323.83	0.0001795
A'_14	0.142	31165.397	320.87	0.0039766
A'_15	0.1429	31362.924	318.85	0.0029724
A"_14	0.1429	31362.924	318.85	6.16E-05
A"_15	0.1446	31736.031	315.1	0.0001888
A'_16	0.1459	32021.348	312.29	0.0015194
A"_16	0.1461	32065.243	311.86	4.89E-05
A"_17	0.1513	33206.511	301.15	8.5E-05
A'_17	0.1528	33535.723	298.19	0.0356867
A"_18	0.1565	34347.779	291.14	0.0084087
A"_19	0.157	34457.516	290.21	7.2E-06
A'_18	0.1571	34479.464	290.03	0.0001804
A'_19	0.1579	34655.044	288.56	0.0536702
A"_20	0.1616	35467.100	281.95	0.0171972
A'_20	0.1654	36301.103	275.47	0.0017630
A"_21	0.1672	36696.158	272.51	8.9E-07
A'_21	0.1681	36893.685	271.05	0.0035113
A"_22	0.1683	36937.580	270.73	0.0020081
A'_22	0.1733	38034.953	262.92	0.0001103
A"_23	0.1733	38034.953	262.92	3.61E-06
A'_23	0.1739	38166.638	262.01	0.0009818
A"_24	0.1754	38495.850	259.77	3.18E-06
A'_24	0.1764	38715.324	258.3	0.0065748
A"_25	0.1803	39571.275	252.71	2.01E-05
A'_25	0.1804	39593.223	252.57	1.2E-05

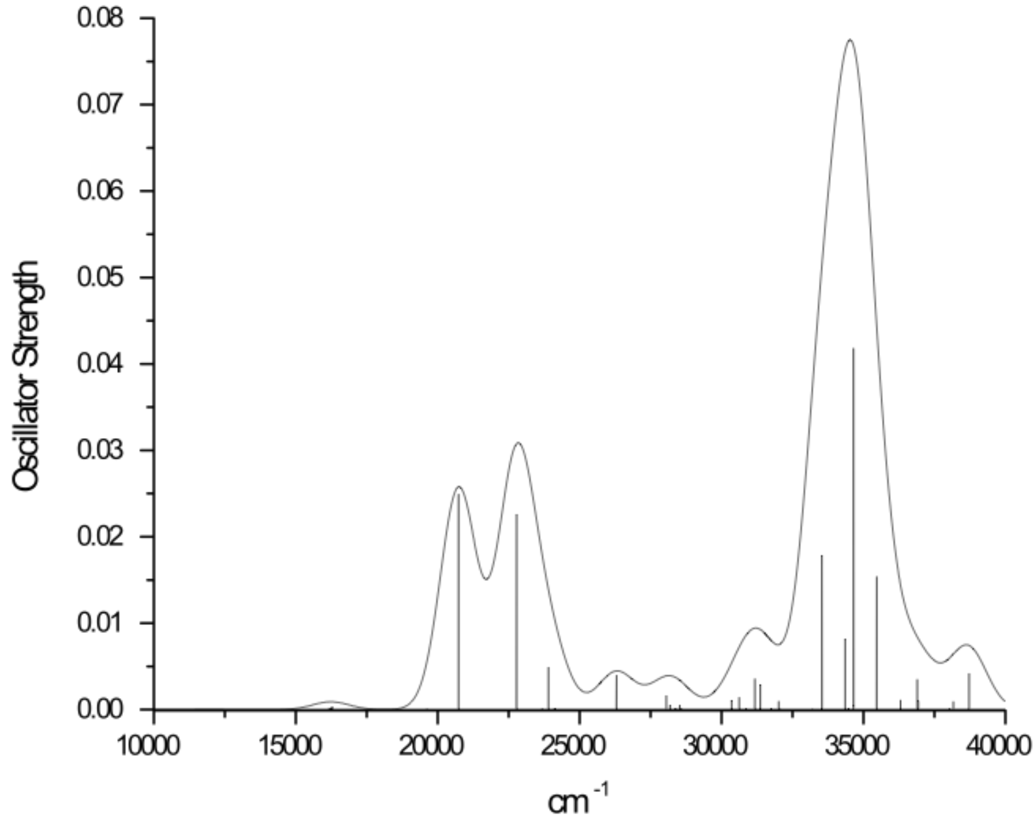

Figure A2: Calculated SOC-B88P86 TDDFT Electronic Spectrum of 1c

1e SOC-TDDFT Excitations

Label	Hartree	cm^{-1}	nm	Oscillator Strength a.u.
A2_1	0.0433	9503.2514	1052.2714	0
B2_1	0.0434	9525.1989	1049.8468	0.0001266
A1_1	0.044	9656.8837	1035.5307	0.0007561
B1_1	0.0499	10951.784	913.09324	0.0005792
B1_2	0.072	15802.173	632.82434	0.0001047
B2_2	0.0726	15933.858	627.59439	5.23E-05
A1_2	0.0733	16087.490	621.60099	1.6E-05
B1_3	0.0844	18523.658	539.85015	6.17E-07
A1_3	0.0846	18567.553	538.57391	2.36E-05
B2_3	0.0851	18677.291	535.40955	0.0001522
A2_2	0.088	19313.767	517.76537	0
A2_3	0.095	20850.089	479.61424	0
B1_4	0.0964	21157.354	472.64888	0.0001570
A1_4	0.0966	21201.249	471.67031	0.0005918
A2_4	0.1008	22123.042	452.01738	0
B1_5	0.109	23922.734	418.01241	4.76E-05
A1_5	0.1094	24010.524	416.48402	0.0005587
A2_5	0.1104	24229.999	412.71152	0
B2_4	0.1171	25700.479	389.09780	0.0036757
A2_6	0.1182	25941.901	385.47675	0
B2_5	0.1184	25985.796	384.82561	0.0038051
B2_6	0.1201	26358.903	379.37845	0.0092631
A1_6	0.1233	27061.221	369.53246	0.0065447
B1_6	0.1234	27083.169	369.23300	0.0085464
A2_7	0.1351	29651.022	337.25649	0
B2_7	0.1354	29716.864	336.50925	0.0002226
A1_7	0.1369	30046.076	332.82215	0.0001212
A2_8	0.1371	30089.971	332.33663	0
B2_8	0.1377	30221.656	330.88854	0.0007978
B1_7	0.1391	30528.921	327.55825	0.003846
B2_9	0.1448	31779.926	314.66403	8.4E-05
A2_9	0.1448	31779.926	314.66403	0
B1_8	0.1477	32416.402	308.48580	0.0011023
A2_10	0.1479	32460.297	308.06864	0
B2_10	0.148	32482.245	307.86049	0.0001534
B1_9	0.1484	32570.035	307.03067	0.0022264
B1_10	0.1502	32965.089	303.35121	0.0059645
A1_8	0.1516	33272.353	300.54982	0.0250228
A1_9	0.1578	34633.096	288.74114	7.3E-05
B1_11	0.1582	34720.886	288.01107	0.0009272
A2_11	0.1607	35269.573	283.53050	0
B2_11	0.1612	35379.310	282.65107	0.0005034
A1_10	0.1634	35862.154	278.84548	9.75E-06
B1_12	0.166	36432.788	274.47802	3.52E-05
A1_11	0.1661	36454.736	274.31278	0.0002056
A2_12	0.1684	36959.527	270.56622	0
B2_12	0.1687	37025.370	270.08507	0.0003078
A1_12	0.1722	37793.531	264.59554	0.0010158
A2_13	0.1743	38254.428	261.40764	0
A1_13	0.1758	38583.639	259.17720	0.0010216

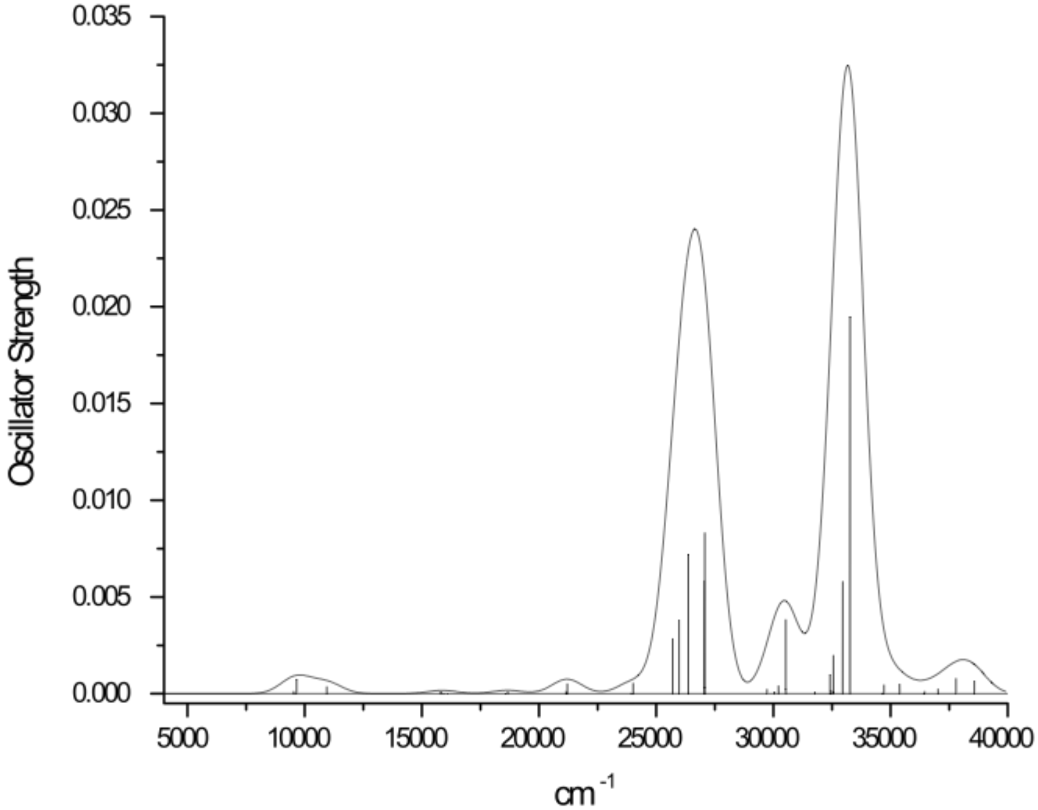

Figure A3: Calculated SOC-B88P86 TDDFT Electronic Spectrum of 1e

Appendix B: Additional Spectra for "Chapter 3: Revisiting the Photochemistry of Vaska's O_2 Complex: Competitive Reductive and Non-Reductive Elimination Reactions"

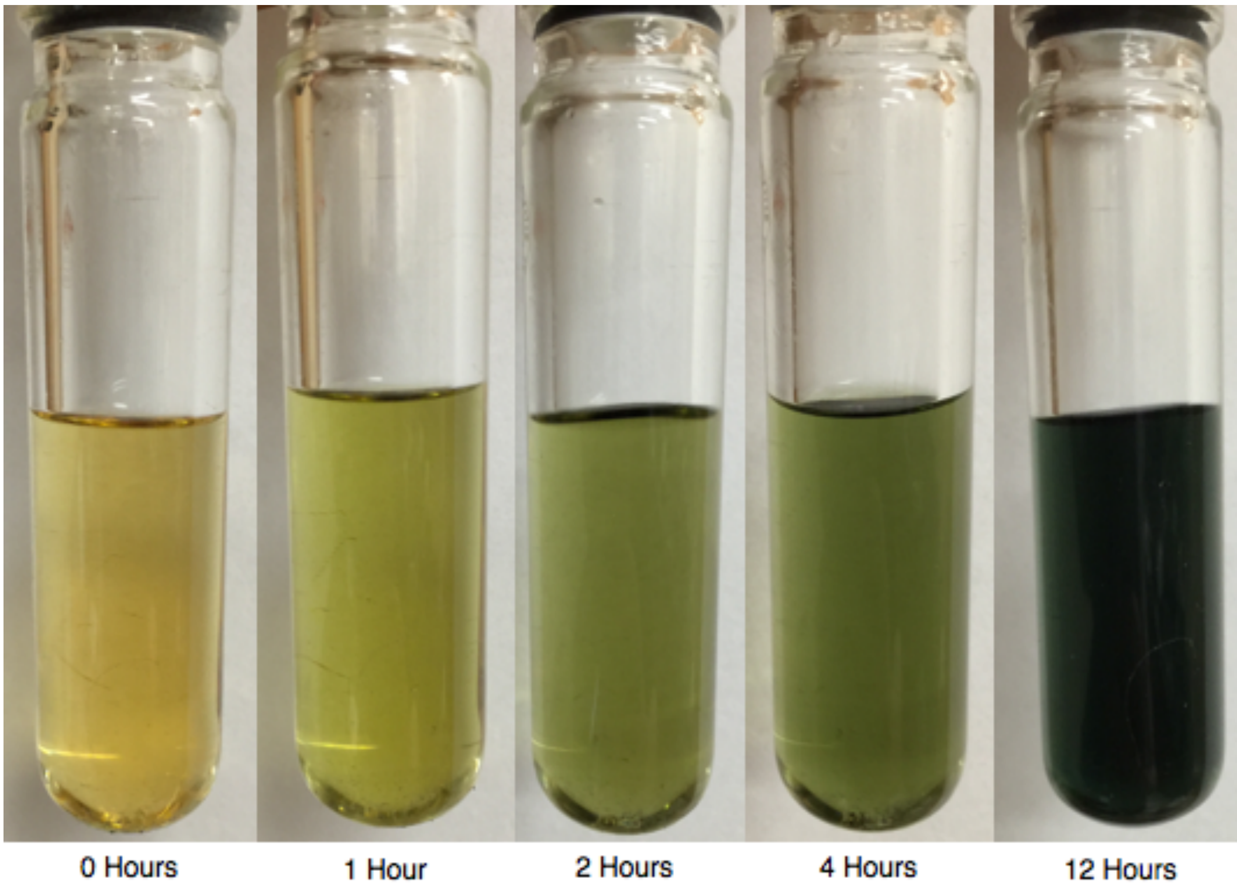

Figure B1: Observed color change following 350 ± 70 nm photolysis of $Ir^{III}Cl(CO)O_2[P(C_6H_5)_3]_2$ in CH_2Cl_2 under 20 PSI O_2.

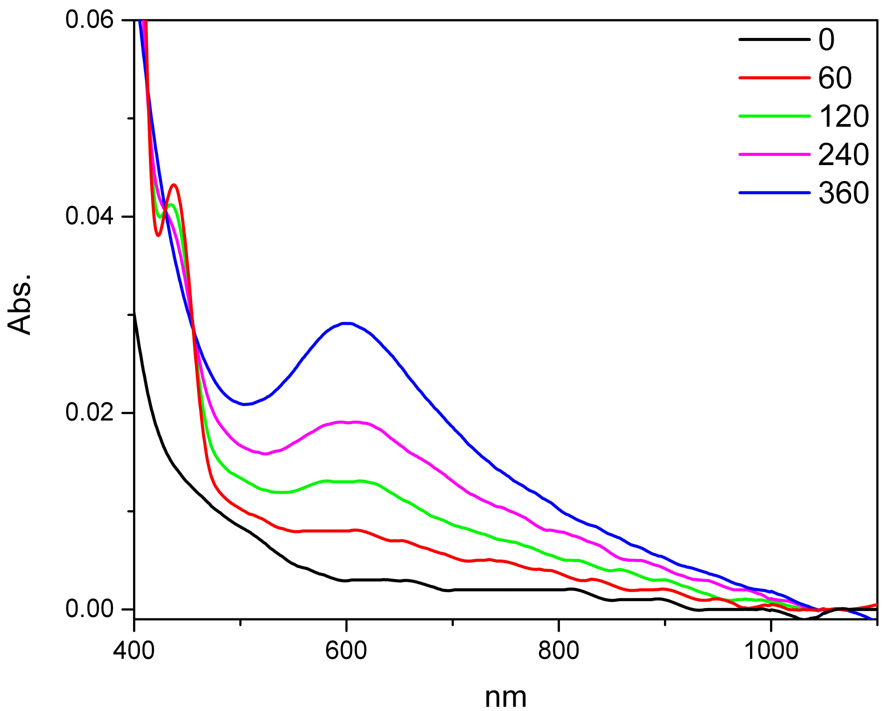

Figure B2: Observed UV-Vis spectral evolution of $Ir^{III}Cl(CO)O_2[P(C_6H_5)_3]_2$ in toluene under 20 PSI O_2 at intervals between 0-360 minutes during 350 ± 70 nm photolysis.

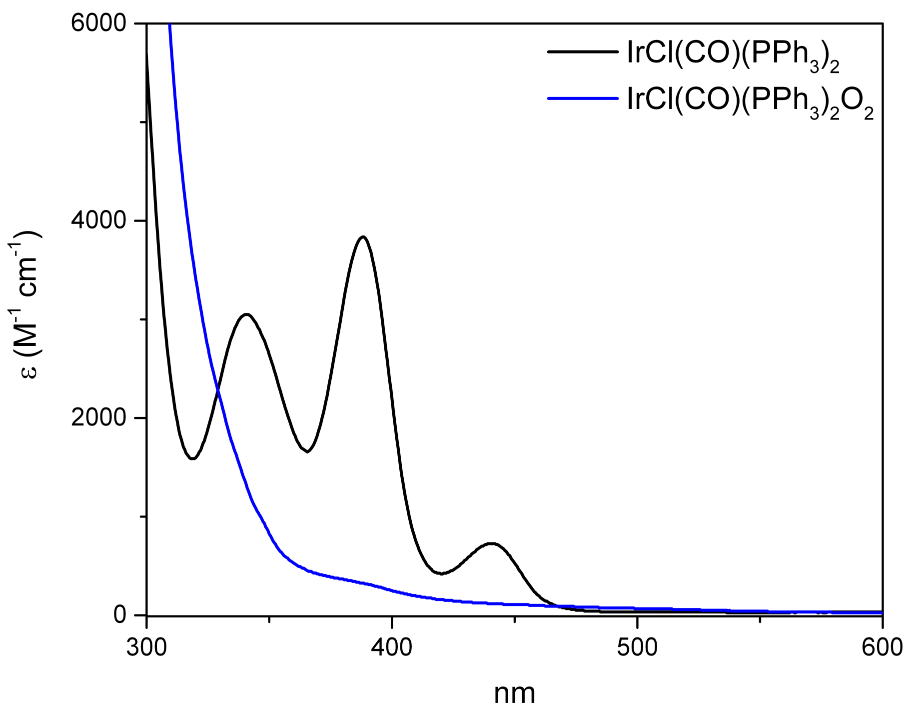

Figure B3: UV-Vis spectra of $Ir^{III}Cl(CO)O_2[P(C_6H_5)_3]_2$ and $Ir^{I}Cl(CO)[P(C_6H_5)_3]_2$ in toluene.

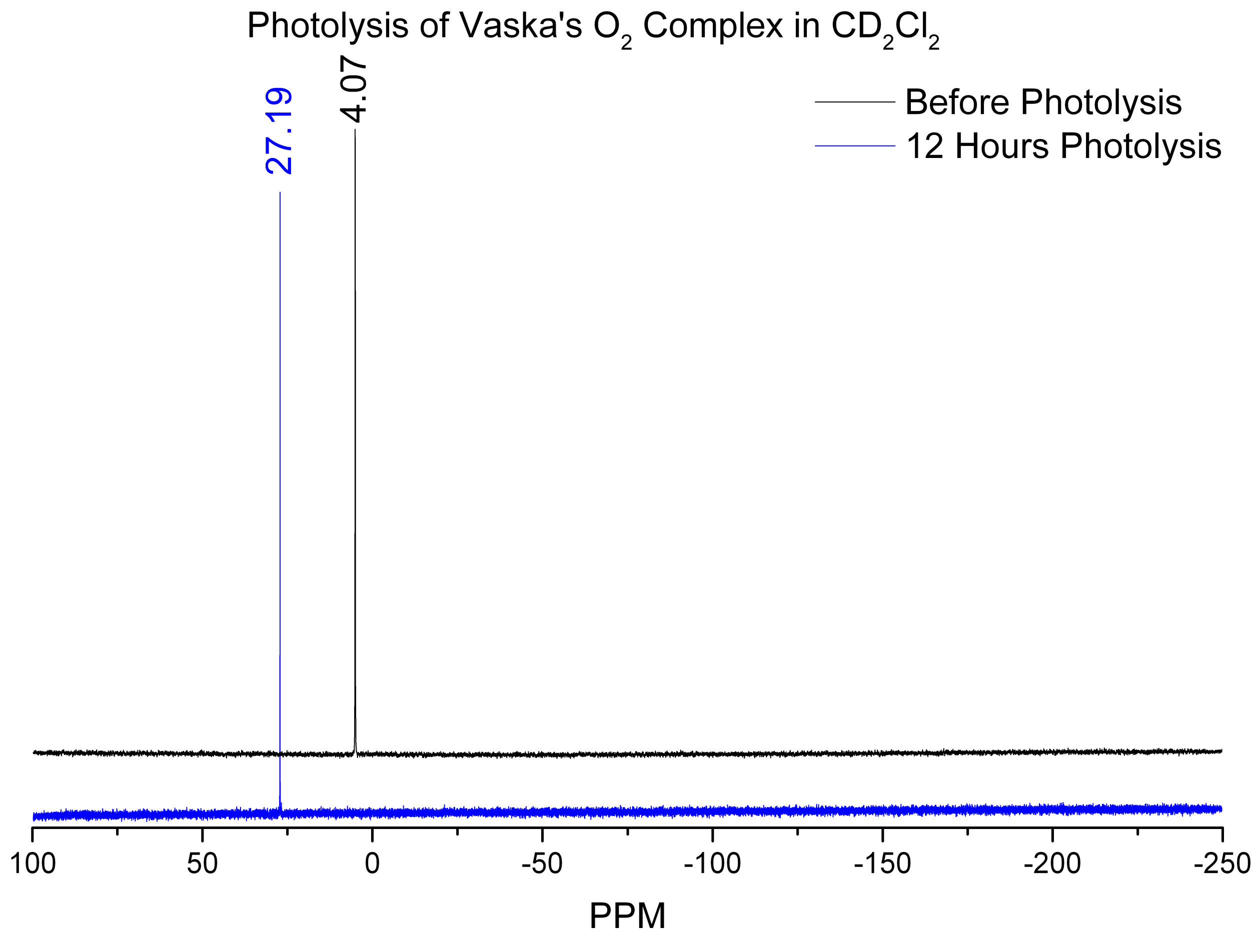

Figure B4: $Ir^{III}Cl(^{13}CO)O_2[P(C_6H_5)_3]_2$ (black trace). ^{31}P NMR (120 MHz, [D$_2$]Methylene Chloride, 30 °C): δ = 4.07 (d, $J^{P\text{-}13CO}$ = 8.70 Hz; *ipso*).

Photolysis product – $OPPh_3$ (blue trace). ^{31}P NMR (120 MHz, [D$_2$]Methylene Chloride, 30 °C): δ = 27.19.

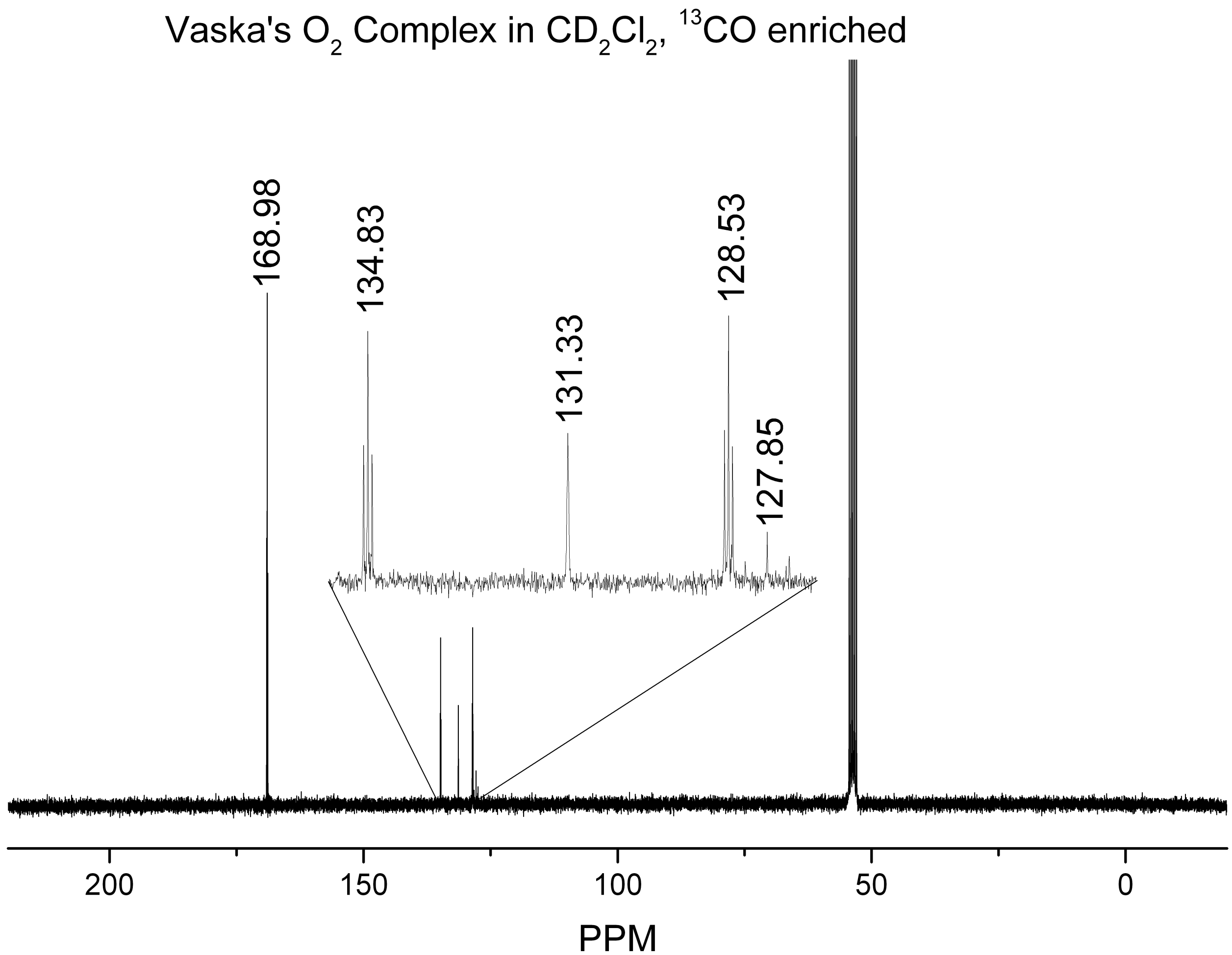

Figure B5: $Ir^{III}Cl(^{13}CO)O_2[P(C_6H_5)_3]_2$. ^{13}C NMR (75 MHz, [D2]Methylene Chloride, 30 °C): δ = 127.85 (t, J = 29.05 Hz; *ipso*), 128.53 (t, J = 5.31 Hz; *ortho*), 131.33 (t, J = 0.91 Hz; *para*), 134.83 (t, J = 5.57 Hz; *meta*), 168.98 (t, J = 8.71 Hz; ^{13}CO)

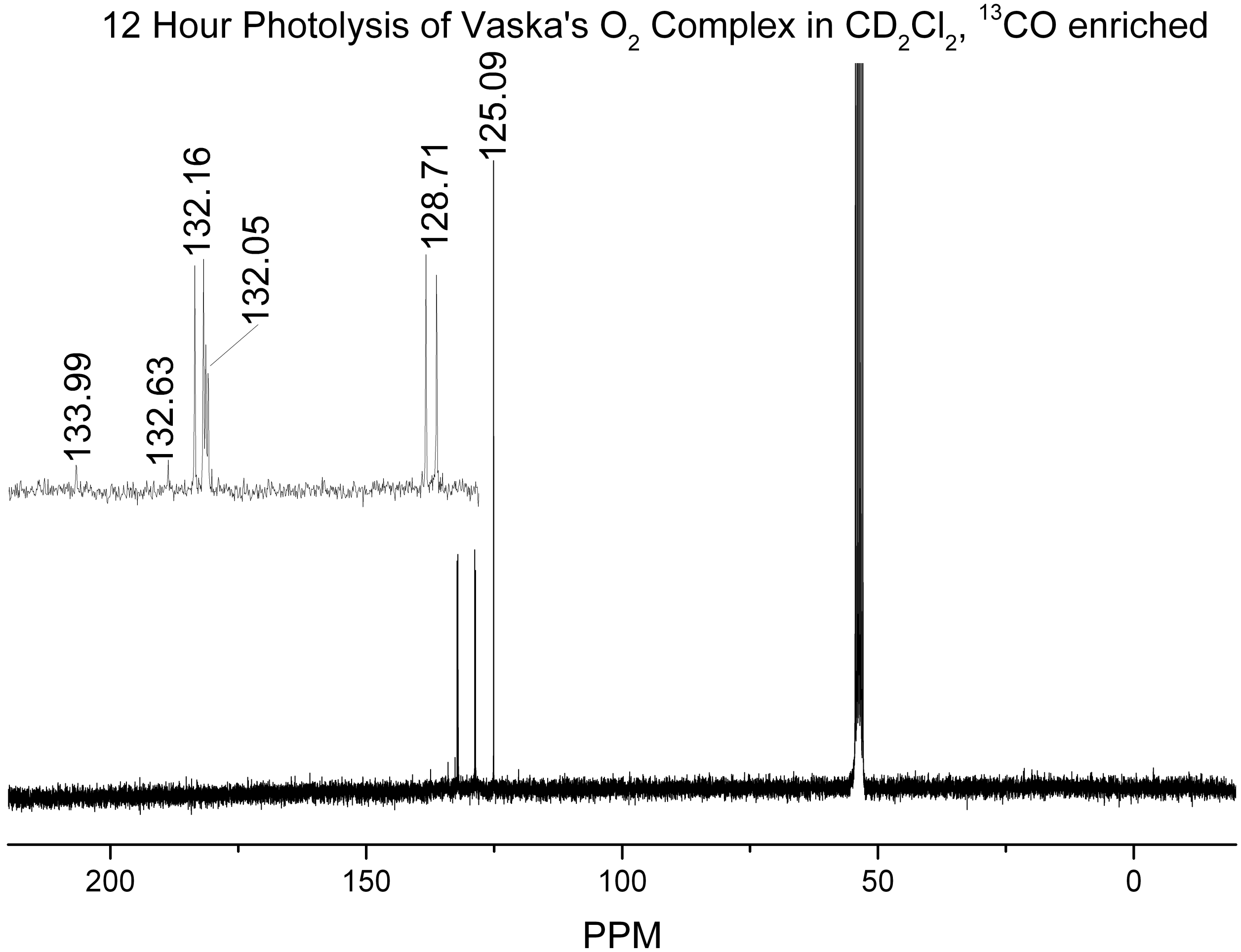

Figure B6: Photolysis products - CO_2/$OPPh_3$. ^{13}C NMR (75 MHz, [D_2]Methylene Chloride, 30 °C): δ = 125.09 (s; CO_2), 128.71 (d, J = 6.04 Hz; *meta*), 132.05 (d, J = 1.24 Hz; *para*), 132.16 (d, J = 4.93 Hz; *ortho*), 133.31 (d, J = 51.61 Hz; *ipso*)

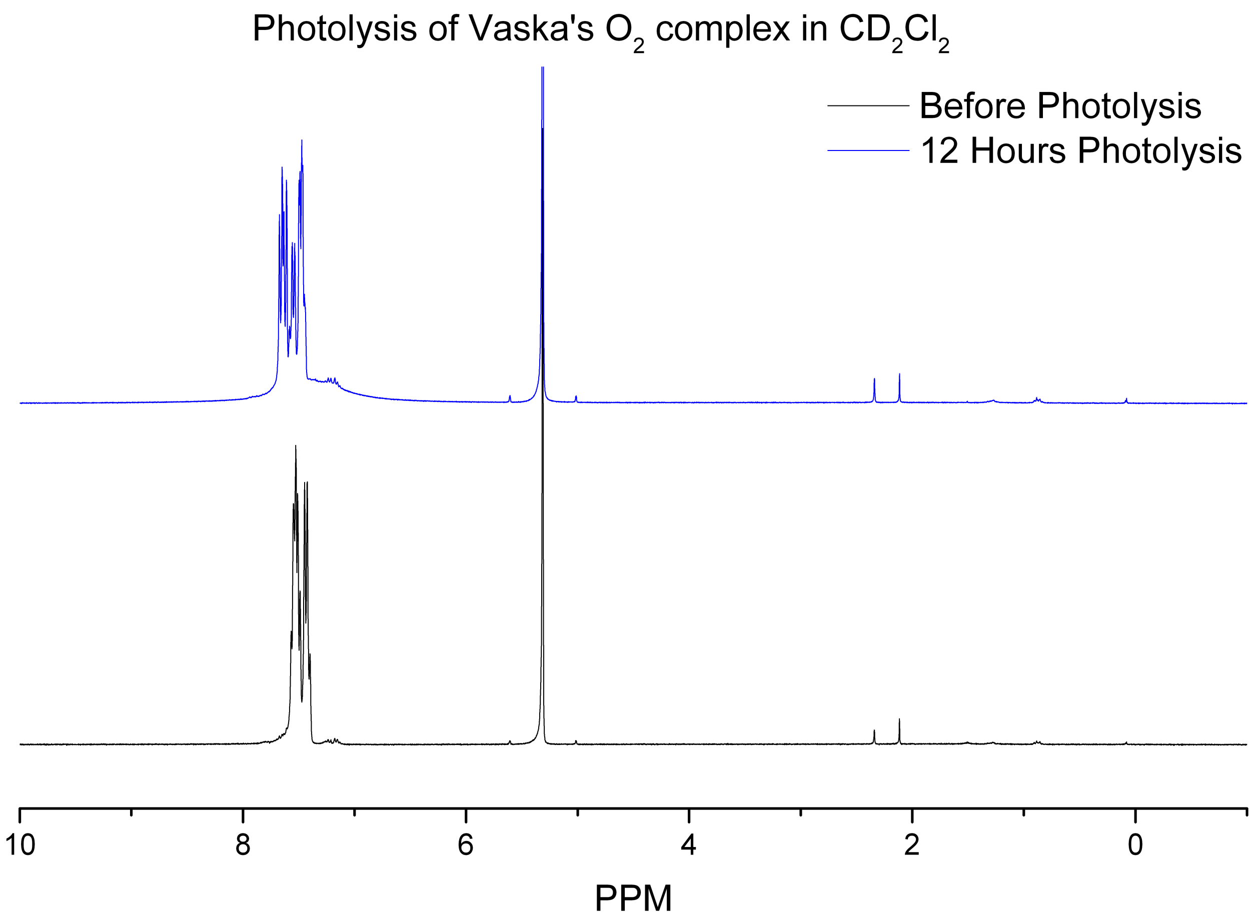

Figure B7: $Ir^{III}Cl(^{13}CO)O_2[P(C_6H_5)_3]_2$ (black trace). ^1H NMR (300 MHz, [D_2]Methylene Chloride, 30 °C): δ = 7.44 (m; 2H), 7.53 (m, 3H).

Photolysis product - $OPPh_3$ (blue trace). ^1H NMR (300 MHz, [D_2]Methylene Chloride, 30 °C): δ = 7.48 (m; 2H), 7.55 (m, 1H), 7.63 (m, 2H).

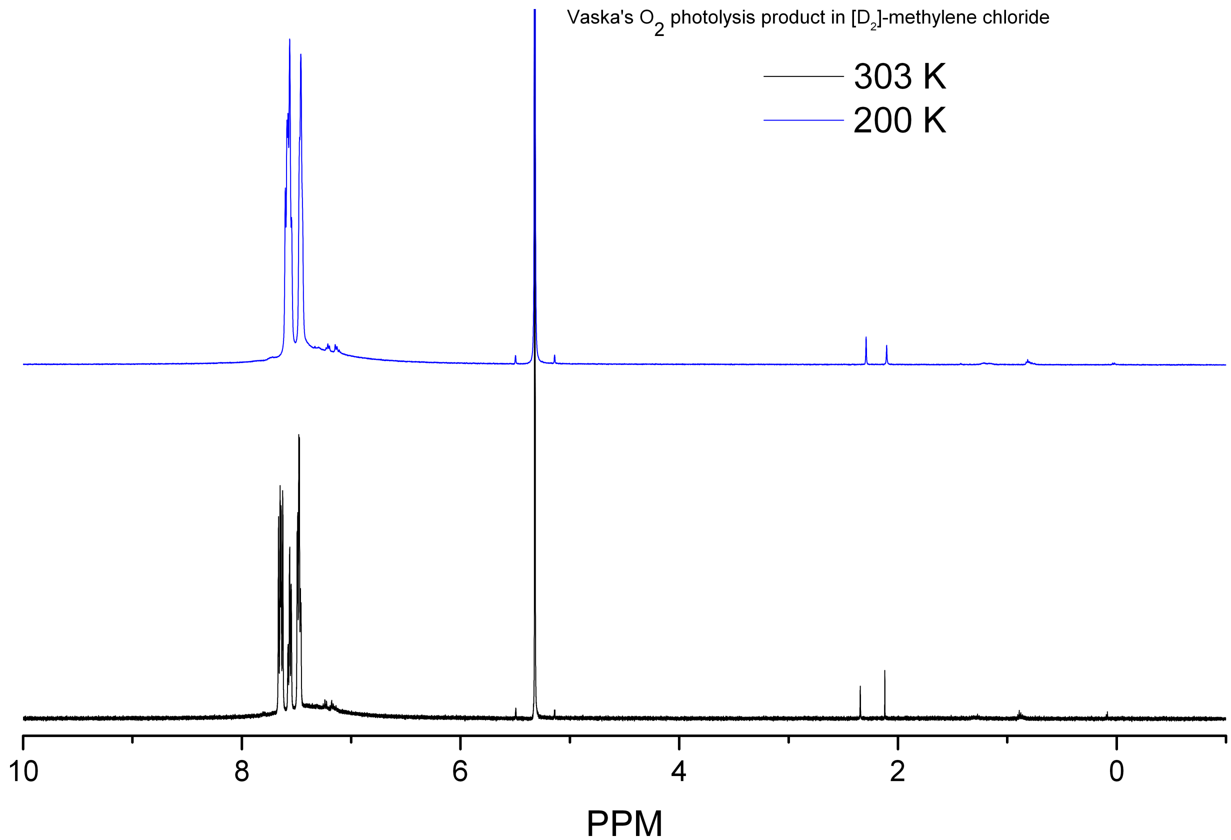

Figure B8: Low-temperature 500 MHz [1]H NMR of photoproducts following 12 hours irradiation of Vaska's O_2 complex in CD_2Cl_2 under 7 PSI O_2.

Appendix C: DFT Calculated Energies and Geometries for "Chapter 4: Intramolecular C-H Activation and Metallacycle Aromaticity in the Photochemistry of [FeFe]-Hydrogenase Model Compounds in Low-Temperature Frozen Matrices"

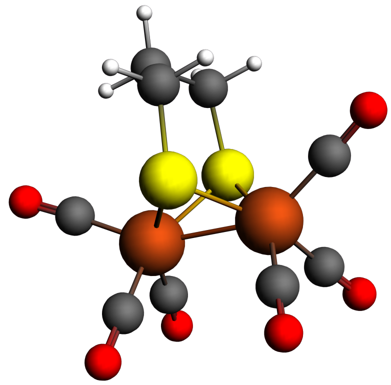

4.1 B: (μ-pdt)[Fe(CO)$_3$]$_2$

B88P86/TZP

Fe	-2.65515848	-1.78097549	1.36089951
O	-5.53085168	-1.43640330	1.92371634
O	-2.76333552	-4.60570440	2.20015408
S	-2.73699861	0.13099858	0.11050581
O	-1.46648928	-0.64948707	3.80094636
Fe	-2.60501647	-1.75140938	-1.19268713
S	-0.80605279	-2.28419539	0.12185319
O	-1.58977696	-0.79489044	-3.78467560
O	-5.47612013	-1.40846922	-1.75489937
O	-2.71740720	-4.58238238	-1.99498373
C	-2.67704701	-3.47564740	-1.65508084
C	-4.34653227	-1.53716390	-1.53248276
C	-1.96040691	-1.15395585	-2.74446527
C	-1.94800084	-1.11556492	2.85229028
C	-2.72678742	-3.50331156	1.84559038
C	-4.40135682	-1.56644011	1.70139651
C	0.45732347	-0.93557713	0.20058428
C	0.07680595	0.39692347	-0.42341775
C	-1.13923809	1.05965853	0.20378829
H	1.33115149	-1.36264938	-0.31047015
H	0.70950196	-0.82867929	1.26575901
H	-0.08970923	0.26423946	-1.50185034
H	0.93512023	1.08321621	-0.32080943
H	-1.35778888	2.01153395	-0.29904972
H	-0.98049562	1.27115606	1.27120801

TPSS-D3(BJ)/TZP

Fe	-2.66837000	-1.79111000	1.50439000
O	-5.54101000	-1.38338000	2.08609000
O	-2.72201000	-4.59294000	2.44336000
S	-2.77416000	0.06423620	0.09720590
O	-1.36034000	-0.53254800	3.81756000
Fe	-2.61416000	-1.76825000	-1.34055000
S	-0.87937900	-2.33825000	0.11987400
O	-1.44305000	-0.60575600	-3.77821000
O	-5.49733000	-1.39962000	-1.87045000
O	-2.66333000	-4.57831000	-2.24320000
C	-2.64843000	-3.48200000	-1.87734000
C	-4.36669000	-1.54141000	-1.67706000
C	-1.88942000	-1.06004000	-2.80845000
C	-1.88144000	-1.04184000	2.91473000
C	-2.71002000	-3.50159000	2.06268000
C	-4.41642000	-1.54106000	1.87046000
C	0.40139700	-1.00889000	0.20490200
C	0.03058380	0.31834100	-0.43679100
C	-1.18233000	0.99999600	0.17745100
H	1.27046000	-1.44175000	-0.29786900
H	0.63646600	-0.89524900	1.26694000
H	-0.13778200	0.16864400	-1.50618000
H	0.88871200	0.99724600	-0.33983600
H	-1.39582000	1.93502000	-0.34739500
H	-1.02748000	1.22476000	1.23644000

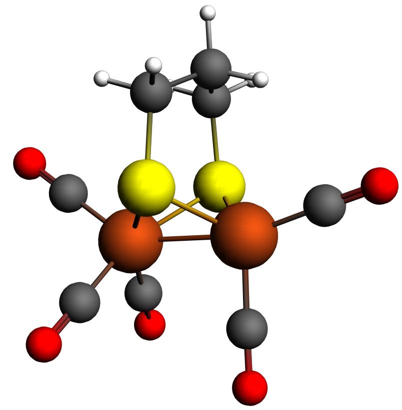

4.1a: (μ-pdt)$Fe_2(CO)_5$

<u>B88P86/TZP</u>

Fe	-2.21662687	-1.16159718	1.36680833
O	-4.98972979	-0.48600297	2.11454632
O	-2.73421057	-4.00562931	1.95814662
S	-2.13116244	0.82297298	0.22411940
O	-0.88337333	-0.43036132	3.89056403
Fe	-2.08715998	-0.94203167	-1.18309604
S	-0.44357440	-1.83756479	0.08186984
H	-0.53743752	2.54251376	-0.16835276
O	-4.60154201	-2.53749099	-1.40143128
O	-1.24087015	-0.28599342	-3.94769768
C	-1.56632203	-0.53337684	-2.85794552
C	-3.62495846	-1.91739347	-1.30291725
H	-0.22900429	1.72403845	1.37730005
C	-1.41002524	-0.72267691	2.89827179
C	-2.52824464	-2.89370759	1.70666097
C	-3.90322759	-0.74322857	1.80608548
C	0.95080601	-0.62279707	0.19686831
C	0.68758789	0.77129432	-0.36446079
C	-0.43240007	1.55888404	0.30988537
H	1.77361172	-1.09830848	-0.35475757
H	1.23366925	-0.58844808	1.25842792
H	0.48119863	0.69640832	-1.44186110
H	1.61880958	1.35605192	-0.26148410

ΔH = + 4.7 kcal mol^{-1}
ΔG = + 3.8 kcal mol^{-1}

<u>TPSS-D3(BJ)/TZP</u>

Fe	-2.22614500	-1.15577500	1.33207000
O	-5.02084700	-0.46546800	1.99387200
O	-2.76118600	-4.01607400	1.84104800
S	-2.11990800	0.83672500	0.23079800
O	-0.89582400	-0.41369500	3.85300200
Fe	-2.04021000	-0.92554500	-1.17790600
S	-0.42318100	-1.83184900	0.11340400
H	-0.51666400	2.54750600	-0.10313000
O	-4.55792600	-2.53477000	-1.24977500
O	-1.16707200	-0.23379900	-3.93516700
C	-1.50553200	-0.50465500	-2.85873000
C	-3.58123600	-1.91049100	-1.21555900
H	-0.23159900	1.69480800	1.42431400
C	-1.43365400	-0.71584500	2.87267800
C	-2.54751600	-2.89885100	1.63627000
C	-3.92769800	-0.73097900	1.72929100
C	0.95675000	-0.61172900	0.26379100
C	0.69085200	0.77104600	-0.32159400
C	-0.42509500	1.55959300	0.35624100
H	1.79267800	-1.08368300	-0.25983900
H	1.20250900	-0.56072000	1.32811100
H	0.47213700	0.67656000	-1.39011500
H	1.61639300	1.35706700	-0.23137000

ΔH = 0.0 kcal mol^{-1}
ΔG = 0.0 kcal mol^{-1}

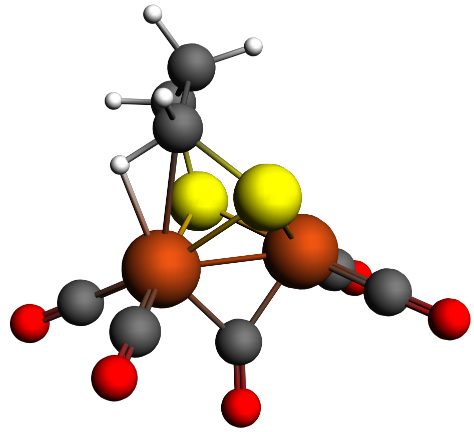

4.1b: (μ-pdt)$Fe_2(CO)_5$

B88P86/TZP

Fe	-2.45464767	-1.47492471	2.01844243
O	-4.81050412	-0.52868980	3.50309062
O	-4.12320700	-3.70292439	1.12267110
S	-2.78140461	0.20340826	0.52490576
O	-1.67354384	-3.14671565	4.30237193
Fe	-2.42762851	-1.92179858	-0.50083344
S	-0.57055774	-2.19785438	0.92549892
H	-1.37228119	-0.53648701	-1.39337885
O	-4.84364866	-1.62618168	-2.14957074
O	-1.61384905	-4.30803676	-1.98443772
C	-1.93863717	-3.36517883	-1.38627883
C	-3.89572587	-1.72842756	-1.48690505
H	-1.63853132	1.19920601	-1.30575270
C	-1.99791235	-2.50436379	3.38937408
C	-3.36655469	-2.80596664	0.99269674
C	-3.89308316	-0.90440989	2.89658935
C	0.60122604	-0.87839816	0.34232599
C	-0.00689968	0.47542455	-0.00355402
C	-1.38364056	0.34508602	-0.66442886
H	1.07476373	-1.32658527	-0.54389473
H	1.36804420	-0.79354792	1.12373458
H	0.67848790	1.00014753	-0.68930365
H	-0.10887511	1.10002848	0.89514265

ΔH = 2.0 kcal mol
ΔG = 3.0 kcal mol

TPSS-D3(BJ)/TZP

Fe	-2.44204000	-1.46296000	2.01076600
O	-4.85031300	-0.59192400	3.44717500
O	-4.09465200	-3.69395600	1.12341400
S	-2.77536300	0.20115500	0.52604200
O	-1.70752600	-3.17656700	4.27402900
Fe	-2.40976800	-1.89339700	-0.48712300
S	-0.57530100	-2.19035600	0.92279200
H	-1.38527100	-0.62418800	-1.38359500
O	-4.85371200	-1.60869200	-2.08958700
O	-1.63489100	-4.31545500	-1.92343800
C	-1.93909800	-3.35299700	-1.35512100
C	-3.89257600	-1.70310500	-1.45344400
H	-1.66441000	1.10402100	-1.36105300
C	-2.00379300	-2.50732300	3.37628600
C	-3.34321600	-2.79574200	0.99008400
C	-3.90615800	-0.92730900	2.86686600
C	0.59719100	-0.89529100	0.31753900
C	-0.02398400	0.44836300	-0.03504100
C	-1.40271000	0.28677700	-0.68625400
H	1.05031100	-1.35319700	-0.56709400
H	1.36737400	-0.79982300	1.08610900
H	0.64613800	0.97429500	-0.72493600
H	-0.13884900	1.06724300	0.85875500

ΔH = 0.0 kcal mol
ΔG = 1.0 kcal mol

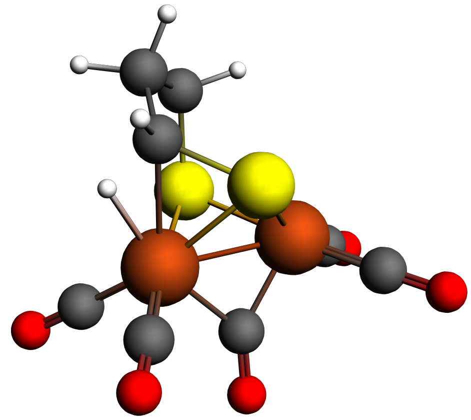

4.1c: (μ-pdt)$Fe_2(CO)_5$

B88P86/TZP

Fe	-2.46872205	-1.52625725	2.01298514
O	-4.81615702	-0.54099674	3.48798087
O	-4.10644365	-3.75106874	1.09125407
S	-2.67114075	0.24645020	0.56797935
O	-1.68896430	-3.16376818	4.31732180
Fe	-2.41956001	-1.88588379	-0.50646307
S	-0.55749040	-2.17843546	0.90911240
H	-1.55277552	-0.70441438	-1.48084701
O	-4.90384902	-1.61795538	-2.05396757
O	-1.62463556	-4.25044899	-2.03019635
C	-1.94677470	-3.31781272	-1.41601788
C	-3.92956943	-1.71161060	-1.43061180
H	-1.70106594	1.02629563	-1.45814377
C	-2.01543992	-2.53090517	3.39810737
C	-3.36181829	-2.83844522	1.00751788
C	-3.90080580	-0.92742537	2.88519233
C	0.45505706	-0.61264376	0.77305305
C	0.07049935	0.28047374	-0.40286777
C	-1.41660525	0.21678855	-0.77178829
H	1.49621036	-0.94996373	0.68572343
H	0.34706109	-0.09430904	1.73086448
H	0.64523365	-0.00096695	-1.29912731
H	0.33819848	1.32297579	-0.16979881

$\Delta H = + 2.5$ kcal mol^{-1}
$\Delta G = + 3.7$ kcal mol^{-1}

TPSS-D3(BJ)/TZP

Fe	-2.44866700	-1.51690900	1.99937500
O	-4.85103000	-0.59557900	3.41693500
O	-4.07649100	-3.74233400	1.08745900
S	-2.65681400	0.23878900	0.55040100
O	-1.72617300	-3.21405000	4.27391300
Fe	-2.40460600	-1.87104800	-0.49154600
S	-0.54865700	-2.16021800	0.90201300
H	-1.53854100	-0.73673400	-1.48670800
O	-4.92761100	-1.58866700	-1.96655900
O	-1.67994000	-4.28830700	-1.96208400
C	-1.96515500	-3.32880900	-1.38039600
C	-3.93384400	-1.68740500	-1.38454900
H	-1.70487800	0.98542200	-1.48929400
C	-2.02062800	-2.54567100	3.37394300
C	-3.33604100	-2.82930800	0.99607100
C	-3.90671300	-0.94514400	2.84457100
C	0.41347400	-0.56745800	0.81009800
C	0.06743300	0.26799100	-0.41455700
C	-1.41398200	0.19276800	-0.79681800
H	1.46488100	-0.86199000	0.80232700
H	0.20851100	-0.03093000	1.73455300
H	0.65100300	-0.06751600	-1.27876000
H	0.33294800	1.31319600	-0.22346500

$\Delta H = 0.0$ kcal mol^{-1}
$\Delta G = 1.1$ kcal mol^{-1}

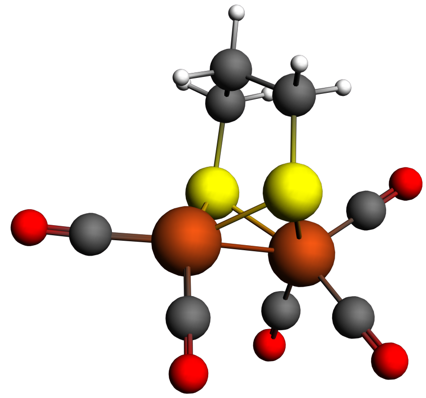

4.1d: (μ-pdt)$Fe_2(CO)_5$

B88P86/TZP

Fe	-2.70561250	-1.69454935	1.52324037
O	-5.46614231	-0.98935748	2.30198132
O	-3.06600801	-4.44337825	2.54529734
S	-2.79910184	0.07359798	0.00417033
O	-1.28471893	-0.52187814	3.83483834
Fe	-2.71469453	-1.99167734	-1.02382364
S	-0.92951912	-2.48092313	0.30336285
H	-1.29230130	1.78053591	-0.64223905
O	-5.61217465	-2.06481374	-1.57225469
O	-1.89519910	-3.46736942	-3.47974402
C	-2.22458459	-2.92255645	-2.50856842
C	-4.46802753	-2.00679927	-1.36611521
H	-0.87651438	1.17060203	0.97398598
C	-1.84865316	-0.97785153	2.92675462
C	-2.92104480	-3.36847294	2.13379790
C	-4.38684683	-1.26603943	1.98113384
C	0.39303666	-1.19829569	0.10456341
C	0.00144744	0.04904232	-0.67854505
C	-1.12146541	0.86735153	-0.05425797
H	1.21149694	-1.72866639	-0.40271047
H	0.73230850	-0.95017875	1.12083253
H	-0.27259395	-0.23296927	-1.70779947
H	0.89432403	0.69481686	-0.75425884

ΔH = + 7.2 kcal mol-1
ΔG = + 6.1 kcal mol-1

TPSS-D3(BJ)/TZP

Fe	-2.70557464	-1.68803985	1.48143568
O	-5.49517376	-1.02331445	2.17678901
O	-3.10009799	-4.46187266	2.40939462
S	-2.77813558	0.08836530	0.01376160
O	-1.29912628	-0.52801897	3.79979192
Fe	-2.68525227	-1.97390683	-0.99422434
S	-0.90245166	-2.45768396	0.32238344
H	-1.27591916	1.79413103	-0.60631049
O	-5.60446067	-2.07920437	-1.36918627
O	-1.98380027	-3.54961499	-3.42379130
C	-2.25856714	-2.94821321	-2.47416107
C	-4.45301590	-2.01194363	-1.24342757
H	-0.85949648	1.15703827	0.99498915
C	-1.86908409	-0.98400819	2.90084096
C	-2.93913694	-3.37760598	2.04254656
C	-4.40343934	-1.27839513	1.89822051
C	0.40474935	-1.16884137	0.13742602
C	-0.00223241	0.05352013	-0.67204682
C	-1.10856533	0.87911651	-0.03257532
H	1.23250357	-1.69272168	-0.34687768
H	0.71331086	-0.89821077	1.15084349
H	-0.30877883	-0.25889660	-1.67683218
H	0.88217527	0.69495580	-0.78417468

ΔH = 3.6 kcal mol-1
ΔG = 1.5 kcal mol-1

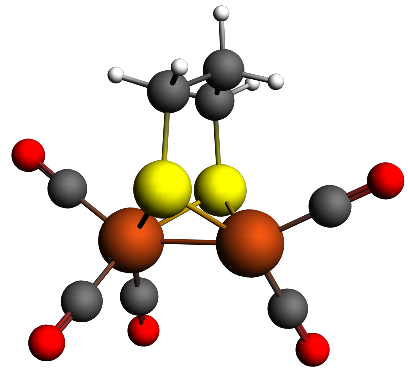

4.1e: (μ-pdt)$Fe_2(CO)_5$

B88P86/TZP

Fe	-2.15358489	-1.22182344	1.43953278
O	-5.02125917	-0.88195508	2.01238242
O	-2.33564958	-4.07076544	2.19221112
S	-2.25783369	0.60487389	0.11220346
O	-0.88479335	-0.11728807	3.86812575
Fe	-2.10675934	-1.22075809	-1.10322374
S	-0.36295635	-1.78839552	0.12793412
H	-0.84577404	2.46875871	-0.32856160
O	-4.94328919	-1.18319842	-1.89910470
O	-1.15008970	-0.37185432	-3.74074285
C	-1.50674796	-0.73873857	-2.69255637
C	-3.83142153	-1.17970013	-1.56051961
H	-0.45857747	1.71860291	1.23831833
C	-1.38676265	-0.56741102	2.92232130
C	-2.26688637	-2.95503807	1.88311826
C	-3.89186668	-1.01053476	1.78140182
C	0.96234070	-0.50188976	0.13128974
C	0.56343675	0.83674892	-0.48004693
C	-0.63627010	1.51374403	0.17257866
H	1.79493890	-0.94593966	-0.43210853
H	1.27728285	-0.39935367	1.17896761
H	0.36927923	0.70406976	-1.55319820
H	1.42721882	1.51989643	-0.40117284

ΔH = 0.0 kcal mol^{-1}
ΔG = 0.0 kcal mol^{-1}

TPSS-D3(BJ)/TZP

Fe	-2.17503000	-1.26035000	1.55866000
O	-5.04713000	-0.88899800	2.13289000
O	-2.23012000	-4.05955000	2.50325000
S	-2.28961000	0.53100800	0.08380150
O	-0.81121500	0.00104595	3.85290000
Fe	-2.11466000	-1.22855000	-1.25786000
S	-0.43630200	-1.84818000	0.04655230
H	-0.87228700	2.39018000	-0.33885800
O	-4.95260000	-1.11005000	-2.07595000
O	-0.98245900	-0.08961240	-3.70350000
C	-1.42689000	-0.58908900	-2.75016000
C	-3.84284000	-1.14130000	-1.74464000
H	-0.49938900	1.63166000	1.22421000
C	-1.33994000	-0.50454800	2.95099000
C	-2.21820000	-2.96569000	2.12310000
C	-3.92052000	-1.03647000	1.90792000
C	0.91477700	-0.59120000	0.09558520
C	0.53088200	0.76319500	-0.49006600
C	-0.66955000	1.43953000	0.16167200
H	1.73990000	-1.02813000	-0.47367300
H	1.21129000	-0.51841000	1.14451000
H	0.34869000	0.65326800	-1.56086000
H	1.39424000	1.43446000	-0.38367000

ΔH = + 1.8 kcal mol^{-1}
ΔG = + 2.4 kcal mol^{-1}

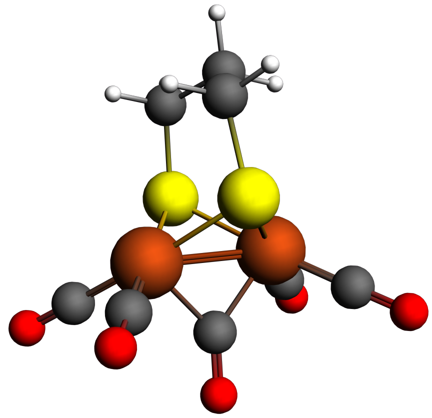

4.1f: (μ-pdt)$Fe_2(CO)_5$

B88P86/TZP

Fe	-2.41474686	-1.45917021	1.99943637
O	-4.74752176	-0.47821048	3.48448376
O	-4.24834175	-3.54367019	1.14650638
S	-2.81683295	0.11870488	0.30712814
O	-1.67456659	-3.40216188	4.06888820
Fe	-2.42323579	-2.01506957	-0.52508090
S	-0.50659236	-2.09517671	0.78498127
H	-1.60881979	2.00222933	-0.45376704
O	-4.79233428	-1.72849578	-2.22882824
O	-1.73661411	-4.66303764	-1.58164833
C	-2.01802943	-3.61693319	-1.16476321
C	-3.85589117	-1.85142423	-1.55407640
H	-1.13111164	1.60934539	1.20795854
C	-1.97921537	-2.63707973	3.25117144
C	-3.41762600	-2.72399354	0.95696810
C	-3.82970507	-0.86933244	2.89139676
C	0.51857271	-0.55811549	0.59971581
C	-0.03462286	0.51958624	-0.31782491
C	-1.29724642	1.18268932	0.20752227
H	1.47488419	-0.94019858	0.21817934
H	0.70074102	-0.16072339	1.60947956
H	-0.21422095	0.10481054	-1.32251343
H	0.73789749	1.30184453	-0.42439329

ΔH = + 2.1 kcal mol⁻¹
ΔG = + 2.3 kcal mol⁻¹

TPSS-D3(BJ)/TZP

Fe	-2.39796000	-1.44951000	1.99727000
O	-4.75680000	-0.51630800	3.47587000
O	-4.22803000	-3.53539000	1.15009000
S	-2.81236000	0.11284300	0.31874400
O	-1.74145000	-3.42356000	4.06879000
Fe	-2.40737000	-2.00147000	-0.52022300
S	-0.50757700	-2.08604000	0.79111500
H	-1.62283000	1.98543000	-0.47934000
O	-4.79174000	-1.75345000	-2.21239000
O	-1.77681000	-4.66169000	-1.58698000
C	-2.02072000	-3.61262000	-1.16185000
C	-3.85090000	-1.84984000	-1.54429000
H	-1.12091000	1.61132000	1.17644000
C	-1.99168000	-2.64354000	3.25073000
C	-3.40068000	-2.71456000	0.95877600
C	-3.82782000	-0.87617500	2.88617000
C	0.51153600	-0.55063800	0.58944100
C	-0.05521340	0.50033900	-0.35009300
C	-1.30355000	1.18007000	0.18693300
H	1.46493000	-0.93152700	0.21486400
H	0.68197600	-0.13399700	1.58735000
H	-0.26369000	0.05277810	-1.32947000
H	0.71268500	1.27314000	-0.49579000

ΔH = 1.8 kcal mol⁻¹
ΔG = 2.7 kcal mol⁻¹

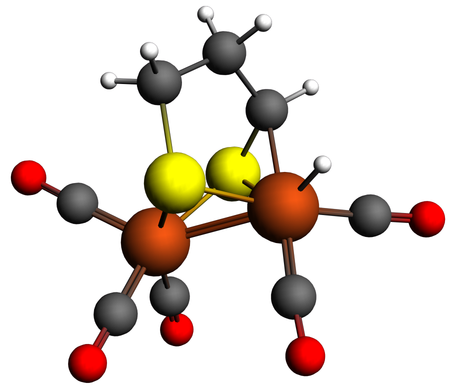

4.1g: (μ-pdt)$Fe_2(CO)_5$

B88P86/TZP

Fe	-2.61354533	-1.82965333	1.48600972
O	-5.41104730	-1.68441737	2.45560817
O	-2.40834565	-4.64322560	2.37398585
S	-3.08281028	-0.01528195	0.22723633
O	-1.21999397	-0.64004396	3.78159451
Fe	-2.63749068	-1.73520871	-1.17230045
S	-0.83780852	-2.29518130	0.10876568
H	-1.71579308	-1.84988078	-2.33973969
O	-4.53160566	-1.05650183	-3.30243708
O	-3.55001392	-4.53986428	-1.39002375
C	-3.20271528	-3.43946047	-1.24867162
C	-3.81331032	-1.31485838	-2.42502385
H	-2.22880182	0.89911427	-1.75494827
C	-1.77431848	-1.12431117	2.88398203
C	-2.49510180	-3.54469328	2.02021067
C	-4.32324119	-1.72930673	2.06246689
C	0.23952991	-0.78336688	0.07329602
C	-0.35693969	0.28349330	-0.83640508
C	-1.85408403	0.15112031	-1.04583402
H	1.22105289	-1.12356535	-0.28240858
H	0.35585624	-0.44958496	1.11005510
H	0.09713767	0.21334587	-1.83684803
H	-0.11286013	1.29117609	-0.45493309

ΔH = 7.4 kcal mol
ΔG = 7.3 kcal mol

TPSS-D3(BJ)/TZP

Fe	-2.59499200	-1.83171200	1.43509600
O	-5.44474400	-1.72412700	2.22518200
O	-2.43994900	-4.66585700	2.24484400
S	-3.00237200	0.02723600	0.22202900
O	-1.29169600	-0.71582600	3.81370200
Fe	-2.62747200	-1.72501200	-1.12591400
S	-0.79425600	-2.25771000	0.11617400
H	-1.76678500	-1.92518700	-2.33195400
O	-4.66210200	-1.08148800	-3.12911100
O	-3.55919000	-4.52631700	-1.15552500
C	-3.20181200	-3.42551500	-1.09862900
C	-3.88181900	-1.32467300	-2.30798000
H	-2.21330200	0.86252300	-1.81854400
C	-1.81421200	-1.17092900	2.88783700
C	-2.50485300	-3.55890400	1.92933100
C	-4.33381500	-1.74618200	1.91619300
C	0.21640600	-0.70397100	0.11869100
C	-0.32259400	0.24632700	-0.93442300
C	-1.82299400	0.13437000	-1.10648200
H	1.24655100	-1.00443000	-0.08190800
H	0.16178700	-0.28770400	1.12405900
H	0.11964600	0.01212300	-1.90866100
H	-0.04133500	1.28032800	-0.68944000

ΔH = 4.0 kcal mol
ΔG = 4.1 kcal mol

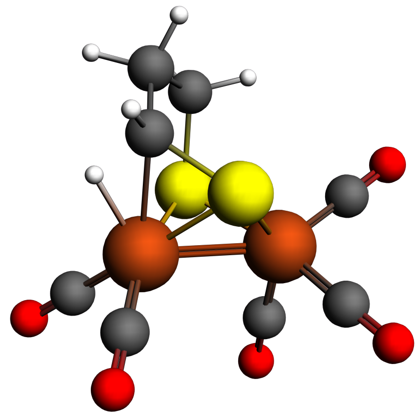

4.1h: (μ-pdt)$Fe_2(CO)_5$

B88P86/TZP

Fe	-2.66504609	-1.67582389	1.49903547
O	-5.31345375	-0.92191537	2.57615615
O	-3.25044168	-4.54079411	1.86994750
S	-2.92961924	0.10166619	0.06540245
O	-1.17461997	-1.06693535	3.96910016
Fe	-2.65350440	-1.89089800	-1.08079119
S	-0.84297423	-2.28143795	0.26603704
H	-1.86062582	-0.72569105	-2.06286698
O	-5.39306032	-1.87219886	-2.14536540
O	-2.21200338	-4.41607334	-2.48976737
C	-2.37497799	-3.41518071	-1.91287553
C	-4.30791170	-1.85321784	-1.72285765
H	-1.97612414	1.02026178	-1.89485373
C	-1.77172648	-1.30015494	3.00051310
C	-3.01248215	-3.41691414	1.71396977
C	-4.28214642	-1.21917957	2.13814637
C	0.22472572	-0.75219689	0.17682883
C	-0.18981636	0.20159802	-0.94200724
C	-1.68390221	0.15828641	-1.27957822
H	1.24823923	-1.11782285	0.02422904
H	0.18026233	-0.27346737	1.16021364
H	0.36288879	-0.03110030	-1.86551068
H	0.07911154	1.23261302	-0.66295768

ΔH = + 8.4 kcal mol^{-1}
ΔG = + 8.3 kcal mol^{-1}

TPSS-D3(BJ)/TZP

Fe	-2.64669100	-1.66714200	1.45139100
O	-5.34988300	-0.98165100	2.41892600
O	-3.26486200	-4.53695000	1.62346800
S	-2.87539500	0.14446000	0.04171300
O	-1.24585700	-1.17724700	3.99479500
Fe	-2.63949400	-1.87510600	-1.02427100
S	-0.78774200	-2.22747200	0.27460400
H	-1.87089100	-0.77511200	-2.07958100
O	-5.44288600	-1.88127500	-1.89016600
O	-2.28396000	-4.48706000	-2.28821200
C	-2.40747200	-3.44867100	-1.77938000
C	-4.32904200	-1.85313100	-1.56431000
H	-1.97152000	0.96685300	-1.97879500
C	-1.80783500	-1.35222900	2.99751600
C	-3.01449900	-3.41042000	1.54817500
C	-4.29183800	-1.24281500	2.03366300
C	0.19383200	-0.64948900	0.20569000
C	-0.17428500	0.17740100	-1.01861300
C	-1.67217400	0.13273600	-1.34026400
H	1.24427600	-0.94597800	0.18388100
H	-0.00221600	-0.10807400	1.12989600
H	0.36930100	-0.18160500	-1.89919700
H	0.11757000	1.22052400	-0.85288300

ΔH = 5.4 kcal mol^{-1}
ΔG = 7.1 kcal mol^{-1}

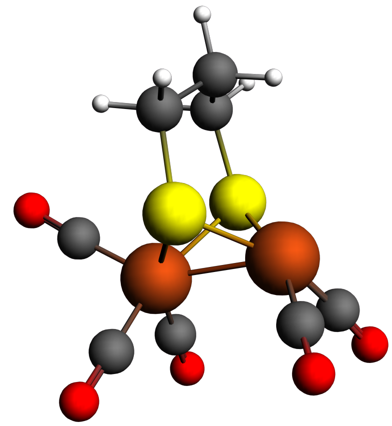

4.1i: (μ-pdt)$Fe_2(CO)_5$

B88P86/TZP

Fe	-2.65720679	-1.79016109	1.37462725
O	-5.51956216	-1.42043584	1.98779426
O	-2.71975215	-4.60734134	2.24391828
S	-2.76716767	0.15056044	0.12421044
O	-1.45109786	-0.64973053	3.80298066
Fe	-2.65238748	-1.77372998	-1.13058292
S	-0.79554243	-2.30259509	0.11199652
H	-1.36966342	2.02113215	-0.25988086
O	-5.46598865	-1.42322953	-1.86203050
O	-2.75892009	-4.54967279	-2.05847359
C	-2.70871076	-3.44621998	-1.68969587
C	-4.33815718	-1.53733164	-1.59513544
H	-0.95476779	1.24623018	1.28141729
C	-1.94486199	-1.12513328	2.86630631
C	-2.69643433	-3.50734500	1.88375998
C	-4.39457017	-1.55807208	1.75300294
C	0.44906564	-0.93264027	0.17832174
C	0.03630453	0.38626493	-0.45676197
C	-1.15223535	1.05549952	0.21650115
H	1.32327650	-1.35159537	-0.33877985
H	0.71855825	-0.80237884	1.23664342
H	-0.17864978	0.23350911	-1.52676842
H	0.89620883	1.07716182	-0.40417822

ΔH = + 4.6 kcal mol^{-1}
ΔG = + 4.3 kcal mol^{-1}

TPSS-D3(BJ)/TZP

Fe	-2.67584000	-1.81200000	1.51712000
O	-5.54328000	-1.38684000	2.11440000
O	-2.68572000	-4.61556000	2.44916000
S	-2.79744000	0.11053600	0.08362380
O	-1.38315000	-0.56945900	3.85277000
Fe	-2.62470000	-1.75201000	-1.26934000
S	-0.84814700	-2.33792000	0.07560550
H	-1.39149000	1.97614000	-0.27976700
O	-5.45320000	-1.37596000	-1.94211000
O	-2.68964000	-4.51104000	-2.26565000
C	-2.65205000	-3.41348000	-1.88903000
C	-4.31801000	-1.49784000	-1.73026000
H	-0.99902300	1.19641000	1.26245000
C	-1.90034000	-1.07501000	2.94619000
C	-2.68377000	-3.52215000	2.07424000
C	-4.42045000	-1.55007000	1.89579000
C	0.40358000	-0.98061400	0.18805400
C	-0.00307641	0.33136100	-0.46613900
C	-1.18731000	1.01551000	0.20056500
H	1.28721000	-1.39423000	-0.30543800
H	0.63376700	-0.84585500	1.24869000
H	-0.22757600	0.15773600	-1.52594000
H	0.85534500	1.01631000	-0.42584700

ΔH = 6.8 kcal mol^{-1}
ΔG = 7.3 kcal mol^{-1}

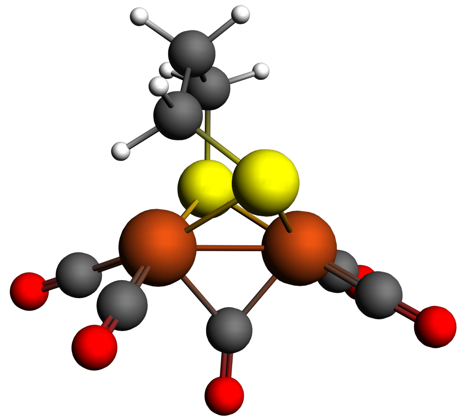

4.1b↔4.1c transition state: (μ-pdt)$Fe_2(CO)_5$

B88P86/TZP

Fe	-2.46487700	-1.50154700	2.01851200
O	-4.81929400	-0.53944900	3.49855600
O	-4.11286600	-3.72780400	1.09864200
S	-2.70928400	0.22856100	0.56254700
O	-1.67792300	-3.14720500	4.31689800
Fe	-2.41711500	-1.89812500	-0.50856300
S	-0.57688800	-2.18319000	0.91109100
H	-1.45795300	-0.67136600	-1.43402100
O	-4.87240700	-1.60570100	-2.09951700
O	-1.62260700	-4.27480600	-2.01412000
C	-1.94324100	-3.33553600	-1.40839500
C	-3.91032200	-1.70907600	-1.45859400
H	-1.70048200	1.05904800	-1.41665600
C	-2.00760300	-2.51551900	3.39802900
C	-3.36185300	-2.82201900	0.99675600
C	-3.90328000	-0.91953800	2.89277800
C	0.56771700	-0.74276800	0.60910500
C	0.03661500	0.41235400	-0.25745600
C	-1.40942900	0.25125700	-0.73131200
H	1.44699400	-1.20605900	0.14216600
H	0.86835600	-0.40131900	1.60617000
H	0.67116200	0.51980600	-1.15101600
H	0.10571100	1.36113400	0.29398700

ΔH = 2.4 kcal mol
ΔG = 4.5 kcal mol

TPSS-D3(BJ)/TZP

Fe	-2.44602848	-1.48747491	2.00805458
O	-4.85883685	-0.59658975	3.42981504
O	-4.08768635	-3.71098487	1.10102230
S	-2.70484594	0.22129934	0.54935476
O	-1.71920096	-3.20044953	4.27255797
Fe	-2.39862059	-1.88239148	-0.49515117
S	-0.57366564	-2.16715991	0.90780224
H	-1.44326836	-0.70377898	-1.43118814
O	-4.88932064	-1.58710530	-2.02390865
O	-1.67156447	-4.31050194	-1.94406106
C	-1.95671747	-3.34480050	-1.37260165
C	-3.90898534	-1.68903483	-1.41940535
H	-1.71294384	1.01784024	-1.44199345
C	-2.01384124	-2.52870243	3.37535769
C	-3.33870228	-2.80739945	0.99390017
C	-3.91172462	-0.93628135	2.85666640
C	0.56605558	-0.73626955	0.59706598
C	0.01974775	0.42092671	-0.25500428
C	-1.41353890	0.22904728	-0.74884497
H	1.42760953	-1.19877372	0.11128612
H	0.87836993	-0.40006366	1.58588575
H	0.66206069	0.55626655	-1.13168259
H	0.04814821	1.35265290	0.31628679

ΔH = 0.3 kcal mol
ΔG = 2.3 kcal mol

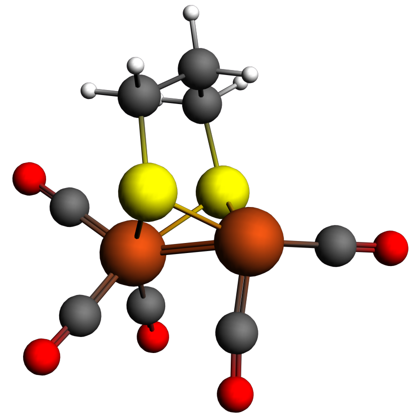

4.1e↔4.1i transition state: (μ-pdt)$Fe_2(CO)_5$

B88P86/TZP

Fe	-2.22212000	-1.21862400	1.31348200
O	-5.00015500	-0.59340300	2.05898000
O	-2.56444600	-4.09138800	1.91592600
S	-2.07846600	0.78438600	0.17240500
O	-1.04291800	-0.44092100	3.89248600
Fe	-1.97137500	-0.95285300	-1.23712000
S	-0.32729600	-1.74972700	0.07618500
H	-0.54747700	2.58776900	0.16109500
O	-4.24952200	-2.77270200	-1.15017000
O	-3.25443800	0.74818500	-3.26143300
C	-2.74474900	0.06526700	-2.46597100
C	-3.29902700	-2.09182300	-1.13112500
H	-0.36424700	1.62814800	1.65215700
C	-1.51077000	-0.73555800	2.87158900
C	-2.44273500	-2.97357500	1.64383800
C	-3.91037600	-0.83876300	1.75653300
C	1.00356800	-0.52389300	0.47824800
C	0.76821000	0.87988700	-0.05633900
C	-0.44521700	1.56760800	0.55672600
H	1.90732100	-0.96046700	0.03052500
H	1.13083500	-0.52736600	1.56998300
H	0.64814600	0.84338800	-1.15095200
H	1.66258400	1.49177600	0.15196100

ΔH = 16.0 kcal mol^{-1}
ΔG = 17.1 kcal mol^{-1}

TPSS-D3(BJ)/TZP

Fe	-2.22576000	-1.21933100	1.29063500
O	-5.01843900	-0.57504300	1.97688300
O	-2.56830100	-4.09811600	1.87330500
S	-2.07895700	0.77993600	0.17698800
O	-1.01042900	-0.41099400	3.84253400
Fe	-1.95403700	-0.95649300	-1.22758200
S	-0.32508300	-1.75767200	0.09673800
H	-0.54999100	2.57386200	0.17921000
O	-4.23191800	-2.77273900	-1.06982600
O	-3.29661900	0.76853300	-3.19452800
C	-2.76278700	0.07337300	-2.43106100
C	-3.27780400	-2.10005200	-1.07200800
H	-0.36512500	1.60368900	1.65839200
C	-1.50138200	-0.72658900	2.84214900
C	-2.44796200	-2.97920200	1.61792000
C	-3.92590800	-0.83087200	1.70653000
C	0.99297500	-0.52890500	0.50457900
C	0.75149300	0.86258900	-0.05767600
C	-0.45032700	1.55692500	0.56844300
H	1.89995800	-0.96485200	0.07666200
H	1.09761900	-0.51216300	1.59289700
H	0.60486600	0.80078700	-1.14291300
H	1.64428900	1.47501700	0.12480100

ΔH = 11.9 kcal mol^{-1}
ΔG = 13.0 kcal mol^{-1}

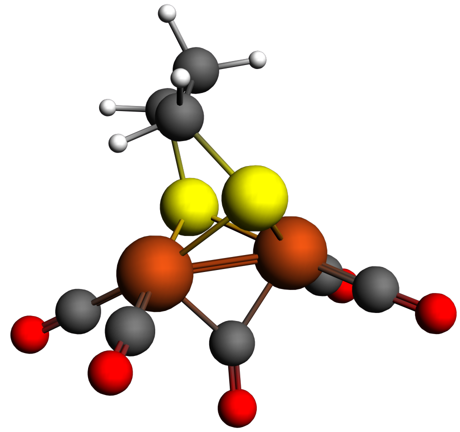

4.1f↔4.1b transition state: (μ-pdt)$Fe_2(CO)_5$

B88P86/TZP

Fe	-2.43330700	-1.46614100	2.00521100
O	-4.78646500	-0.50354000	3.48320900
O	-4.14376000	-3.68081400	1.14953800
S	-2.78449600	0.18562100	0.47045900
O	-1.66613100	-3.18804300	4.25597800
Fe	-2.45061000	-1.96807200	-0.50534000
S	-0.55352600	-2.17446700	0.89196500
H	-1.23364900	-0.08975300	-1.42659200
O	-4.85622400	-1.63921700	-2.16018200
O	-1.67339300	-4.40262100	-1.93884400
C	-1.98260700	-3.44273600	-1.36097100
C	-3.91335300	-1.76290100	-1.49356200
H	-1.52104600	1.58738200	-0.96486900
C	-1.98671900	-2.52643600	3.35585600
C	-3.37618200	-2.79748800	0.98682000
C	-3.87038800	-0.88745800	2.88055000
C	0.60260900	-0.82256700	0.35193600
C	0.02452900	0.57928700	0.22428400
C	-1.29089100	0.59609500	-0.55004200
H	0.99618200	-1.16452000	-0.61769600
H	1.42852200	-0.85415400	1.07587300
H	0.76372900	1.20380800	-0.30631000
H	-0.13158800	1.03076000	1.21561600

ΔH = 2.3 kcal mol
ΔG = 4.1 kcal mol

TPSS-D3(BJ)/TZP

Fe	-2.40160700	-1.44583600	1.98568500
O	-4.79990800	-0.54139800	3.41974200
O	-4.13714400	-3.63853100	1.16027800
S	-2.78414600	0.16873900	0.42357000
O	-1.70328800	-3.26639200	4.17719200
Fe	-2.44289500	-1.96582400	-0.51030900
S	-0.54585600	-2.15401900	0.85487700
H	-1.15369200	0.12640000	-1.40361100
O	-4.89513400	-1.67150100	-2.09594900
O	-1.74717900	-4.49767500	-1.80970200
C	-2.01385800	-3.49252000	-1.30040200
C	-3.92704700	-1.77769600	-1.47122800
H	-1.48350500	1.73610100	-0.76652600
C	-1.98288500	-2.55414200	3.30788900
C	-3.36251800	-2.76711200	0.97960900
C	-3.85707800	-0.89036200	2.84575800
C	0.59607800	-0.78872800	0.35076700
C	0.01352800	0.61395200	0.36343000
C	-1.25633900	0.70831200	-0.47299100
H	0.93628300	-1.05135600	-0.65625900
H	1.44542300	-0.87765800	1.03256200
H	0.76738400	1.29481000	-0.05325100
H	-0.19935500	0.93445600	1.38873200

ΔH = 1.5 kcal mol
ΔG = 3.0 kcal mol

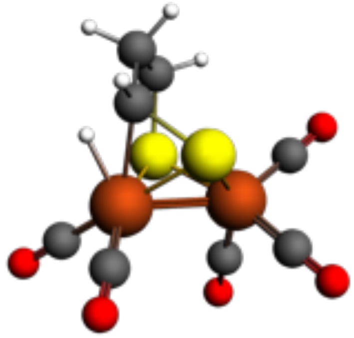

4.1i↔4.1h transition state: (μ-pdt)$Fe_2(CO)_5$

B88P86/TZP

Fe	-2.67062500	-1.68990700	1.50182000
O	-5.34717600	-0.99660000	2.55387800
O	-3.13991100	-4.55115900	2.04244700
S	-2.94768900	0.07940600	0.07928700
O	-1.15410100	-0.91745400	3.90953600
Fe	-2.66028300	-1.88395400	-1.10300000
S	-0.88108900	-2.33045500	0.24998200
H	-1.77757100	-0.69521200	-2.01424700
O	-5.37059700	-1.79270400	-2.23825500
O	-2.27345000	-4.40295300	-2.53883300
C	-2.41067800	-3.40482800	-1.95051500
C	-4.29783700	-1.80240000	-1.78386500
H	-1.93465900	1.04888700	-1.82119900
C	-1.76401700	-1.21922600	2.96817200
C	-2.94999600	-3.42892800	1.82543300
C	-4.30468600	-1.26624000	2.12525500
C	0.27792700	-0.87532900	0.13674400
C	-0.18702700	0.24875600	-0.79992100
C	-1.65828600	0.17469200	-1.21578600
H	1.22444300	-1.30806200	-0.21245200
H	0.43454900	-0.52311700	1.16196900
H	0.41382900	0.24326200	-1.72230900
H	-0.01858900	1.22469400	-0.32053200

ΔH = 8.2 kcal mol
ΔG = 9.3 kcal mol

TPSS-D3(BJ)/TZP

Fe	-2.66224421	-1.67370234	1.45619052
O	-5.36940171	-1.04488020	2.45784835
O	-3.13817507	-4.54815437	1.90034846
S	-2.96011816	0.08063353	0.05620293
O	-1.15776888	-0.91595287	3.87040183
Fe	-2.64806558	-1.87703692	-1.07958861
S	-0.86704942	-2.31858185	0.24989850
H	-1.64659491	-0.65108049	-1.94579345
O	-5.39413363	-1.80259578	-2.11531398
O	-2.35503851	-4.48947379	-2.35839533
C	-2.44606397	-3.44748717	-1.84838629
C	-4.30171500	-1.80131643	-1.71988107
H	-1.87805295	1.09054654	-1.77729963
C	-1.76774787	-1.20474802	2.92972414
C	-2.94237128	-3.42218816	1.73261397
C	-4.31262979	-1.28372502	2.05594605
C	0.34760119	-0.94777533	0.01747039
C	-0.20697369	0.34949091	-0.58654066
C	-1.61530103	0.21968313	-1.17335248
H	1.09143086	-1.39420571	-0.64753641
H	0.82168609	-0.77993292	0.98649582
H	0.46733337	0.69358476	-1.37859954
H	-0.24447123	1.13559262	0.17214675

ΔH = 7.2 kcal mol
ΔG = 7.6 kcal mol

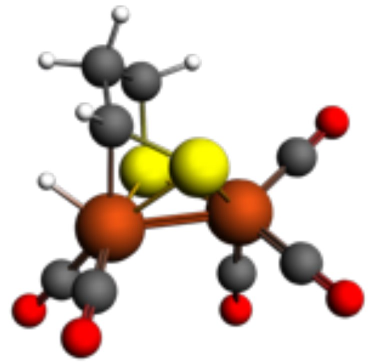

4.1g↔4.1h transition state: (μ-pdt)$Fe_2(CO)_5$

B88P86/TZP

Fe	-2.65681100	-1.71533400	1.52236300
O	-5.38405300	-1.15477900	2.51974700
O	-3.00504900	-4.58380200	2.10952200
S	-2.95692600	0.05896400	0.12491400
O	-1.17965100	-0.89567600	3.94084800
Fe	-2.63910500	-1.81656900	-1.13202800
S	-0.86307800	-2.30707200	0.23231600
H	-1.86906600	-1.20549500	-2.28353400
O	-5.24629500	-1.50186000	-2.45053200
O	-2.43227900	-4.50431000	-2.30188000
C	-2.52064400	-3.45813100	-1.80298200
C	-4.22014900	-1.61583400	-1.91404600
H	-2.09407600	0.79766700	-1.93942700
C	-1.76686500	-1.22167100	2.99327100
C	-2.86504200	-3.45792600	1.87296100
C	-4.31982000	-1.36674500	2.11259800
C	0.22074700	-0.79580400	0.14343600
C	-0.25354600	0.12902800	-0.96978600
C	-1.75589800	0.05242300	-1.21109800
H	1.23944200	-1.16151700	-0.03718500
H	0.19886800	-0.31430500	1.12639200
H	0.24662500	-0.12634400	-1.91650000
H	0.02018700	1.17287800	-0.73966500

ΔH = 11.4 kcal mol⁻¹
ΔG = 11.8 kcal mol⁻¹

TPSS-D3(BJ)/TZP

Fe	-2.64854800	-1.63096700	1.48013500
O	-5.29301700	-0.95020000	2.59355700
O	-3.34117400	-4.48865500	1.53967600
S	-2.95535100	0.09917100	0.03733800
O	-1.18249300	-1.31004600	4.01186200
Fe	-2.60330200	-1.86498000	-1.04773000
S	-0.78273800	-2.18228700	0.29676300
H	-1.92127600	-1.32255300	-2.28692100
O	-5.32681200	-1.77284300	-2.14288700
O	-2.25993800	-4.57628700	-2.10962700
C	-2.39777400	-3.51881600	-1.65890800
C	-4.25143600	-1.79826400	-1.71238400
H	-2.15768600	0.66898400	-2.10459900
C	-1.76687100	-1.41618500	3.01821000
C	-3.06064100	-3.36706600	1.48538700
C	-4.25949000	-1.20769900	2.14520900
C	0.16207300	-0.59362000	0.15769900
C	-0.29220100	0.13665500	-1.09346800
C	-1.79309300	0.01321100	-1.31603300
H	1.22000700	-0.85862700	0.11534500
H	-0.02684700	-0.01866600	1.06299000
H	0.21348800	-0.27026000	-1.97512600
H	-0.03051500	1.20061900	-1.02595600

ΔH = 7.8 kcal mol⁻¹
ΔG = 10.0 kcal mol⁻¹

4.1i↔4.1f transition state: (μ-pdt)$Fe_2(CO)_5$

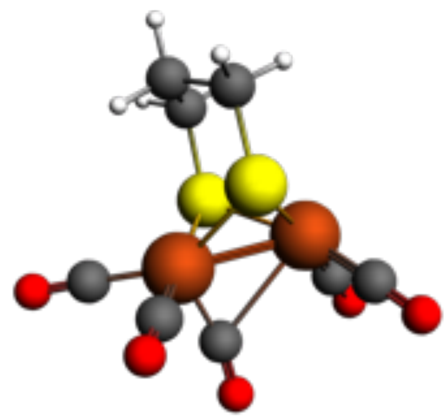

B88P86/TZP

Fe	-2.34077000	-1.26955000	2.09227000
O	-4.99038000	-0.47053900	3.06629000
O	-3.83795000	-4.14821000	1.32153000
S	-2.64397000	0.15697000	0.29044500
O	-2.11596000	-3.29134000	4.21273000
Fe	-2.54608000	-2.09266000	-0.30690600
S	-0.57587100	-2.17948000	0.91062100
H	-1.30659000	1.84836000	-0.67153200
O	-5.01121000	-1.62937000	-1.83919000
O	-1.51922000	-3.96425000	-2.31402000
C	-1.91935000	-3.20516000	-1.53093000
C	-4.04321000	-1.80658000	-1.22728000
H	-0.71703100	1.48000000	0.95984100
C	-2.17721000	-2.49555000	3.36853000
C	-3.28466000	-3.25778000	0.81107800
C	-3.93279000	-0.77838300	2.69501000
C	0.61934300	-0.87886700	0.34724300
C	0.07935420	0.18299300	-0.59715600
C	-1.02945000	1.02901000	0.00549358
H	1.42628000	-1.44986000	-0.13158200
H	1.03078000	-0.42154400	1.26017000
H	-0.28163500	-0.28878900	-1.52476000
H	0.91476300	0.84979800	-0.87445700

ΔH = 9.3 kcal mol^{-1}
ΔG = 10.2 kcal mol^{-1}

TPSS-D3(BJ)/TZP

Fe	-2.34593000	-1.28476000	2.07981000
O	-5.02229000	-0.51508600	3.01329000
O	-3.84018000	-4.08054000	1.35749000
S	-2.64555000	0.15988900	0.30868700
O	-2.12224000	-3.33044000	4.18245000
Fe	-2.52574000	-2.07164000	-0.30759200
S	-0.57359400	-2.17058000	0.91518000
H	-1.31820000	1.83783000	-0.66771700
O	-5.00045000	-1.61750000	-1.82954000
O	-1.51227000	-3.98950000	-2.27631000
C	-1.90963000	-3.21866000	-1.50655000
C	-4.03002000	-1.79251000	-1.22514000
H	-0.70450000	1.46742000	0.95150800
C	-2.17789000	-2.52464000	3.35242000
C	-3.27451000	-3.19282000	0.85556300
C	-3.95794000	-0.81061000	2.66328000
C	0.61391700	-0.87227400	0.34567500
C	0.05124000	0.16252000	-0.61447700
C	-1.03485000	1.02516000	0.00603700
H	1.41916000	-1.44113000	-0.12621400
H	1.01340000	-0.39611000	1.24717000
H	-0.34536100	-0.33644900	-1.50677000
H	0.87514200	0.81639800	-0.93240100

ΔH = 6.1 kcal mol^{-1}
ΔG = 8.7 kcal mol^{-1}

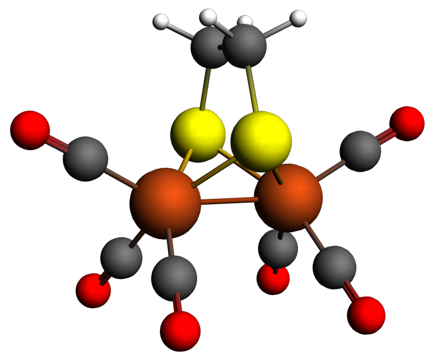

Scheme 4.1 C: (μ-edt)[Fe(CO)$_3$]$_2$

B88P86/TZP

Fe	-2.63724584	-1.77050775	1.38395962
O	-5.51282285	-1.39439224	1.90192963
O	-2.78238235	-4.63116404	2.07379830
S	-2.63015349	0.12177314	0.12125276
O	-1.63669051	-0.83896452	3.98932734
Fe	-2.61676437	-1.75972722	-1.15938997
S	-0.78102335	-2.15939603	0.12674771
O	-1.53791853	-0.80605115	-3.72542695
O	-5.47961243	-1.37871115	-1.74200566
O	-2.73887412	-4.60980371	-1.89539955
C	-2.69401354	-3.49430446	-1.58650241
C	-4.35347856	-1.52504965	-1.51351283
C	-1.94565379	-1.17315553	-2.70274928
C	-2.00996078	-1.19687813	2.95042867
C	-2.72539030	-3.51023190	1.78727152
C	-4.38172178	-1.53965334	1.69860127
C	0.10087559	-0.53445586	0.14323795
H	-0.74016356	1.27770440	1.02818687
C	-0.85840252	0.64869377	0.13673157
H	0.75445751	-0.53941151	-0.73837647
H	0.73239241	-0.54690329	1.04071267
H	-0.72540490	1.27984536	-0.75113954

TPSS-D3(BJ)/TZP

Fe	-2.63073000	-1.76537000	1.35874000
O	-5.51137000	-1.38989000	1.85232000
O	-2.85235000	-4.66109000	1.86044000
S	-2.64212000	0.12576400	0.11632800
O	-1.60395000	-0.86320700	3.96630000
Fe	-2.60325000	-1.75863000	-1.13658000
S	-0.76441900	-2.12427000	0.13071100
O	-1.51929000	-0.81631800	-3.70675000
O	-5.47910000	-1.39528000	-1.66679000
O	-2.77816000	-4.64794000	-1.69312000
C	-2.69779000	-3.51420000	-1.48272000
C	-4.34867000	-1.53487000	-1.47019000
C	-1.93274000	-1.18492000	-2.68980000
C	-1.99196000	-1.21540000	2.93368000
C	-2.74990000	-3.52503000	1.67337000
C	-4.37941000	-1.53360000	1.66810000
C	0.09328100	-0.49011900	0.14926900
H	-0.77706900	1.30943000	1.01718000
C	-0.88328400	0.67920800	0.13181900
H	0.74608100	-0.48676200	-0.72601800
H	0.71037800	-0.48960300	1.05007000
H	-0.75870100	1.29785000	-0.75925200

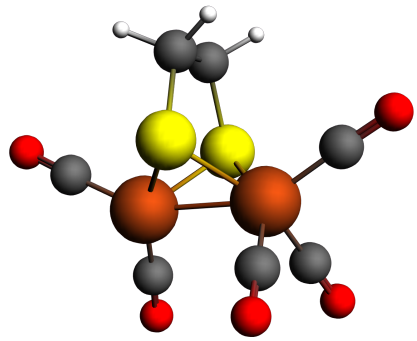

4.2a: (μ-edt)$Fe_2(CO)_5$

B88P86/TZP

Fe	-2.63711954	-1.77062424	1.28134993
O	-5.48944580	-1.65162482	2.00982077
H	0.68783026	-0.58030620	1.09637535
S	-2.65809106	0.09115372	0.13066841
O	-1.66129346	-0.98223795	3.93099814
Fe	-2.61155175	-1.69309619	-1.23832676
S	-0.79964165	-2.15136005	0.06746952
O	-1.39979226	-0.78966318	-3.78019511
O	-5.45408768	-1.26636218	-1.87060165
O	-2.90481105	-4.58088506	-1.75898011
C	-2.77776412	-3.44428840	-1.56433501
C	-4.33335181	-1.42937168	-1.62154448
C	-1.85876524	-1.13368645	-2.77140601
C	-2.03218553	-1.33548966	2.88404229
H	-0.75261265	1.32688036	-0.64697152
C	-4.36927100	-1.68525964	1.70338378
C	0.08898935	-0.52419316	0.17928021
H	-0.79742869	1.22861396	1.13049073
C	-0.88607715	0.64624096	0.20405381
H	0.76593576	-0.48026011	-0.68205302

ΔH = 0.0 kcal mol^{-1}
ΔG = 0.0 kcal mol^{-1}

TPSS-D3(BJ)/TZP

Fe	-2.62247000	-1.79710000	1.26409000
O	-5.51469000	-1.58409000	1.79853000
H	0.69730400	-0.57185200	1.06052000
S	-2.65450000	0.08310400	0.14822900
O	-1.64442000	-0.96598600	3.90239000
Fe	-2.61607000	-1.69595000	-1.21234000
S	-0.78914800	-2.14710000	0.04909000
O	-1.40051000	-0.74302700	-3.73309000
O	-5.47988000	-1.28120000	-1.75600000
O	-2.90402000	-4.59012000	-1.69956000
C	-2.77921000	-3.45221000	-1.52528000
C	-4.35126000	-1.43730000	-1.55470000
C	-1.87311000	-1.11353000	-2.74288000
C	-2.02237000	-1.34311000	2.86937000
H	-0.77420300	1.32430000	-0.64816200
C	-4.37658000	-1.68463000	1.60248000
C	0.08914900	-0.51852700	0.15622500
H	-0.79311200	1.21992000	1.12584000
C	-0.89181000	0.64735600	0.20103000
H	0.74336000	-0.46637800	-0.71515300

ΔH = 0.0 kcal mol^{-1}
ΔG = 0.0 kcal mol^{-1}

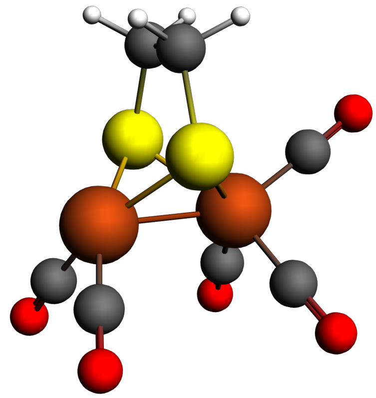

4.2b: (μ-edt)$Fe_2(CO)_5$

B88P86/TZP

Fe	-2.69323596	-1.80122504	1.34081102
O	-5.52914049	-1.41008523	1.96006899
O	-2.86076593	-4.61628277	2.13536192
S	-2.65725543	0.12863012	0.12331706
H	0.70970063	-0.52962194	1.04417336
Fe	-2.62687898	-1.78009109	-1.15552486
S	-0.78379432	-2.18054840	0.15391239
O	-1.45683228	-0.70583309	-3.63354588
O	-5.48630523	-1.39889833	-1.76303381
O	-2.67356058	-4.60899269	-1.98151761
C	-2.65633913	-3.50365938	-1.63820748
C	-4.36078248	-1.54215889	-1.53423293
C	-1.92762513	-1.14605162	-2.66911952
H	-0.74604478	1.23327392	-0.81798249
C	-2.78105071	-3.49497113	1.83153261
C	-4.39256750	-1.54876754	1.74804143
C	0.08451202	-0.54353977	0.14176119
H	-0.74270643	1.31061046	0.95547106
C	-0.87650479	0.64055781	0.09609334
H	0.75077205	-0.55996898	-0.73003725

ΔH = 2.7 kcal mol^{-1}
ΔG = 2.3 kcal mol^{-1}

TPSS-D3(BJ)/TZP

Fe	-2.67670000	-1.78757000	1.33407000
O	-5.52555000	-1.38990000	1.89435000
O	-2.94036000	-4.65166000	1.88284000
S	-2.65646000	0.13120800	0.11729700
H	0.68605600	-0.46759400	1.02347000
Fe	-2.62465000	-1.78873000	-1.11988000
S	-0.76887000	-2.15650000	0.15763000
O	-1.43273000	-0.68561400	-3.57650000
O	-5.50013000	-1.43368000	-1.66438000
O	-2.67790000	-4.64855000	-1.84101000
C	-2.65535000	-3.53053000	-1.55173000
C	-4.36968000	-1.56733000	-1.46903000
C	-1.92104000	-1.14835000	-2.63431000
H	-0.78759200	1.17689000	-0.93996400
C	-2.80773000	-3.51007000	1.71276000
C	-4.38636000	-1.53051000	1.71634000
C	0.08483100	-0.51623500	0.11326100
H	-0.73678400	1.37660000	0.82056500
C	-0.88663900	0.65579700	0.01395100
H	0.75814900	-0.55225800	-0.74548100

ΔH = 2.7 kcal mol^{-1}
ΔG = 3.2 kcal mol^{-1}

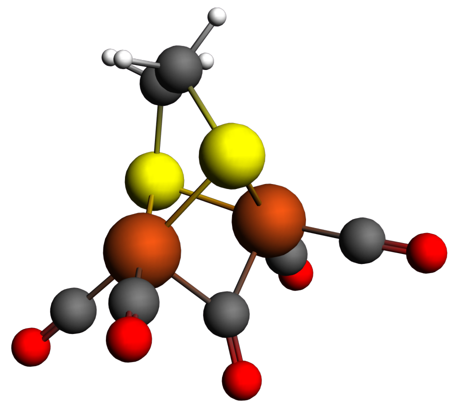

4.2c: (μ-edt)$Fe_2(CO)_5$

B88P86/TZP

Fe	-2.43490428	-1.48855363	2.02894667
O	-4.78769115	-0.50631759	3.48032487
O	-4.25414387	-3.55590249	1.11415539
S	-2.68005821	0.14243692	0.37773477
O	-1.70947428	-3.47201830	4.06087277
Fe	-2.41850686	-1.99229832	-0.50033589
S	-0.50016107	-1.94765565	0.82034501
H	-0.82136335	0.83682012	-0.98861891
O	-4.80532082	-1.67454931	-2.17176340
O	-1.70629683	-4.63603575	-1.55455798
C	-1.99670855	-3.58963341	-1.14613464
C	-3.85841310	-1.81520859	-1.51582994
H	-0.88781681	1.74076649	0.53730107
C	-2.01720719	-2.69261424	3.25786102
C	-3.42209739	-2.72885546	0.96369599
C	-3.86262891	-0.90653342	2.90522433
C	0.09668014	-0.19770478	0.69385546
H	0.37829365	0.11203544	1.70750007
C	-0.94732638	0.73649879	0.09607036
H	1.00979100	-0.22412682	0.08373778

ΔH = 1.1 kcal mol^{-1}
ΔG = 1.8 kcal mol^{-1}

TPSS-D3(BJ)/TZP

Fe	-2.42806000	-1.48474000	2.02097000
O	-4.80000000	-0.51273000	3.45296000
O	-4.25223000	-3.54968000	1.10952000
S	-2.68159000	0.13512100	0.38066800
O	-1.69852000	-3.48663000	4.03655000
Fe	-2.41397000	-1.98359000	-0.49830200
S	-0.50923200	-1.95181000	0.81875800
H	-0.81895200	0.76827900	-1.00364000
O	-4.82141000	-1.65838000	-2.14213000
O	-1.69660000	-4.64319000	-1.51474000
C	-1.98970000	-3.59127000	-1.13103000
C	-3.86626000	-1.80356000	-1.50449000
H	-0.88872300	1.73086000	0.48251500
C	-2.00812000	-2.70038000	3.24522000
C	-3.42016000	-2.72448000	0.96061500
C	-3.86629000	-0.90458000	2.89194000
C	0.08158800	-0.20068800	0.71879400
H	0.31230000	0.11217900	1.73865000
C	-0.95063400	0.71688200	0.07840800
H	1.01214000	-0.21840100	0.14521700

ΔH = 5.0 kcal mol^{-1}
ΔG = 6.3 kcal mol^{-1}

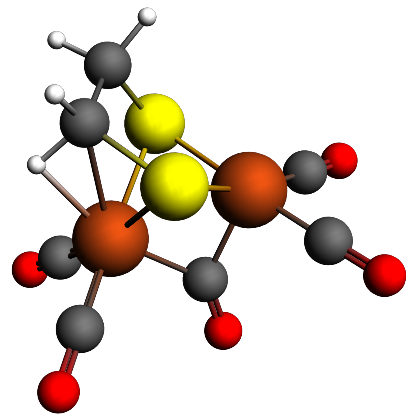

4.2d: (μ-edt)$Fe_2(CO)_5$

B88P86/TZP

Fe	-1.57360500	0.33823100	2.13783400
O	-4.05193200	1.30221000	3.38482900
O	-3.29622400	-1.71642900	0.99383700
S	-1.55284200	2.10522000	0.71426200
O	-1.17334300	-1.56451800	4.33093000
Fe	-1.35071900	-0.01356400	-0.37962900
S	0.41652800	-0.26333400	1.19961400
H	-0.09826400	1.41338300	-1.14323000
O	-3.59109800	0.49292900	-2.20283400
O	-0.62507100	-2.44814800	-1.82160200
C	-0.90600000	-1.48020700	-1.24455500
C	-2.70488300	0.30766300	-1.47741400
H	0.29473700	3.02263600	-0.54457500
C	-1.33791400	-0.82164700	3.45362000
C	-2.46991000	-0.87327500	0.96333000
C	-3.07734600	0.92636900	2.87845200
C	1.13463300	1.34717400	0.63596000
H	1.44194700	1.95227000	1.49705000
C	0.05644200	2.00897300	-0.19032000
H	2.02019900	1.10310400	0.02997600

ΔH = 2.5 kcal mol^{-1}
ΔG = 3.6 kcal mol^{-1}

TPSS-D3(BJ)/TZP

Fe	-1.57050985	0.34116452	2.13425974
O	-4.07044871	1.30446374	3.34018860
O	-3.29441476	-1.71013591	0.99132389
S	-1.54405923	2.10099089	0.71639936
O	-1.18285706	-1.57528419	4.31925619
Fe	-1.33880495	0.00011794	-0.36984438
S	0.40856176	-0.27499475	1.20296302
H	-0.14030819	1.30525010	-1.14421629
O	-3.60090700	0.52296289	-2.16411259
O	-0.61825646	-2.45091182	-1.78706613
C	-0.89823799	-1.47684084	-1.22641013
C	-2.70455115	0.33198737	-1.45791293
H	0.26739981	2.93764518	-0.64095457
C	-1.34209058	-0.82404802	3.45111318
C	-2.46697550	-0.86985808	0.96441403
C	-3.08612082	0.93127081	2.85690751
C	1.12976149	1.32149056	0.60726081
H	1.43525482	1.94483613	1.44860554
C	0.03787372	1.95280445	-0.22432913
H	2.00298903	1.06241927	-0.00006703

ΔH = 5.2 kcal mol^{-1}
ΔG = 7.1 kcal mol^{-1}

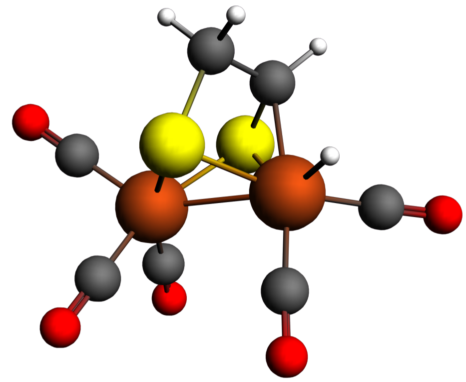

4.2e: (μ-edt)$Fe_2(CO)_5$

B88P86/TZP

Fe	-2.56094171	-1.73653328	1.39263583
O	-5.44331241	-2.28623714	1.76206545
O	-1.93813835	-3.64737039	3.52320820
S	-2.75355260	0.17384835	0.11011830
H	-2.49810324	-0.79772785	2.55173512
Fe	-2.76528635	-1.66401418	-1.26036212
S	-0.99293288	-2.39062788	-0.09174458
O	-1.50748445	-0.48467552	-3.64128146
O	-5.56430007	-1.00896229	-1.95335715
O	-3.14037781	-4.43604150	-2.22206426
C	-2.98367723	-3.35615038	-1.83595802
C	-4.47064952	-1.26237391	-1.67195355
C	-2.01453003	-0.94677508	-2.70657778
H	-0.36047361	0.68548066	-0.38660406
C	-2.18355152	-2.92169184	2.64818042
C	-4.31426698	-2.08709646	1.57152734
C	-0.66898147	-1.03591644	0.99242158
H	-0.87022810	1.08734334	1.28812109
C	-0.94754207	0.34491059	0.48102810
H	0.19494971	-1.20087964	1.64306393

ΔH = 10.3 kcal mol⁻¹
ΔG = 11.3 kcal mol⁻¹

TPSS-D3(BJ)/TZP

Fe	-2.54957581	-1.72704877	1.34653102
O	-5.43108290	-2.34714357	1.52515015
O	-1.97714097	-3.72081188	3.41138376
S	-2.73674083	0.19628954	0.11532186
H	-2.56191053	-0.82002760	2.53725939
Fe	-2.76125166	-1.64667257	-1.21327666
S	-0.95631595	-2.34509088	-0.09304800
O	-1.54937028	-0.55741117	-3.65433138
O	-5.56671118	-0.98830113	-1.85305743
O	-3.19115412	-4.45867471	-2.00754886
C	-3.01185874	-3.36223883	-1.69815442
C	-4.47107654	-1.24277898	-1.59902088
C	-2.04023718	-0.98503794	-2.69985213
H	-0.35032774	0.71787090	-0.34629912
C	-2.19677033	-2.95899270	2.56706629
C	-4.30062092	-2.11406226	1.42341438
C	-0.66576820	-1.00855445	1.01582745
H	-0.88333600	1.10487174	1.32106933
C	-0.94196876	0.37469665	0.50932982
H	0.18282301	-1.17649981	1.67606431

ΔH = 11.7 kcal mol⁻¹
ΔG = 12.8 kcal mol⁻¹

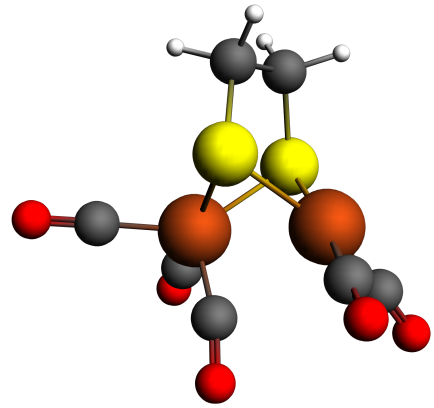

4.2b↔4.2c transition state: (μ-edt)$Fe_2(CO)_5$

B88P86/TZP

Fe	-2.55592000	-1.67345000	1.87898000
O	-4.95375000	-0.51819700	3.12644000
O	-3.94484000	-4.13549000	1.13560000
S	-2.48410000	0.17919600	0.47755000
O	-1.56911000	-2.60624000	4.47672000
Fe	-2.34133000	-1.83625000	-0.63661900
S	-0.55978100	-2.11499000	0.79776200
H	-0.48377700	0.87216100	-0.67657600
O	-5.02718000	-1.58772000	-1.78450000
O	-2.03792000	-4.51881000	-1.79397000
C	-2.14589000	-3.46122000	-1.32573000
C	-3.95217000	-1.66277000	-1.34899000
H	-0.58902100	1.58537000	0.94514100
C	-1.95447000	-2.23010000	3.44782000
C	-3.33583000	-3.15276000	1.28603000
C	-4.02303000	-0.98750300	2.61945000
C	0.22324900	-0.43951400	0.91315200
H	0.45983900	-0.28240700	1.97208000
C	-0.69237100	0.65034400	0.37795600
H	1.16744000	-0.49264900	0.35341200

ΔH = 8.1 kcal mol^{-1}
ΔG = 8.5 kcal mol^{-1}

TPSS-D3(BJ)/TZP

Fe	-2.54422151	-1.63395281	1.87829044
O	-5.00755556	-0.58049511	3.09148242
O	-3.94141104	-4.07240267	1.09355936
S	-2.47657439	0.18405927	0.45050616
O	-1.55763410	-2.70720390	4.42043460
Fe	-2.34538604	-1.85143490	-0.61421987
S	-0.56030644	-2.10712047	0.81315019
H	-0.47059773	0.75768871	-0.75460280
O	-5.05498186	-1.54957216	-1.69777318
O	-1.99613165	-4.55068120	-1.72714187
C	-2.13224685	-3.48779834	-1.28910639
C	-3.97065456	-1.66063706	-1.30514332
H	-0.56888697	1.59609954	0.80388485
C	-1.95738068	-2.26788522	3.42463916
C	-3.32444768	-3.08855894	1.20920480
C	-4.04195548	-0.99091149	2.60567743
C	0.21125553	-0.43226256	0.92917655
H	0.37639815	-0.24365761	1.99111723
C	-0.68303378	0.62777134	0.30882491
H	1.18048701	-0.49115668	0.42573129

ΔH = 8.8 kcal mol^{-1}
ΔG = 10.7 kcal mol^{-1}

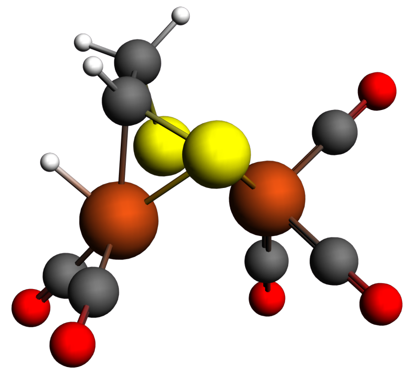

4.2b↔4.2e transition state: (μ-edt)$Fe_2(CO)_5$

B88P86/TZP

Fe	-2.65257309	-1.74533774	1.36258581
O	-5.20987787	-1.17640939	2.69300136
O	-2.51850173	-4.31735805	2.77568652
S	-2.85481118	0.12843960	0.02087131
H	-1.82310115	-0.99599800	2.40394154
Fe	-2.65364857	-1.72017715	-1.31599311
S	-0.90501054	-2.26366500	-0.00063432
O	-1.66694108	-0.38915280	-3.75662298
O	-5.56047319	-1.55794216	-1.80258073
O	-2.58271038	-4.49378267	-2.32527665
C	-2.60937543	-3.40779010	-1.92057458
C	-4.42014856	-1.61703343	-1.60268560
C	-2.05082559	-0.91229426	-2.79423883
H	-0.45263825	0.78972702	-0.25732805
C	-2.55826013	-3.30825797	2.19654184
C	-4.21516451	-1.41301643	2.13860341
C	-0.76674746	-0.89707555	1.13289516
H	-1.17041645	1.22469660	1.33275649
C	-1.11117838	0.44948774	0.55555820
H	0.11861196	-0.98771404	1.76991807

ΔH = 15.4 kcal mol^{-1}
ΔG = 16.4 kcal mol^{-1}

TPSS-D3(BJ)/TZP

Fe	-2.65393200	-1.72199900	1.29586300
O	-5.31336700	-1.17594400	2.41202000
O	-2.63660900	-4.35274600	2.59678700
S	-2.76123900	0.17475700	0.00145300
H	-1.85705100	-0.98634700	2.38611900
Fe	-2.61075900	-1.71635600	-1.26530900
S	-0.86076000	-2.25617100	0.02946300
O	-1.85096700	-0.38076900	-3.77836400
O	-5.55186500	-1.67621100	-1.43911400
O	-2.56133500	-4.49084000	-2.25761300
C	-2.57413100	-3.40340200	-1.86665600
C	-4.39790000	-1.68311900	-1.36769700
C	-2.13899800	-0.91313800	-2.79219300
H	-0.34180900	0.75771600	-0.17816800
C	-2.62727700	-3.31597600	2.07642200
C	-4.27150900	-1.39678600	1.95523000
C	-0.75456300	-0.91237400	1.19180200
H	-1.10750700	1.21424900	1.37888200
C	-1.03695600	0.44430800	0.60579100
H	0.09235200	-1.03074000	1.86496100

ΔH = 17.3 kcal mol^{-1}
ΔG = 20.2 kcal mol^{-1}

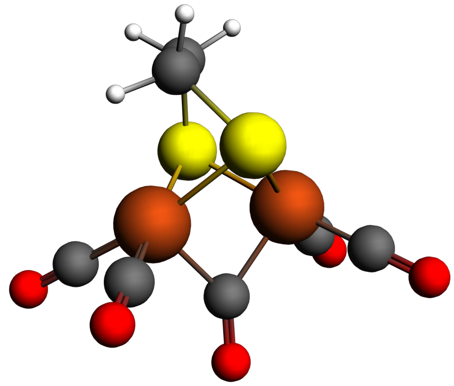

4.2c↔4.2d transition state: (μ-edt)$Fe_2(CO)_5$

B88P86/TZP

Fe	-1.55423988	0.35105087	2.13403670
O	-4.05320724	1.31920783	3.33913550
O	-3.31135510	-1.68396960	1.01128059
S	-1.55668228	2.08576007	0.65775222
O	-1.18103467	-1.64452113	4.24960549
Fe	-1.36110795	-0.03292471	-0.37557652
S	0.41747054	-0.24090678	1.16251065
H	0.07967113	1.70247317	-1.10759585
O	-3.61427205	0.49450377	-2.17829080
O	-0.66270958	-2.52997297	-1.73316607
C	-0.93250319	-1.53903038	-1.19683886
C	-2.72289332	0.29300737	-1.46790809
H	0.37817059	3.21097488	-0.23972237
C	-1.33565148	-0.85972948	3.41161452
C	-2.47298432	-0.85472699	0.95813823
C	-3.06962034	0.94263148	2.85835704
C	1.14825710	1.40458429	0.74497717
H	1.38866415	1.93466272	1.66739569
C	0.13793190	2.15288144	-0.09819706
H	2.07034619	1.20780570	0.18866277

ΔH = 2.4 kcal mol^{-1}
ΔG = 4.7 kcal mol^{-1}

TPSS-D3(BJ)/TZP

Fe	-1.55423988	0.35105087	2.13403670
O	-4.05320724	1.31920783	3.33913550
O	-3.31135510	-1.68396960	1.01128059
S	-1.55668228	2.08576007	0.65775222
O	-1.18103467	-1.64452113	4.24960549
Fe	-1.36110795	-0.03292471	-0.37557652
S	0.41747054	-0.24090678	1.16251065
H	0.07967113	1.70247317	-1.10759585
O	-3.61427205	0.49450377	-2.17829080
O	-0.66270958	-2.52997297	-1.73316607
C	-0.93250319	-1.53903038	-1.19683886
C	-2.72289332	0.29300737	-1.46790809
H	0.37817059	3.21097488	-0.23972237
C	-1.33565148	-0.85972948	3.41161452
C	-2.47298432	-0.85472699	0.95813823
C	-3.06962034	0.94263148	2.85835704
C	1.14825710	1.40458429	0.74497717
H	1.38866415	1.93466272	1.66739569
C	0.13793190	2.15288144	-0.09819706
H	2.07034619	1.20780570	0.18866277

ΔH = 5.4 kcal mol^{-1}
ΔG = 7.7 kcal mol^{-1}

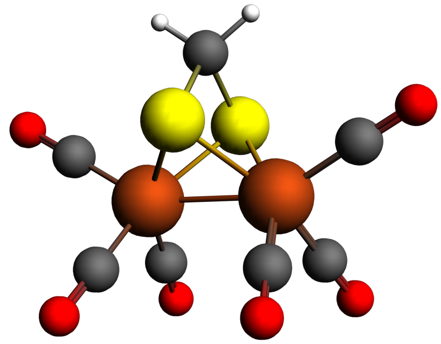

Scheme 4.1 D: (μ-mdt)$Fe_2(CO)_6$

B88P86/TZP

Fe	-2.67290123	-1.78079916	1.38877801
O	-5.54375246	-1.41263764	1.96883084
O	-2.77379556	-4.66705089	1.99717606
S	-2.49376469	0.13616191	0.12344256
O	-1.61195331	-0.85392732	3.98342803
Fe	-2.64528352	-1.76534842	-1.16813737
S	-0.75127777	-1.94560497	0.12969097
O	-1.52530788	-0.82103956	-3.73165871
O	-5.50131699	-1.38684890	-1.81091337
O	-2.73833118	-4.64648143	-1.80153886
C	-2.70976359	-3.51638904	-1.54380501
C	-4.38279905	-1.53948882	-1.54578697
C	-1.95864993	-1.18604901	-2.71823539
C	-2.02185628	-1.21346029	2.95841864
C	-2.74218323	-3.53505085	1.74826502
C	-4.41912847	-1.56115289	1.72828361
H	-0.17920449	0.30036517	-0.75699328
H	-0.19857403	0.28978082	1.05501797
C	-0.66380841	-0.10204816	0.14162540

TPSS-D3(BJ)/TZP

Fe	0.00000000	1.24519752	-0.19584084
O	2.13614743	1.76953626	-2.15746391
O	-2.13614743	1.76953626	-2.15746391
S	1.35577053	0.00000000	1.16159081
O	0.00000000	3.83530850	1.20942348
Fe	0.00000000	-1.24519752	-0.19584084
S	-1.35577053	0.00000000	1.16159081
O	0.00000000	-3.83530850	1.20942348
O	2.13614743	-1.76953626	-2.15746391
O	-2.13614743	-1.76953626	-2.15746391
C	-1.29575804	-1.56629884	-1.39095828
C	1.29575804	-1.56629884	-1.39095828
C	0.00000000	-2.81654897	0.66140214
C	0.00000000	2.81654897	0.66140214
C	-1.29575804	1.56629884	-1.39095828
C	1.29575804	1.56629884	-1.39095828
H	0.00000000	-0.90318163	3.02031791
H	0.00000000	0.90318163	3.02031791
C	0.00000000	0.00000000	2.40765102

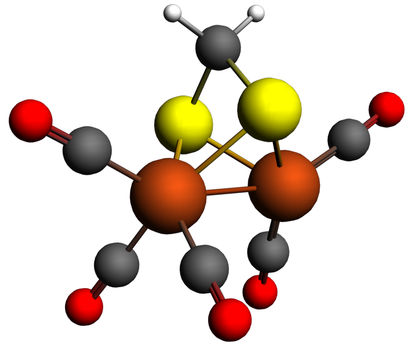

4.3a: (μ-mdt)$Fe_2(CO)_5$

B88P86/TZP

Fe	-2.67221435	-1.73166307	1.40922980
O	-5.53033714	-1.34628771	2.02296330
O	-2.88037469	-4.65667921	1.77140503
S	-2.52394259	0.12015687	0.09806929
O	-1.53896983	-0.95567913	4.03988733
Fe	-2.62314503	-1.72578392	-1.12093932
S	-0.74219947	-1.91748577	0.14126012
O	-1.55189852	-0.89794289	-3.73091667
O	-5.47349583	-1.57546996	-1.86515267
H	-0.24705202	0.34001654	1.04790287
C	-0.69618376	-0.05722385	0.12889750
C	-4.35175768	-1.62689688	-1.56030187
C	-1.97238780	-1.26719799	-2.70801072
C	-1.97058727	-1.24700646	3.00250437
C	-2.80696603	-3.50621209	1.62905692
C	-4.40838875	-1.49966008	1.76830306
H	-0.21495482	0.35132463	-0.76895263

ΔH = 3.2 kcal mol
ΔG = 2.4 kcal mol

TPSS-D3(BJ)/TZP

Fe	-2.67136181	-1.70883178	1.38325113
O	-5.52607769	-1.26575273	1.95302264
O	-2.96588166	-4.63499549	1.57947817
S	-2.52789473	0.11996256	0.06095653
O	-1.54189896	-0.99292696	4.02366157
Fe	-2.58923261	-1.77228283	-1.07997224
S	-0.71449835	-1.88230256	0.18433995
O	-1.59790546	-0.86335896	-3.68898716
O	-5.47255866	-1.66285892	-1.67586475
H	-0.28467662	0.39458248	1.04160284
C	-0.70334470	-0.02820868	0.12687617
C	-4.33757130	-1.71318568	-1.44680515
C	-1.97887698	-1.28464017	-2.67556438
C	-1.98143803	-1.25176423	2.98522044
C	-2.84864699	-3.48414779	1.52000071
C	-4.40609057	-1.44695171	1.72793292
H	-0.21724400	0.36323682	-0.76852463

ΔH = 0.0 kcal mol
ΔG = 0.0 kcal mol

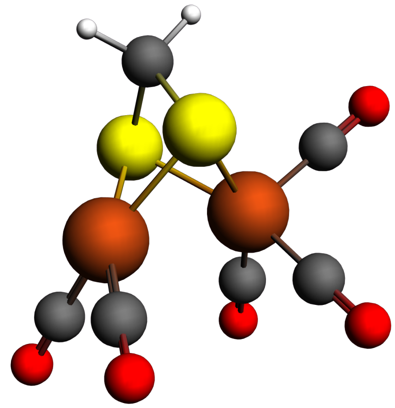

4.3b: (μ-mdt)$Fe_2(CO)_5$

B88P86/TZP

Fe	-2.66360276	-1.76937129	1.40664636
O	-5.53401299	-1.36942628	1.97155859
O	-2.73841564	-4.66369185	1.98291564
S	-2.50467823	0.15096642	0.11899743
O	-1.60551937	-0.85181421	4.00975642
Fe	-2.68404924	-1.80705698	-1.09671439
S	-0.73401283	-1.95035573	0.13523322
H	-0.17589444	0.32436756	0.97563723
O	-5.47029303	-1.40626987	-1.92388737
O	-2.75885632	-4.61829688	-1.93403059
C	-2.72116714	-3.50043824	-1.60630272
C	-4.36014233	-1.55915530	-1.60355955
C	-0.67203488	-0.10059383	0.09339454
C	-2.02513031	-1.21528411	2.99101302
C	-2.71461193	-3.52694390	1.76206800
C	-4.40811973	-1.52885282	1.75107168
H	-0.20915664	0.28322740	-0.82470758

ΔH = 4.1 kcal mol^{-1}
ΔG = 3.3 kcal mol^{-1}

TPSS-D3(BJ)/TZP

Fe	0.78583464	0.39539487	0.00000000
O	0.55829171	2.40317971	-2.14648379
O	0.55829171	2.40317971	2.14648379
S	0.12100663	-1.33336466	-1.37032584
O	3.71882627	0.06503489	0.00000000
Fe	-1.50836210	-0.46093365	0.00000000
S	0.12100663	-1.33336466	1.37032584
H	1.62969032	-2.73738651	0.00000000
O	-2.79494007	1.14228059	-2.08760258
O	-2.79494007	1.14228059	2.08760258
C	-2.31106314	0.47609674	1.26853288
C	-2.31106314	0.47609674	-1.26853288
C	0.56742633	-2.48647419	0.00000000
C	2.57052775	0.19993598	0.00000000
C	0.65823174	1.61986378	1.30429661
C	0.65823174	1.61986378	-1.30429661
H	-0.04573625	-3.38938095	0.00000000

ΔH = 0.7 kcal mol^{-1}
ΔG = 1.0 kcal mol^{-1}

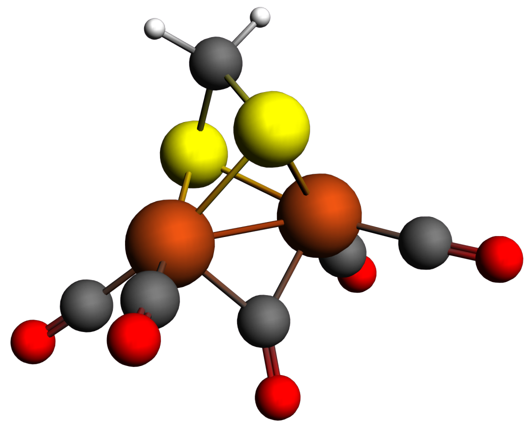

4.3c: (μ-mdt)$Fe_2(CO)_5$

B88P86/TZP

Fe	-2.85648817	-1.94445036	1.40791484
O	-5.11751412	-1.03005833	3.04717624
O	-2.35210394	-4.28200812	3.11404985
S	-2.73006245	-0.00343049	0.12305152
O	-4.82633091	-3.64063485	0.10017531
Fe	-2.83862818	-1.93847935	-1.17280355
S	-0.91552066	-2.13940748	0.13015446
H	-0.41918288	0.12753485	1.04103083
O	-5.07858591	-1.01751196	-2.83732532
O	-2.30859717	-4.27011861	-2.87930243
C	-2.53487349	-3.36438646	-2.18860967
C	-4.20718900	-1.39854880	-2.17086063
C	-0.88956805	-0.27668621	0.13728844
C	-3.92837206	-2.87083256	0.10822882
C	-2.56775065	-3.37429345	2.42262817
C	-4.23787152	-1.40815565	2.39000125
H	-0.40397993	0.13421394	-0.75530366

ΔH = 0.0 kcal mol
ΔG = 0.0 kcal mol

TPSS-D3(BJ)/TZP

Fe	1.27878493	0.00000000	0.00764795
O	2.89054607	-2.13021199	-1.21093988
O	2.89054607	2.13021199	-1.21093988
S	0.00000000	-1.39795615	1.33912681
O	0.00000000	0.00000000	-2.59479425
Fe	-1.27878493	0.00000000	0.00764795
S	0.00000000	1.39795615	1.33912681
H	0.89558556	0.00000000	3.18176391
O	-2.89054607	-2.13021199	-1.21093988
O	-2.89054607	2.13021199	-1.21093988
C	-2.25317325	1.29106824	-0.73306019
C	-2.25317325	-1.29106824	-0.73306019
C	0.00000000	0.00000000	2.56115057
C	0.00000000	0.00000000	-1.41357609
C	2.25317325	1.29106824	-0.73306019
C	2.25317325	-1.29106824	-0.73306019
H	-0.89558556	0.00000000	3.18176391

ΔH = 0.7 kcal mol
ΔG = 1.8 kcal mol

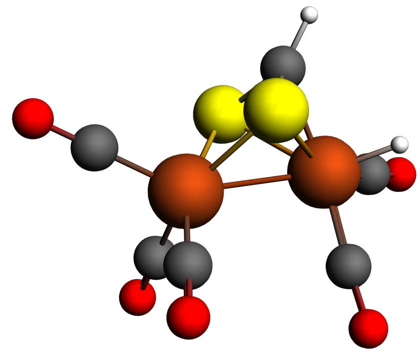

4.3d: (μ-mdt)$Fe_2(CO)_5$

B88P86/TZP

Fe	-0.10436525	-0.21078992	-1.24843476
O	1.72139392	-2.52420515	-1.49564589
O	-2.49705339	-1.92874257	-1.51983552
S	1.51286902	1.10129562	-0.35101776
O	-0.04384130	0.76629737	-4.02435610
Fe	0.13542634	0.34610196	1.31442222
S	-1.28005366	1.43042880	-0.15445967
H	0.40080044	3.11701337	0.73161111
O	2.03790948	0.27286911	3.52748232
O	-1.07421994	-2.21301353	2.10261911
C	-0.57931336	-1.21723293	1.76182223
C	1.30490293	0.28953327	2.62421788
C	0.25567987	2.11505772	0.32812377
C	-0.07738737	0.38288934	-2.93088082
C	-1.55836105	-1.26160651	-1.40320739
C	1.00839905	-1.61799119	-1.39549014
H	-0.62157543	1.03968206	2.39016861

ΔH = 3.4 kcal mol^{-1}
ΔG = 2.7 kcal mol^{-1}

TPSS-D3(BJ)/TZP

Fe	-0.09820009	-0.18689854	-1.21057754
O	1.72380952	-2.50825548	-1.33541865
O	-2.46900682	-1.94093481	-1.39324579
S	1.50586938	1.13571367	-0.34577051
O	-0.06207219	0.70038817	-4.01184567
Fe	0.12182064	0.35465971	1.26918556
S	-1.27705469	1.45907301	-0.16105051
H	0.39388071	3.13069093	0.75684880
O	2.05911460	0.16848655	3.44223756
O	-1.07743160	-2.24805237	1.89966726
C	-0.59072267	-1.23076499	1.63061222
C	1.30935350	0.23486717	2.56139846
C	0.25038591	2.13980015	0.34261879
C	-0.08306147	0.35204558	-2.91077129
C	-1.54329011	-1.25686338	-1.32280374
C	1.01804322	-1.59691249	-1.29448088
H	-0.63529972	1.00080832	2.37865695

ΔH = 2.8 kcal mol^{-1}
ΔG = 3.0 kcal mol^{-1}

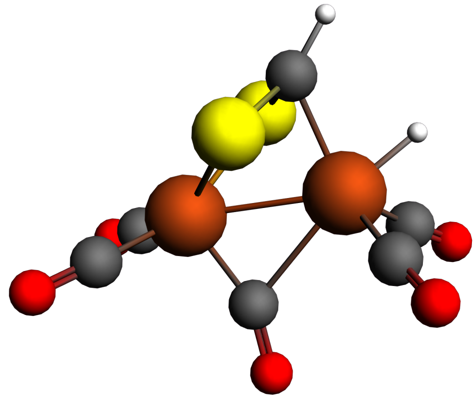

4.3e: (μ-mdt)$Fe_2(CO)_5$

B88P86/TZP

Fe	0.11286110	-1.47138090	0.00000000
O	-0.54555418	-3.41204473	2.10344833
O	-0.54555418	-3.41204473	-2.10344833
S	1.52663453	-0.30839918	1.41532342
O	-2.57754990	-0.33822439	0.00000000
Fe	0.29547818	1.12515792	0.00000000
S	1.52663453	-0.30839918	-1.41532342
H	3.09843374	1.09016878	0.00000000
O	-1.02423470	2.58206218	2.16896098
O	-1.02423470	2.58206218	-2.16896098
C	-0.53304141	1.98085510	-1.30814840
C	-0.53304141	1.98085510	1.30814840
C	2.20181061	0.46996301	0.00000000
C	-1.41949273	-0.51570725	0.00000000
C	-0.30399050	-2.63975984	-1.26883732
C	-0.30399050	-2.63975984	1.26883732
H	1.15790594	2.34106322	0.00000000

ΔH = 8.6 kcal mol
ΔG = 7.9 kcal mol

TPSS-D3(BJ)/TZP

Fe	0.15122400	-1.45301200	0.00000000
O	-0.63105000	-3.34269800	2.10276200
O	-0.63105000	-3.34269800	-2.10276200
S	1.54621200	-0.29539500	1.40994300
O	-2.52062000	-0.30687100	0.00000000
Fe	0.29925700	1.09238800	0.00000000
S	1.54621200	-0.29539500	-1.40994300
H	3.08322500	1.13778600	0.00000000
O	-1.07066800	2.48158200	2.18050200
O	-1.07066800	2.48158200	-2.18050200
C	-0.55340300	1.91649000	-1.31711600
C	-0.55340300	1.91649000	1.31711600
C	2.20986700	0.49644400	0.00000000
C	-1.36024300	-0.46340900	0.00000000
C	-0.32796400	-2.59697400	-1.26963500
C	-0.32796400	-2.59697400	1.26963500
H	1.13056700	2.33409400	0.00000000

ΔH = 8.4 kcal mol
ΔG = 8.6 kcal mol

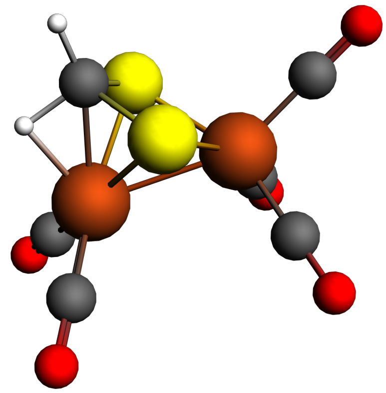

4.3f: (μ-mdt)$Fe_2(CO)_5$

B88P86/TZP

Fe	-0.25218294	1.24990969	0.00000000
O	-2.28795628	1.47181296	-2.12944662
O	-2.28795628	1.47181296	2.12944662
S	1.21318139	0.21339331	-1.41390299
O	0.69449958	4.04577698	0.00000000
Fe	0.22197849	-1.33354515	0.00000000
S	1.21318139	0.21339331	1.41390299
H	3.23436313	-0.38188951	0.00000000
O	-1.05936010	-2.95473831	-2.07205270
O	-1.05936010	-2.95473831	2.07205270
C	-0.54647370	-2.29976492	1.25573015
C	-0.54647370	-2.29976492	-1.25573015
C	2.14080866	-0.47035702	0.00000000
C	0.32618332	2.94586463	0.00000000
C	-1.49171803	1.38250966	1.29306910
C	-1.49171803	1.38250966	-1.29306910
H	1.97874119	-1.66045539	0.00000000

ΔH = 11.6 kcal mol^{-1}
ΔG = 10.7 kcal mol^{-1}

TPSS-D3(BJ)/TZP

Fe	-0.21281000	1.19012500	0.00000000
O	-2.26868900	1.23394400	-2.11338300
O	-2.26868900	1.23394400	2.11338300
S	1.29038100	0.21711500	-1.40987200
O	0.55721400	4.03635200	0.00000000
Fe	0.24438500	-1.27603300	0.00000000
S	1.29038100	0.21711500	1.40987200
H	3.30283500	-0.37352000	0.00000000
O	-1.24125500	-2.70436000	-2.07061700
O	-1.24125500	-2.70436000	2.07061700
C	-0.62921700	-2.14512900	1.25713100
C	-0.62921700	-2.14512900	-1.25713100
C	2.21677400	-0.47840000	0.00000000
C	0.26227900	2.91880100	0.00000000
C	-1.46207600	1.22938600	1.28736300
C	-1.46207600	1.22938600	-1.28736300
H	2.04504500	-1.64427800	0.00000000

ΔH = 11.8 kcal mol^{-1}
ΔG = 11.5 kcal mol^{-1}

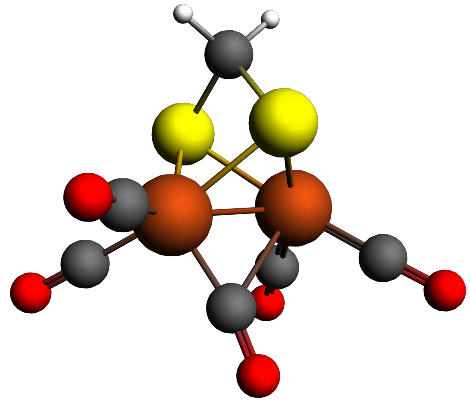

4.3b↔4.3c transition state: (μ-mdt)$Fe_2(CO)_5$

B88P86/TZP

Fe	-2.69067625	-1.52862965	1.48068765
O	-5.22433468	-0.63522297	2.68850455
O	-3.63769690	-4.28792407	1.20613232
S	-2.76243134	0.15465483	-0.13115595
O	-1.35697777	-1.84629709	4.07977369
Fe	-2.64075713	-2.00359285	-1.00126434
S	-0.71909375	-1.68160696	0.24501411
H	-0.48929337	0.75509216	0.66520141
O	-5.39465630	-2.08568701	-2.02272136
O	-2.05895371	-4.73421300	-1.92881487
C	-2.29302683	-3.66398522	-1.53944824
C	-4.30055074	-2.05318479	-1.62725490
C	-0.90684039	0.12325197	-0.12786632
C	-1.89695114	-1.71194574	3.05965425
C	-3.22859334	-3.19604626	1.15847557
C	-4.23437867	-1.00078833	2.20833605
H	-0.47432818	0.39647979	-1.09813430

ΔH = 8.5 kcal mol^{-1}
ΔG = 9.1 kcal mol^{-1}

TPSS-D3(BJ)/TZP

Fe	-2.67852900	-1.51083800	1.44962600
O	-5.23765700	-0.67360400	2.63441400
O	-3.66969100	-4.23969400	1.11828600
S	-2.74889100	0.16232300	-0.15020900
O	-1.41251500	-1.93911800	4.06089000
Fe	-2.62300800	-1.99007800	-0.99135300
S	-0.70864300	-1.66345300	0.24273600
H	-0.49882600	0.75979400	0.67752100
O	-5.43009500	-2.13322400	-1.83617900
O	-2.06331500	-4.75435700	-1.82724900
C	-2.27893000	-3.66679000	-1.49433400
C	-4.31154000	-2.06779100	-1.54022100
C	-0.89817200	0.13737700	-0.12346100
C	-1.91993600	-1.75122100	3.03621500
C	-3.23136300	-3.16051100	1.07278400
C	-4.23659900	-1.00934900	2.16444200
H	-0.45994500	0.41166100	-1.08382000

ΔH = 6.4 kcal mol^{-1}
ΔG = 7.9 kcal mol^{-1}

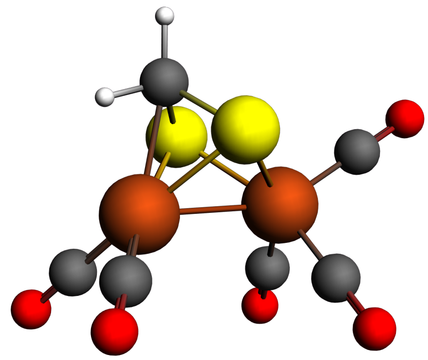

4.3b↔4.3f transition state: (μ-mdt)$Fe_2(CO)_5$

B88P86/TZP

Fe	0.00838400	-0.18121300	-1.26988900
O	2.21265700	-2.13613900	-1.49264100
O	-2.04600900	-2.30086800	-1.39262000
S	1.38296300	1.38011700	-0.31702500
O	-0.11883500	0.71662100	-4.07982500
Fe	0.08947800	0.29625500	1.27823700
S	-1.43444700	1.23369200	-0.20139700
H	-0.12262300	3.37398700	0.06760600
O	2.28475100	-0.95143700	2.75548100
O	-1.84969500	-1.13910700	2.93275700
C	-1.08466000	-0.56439200	2.26655800
C	1.41922400	-0.44675800	2.15899100
C	-0.05365000	2.31113000	0.33665900
C	-0.06746600	0.36277200	-2.97640800
C	-1.23842100	-1.47179500	-1.34615300
C	1.34884600	-1.36906800	-1.40925200
H	-0.00526500	2.28986300	1.48776400

ΔH = 11.4 kcal mol^{-1}
ΔG = 11.1 kcal mol^{-1}

TPSS-D3(BJ)/TZP

Fe	-0.25017600	1.14850084	0.00000000
O	-2.30324445	1.13712696	-2.11675458
O	-2.30324445	1.13712696	2.11675458
S	1.28174837	0.21786166	-1.40793281
O	0.45043028	4.01305722	0.00000000
Fe	0.26093071	-1.30014110	0.00000000
S	1.28174837	0.21786166	1.40793281
H	3.33679359	-0.17113020	0.00000000
O	-1.23208299	-2.72601113	-2.06623646
O	-1.23208299	-2.72601113	2.06623646
C	-0.61341513	-2.16963641	1.25535144
C	-0.61341513	-2.16963641	-1.25535144
C	2.26958755	-0.40277666	0.00000000
C	0.18034783	2.88938725	0.00000000
C	-1.49840301	1.15703814	1.28935217
C	-1.49840301	1.15703814	-1.28935217
H	2.20705454	-1.55276809	0.00000000

ΔH = 11.4 kcal mol^{-1}
ΔG = 12.1 kcal mol^{-1}

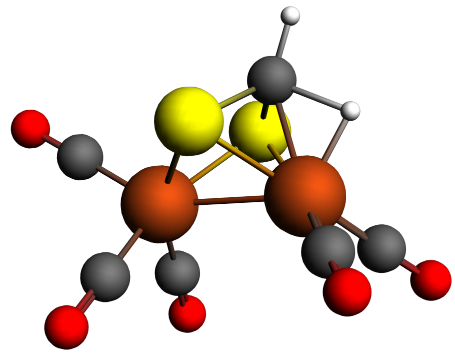

4.3d↔4.3f transition state: (μ-mdt)$Fe_2(CO)_5$

B88P86/TZP

Fe	0.01038700	-0.19424200	-1.31125900
O	2.19601900	-2.15381400	-1.63546800
O	-2.04216800	-2.30978500	-1.49257800
S	1.39170200	1.31918500	-0.29778300
O	-0.13871100	0.79397600	-4.08757700
Fe	0.09066200	0.28540500	1.30643800
S	-1.42449300	1.18259000	-0.18498400
H	-0.07350900	3.17011000	0.65993100
O	2.30310200	-0.81267500	2.88163900
O	-1.88009000	-1.01502400	3.04019300
C	-1.10042700	-0.51084000	2.33858800
C	1.42821100	-0.38975900	2.24089400
C	-0.02899500	2.09358400	0.47399200
C	-0.07720100	0.41657000	-2.99217600
C	-1.23315100	-1.48347900	-1.41419200
C	1.33907700	-1.38530100	-1.50014900
H	0.04352900	1.73538900	1.89784700

ΔH = 11.1 kcal mol^{-1}
ΔG = 10.6 kcal mol^{-1}

TPSS-D3(BJ)/TZP

Fe	-0.01064100	-0.14843500	-1.26158800
O	2.16319400	-2.13721500	-1.31133700
O	-2.05413300	-2.27035600	-1.31651100
S	1.37129100	1.40048300	-0.31214400
O	-0.06855100	0.66054700	-4.09458400
Fe	0.10055800	0.28724200	1.22965000
S	-1.43609700	1.24948500	-0.16624900
H	-0.08269800	3.19588500	0.74549500
O	2.34517900	-0.94620200	2.64387500
O	-1.85841500	-1.18467500	2.82804100
C	-1.08103100	-0.60549500	2.19159200
C	1.45777800	-0.46057100	2.07656500
C	-0.03801800	2.13486000	0.51332200
C	-0.05102400	0.35885000	-2.97831800
C	-1.25265700	-1.43850400	-1.30527400
C	1.31058600	-1.35781500	-1.30173600
H	0.05600800	1.70736400	1.90599800

ΔH = 11.4 kcal mol^{-1}
ΔG = 11.6 kcal mol^{-1}

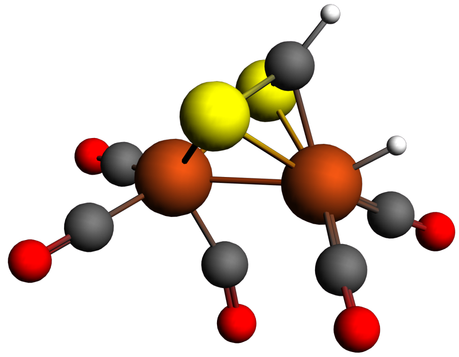

3d↔4.3e transition state: (μ-mdt)$Fe_2(CO)_5$

B88P86/TZP

Fe	-0.23694989	-0.01772729	-1.29591306
O	1.18376589	-2.43470012	-0.46579906
O	-2.41149266	-1.62334323	-2.44267481
S	1.02406041	1.69765314	-0.40384582
O	1.09125920	0.13206414	-3.90531938
Fe	0.26992326	0.21647437	1.23167272
S	-1.66474261	1.05619214	0.16134019
H	-0.39426594	2.93620794	1.29199882
O	2.91063819	-0.36616783	2.32706367
O	-1.10930239	-1.85608737	2.77189840
C	-0.55439863	-1.05730417	2.14343206
C	1.86657339	-0.15954448	1.86720023
C	-0.32105950	2.05495147	0.65547932
C	0.56107051	0.07405208	-2.87295634
C	-1.55189416	-0.99326306	-1.98304960
C	0.64716237	-1.40154250	-0.56851364
H	0.14865747	0.99235258	2.49701865

ΔH = 8.1 kcal mol^{-1}
ΔG = 9.0 kcal mol^{-1}

TPSS-D3(BJ)/TZP

Fe	-0.24594100	-0.00092300	-1.28089900
O	1.14631900	-2.41406600	-0.41173500
O	-2.39442100	-1.63823300	-2.43255700
S	1.00301200	1.71618000	-0.40376800
O	1.15336000	0.09712100	-3.85555800
Fe	0.27449900	0.20965700	1.19989700
S	-1.66719000	1.04305500	0.18186500
H	-0.40086500	2.91209800	1.32537200
O	2.93721700	-0.36950400	2.25082400
O	-1.13030600	-1.86108900	2.72287300
C	-0.56326900	-1.06494300	2.10945500
C	1.88764000	-0.16578100	1.81373300
C	-0.32983100	2.04851700	0.67451200
C	0.59388900	0.05755600	-2.84110900
C	-1.54916600	-0.99445900	-1.97259100
C	0.62719800	-1.37113500	-0.50509800
H	0.16875300	0.97735200	2.47573600

ΔH = 7.9 kcal mol^{-1}
ΔG = 10.2 kcal mol^{-1}

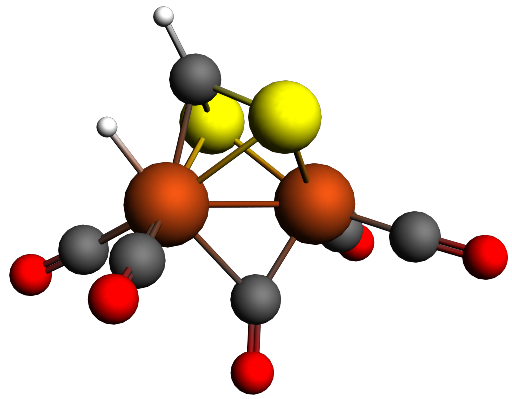

4.3c↔4.3e transition state: (μ-mdt)$Fe_2(CO)_5$

B88P86/TZP

Fe	0.17798300	-1.50588900	0.00000000
O	-0.61614800	-3.39850700	2.09807300
O	-0.61614800	-3.39850700	-2.09807300
S	1.54027600	-0.29389700	1.42212600
O	-2.50863600	-0.38606400	0.00000000
Fe	0.21125100	1.06639100	0.00000000
S	1.54027600	-0.29389700	-1.42212600
H	3.11842400	1.09841900	0.00000000
O	-0.98689500	2.65361500	2.14845900
O	-0.98689500	2.65361500	-2.14845900
C	-0.53998700	2.00600200	-1.29699600
C	-0.53998700	2.00600200	1.29699600
C	2.15883700	0.57544800	0.00000000
C	-1.33407800	-0.45010600	0.00000000
C	-0.32306100	-2.64030500	-1.26726100
C	-0.32306100	-2.64030500	1.26726100
H	1.40876200	2.02483400	0.00000000

ΔH = 9.3 kcal mol^{-1}
ΔG = 9.7 kcal mol^{-1}

TPSS-D3(BJ)/TZP

Fe	0.20636600	-1.49070800	0.00000000
O	-0.68417300	-3.33795700	2.09511800
O	-0.68417300	-3.33795700	-2.09511800
S	1.54942600	-0.28275200	1.41672100
O	-2.47304300	-0.37467000	0.00000000
Fe	0.22728500	1.04229700	0.00000000
S	1.54942600	-0.28275200	-1.41672100
H	3.12203300	1.11313600	0.00000000
O	-1.03058500	2.57711800	2.15042800
O	-1.03058500	2.57711800	-2.15042800
C	-0.55181600	1.95760700	-1.30137200
C	-0.55181600	1.95760700	1.30137200
C	2.17142500	0.58825400	0.00000000
C	-1.29913200	-0.42724900	0.00000000
C	-0.33797000	-2.60541800	-1.26733500
C	-0.33797000	-2.60541800	1.26733500
H	1.41130500	2.02009500	0.00000000

ΔH = 9.4 kcal mol^{-1}
ΔG = 10.6 kcal mol^{-1}

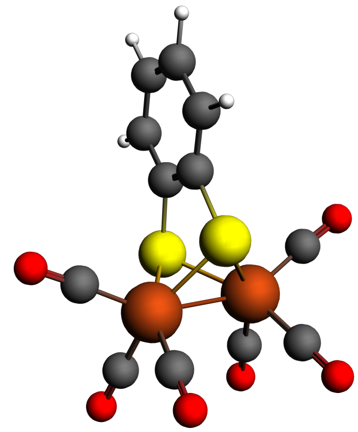

Scheme 4.1 E: (μ-bdt)$Fe_2(CO)_6$

B88P86/TZP

Fe	-2.61086413	-1.77184918	1.36916514
O	-5.47255585	-1.32021297	1.88556607
O	-2.93394805	-4.64069283	1.94092827
S	-2.49526875	0.15813707	0.11931393
O	-1.60374822	-0.90461842	4.00160501
Fe	-2.57890918	-1.76676545	-1.14201949
S	-0.71781652	-2.21856527	0.13739781
O	-1.50846014	-0.88298279	-3.74383018
O	-5.42712123	-1.31385433	-1.72860320
O	-2.87000070	-4.62739814	-1.77033003
C	-2.75172795	-3.50182007	-1.52140690
C	-4.30467269	-1.48529391	-1.49700407
C	-1.89687893	-1.21968012	-2.70652859
C	-1.96774370	-1.23546692	2.95360670
C	-2.80102693	-3.51102248	1.71927273
C	-4.34434923	-1.48981057	1.68222161
H	-0.85524611	2.65250852	0.16153316
C	0.10878164	-0.62058398	0.16185365
C	1.49089683	-0.47612541	0.19684166
C	2.03478952	0.82111205	0.21884525
C	1.20006261	1.93777186	0.20583917
C	-0.19784592	1.78327050	0.17083796
C	-0.72780572	0.49839112	0.15093727
H	2.13798650	-1.35313786	0.20713911
H	3.11730618	0.94729654	0.24662085
H	1.62757201	2.94048890	0.22318602

TPSS-D3(BJ)/TZP

Fe	-2.60865000	-1.77084000	1.34521000
O	-5.47966000	-1.32109000	1.81749000
O	-2.94116000	-4.65255000	1.84961000
S	-2.49183000	0.15880300	0.11585300
O	-1.58386000	-0.89704000	3.96906000
Fe	-2.57283000	-1.76349000	-1.12621000
S	-0.71436800	-2.21338000	0.13530100
O	-1.49756000	-0.87380100	-3.72458000
O	-5.43536000	-1.31499000	-1.64800000
O	-2.88750000	-4.64235000	-1.65814000
C	-2.75627000	-3.51014000	-1.46371000
C	-4.30790000	-1.48316000	-1.45402000
C	-1.89145000	-1.21711000	-2.69426000
C	-1.96093000	-1.23515000	2.93088000
C	-2.80391000	-3.51940000	1.66501000
C	-4.34945000	-1.48882000	1.64005000
H	-0.86071600	2.64336000	0.16615400
C	0.10530400	-0.61971200	0.16320400
C	1.48438000	-0.47485600	0.20193100
C	2.02535000	0.82030200	0.22793100
C	1.19099000	1.93419000	0.21452900
C	-0.20375700	1.77949000	0.17508400
C	-0.73111500	0.49668000	0.15167700
H	2.12776000	-1.34895000	0.21279300
H	3.10349000	0.94734900	0.25937300
H	1.61628000	2.93325000	0.23519300

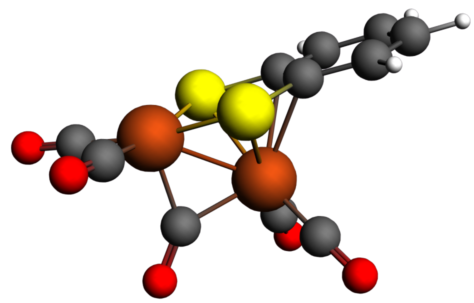

4.4a: (μ-bdt)$Fe_2(CO)_5$

B88P86/TZP

Fe	-2.06601605	-1.25448771	1.67954732
O	-3.89631152	0.24806259	3.39015642
O	-4.13311683	-3.34235252	1.49570825
S	-2.59448864	0.03091944	-0.28568607
O	-1.09119139	-2.69016293	4.02960797
Fe	-2.52409624	-2.19078318	-0.64125413
S	-0.43046333	-2.19990902	0.19400298
C	-3.18312081	-0.35608115	2.70273301
O	-5.01366421	-1.95533120	-2.17154134
O	-2.27502088	-4.95926061	-1.57633042
C	-2.35410504	-3.86723939	-1.18991431
C	-4.03619019	-2.06097058	-1.55393065
H	-1.59065830	2.55551059	0.79681971
C	-1.47723948	-2.13243336	3.08798207
C	-3.31873400	-2.61954909	1.04214422
C	-0.09243042	-0.53735257	0.73681775
C	1.11267113	-0.21064589	1.40792051
C	1.33870260	1.09540144	1.80949860
C	0.36649502	2.09656460	1.58929442
C	-0.83116658	1.79273063	0.96513706
C	-1.06938404	0.46958685	0.51704119
H	1.85374868	-0.99012931	1.58125849
H	2.27416372	1.35010272	2.30803824
H	0.55705632	3.11875432	1.91697728

ΔH = 0.0 kcal mol^{-1}
ΔG = 0.0 kcal mol^{-1}

TPSS-D3(BJ)/TZP

Fe	-2.05340000	-1.24455000	1.64184000
O	-3.85576000	0.31014300	3.33889000
O	-4.12681000	-3.33297000	1.50442000
S	-2.59242000	0.02193700	-0.30204900
O	-0.96259600	-2.62784000	3.97473000
Fe	-2.52623000	-2.19353000	-0.64592300
S	-0.44023300	-2.20667000	0.18295700
C	-3.15872000	-0.31839500	2.66169000
O	-5.02933000	-1.95495000	-2.15626000
O	-2.29913000	-4.97736000	-1.54429000
C	-2.36768000	-3.88125000	-1.17465000
C	-4.04852000	-2.06260000	-1.54854000
H	-1.62484000	2.52126000	0.84872100
C	-1.41065000	-2.09618000	3.04942000
C	-3.31484000	-2.61273000	1.04572000
C	-0.11402800	-0.55558700	0.75450500
C	1.06584000	-0.24495600	1.47333000
C	1.26867000	1.04603000	1.91787000
C	0.30247900	2.04950000	1.69029000
C	-0.86813500	1.76323000	1.01829000
C	-1.08551000	0.45289800	0.52933500
H	1.79521000	-1.02668000	1.65445000
H	2.17800000	1.28923000	2.45878000
H	0.47658800	3.05693000	2.05559000

ΔH = 0.0 kcal mol^{-1}
ΔG = 0.0 kcal mol^{-1}

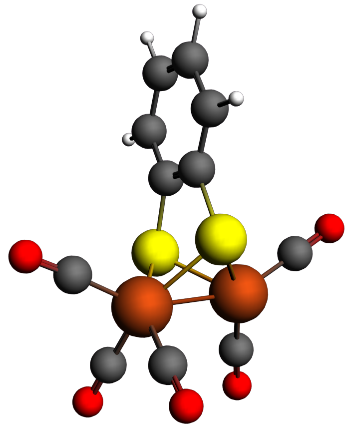

4.4b: (μ-bdt)$Fe_2(CO)_5$

B88P86/TZP

Fe	-2.56116987	-1.76979569	1.23476657
H	3.07416318	0.95575316	0.53293989
O	-3.19809755	-4.52790041	2.00798800
S	-2.51998621	0.15303319	0.00868458
O	-1.69671676	-0.92217640	3.91208865
Fe	-2.52007657	-1.79037676	-1.24183257
S	-0.72701464	-2.21993485	0.09141856
O	-1.51296792	-0.86083487	-3.86711829
O	-5.40845492	-1.42278544	-1.68740225
O	-2.80938187	-4.66042346	-1.80100508
C	-2.68640444	-3.52755434	-1.58360721
C	-4.26923076	-1.56589727	-1.51807515
C	-1.86988357	-1.20949407	-2.82245234
C	-2.05562769	-1.23933891	2.85235146
C	-2.90823548	-3.44771392	1.68736312
H	1.57696643	2.94135761	0.45360276
H	-0.89187715	2.65073331	0.21675238
C	0.08547825	-0.61987269	0.18889296
C	1.46302905	-0.47074179	0.33519147
C	1.99749589	0.82399481	0.42511605
C	1.15618767	1.93793422	0.38338526
C	-0.23421868	1.78227946	0.24723587
C	-0.75882514	0.49810768	0.14892159
H	2.10889195	-1.34762852	0.38106974

ΔH = 7.7 kcal mol^{-1}
ΔG = 6.3 kcal mol^{-1}

TPSS-D3(BJ)/TZP

Fe	-2.58804000	-1.75161000	1.22176000
H	3.06535000	0.93095400	0.53598900
O	-3.11005000	-4.57579000	1.84605000
S	-2.51561000	0.15927400	-0.00387600
O	-1.68612000	-0.89789200	3.88718000
Fe	-2.52238000	-1.79005000	-1.21724000
S	-0.73956500	-2.21538000	0.11412500
O	-1.48361000	-0.86832800	-3.83278000
O	-5.41351000	-1.41258000	-1.63933000
O	-2.81169000	-4.66947000	-1.73742000
C	-2.68790000	-3.53530000	-1.54196000
C	-4.27501000	-1.55864000	-1.48272000
C	-1.85472000	-1.21917000	-2.79633000
C	-2.06347000	-1.21957000	2.83843000
C	-2.89990000	-3.45964000	1.60780000
H	1.58625000	2.91900000	0.41864200
H	-0.87755200	2.64115000	0.17605200
C	0.07764100	-0.62534900	0.19862700
C	1.45217000	-0.48476600	0.34902000
C	1.99277000	0.80527700	0.42457200
C	1.16076000	1.92157000	0.36160400
C	-0.22745000	1.77380000	0.22234600
C	-0.75761300	0.49433200	0.14014600
H	2.08731000	-1.36257000	0.40889400

ΔH = 6.1 kcal mol^{-1}
ΔG = 5.2 kcal mol^{-1}

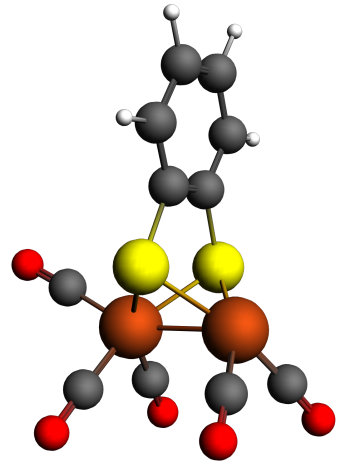

4.4c: (μ-bdt)$Fe_2(CO)_5$

B88P86/TZP

Fe	-2.62947767	-1.78835872	1.26945205
O	-5.41771155	-1.31049617	2.01806128
O	-2.92924748	-4.58454953	2.07915194
S	-2.51724065	0.17012565	0.02725834
H	3.07182513	0.92994893	0.64959485
Fe	-2.59118662	-1.77731193	-1.20456349
S	-0.70996449	-2.23686029	0.04569201
O	-1.56346424	-0.92949272	-3.83801137
O	-5.45167603	-1.33138467	-1.73904718
O	-2.90166634	-4.65217817	-1.75847550
C	-2.76818192	-3.52077471	-1.55281378
C	-4.32318889	-1.49448195	-1.53890607
C	-1.94177149	-1.25762297	-2.79481712
H	1.57835768	2.92259882	0.62141072
C	-2.78959052	-3.46870850	1.77593016
C	-4.29806562	-1.47997225	1.74536057
H	-0.88638703	2.63832502	0.32504680
C	0.08801368	-0.63148931	0.20037039
C	1.46230980	-0.48458899	0.36769290
C	1.99625964	0.80648080	0.52110928
C	1.15926771	1.92283732	0.50585128
C	-0.22775403	1.77004551	0.33786996
C	-0.75296810	0.48934662	0.18816550
H	2.11057454	-1.36073745	0.37745876

ΔH = 9.1 kcal mol^{-1}
ΔG = 7.7 kcal mol^{-1}

TPSS-D3(BJ)/TZP

Fe	-2.63367000	-1.78985000	1.28082000
O	-5.46686000	-1.33510000	1.85905000
O	-2.97783000	-4.63502000	1.87460000
S	-2.50671000	0.17219500	0.06565500
H	3.07907000	0.94308900	0.52347700
Fe	-2.58176000	-1.77195000	-1.15327000
S	-0.70438500	-2.22607000	0.08844400
O	-1.53831000	-0.90950400	-3.77672000
O	-5.44860000	-1.32575000	-1.65872000
O	-2.89519000	-4.65602000	-1.66373000
C	-2.76090000	-3.52289000	-1.48371000
C	-4.31939000	-1.48919000	-1.47784000
C	-1.92616000	-1.24739000	-2.74282000
H	1.58985000	2.92903000	0.47939900
C	-2.81818000	-3.49952000	1.68678000
C	-4.33023000	-1.49228000	1.67610000
H	-0.87712000	2.63851000	0.25668700
C	0.09424000	-0.62349700	0.19386200
C	1.46904000	-0.47522200	0.32048700
C	2.00478000	0.81691400	0.42500000
C	1.16924000	1.93069000	0.40128500
C	-0.21905200	1.77543000	0.27411900
C	-0.74498600	0.49409600	0.17548800
H	2.11297000	-1.34899000	0.33695900

ΔH = 7.6 kcal mol^{-1}
ΔG = 7.1 kcal mol^{-1}

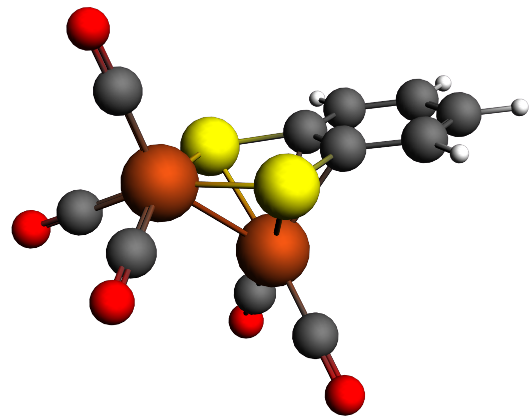

4.4d: (μ-bdt)$Fe_2(CO)_5$

B88P86/TZP

Fe	-1.43935649	-1.62289630	0.00000000
O	-2.21961246	-3.61846910	-1.99073064
O	2.58732581	1.91071587	0.00000000
S	-0.63063209	-0.11550321	-1.56107866
O	-2.21961246	-3.61846910	1.99073064
Fe	0.94287627	-0.53642560	0.00000000
S	-0.63063209	-0.11550321	1.56107866
C	-1.89137673	-2.80890235	-1.21979610
O	2.36399635	-2.00107212	-2.12387457
O	2.36399635	-2.00107212	2.12387457
C	1.80988688	-1.43524806	1.27986984
C	1.80988688	-1.43524806	-1.27986984
H	-3.23519649	0.84644610	-2.50450401
C	-1.89137673	-2.80890235	1.21979610
C	1.93186825	0.95659242	0.00000000
C	-2.08307078	0.45272672	0.70893141
C	-3.24297712	0.85428839	1.41521810
C	-4.36316153	1.25755031	0.70625753
C	-4.36316153	1.25755031	-0.70625753
C	-3.24297712	0.85428839	-1.41521810
C	-2.08307078	0.45272672	-0.70893141
H	-3.23519649	0.84644610	2.50450401
H	-5.25519559	1.57357131	1.24730850
H	-5.25519559	1.57357131	-1.24730850

ΔH = 10.5 kcal mol^{-1}
ΔG = 8.7 kcal mol^{-1}

TPSS-D3(BJ)/TZP

Fe	-1.42079093	-1.54582269	0.00000000
O	-2.00451242	-3.58593659	-2.01287428
O	2.68947838	1.82494996	0.00000000
S	-0.63791804	-0.03397050	-1.56116519
O	-2.00451242	-3.58593659	2.01287428
Fe	0.90707040	-0.52673484	0.00000000
S	-0.63791804	-0.03397050	1.56116519
C	-1.78266945	-2.75386026	-1.23197077
O	2.21802839	-2.16179965	-2.07157732
O	2.21802839	-2.16179965	2.07157732
C	1.70896939	-1.51033681	1.26587133
C	1.70896939	-1.51033681	-1.26587133
H	-3.27931551	0.79675520	-2.49832417
C	-1.78266945	-2.75386026	1.23197077
C	1.98894745	0.90651137	0.00000000
C	-2.10968352	0.46485051	0.70821788
C	-3.28681758	0.81040009	1.41386681
C	-4.42016923	1.15946324	0.70526049
C	-4.42016923	1.15946324	-0.70526049
C	-3.28681758	0.81040009	-1.41386681
C	-2.10968352	0.46485051	-0.70821788
H	-3.27931551	0.79675520	2.49832417
H	-5.32422074	1.42709098	1.24250635
H	-5.32422074	1.42709098	-1.24250635

ΔH = 11.5 kcal mol^{-1}
ΔG = 10.4 kcal mol^{-1}

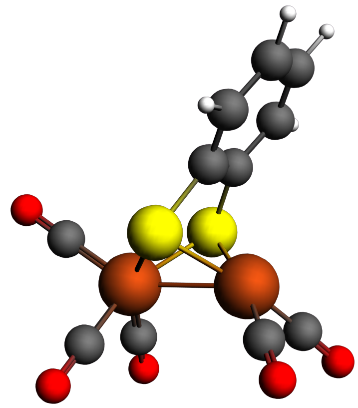

4.4c↔4.4d transition state: (μ-bdt)$Fe_2(CO)_5$

B88P86/TZP

Fe	-2.41687439	-1.64781471	1.12099422
O	-4.80413230	-0.91923210	2.65280565
O	-2.38573741	-4.15039116	2.64004375
S	-2.62253745	0.14660225	-0.34477060
H	2.60504805	0.61498910	1.80891103
Fe	-2.66770632	-1.82214341	-1.45967624
S	-0.75041055	-2.31121575	-0.35493779
O	-1.63602366	-1.09284791	-4.12932894
O	-5.54646299	-1.36399399	-1.92966532
O	-3.04026247	-4.72636488	-1.84650035
C	-2.89029998	-3.58753439	-1.69630594
C	-4.41693911	-1.54055859	-1.74281174
C	-2.04910025	-1.38009259	-3.08497793
H	1.10600351	2.60423405	1.78847718
C	-2.36982154	-3.15606715	2.02974050
C	-3.84933574	-1.18644319	2.03779131
H	-1.18700794	2.43961458	0.82907375
C	-0.11245113	-0.77314597	0.29291986
C	1.17369001	-0.68073520	0.85539061
C	1.60182714	0.53530043	1.38739647
C	0.75674865	1.65584676	1.37710377
C	-0.52703168	1.57143194	0.83896955
C	-0.96555002	0.35368292	0.28827047
H	1.82722555	-1.55384143	0.85861816

ΔH = 11.1 kcal mol
ΔG = 10.8 kcal mol

TPSS-D3(BJ)/TZP

Fe	-2.38363569	-1.61916149	1.05474716
O	-4.89095296	-0.96382738	2.40544187
O	-2.44605075	-4.20885686	2.40694139
S	-2.56255235	0.19215573	-0.39480175
H	2.54912716	0.57311152	1.98745269
Fe	-2.64950206	-1.81040752	-1.42113820
S	-0.69185892	-2.27049053	-0.39814524
O	-1.79353162	-1.20239598	-4.17888896
O	-5.55503947	-1.39204755	-1.67426129
O	-3.05843567	-4.72317769	-1.60250684
C	-2.88920458	-3.58260805	-1.54765505
C	-4.41459697	-1.54926504	-1.58835463
C	-2.13255621	-1.43934395	-3.10033746
H	1.05238459	2.55564179	1.97471259
C	-2.38497726	-3.17308344	1.88207531
C	-3.87691369	-1.19349683	1.88497368
H	-1.18535593	2.42802798	0.90023963
C	-0.08030922	-0.75036198	0.29528314
C	1.17626507	-0.67982007	0.91692257
C	1.57459969	0.51260814	1.51340405
C	0.72998353	1.63079036	1.50691174
C	-0.52326219	1.56857764	0.90527642
C	-0.93170629	0.37445543	0.29154475
H	1.82222763	-1.55148423	0.92092015

ΔH = 11.6 kcal mol
ΔG = 11.0 kcal mol

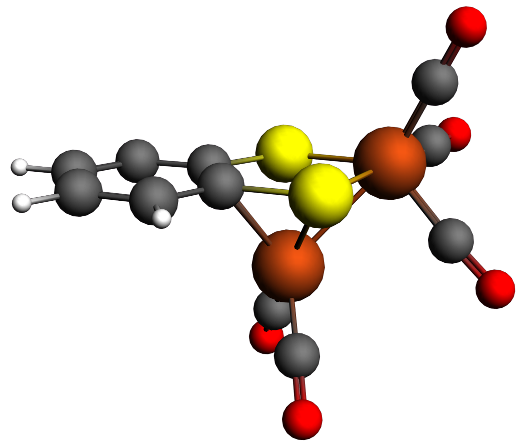

4.4a↔4.4d transition state: (μ-bdt)$Fe_2(CO)_5$

B88P86/TZP

Fe	-1.40263600	-1.61363600	0.11979300
O	-2.15719100	-3.82058500	-1.65153300
O	2.72613100	1.74301000	0.62658000
S	-0.68994900	-0.23606100	-1.64022500
O	-2.15030100	-3.36785800	2.34063500
Fe	0.94269000	-0.48390800	-0.11603700
S	-0.59261900	0.09324400	1.47048200
C	-1.85240800	-2.92819900	-0.96682300
O	2.70065300	-1.35280800	-2.31437900
O	1.85996700	-2.71597300	1.58390400
C	1.44869300	-1.85047800	0.92879000
C	2.00530900	-1.02254100	-1.44776700
H	-3.35751500	0.54950700	-2.59179700
C	-1.84285600	-2.65329400	1.47279800
C	2.02832900	0.86722900	0.32230900
C	-2.09428600	0.51426000	0.60766600
C	-3.24396100	0.96754200	1.30442100
C	-4.39100600	1.27906000	0.59323000
C	-4.43468500	1.12999400	-0.81086100
C	-3.33033100	0.66914200	-1.50824100
C	-2.13632900	0.36571300	-0.80470300
H	-3.20630800	1.07811200	2.38850100
H	-5.27165100	1.64030900	1.12625400
H	-5.34821200	1.37899700	-1.35282500

ΔH = 10.5 kcal mol-
ΔG = 10.6 kcal mol-

TPSS-D3(BJ)/TZP

Fe	-1.42283900	-1.54410900	0.03509500
O	-2.02080400	-3.62856700	-1.92746300
O	2.68681000	1.81276400	0.13531900
S	-0.65694300	-0.07886200	-1.58263400
O	-1.96942700	-3.53725100	2.10348700
Fe	0.90218800	-0.52992600	-0.03722400
S	-0.61871900	0.01103800	1.53787800
C	-1.79665700	-2.78103700	-1.16454300
O	2.35746000	-1.98138100	-2.14837500
O	2.09124100	-2.32990100	1.97040200
C	1.62384500	-1.61654500	1.19244000
C	1.78529500	-1.40666500	-1.32665300
H	-3.30479800	0.73531800	-2.51492600
C	-1.76570900	-2.72275300	1.29954400
C	1.98524800	0.89789900	0.06253200
C	-2.10215600	0.48138200	0.68665700
C	-3.27141300	0.84624000	1.39573000
C	-4.41168700	1.17919600	0.69051600
C	-4.42686600	1.14397100	-0.71955700
C	-3.30161700	0.77524300	-1.43090300
C	-2.11709900	0.44758600	-0.72947800
H	-3.25265300	0.85992600	2.48018300
H	-5.30848500	1.46517300	1.23065800
H	-5.33504400	1.40346600	-1.25411000

ΔH = 11.5 kcal mol-
ΔG = 10.4 kcal mol-

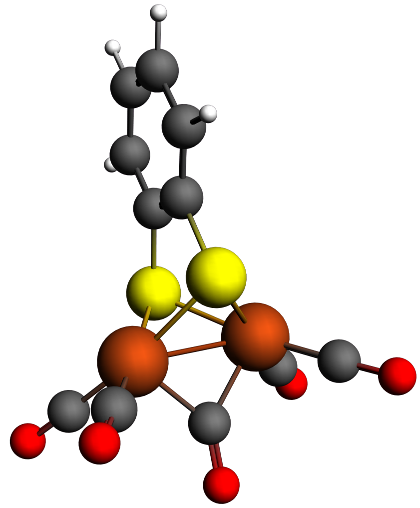

4.4a ring flop transition state: (μ-bdt)$Fe_2(CO)_5$

B88P86/TZP

Fe	0.00000000	-1.28908628	1.21217964
O	2.12895195	-2.94251581	2.37701598
O	0.00000000	0.00000000	3.81960773
S	1.54269001	0.00000000	-0.00985764
O	-2.12895195	-2.94251581	2.37701598
Fe	0.00000000	1.28908628	1.21217964
S	-1.54269001	0.00000000	-0.00985764
C	1.28583192	-2.28083217	1.93059888
O	2.12895195	2.94251581	2.37701598
O	-2.12895195	2.94251581	2.37701598
C	-1.28583192	2.28083217	1.93059888
C	1.28583192	2.28083217	1.93059888
H	2.49645990	0.00000000	-2.80975772
C	-1.28583192	-2.28083217	1.93059888
C	0.00000000	0.00000000	2.63626206
C	-0.70109139	0.00000000	-1.61076861
C	-1.40530143	0.00000000	-2.81297967
C	-0.69644733	0.00000000	-4.02868017
C	0.69644733	0.00000000	-4.02868017
C	1.40530143	0.00000000	-2.81297967
C	0.70109139	0.00000000	-1.61076861
H	-2.49645990	0.00000000	-2.80975772
H	-1.24625412	0.00000000	-4.97119346
H	1.24625412	0.00000000	-4.97119346

ΔH = 6.7 kcal mol^{-1}
ΔG = 8.1 kcal mol^{-1}

TPSS-D3(BJ)/TZP

Fe	0.00000000	-1.28120282	1.18620103
O	2.12436820	-2.88588651	2.41813645
O	0.00000000	0.00000000	3.78888051
S	1.53863506	0.00000000	-0.00973662
O	-2.12436820	-2.88588651	2.41813645
Fe	0.00000000	1.28120282	1.18620103
S	-1.53863506	0.00000000	-0.00973662
C	1.28663312	-2.25239644	1.93290944
O	2.12436820	2.88588651	2.41813645
O	-2.12436820	2.88588651	2.41813645
C	-1.28663312	2.25239644	1.93290944
C	1.28663312	2.25239644	1.93290944
H	2.48880587	0.00000000	-2.79216523
C	-1.28663312	-2.25239644	1.93290944
C	0.00000000	0.00000000	2.60778163
C	-0.69931223	0.00000000	-1.60258613
C	-1.40332831	0.00000000	-2.79990629
C	-0.69528228	0.00000000	-4.01200756
C	0.69528228	0.00000000	-4.01200756
C	1.40332831	0.00000000	-2.79990629
C	0.69931223	0.00000000	-1.60258613
H	-2.48880587	0.00000000	-2.79216523
H	-1.24272050	0.00000000	-4.94926199
H	1.24272050	0.00000000	-4.94926199

ΔH = 8.9 kcal mol^{-1}
ΔG = 9.0 kcal mol^{-1}

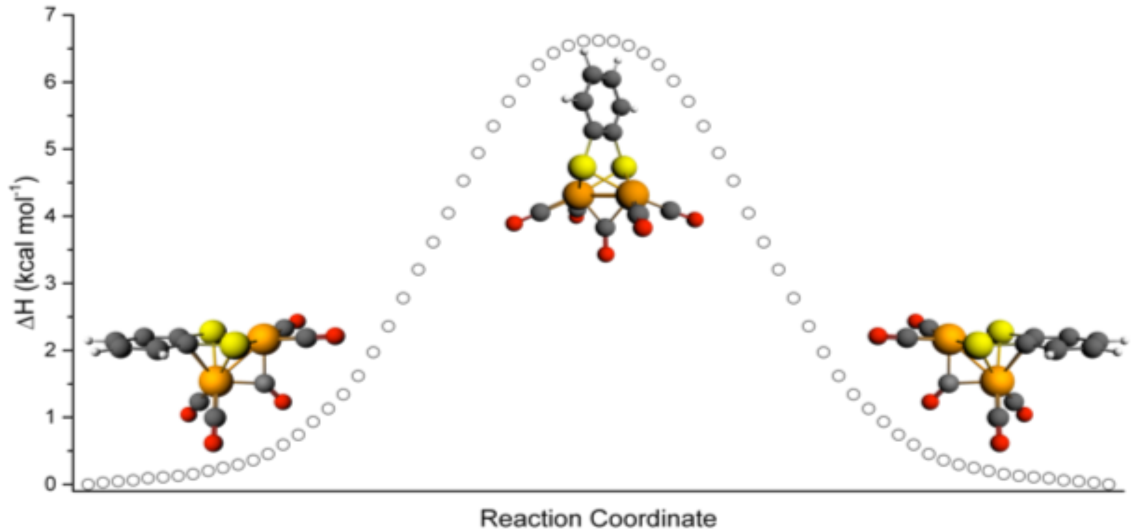

Figure C1: Potential energy (B88P86) surface of the bdt ligand of 4a along the Fe-Fe C_s plane.

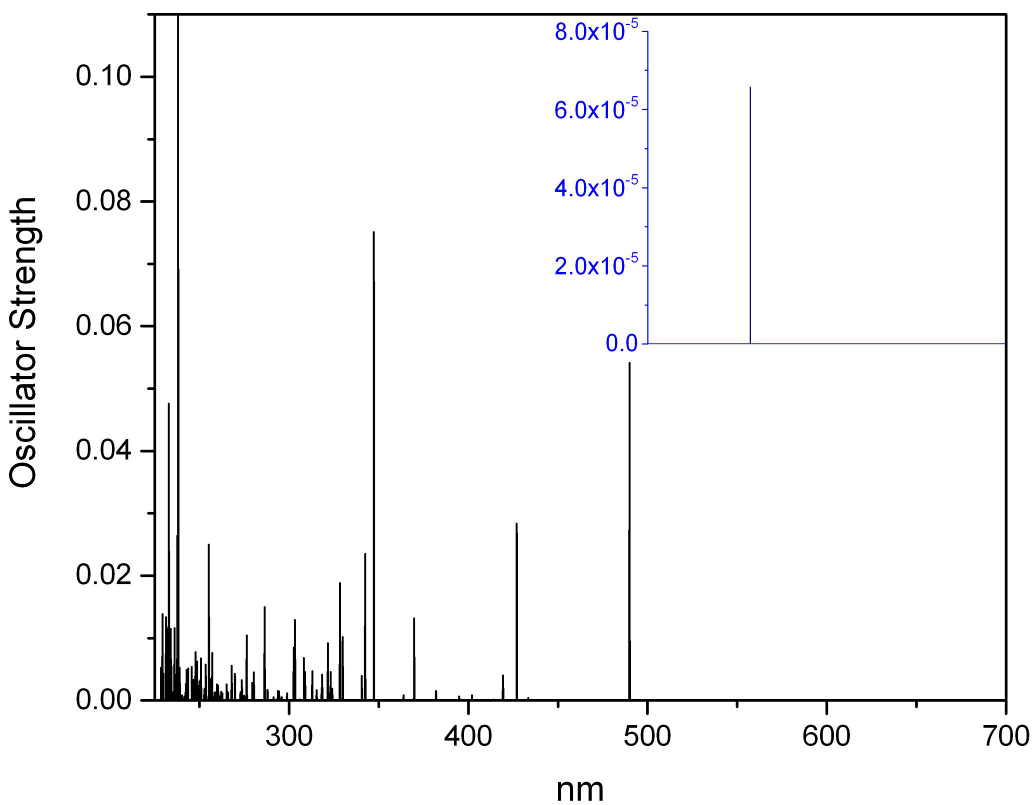

Figure C2: SAOP calculated excitations of (pdt)$Fe_2(CO)_6$.